

A NOVEL ANTINEOPLASTIC NANO-LIPOBUBBLE DRUG DELIVERY SYSTEM FOR PASSIVELY TARGETED OVARIAN CANCER THERAPY

DERUSHA FRANK



A dissertation submitted to the Faculty of Health Sciences, University of the Witwatersrand, in fulfillment of the requirements for the degree of Master of Pharmacy

Supervisor:

Professor Viness Pillay

Department of Pharmacy and Pharmacology, University of the Witwatersrand, South Africa

Co-Supervisors:

Professor Yahya E. Choonara

Department of Pharmacy and Pharmacology, University of the Witwatersrand, South Africa

Dr Lisa C. du Toit

Department of Pharmacy and Pharmacology, University of the Witwatersrand, South Africa

Dr Clement Penny

Department of Medical Oncology, University of the Witwatersrand, South Africa

Johannesburg, 2014

DECLARATION

I, Derusha Frank, declare that this dissertation is my own work. It has been submitted for the degree of Master of Pharmacy in the Faculty of Health Sciences at the University of the Witwatersrand, Johannesburg, South Africa. It has not been submitted before for any other degree or examination at this or any other University.

This the 07th day of October 2014

RESEARCH OUTPUTS

Research Publications

Derusha Frank, Charu Tyagi, Lomas K. Tomar, Yahya E. Choonara, Lisa C. du Toit, Pradeep Kumar, Clement Penny, Viness Pillay. Overview of the role of nanotechnological innovations in the detection and treatment of solid tumours. *International Journal of Nanomedicine*, (2014); 9: 589-613. (Abstract in Appendix A).

Conference Proceedings

Poster Presentations

Derusha Frank, Viness Pillay, Yahya E. Choonara, Lisa C. du Toit. Characterization of Chitosan-Poly(ϵ -caprolactone) Interpenetrating Polymeric Complexes. Poster presented at the 5th International Conference on Pharmaceutical and Pharmacological Sciences, 23-26 September 2009, Potchefstroom, South Africa (Abstract in Appendix B1).

Derusha Frank, Pradeep Kumar, Lisa C. du Toit, Yahya E. Choonara, Clement Penny, Viness Pillay. Fabrication and Evaluation of Camptothecin-loaded Nano-liposomes for Targeted Ovarian Cancer Therapy. Poster presented at the 12th NanoBio Conference, 18-20 June 2012, Varese, Italy (Abstract in Appendix B2).

Podium Presentations

Derusha Frank, Viness Pillay, Yahya E. Choonara, Lisa C. du Toit, Clement Penny. Design and Characterization of Intravenously Administered Nanolipobubbles for Targeted Ovarian Cancer Therapy. Podium presentation for the Young Scientist Competition at the 6th International Conference on Pharmaceutical and Pharmacological Sciences, 25-28 September 2011, Durban, South Africa (Abstract in Appendix B3).

Derusha Frank, Pradeep Kumar, Lisa C. du Toit, Yahya E. Choonara, Clement Penny, Viness Pillay. Fabrication and Evaluation of Camptothecin-loaded Nano-liposomes for Targeted Ovarian Cancer Therapy. Podium presentation for the Best Student Competition at the 12th NanoBio Conference, 18-20 June 2012, Varese, Italy (Abstract in Appendix B2).

Derusha Frank, Yahya E. Choonara, Lisa C. du Toit, Clement Penny, Pradeep Kumar, Viness Pillay. Characterization and Optimization of Camptothecin Nano-liposomes for

Targeted Ovarian Cancer Therapy. Podium presentation at the University of the Witwatersrand Faculty of Health Sciences Research Day, 19 September 2012, Johannesburg, South Africa (Abstract in Appendix B4).

Accolades

University of the Witwatersrand Postgraduate Merit Award, 2009 and 2010.

TATA Africa Scholarship, 2011 and 2012.

First runner-up in the Adcock Ingram Young Scientist Competition: Design and Characterization of Intravenously Administered Nanolipobubbles for Targeted Ovarian Cancer Therapy. 6th International Conference on Pharmaceutical and Pharmacological Sciences, 25-28 September 2011, Durban, South Africa.

Winner of the Best Student Oral Presentation in the Clinical Sciences and Therapeutics for Health theme track: Characterization and Optimization of Camptothecin Nanoliposomes for Targeted Ovarian Cancer Therapy. University of the Witwatersrand Faculty of Health Sciences Research Day, 19 September 2012, Johannesburg, South Africa.

PATENT

Targeted Ovarian Cancer Therapy. Lisa C. du Toit, Derusha Frank, Viness Pillay, Yayha E. Choonara. *SA Patent Application No: 2012/07435*, 4 October 2012 (Abstract in Appendix C).

SUMMARY

Ovarian cancer (OC) is the most aggressive gynecological cancer with in excess of 22000 new cases diagnosed annually in the United States alone. OC is predominantly diagnosed at advanced stages due to the presentation of non-specific symptoms and the absence of adequate clinical markers for routine screening. The consequent prognosis associated with OC is appalling, with an extremely low 5-year survival rate, high incidence of recurrence and drug resistance. The current Gold Standard for the treatment of OC involves a combination of surgical resection and aggressive chemotherapy. However, many factors compromise the safety and efficacy of antineoplastic drugs, not least of all being systemic toxicity of the drugs which affect the quality of life of the patient during and after treatment, and may sometimes prove fatal. Camptothecin (CPT) is a highly efficacious, broad-spectrum antineoplastic drug, the clinical use of which has been hindered by a deleterious side-effect profile, poor aqueous solubility and instability under physiological conditions. This study aimed to address the shortfalls associated with the delivery and *in vivo* activity of CPT by applying nano-technological engineering to produce a novel nano-enabled drug delivery system (DDS) that will be passively targeted to the tumour site following intravenous administration. Tumour tissue displays unique characteristics that collectively have been termed the Enhanced Permeability and Retention (EPR) phenomenon. Passive targeting of the formulated antineoplastic nano-lipobubbles (NLB) through this phenomenon will enable preferential accumulation of the DDS within tumour tissue, thereby reducing systemic side-effects and enhancing therapeutic activity. In addition, formulation as NLB improved the solubility of CPT thereby facilitating administration and enhancing the pharmacokinetic profile of the drug. Nano-sizing was the central consideration in this study and a size threshold of 200 nm was delineated for effective passive targeting. Pre-formulation studies highlighted 2 feasible lipid combinations and the concentration ranges thereof, as well as an appropriate solvent system, emulsifier and CPT concentration for the formulation of nano-liposomes (NLS). The merits of two methods of NLS formulation were investigated as well as various formulation parameters. The Reverse-Phase Solvent Evaporation (RPSE) method was deemed the most suitable method of NLS preparation for this study. The delineation of independent variables and measured outcomes was central to the generation of a Face-centered Central Composite experimental design for each of the two lipid combinations. Systematic analysis of the fifteen formulations of each of these experimental designs produced experimental data that was mathematically modeled employing regression models to predict the effect of formulation variables on measured outcomes and hence, statistically optimize the formulations based on the desired average size, zeta potential, drug incorporation and mean dissolution time of formulated NLS. Each of the 2 statistically optimized formulations demonstrated a composite desirability >0.9. The effect of gaseous incorporation and sonication parameters involved in the conversion of NLS to NLB on the measured outcomes were assessed and optimized. Optimized NLB formulations were further modified to incorporate silibinin (SB), for the achievement of synergistic antineoplastic activity with CPT. The application of sequential polymeric coating proved substantially beneficial to the stability characteristics and drug release profiles of both NLB formulations, whilst the average size of NLB was maintained below 200 nm (141-190 nm). Substantial inversion of zeta potential following the application of CHT and PAA, as well as chemical structural changes determined by FTIR spectroscopy confirmed successful polymeric coating and highlighted the resultant favorable effect on formulation stability. Assessment of the physical stability of optimized formulations further substantiated the positive impact of polymeric coating and suggested excellent feasibility with regards to storage stability and clinical use. *In vitro* drug release studies readily highlighted the positive influence of polymeric coating on the drug release characteristics of CPT and SB. The results of cytotoxicity evaluation on A2780 epithelial ovarian cancer cells, by flow cytometry and real-time cell analysis, further corroborated the benefits of the altered drug release characteristics achieved following polymeric coating. Cumulative cytotoxicity demonstrated by optimized NLB 72 hours post-treatment ranged between 85%-95%. Cellular internalization of formulated NLB was swiftly achieved, with the extent of internalization exhibiting time-dependent and size-dependent characteristics. The slower release of CPT and SB from coated NLB formulations resulted in enhanced and sustained cytotoxicity relative to uncoated NLB formulations and native drug compounds. Quantitation of the hemolytic potential of formulated NLB-DDS was significantly below the safety threshold for intravenous formulations. The optimized NLB-DDS displayed favorable characteristics for the achievement of passive targeting, satisfactory drug incorporation, substantial physical stability, favorable haemocompatibility, as well as enhanced cytotoxicity against A2780 cells relative to the native drugs.

ACKNOWLEDGEMENTS

At the completion of this work I am eternally humbled and deeply grateful to the countless individuals for their generosity of spirit in guiding and assisting me through this most rewarding and challenging task. Without each of you this journey would have held much less value, educational and life lessons.

Of greatest importance, I lay my gratitude at the feet of the Almighty, constant and everlasting companion of my heart, for bringing me to and through this invaluable experience from which I have gained unquantifiable rewards and lessons.

To my mum: The words in every book ever written will never be enough to express my gratitude for always affording me every opportunity possible to live out my dreams and pursue the many crazy ideas I have had. Thank you for being my most ardent supporter, for working tirelessly to provide the necessary means, for constantly encouraging me to reach beyond my boundaries and grounding me in an ethos of honest hard work. Feeling safe to fall because you are my safety net, gives me the courage to reach further and deeper in every endeavor I undertake.

To my siblings, Krenesh and Krelisha: Thank you for always catching me even before I fall, and constantly encouraging, protecting and guiding me. You guys are my constant in the greatest of uncertainties, safe place in troubled times and the reason I can view the world through rose-tinted glasses.

To my Fiancé and best friend, André: I am at a loss for words to adequately express my gratitude for your unwavering support, help and encouragement. Thank you for making my work a priority and going far beyond every expectation to make life smooth and easy for me. Thank you for having faith in me when mine was dwindling, wiping the many tears, indulging my crazy antics and always reminding me of the wonder that lay ahead. You are a symbol of all that is good and you truly inspire me to do and be better.

To my Supervisor, Professor Viness Pillay: Thank you for affording me the opportunity to undertake my Masters in an environment where the nothing is considered impossible! You have provided more than just a technologically advanced research platform. You have provided a window into a world that encourages us to think out of the box and feel comfortable (even inspired) in the realm of outrageous ideas, uncertain outcomes and fearless exploration of the unknown that may indeed bring forth a concept that will change the world someday. Thank you for pushing the boundaries, testing me, frustrating me and teaching me. It was all worthwhile!

To my co-supervisor, Dr Lisa du Toit: You truly are an inspiration. To you I extend my sincerest gratitude for the effort and expertise you have generously put into my work and for your constant encouragement and kindness. Thank you for your patience and guidance throughout my research.

To my co-supervisors, Professor Yahya Choonara and Dr Clement Penny: I extend my sincere appreciation for your valuable input during the undertaking of my research and affording me the opportunity to learn under your guidance and expertise.

To Pradeep Kumar: You are indeed a giant among men and I am most fortunate to have considered you a mentor during my research. Thank you for your humility, passion and willingness to help wherever you could.

To the friends that have become family, Kovanya, Natanya, Kavitha, Ameena: Each one of you has provided something unique that has helped, inspired and motivated me. Thank you for the coffee/lunch/shopping expeditions that were a welcomed distraction, the hours of laughter and conversation on and off campus, for gracefully tolerating my ranting and woes when things just weren't working and for always having an encouraging word. Thank you for the willingness to help with my work and provide guidance or share the lessons learned through each of your own research. Most of all thank you for all the things that only amazing girlfriends can provide!

A special thank you to Thiresen, Thomas, Yashodan and Yusuf for always being there to lend a helping hand, be it in research or my personal endeavors. Thank you for the awesome adventures, many hours of mischief and laughter and treasured friendships.

To my friends and colleagues in the department: Priya, Ndidi, Bongani, Toyin, Caragh, Deshika, Zaheeda, Sherri-lee, Samantha, Mpho, Shivaan, Clare, Yasien, Sajida, Karmani, Poornima, Bibi Fatima, Fatema Mia, Raeesa, Mershen, Sunaina, Pierre, Teboho, Felix, Femi, Khadija, Zama, Nonhlanhla, Khuphukile, Jonathan, Pius and all other postgraduate students, I extend my gratitude for the assistance each have you have provided during my research and for being a part of my journey. A heartfelt thank you to Steven Mufamadi for your unselfish nature and the many hours you have spent assisting, guiding and encouraging me.

My heartfelt appreciation to Dr Tyagi, Dr Tomar and Dr Bijukumar for your kind assistance and perseverance in the publishing of my review article, lending your valued expertise to my *ex vivo* studies and for your general kindness and support.

Thank you to Busi, Tebogo, Sello and Bafana for your assistance. A special thank you to Kleinbooi (KB) for your constant willingness and sometimes going above and beyond your call of duty to assist me. Your dedication is admirable and sincerely appreciated.

To Professor Sandy van Vuuren: You have been the epitome of professionalism and I have learned so much from you through the facilitation of undergraduate practical training and far beyond. I extend my sincere gratitude and appreciation for your generosity in assisting me wherever possible, your understanding and guidance.

To Mr David Bayever, Mrs Veni Padayachee, Ms Neha Singh: Thank you for the constant encouragement, support and insight into the 'bigger picture'. Your kindness and generosity has made a huge contribution to this experience.

To Natasia, Thandiwe, Ezio of the Department of Medical Oncology, I extend my deepest gratitude for assisting me in navigating new territory, coming to my aid on numerous occasions, sharing your knowledge and expertise, accommodating me in the laboratory and always being so willing and good natured about helping me.

I was fortunate to have benefited from the knowledge and expertise of Danny Ramduth and Nдавhe of BD Biosciences during the undertaking of flow cytometry analysis, as well as the kind assistance of Zachariah More from the Department of Surgery. Thank you for patiently answering all my questions, advising and guiding me throughout this process. Thank you also to Miss Pam Sharp for your patient assistance with Transmission Electron Microscopy.

Thank you to the funders who have generously funded this study and eased the financial burden: University of the Witwatersrand, Tata Africa, Gauteng Department of Education, Technology Innovation Agency, Gauteng Department of Agriculture and Rural Development, National Research Foundation, PPS Insurance, The Pharmaceutical Society of South Africa.

This list is by no means complete. There have been countless acts of kindness and amazing people that have assisted me on this journey. I would like to express my gratitude to everyone that I may have mistakenly omitted.

DEDICATION

This research is dedicated firstly, to my mum: For all that you are and all that you have let me be and made me. I am who and where I am because I stand on the shoulders of a Giant.

Secondly: I dedicate this work to the many loved ones we have lost to cancer. It is the memory of each of you and the role you have played in my life that has inspired the completion of this work through the most trying times.

TABLE OF CONTENTS

CHAPTER 1

AN OVERVIEW OF OVARIAN CANCER, RATIONALE AND MOTIVATION FOR THIS STUDY

1.1	Introduction	1
1.2	Detection and diagnosis of ovarian cancer: The initial problem	5
1.3	Micro-environmental tumour physiology: Barrier and potential in drug delivery	6
1.4	Current treatment protocol for ovarian cancer	7
1.5	Statement of the problem	8
1.6	Approach to the problem	9
1.7	Rationale and Motivation for the study	10
1.8	Aim and Objectives of this study	12
1.9	Novelty of this study	13
1.10	Overview of this dissertation	13

CHAPTER 2

INNOVATIVE NANOTECHNOLOGICAL APPROACHES TO THE DETECTION AND TREATMENT OF OVARIAN AND OTHER SOLID TUMOURS

2.1	Introduction	15
2.2	Application of nanotechnology in tumour diagnostics and imaging	17
2.2.1	Biosensors in cancer detection	17
2.2.2	Quantum dots for tumour detection and imaging	20
2.3	A nanotechnological approach to cancer therapy	22
2.3.1	Poor aqueous solubility: A cascading pharmaceutical challenge	23
2.3.2	Targeted therapy: The future of medicine	24
2.3.2.1	Passive targeting of cancer nanotherapeutics	24
2.3.2.2	Enhancing therapeutic efficacy through active targeting	24
2.3.2.2.1	Folate receptor- α	25
2.3.2.2.2	Heat shock protein 90 (Hsp90)	26
2.3.2.2.3	Human epidermal growth factor receptor (HER)-2	27
2.3.2.2.4	Aptamer-based targeted nanosystems	28
2.3.3	Tumour drug resistance: A progressive challenge	28
2.4	Antineoplastic drug challenges: Innovative nanotechnological solutions	30
2.4.1	Doxorubicin	30
2.4.2	Camptothecin	32
2.4.3	Paclitaxel	35
2.4.4	Nutlin-3a	36
2.4.5	Indisulam	36
2.4.6	Curcumin	37
2.5	Nano-enabled antisense oligonucleotides in cancer therapeutics	39
2.6	Nano-theranostics	41
2.6.1	Magnetic nanoparticles	41
2.6.2	Photodynamic therapy	42
2.7	Concluding Remarks	46

CHAPTER 3
PRELIMINARY STUDIES FOR THE DESIGN AND DEVELOPMENT OF A PARENTERAL
ANTINEOPLASTIC NANO-LIPOBUBBLE FORMULATION

3.1	Introduction	47
3.2	Preliminary Studies in the Development of the NLB-DDS	48
3.2.1	Rational Selection of Materials.....	49
3.2.1.1	Lipid Components	49
3.2.1.2	The model drug: Camptothecin.....	53
3.2.1.3	Emulsifiers/Surfactants	54
3.3	Materials and Methods.....	56
3.3.1	Materials	56
3.3.2	Methods.....	56
3.3.2.1	Preparation of Nano-liposomes by the film hydration method.....	57
3.3.2.2	Preparation of Nano-liposomes by the reverse phase solvent evaporation method	57
3.3.2.3	Morphological characterization of nano-liposomal formulations.....	58
3.3.2.4	Construction of a standard curve for the photospectroscopic quantification of camptothecin.....	58
3.3.2.5	Determining favorable camptothecin loading.....	59
3.3.2.6	Size and size distribution characterization of nano-liposomes.....	60
3.3.2.7	Investigating the influence of ultrasonication on the size characteristics of nano-liposomes.....	60
3.4	Results and Discussion.....	61
3.4.1	Morphological analysis of nano-liposomes	61
3.4.2	Generation of a standard curve for quantification of camptothecin	61
3.4.3	Delineation of the most feasible method of nano-liposome preparation	62
3.4.4	Influence of ultrasonication on the properties of formulated nano-liposomes.....	63
3.4.5	Establishment of the influence of formulation variations on nanoliposomes characteristics for the selection of favorable parameters.....	63
3.5	Concluding Remarks.....	66

CHAPTER 4

FORMULATION AND STATISTICAL OPTIMIZATION OF A CAMPTOTHECIN-LOADED INTRAVENOUS NANO-LIPOSOMAL DRUG DELIVERY SYSTEM

4.1	Introduction	67
4.2	Statistical modeling employing a Face-Centered Central Composite Design	68
4.3	Determination of suitable measured responses.....	69
4.4	Materials and Methods.....	71
4.4.1	Materials	71
4.4.2	Methods.....	71
4.4.2.1	Formulation of camptothecin-loaded nano-liposomes	71
4.4.2.2	Determination of the size, size distribution and surface charge characteristics of formulated nano-liposomes.....	73
4.4.2.3	Elucidation of camptothecin incorporation efficiency	73
4.4.2.4	<i>In vitro</i> camptothecin release analysis.....	73
4.4.2.5	Micro-ultrasound imaging of formulated nano-liposomes	74
4.5	Results and Discussion.....	74
4.5.1	Experimental results.....	74
4.5.1.1	Size and size distribution analysis of fabricated nano-liposomes	74
4.5.1.2	Surface charge characterization of formulated nano-liposomes	76
4.5.1.3	Quantification of camptothecin incorporation efficiency.....	77
4.5.1.4	Assessment of the release characteristics of camptothecin from nano-liposomes.....	78
4.5.1.5	Behavioral characterization of formulated nano-liposomes through micro-ultrasound imaging.....	81
4.5.2	Computational modeling of experimental data.....	81
4.5.2.1	Experimental design and statistical optimization of CHO nano-liposomes.....	82
4.5.2.1.1	Validation of statistical optimization through data correlation.....	82
4.5.2.1.2	Characterization of the relationship of independent variables relative to measured outcomes.....	83
4.5.2.1.3	Analysis of the fit of the derived model.....	85
4.5.2.1.4	Constrained optimization of the CHO nano-liposomal drug delivery system	88
4.5.2.2	Experimental design and statistical optimization of DSPE nano-liposomes.....	89
4.5.2.2.1	Validation of statistical optimization through data correlation.....	89
4.5.2.2.2	Characterization of the relationship of independent variables relative to measured outcomes.....	90
4.5.2.2.3	Analysis of the fit of the derived model.....	93

4.5.2.2.4	Constrained optimization of the DSPE nano-liposomal drug delivery system	95
4.6	Concluding Remarks.....	96

CHAPTER 5

MODIFICATION AND PERFORMANCE EVALUATION OF THE OPTIMIZED NANO-LIPOBUBBLE DRUG DELIVERY SYSTEM

5.1	Introduction	98
5.2	Phytochemicals in antineoplastic therapy: Silibinin.....	99
5.3	Materials and Methods.....	100
5.3.1	Materials	100
5.3.2	Methods.....	101
5.3.2.1	Preparation of candidate CHO nano-liposomes and DSPE nano-liposomes.....	101
5.3.2.2	Conversion of formulated nano-liposomes to nano-lipobubbles: Effect of sonication duration.....	101
5.3.2.3	Investigating the effect of lyophilization on nano-lipobubble size and stability.....	102
5.3.2.4	Assessment of lyoprotectant efficacy through water content determination	102
5.3.2.5	Generation of standard curves for the photospectroscopic quantification of silibinin	103
5.3.2.6	Determining the efficacy of phytochemical incorporation.....	103
5.3.2.7	Evaluating polymeric coating by layer-by-layer self-deposition.....	103
5.3.2.8	Determining chemical structural transitions resulting from polymeric coating of nano-liposomes	104
5.3.2.9	Elucidating the size characteristics of formulated nano-liposomes and nano-lipobubbles.....	105
5.3.2.10	Surface charge characterization of formulated nano-liposomes and nano-lipobubbles.....	105
5.3.2.11	Morphological characterization of formulated nano-lipobubbles	106
5.3.2.12	Investigating the efficiency of camptothecin incorporation.....	106
5.3.2.13	Generation of a standard curve for the photospectroscopic quantification of camptothecin.....	106
5.3.2.14	Elucidation of camptothecin and silibinin release characteristics.....	106
5.3.2.15	Delineation of the stability characteristics of optimized nano-lipobubbles.....	107
5.3.2.15.1	Determining stability of nano-lipobubbles in the presence of serum ...	107
5.3.2.15.2	Assessing stability of the formulation after reconstitution	107
5.3.2.15.3	Determining the effect of long-term storage on physicochemical characteristics of formulated nano-lipobubbles.....	108
5.4	Results and Discussion.....	108
5.4.1	Size and surface charge characterization of candidate formulations ..	108
5.4.2	Determination of the effect of lyophilization on formulated nano-lipobubbles.....	110

5.4.3	Determination of lyoprotectant efficacy on formulated nano-liposomes and nano-lipobubbles.....	113
5.4.4	Generation of a standard curve for the photospectroscopic quantification of silibinin	114
5.4.5	Silibinin incorporation and the effect thereof on the physical characteristics of formulated nano-lipobubbles.....	115
5.4.6	Investigating the feasibility of polymeric coating of nano-lipobubbles: Macroscopic and microscopic evaluation	116
5.4.7	Confirmation of polymeric coating through chemical structural transition analyses.....	120
5.4.8	Determining the restoration of nano-lipobubble structure employing fluorescence microscopy.....	121
5.4.9	Establishing the efficiency of camptothecin incorporation.....	122
5.4.10	Generation of a standard curve for the photospectroscopic quantification of CPT at tumoural pH	123
5.4.11	Establishment of drug release characteristics and the effects of modifications on candidate formulations.....	124
5.4.12	Defining the stability characteristics of formulated nano-lipobubbles..	130
5.4.12.1	Determination of the stability of nano-lipobubbles in serum.....	130
5.4.12.2	Characterizing the stability of reconstituted nano-lipobubbles	131
5.4.12.3	Evaluation of the storage stability of nano-lipobubbles	136
5.5	Concluding Remarks.....	137

CHAPTER 6

EX VIVO EVALUATION OF OPTIMIZED NANO-LIPOBUBBLE FORMULATIONS

6.1	Introduction	140
6.2	Materials and Methods.....	141
6.2.1	Materials	141
6.2.2	Methods.....	141
6.2.2.1	Preparation of optimized and control nano-lipobubbles	141
6.2.2.2	Cell culturing and expansion of the A2780 ovarian cancer cell line	141
6.2.2.3	Determination of cell concentration and viability.....	142
6.2.2.4	Delineating experimental controls	142
6.2.2.5	Determination of hemolytic activity of nano-lipobubbles	143
6.2.2.6	Assessing cellular uptake of nano-lipobubbles through fluorescence microscopy.....	144
6.2.2.7	Characterizing the cytotoxicity of formulated nano-lipobubbles	144
6.2.2.7.1	Evaluating cytotoxicity employing flow cytometry	144
6.2.2.7.2	Real-time evaluation of formulation cytotoxicity.....	146
6.3	Results and Discussion.....	147
6.3.1	Hemolytic impact of formulated nano-lipobubble drug delivery systems.....	147
6.3.2	Cellular uptake of nano-lipobubbles	147
6.3.3	Assessment of cytotoxicity by flow cytometry	148
6.3.4	Assessing cellular status through continuous real-time evaluation	151
6.4	Conclusions	159

CHAPTER 7

CONCLUSIONS AND RECOMMENDATIONS

7.1	Conclusions	161
7.2	Recommendations	163

REFERENCES	165
-------------------------	------------

APPENDICES	189
-------------------------	------------

APPENDIX A.....	190
-----------------	-----

APPENDIX B.....	191
-----------------	-----

APPENDIX B1	191
-------------------	-----

APPENDIX B2	192
-------------------	-----

APPENDIX B3	193
-------------------	-----

APPENDIX B4	194
-------------------	-----

APPENDIX C.....	195
-----------------	-----

APPENDIX D.....	196
-----------------	-----

LIST OF FIGURES

- Figure 1.1** A comprehensive view of the estimated number of new cancer cases diagnosed worldwide in 2008 (Source: GLOBOCAN, 2008). *Region estimates do not do not add up to the world estimate due to calculation method. **2**
- Figure 1.2** Brief histological classification of EOC and primary features of each subtype (Adapted from Cloven *et al.*, 2004)..... **4**
- Figure 1.3** Age-specific incidence rates per 100 000 population in the UK, diagnosed annually between 2002 and 2006. Whilst the absolute values are specific to the UK region for a specified time period, the trend is globally representative. (Adapted from Cancer Research UK, 2013)..... **5**
- Figure 1.4** General trend in correlation of tumour stage at the time of diagnosis and the corresponding 5-year survival rate adapted from the latest statistics available from SEER for the USA (Howlader *et al.*, 2012). This trend is significant and representative of current global trends. 1) localized tumour; 2) Spread to regional lymph nodes; 3) Distant metastasis; 4) Unknown stage. The proportion of ovarian cancer diagnoses made after metastasis outside the peritoneal region is in stark contrast to the portion of early diagnoses. The radical decline in 5-year survival rate (expressed as a percentage) as tumour stage progresses, is distinct and accounts for the poor prognosis associated with this condition. **5**
- Figure 1.5** Visual illustration of the tumour micro-environmental factors influencing therapeutic efficacy..... **7**
- Figure 2.1** Illustrative summary of the potential benefits that nanosystems may offer with regards to tumour diagnosis and treatment. **16**
- Figure 2.2** Illustrative representation of the various types of interactions between bioreceptors and analytes, as well as the measurable signals that are produced. **18**
- Figure 2.3** A: is a diagrammatic comparison of the internalization mechanisms of free drug and nano-DDS's in normal tumour cells and MDR tumour cells (Adapted with permission from Gao *et al.*, 2012). B: confocal micrographs highlighting the cellular internalization mechanisms of free drug, a nano-DDS and a functionalized nano-DDS. In this image the drug is indicated in red while the cell nuclei are highlighted in blue. The distinct difference is

drug concentration within the cell after incubation for 2 hours denotes a difference in mechanism of cellular uptake. The significant reduction of free drug after 6 hours and complete absence of free drug after 24 hours indicates efflux of the drug out of the cell. However, drug administered in nanosystems persist within the cell for over 24 hours, indicating a by-pass of the cellular efflux mechanism. Moreover, functionalized nanosystems display superior cellular drug concentration (Source 2.3B: Wate *et al.*, 2012)..... **30**

Figure 2.4 Illustrative representation of the mechanism of PS cytotoxicity for PDT (Adapted with permission from Spyratou *et al.*, 2012)..... **43**

Figure 3.1 Illustrative representation of the ideal properties and key considerations of the intended NLB-DDS **49**

Figure 3.2 Structural illustration of the reversible chemical degradation of CPT from the active lactone form to the poorly active carboxylate form, under physiological conditions..... **54**

Figure 3.3 Transmission Electron Micrographs of NLS at A) 30000x magnification, B) 40000x magnification and C) 50000x magnification..... **61**

Figure 3.4 Three dimensional absorption spectrum of CPT in DMSO:PBS (pH 7.4; 37°C) (1:1)..... **61**

Figure 3.5 Standard curve of the absorbance of CPT in DMSO:PBS (pH 7.4; 37°C) (1:1), as well as 95% confidence and prediction bands (in all cases n=3 and SD<0.02)..... **62**

Figure 4.1 Schematic representation of the experimental runs designated at each of the three levels of the FC-CCD..... **69**

Figure 4.2 Typical size profiles representing CHO-NLS at the minimal (A) and maximal (B) presenting sizes and DSPE-NLS at the minimal (C) and maximal (D) presenting sizes..... **75**

Figure 4.3 Graphical illustration of the relationship between [DOS] and zeta potential. Each set of bars represents formulations containing a particular [DOS].... **76**

Figure 4.4 Fractional drug release profiles for CHO-NLS in PBS (pH 7.4; 37°C) (Design 1) undertaken over a 24 hour period (in all cases n=3 and SD ≤ 0.03)..... **79**

Figure 4.5 Fractional drug release profiles for DSPE-NLS (Design 2) in PBS (pH 7.4; 37°C) undertaken over a 24 hour period (in all cases n=3 and SD ≤ 0.03). **80**

Figure 4.6	Micro-ultrasound images of CHO-NLS following injection into a carageenan hydrogel.....	81
Figure 4.7	Correlation scatter plots of A) Average size ($R^2=62.6\%$); B) Zeta potential ($R^2=97.3\%$); C) DIE ($R^2=80.7\%$) and D) MDT ($R^2=85.7\%$) for the determination of correlation between the experimental and fitted measured responses for CHO-NLS.....	82
Figure 4.8	Graphical illustrations employing A) a 3-D response surface graph and B) a contour plot to depict the influence of independent variables on the average size and zeta potential, respectively, of CHO-NLS.....	83
Figure 4.9	Graphical illustrations employing A) a contour plot and B) a 3-D response surface plot to depict the relationship of independent variables to the measured outcomes DIE and MDT respectively, of CHO-NLS	85
Figure 4.11	Optimization plots for CHO-NLS, indicating optimal levels of independent variables, the predicted outcomes based on these independent variables as well as the desirability of the predicted outcomes.	89
Figure 4.12	Scatter plots of A) Average size ($R^2=83.9\%$); B) Zeta potential ($R^2=81.1\%$); C) DIE ($R^2=63.5\%$) and D) MDT ($R^2=69.3\%$) for the determination of correlation between the experimental and fitted measured responses for DSPE-NLS.	90
Figure 4.13	Graphical illustration employing 3-D response surface graphs (A and C) and a contour plot (B) to depict the influence of independent variables on the average size, zeta potential and MDT of DSPE-NLS.	92
Figure 4.14	Summary of the Residual Plots generated for the measured outcomes of DSPE-NLS.	94
Figure 4.15	Optimization plots for DSPE-NLS, indicating optimal levels of independent variables, the predicted outcomes based on these independent variables and the desirability of the predicted outcomes.	96
Figure 5.1	Schematic summary of the modifications undertaken on candidate NLS formulations and the analytical characterization involved.....	99
Figure 5.2	Size-Intensity profiles of A) candidate CHO-NLS, B) CHO-NLB, C) candidate DSPE-NLS and D) DSPE-NLB (in all cases $n=3$ and $SD<0.02$).	110
Figure 5.3	Schematic representation of the mechanism of lyoprotection afforded by sugar molecules in the lyophilization of liposomes. (Recreated from Chen <i>et al.</i> , 2010 (b))	112

Figure 5.4	Digital images of the post lyophilization products of CHO-NLS A) in the absence of a lyoprotectant, B) with fructose and C) with lactose.	113
Figure 5.5	Three dimensional absorption spectrum of SB in A) DMSO:PBS (pH 7.4; 37°C) (1:1) and B) DMSO:PBS (pH 6.0; 37°C) (1:1).	114
Figure 5.7	Digital images of typical post-lyophilization products of CHO-NLS coated with A) PEI and pectin, B) PEI and alginate, C) CHT and pectin, D) CHT and PAA.	117
Figure 5.8	Effect of the sequential deposition of alternating layers of CHT and PAA on the zeta potential of CHO- and DSPE-NLB.	118
Figure 5.9	Scanning electron micrographs of post-lyophilization products of CHO-NLS coated with A) PEI and pectin (4200x magnification); B) PEI and carrageenan (2800x magnification); C) CHT and pectin (3200x magnification) and D) CHT and PAA (4800x magnification).	119
Figure 5.10	FTIR spectra highlighting the chemical structural transitions of optimized A) CHO-NLS and B) DSPE-NLS following polymeric coating, relative to uncoated CHO- and DSPE-NLS and the native polymers employed in the polyelectrolyte coating.	121
Figure 5.11	Fluorescence micrographs of A) CHO-NLB and B) DSPE-NLB labelled with FITC dye confirming the restoration of NLB structure following lyophilization, reconstitution and SF ₆ gas introduction.	122
Figure 5.12	Graphical illustration of the post-modification DIE's of CPT and SB in CHO-NLB and DSPE-NLB.	123
Figure 5.13	Three dimensional absorption spectrum of CPT in DMSO:PBS (pH 6.0, 37°C) (1:1).	124
Figure 5.14	Standard curve of the absorbance of CPT in DMSO:PBS (pH 6.0; 37°C) (1:1), as well as the 95% confidence and prediction bands (in all cases n=3 and SD<0.02).	124
Figure 5.15	Fractional drug release profiles of CPT from A) candidate CHO- and DSPE-NLS and B) candidate CHO- and DSPE-NLB, at tumoural and physiologic pH over 24 hours (in all cases n=3 and SD<0.02).	125
Figure 5.16	Fractional drug release of A) CPT and B) SB, from CHO- and DSPE-NLB containing SB, at tumoural and physiologic pH over 24 hours (in all cases n=3 and SD<0.02).	127

Figure 5.17	Fractional drug release of A) CPT and B) SB, from coated CHO- and DSPE-NLB, at tumoural and physiologic pH over 24 hours (in all cases n=3 and SD<0.02).	128
Figure 5.20	Defining the A) average size, B) zeta potential, C) CPT incorporation and D) SB incorporation of polymer coated CHO- and DSPE-NLB stored under ambient and refrigeration temperatures over a three month period (in all cases n=3 and SD<0.03).	137
Figure 6.1	Quantitative analysis of the hemolysis induced by optimized CHO- and DSPE-NLS. Despite the concentration-dependent hemolysis displayed, all formulations assessed displayed hemolysis that was below the toxic threshold.....	147
Figure 6.2	Qualitative evaluation of cellular uptake of SRB-labeled optimized CHO- and DSPE-NLB 10 and 30 minutes post-treatment.	148
Figure 6.3	Histograms (A; C; E) and scatter plots (B; D) indicating the intensity of 7-AAD detected as a measure of the cytotoxicity of test controls, CPT and SB formulations. Histograms in the first column provide an indication of the natural cell death that occurred in untreated cells over the analytical period, with an inset of the forward versus side scatter plot for each day, depicting the cell characteristics on each day. (M1 = R2 = cell cytotoxicity).....	152
Figure 6.4	Histograms (A; C; E) and scatter plots (B; D; F) indicating the intensity of 7-AAD detected as a measure of cytotoxicity induced by placebo, uncoated and optimized CHO- and DSPE-NLB. (M1 = R2 = cell cytotoxicity).	153
Figure 6.5	Growth profiles of A2780 cells at densities from 1250-10000 cells/well over a 100 hour period. (in all cases n=3 and SD<0.02)	154
Figure 6.6	Cell index curves highlighting cellular response to serial dilutions of CPT relative to the growth pattern of untreated cells and treatment with the PBS:DMSO solvent system. (in all cases n=3 and SD<0.02).....	156
Figure 6.7	Graphical illustration of the growth and response of A2780 cells to various control preparations establishing the cytotoxic potential of each preparation. (in all cases n=3 and SD<0.02).....	157

LIST OF TABLES

Table 1.1	Comparison of approximate 5-year survival rates for breast and gynecological cancers, highlighting the poor outcome, and critical need, for improvement in the treatment of ovarian cancer (American Cancer Society, 2012; Cancer Research UK, 2013).....	2
Table 2.1	Tabulated nanosystems functionalized for folate receptor targeting in cancer therapeutics.....	26
Table 2.2	A brief outline of commercially available and pre-clinical nanosystems with application in the oncology field.....	40
Table 2.3	Nanosystems investigated for use in PDT, with therapeutic and/or imaging potential.....	45
Table 3.1	Tabulated summary of the properties of surfactants investigated.....	56
Table 3.2	Fixed conditions of rotary evaporation undertaken in the formation of NLS.....	58
Table 3.3	Serial dilutions of CPT in DMSO:PBS (pH 7.4; 37°C) (1:1) for the construction of a standard curve.....	59
Table 4.1	Summary of the minima and maxima of independent variables established from pre-formulation studies and the translation to three analyses levels employed in the experimental design.....	69
Table 4.2	Delineation of the lower and upper limits of the chosen measured responses, and the objective for optimization with respect to each measured response.....	71
Table 4.3	Composition of formulations for each experimental run of the CHO-NLS experimental design.....	72
Table 4.4	Composition of formulations for each experimental run of the DSPE-NLS experimental design.....	72
Table 4.5	Fixed formulation parameters maintained during the preparation of NLS..	73
Table 4.6	Tabulated representation of the average size of NLS for each of the two experimental designs.....	75

Table 4.7	Tabulation of the DIE percentages obtained for formulations in Designs 1 and 2, highlighting the significant distinction between CHO- and DSPE-NLS.....	77
Table 4.8	Calculated MDT values for each experimental run designated for each of the two experimental designs.....	80
Table 4.9	Summary of the <i>p</i> -values for each of the independent variables relative to the measured outcomes.....	88
Table 4.10	Summary of the <i>p</i> -values for each of the independent variables relative to the measured outcomes.....	95
Table 5.1	Composition of the candidate NLS systems obtained by statistical optimization.....	101
Table 5.2	Cationic and anionic polymers investigated for application in NLS coating by the LBL self deposition methodology.....	104
Table 5.3	Summary of average size and size distribution assessments undertaken on candidate NLS and NLB formulations and the modifications that ensued.....	105
Table 5.4	Experimentally determined average size and zeta potential of candidate CHO- and DSPE-NLS and NLB, as well as the percentage deviation from the values predicted for NLS by computational modelling.....	109
Table 5.5	Tabulation of the physical characteristics of CHO- and DSPE-NLB formulations highlighting the effect of lyophilization and lyoprotectant incorporation on the resultant NLB properties.....	111
Table 5.6	Physical characteristics of formulated NLB-DDS and efficiency of SB incorporation relative to quantity of SB added to the formulation.....	116
Table 5.7	Experimentally derived and statistically predicted DIE of CPT for CHO- and DSPE-NLB.....	122
Table 5.8	Physical characteristics of uncoated and polymer coated CHO- and DSPE-NLB in the presence of FBS.....	131
Table 6.1	Test and control preparations evaluated for their cytotoxic effect on A2780 ovarian cancer cells.....	145

LIST OF EQUATIONS

Equation 3.1	Quantitation of Drug Incorporation Efficiency for CPT.....	60
Equation 3.2	Stokes-Einstein equation.....	60
Equation 4.1	Regression equation generated for the average size of CHO-NLB	85
Equation 4.2	Regression equation generated for the zeta potential of CHO-NLB.....	85
Equation 4.3	Regression equation generated for the DIE of CHO-NLB.....	85
Equation 4.4	Regression equation generated for the MDT of CHO-NLB.....	85
Equation 4.5	Regression equation generated for the average size of DSPE-NLB	93
Equation 4.6	Regression equation generated for the zeta potential of DSPE-NLB.....	93
Equation 4.7	Regression equation generated for the DIE of DSPE-NLB.....	93
Equation 4.8	Regression equation generated for the MDT of DSPE-NLB.....	93
Equation 5.1	Water quantitation through oxidation of SO ₂ in Karl Fisher titration	103
Equation 6.1	Quantification of haemolytic activity of optimized CHO- and DSPE-NLB.....	144

LIST OF ABBREVIATIONS

17-AAG	17-allylamino-17-demethoxy geldanamycin
7-AAD	7-amino-actinomycin
ANOVA	Analysis of Variance
APC	allophycocyanin
Au	gold
BaP	benzo[a]pyrene
CCD	Central Composite Design
CHO	cholesterol
CHO-NLS	cholesterol-containing nano-liposomes
CHO-NLB	cholesterol-containing nano-lipobubbles
CHT	chitosan
CI	cell index/indices
CPNT	carboxylated polypyrrole carbon nanotube/s
CPT	camptothecin
CPNT	carboxylated polypyrrole carbon nanotubes
DDS	drug delivery system/s
DIE	drug incorporation efficiency
DMSO	dimethyl sulphoxide
DOS	dioctyl sulfosuccinate
DOX	doxorubicin
DSPC	distearoylphosphatidylcholine
DSPE/DSPE-m-PEG	distearoylphosphatidylethanolamine-methoxy-polyethylene glycol
DSPE-NLS	distearoylphosphatidylethanolamine-containing nano-liposomes
DSPE-NLB	distearoylphosphatidylethanolamine-containing nano-lipobubbles
ELISA	enzyme-linked immunosorbent assay
EOC	epithelial ovarian cancer
EpCAM	epithelial cell adhesion molecule
EPR	Enhanced Permeability and Retention
FBS	foetal bovine serum
FC-CCD	Face-Centered Central Composite Design
FDA	United States Food and Drug Administration
FHM	Film Hydration Method
FIGO	International Federation of Gynecology and Obstetrics
FITC	fluorescein isothiocyanate
FTIR	Fourier Transform Infra-Red

GMO	glycerol monooleate
HDM2	human double minute 2 (oncoprotein)
HER-2	human epidermal growth factor receptor-2
HSA	human serum albumin
Hsp90	heat shock protein 90
ITO	indium tin oxide
KF	Karl Fischer
LBL	layer-by-layer
MDT	mean dissolution time
MDR	multi drug resistance
MNP	magnetic nanoparticles
MRT	mean residence time
Nano-DDS	nano drug delivery system
NLB-DDS	nano-lipobubble drug delivery system/s
NCI	National Cancer Institute
NH ₄ Cl	ammonium chloride
NLB	nano-lipobubble/s
NLB-DDS	nano-lipobubble drug delivery system
NLS	nano-liposome/s
NSCLC	non-small cell lung cancer
Nutlin-PLGANP	nutlin-3a-containing PLGA nanoparticles
ORMOSIL	organically modified silica
PAA	poly(acrylic acid)
PACA	poly(alkyl cyanoacrylate)
PEG	poly(ethylene glycol)
P-gp	P-glycoprotein
PBS	phosphate buffered saline
PC	phosphatidylcholines
PdI	polydispersity index/indices
PE	phosphatidylethanolamine
PE ₂	R-phycoerythrin
PEC	polyelectrolyte complex
PEI	polyethyleneimine
PerCP	peridinin-chlorophyll proteins
PLA	poly(lactic acid)
PLGA	poly(lactic-co-glycolic acid)
PLGANP	poly(lactic-co-glycolic acid) nanoparticles
PLL	poly-L-lysine

PS	photosensitizer/s
PDT	photodynamic Therapy
PTX	paclitaxel
QD	quantum dots
RBC	red blood cells
RES	reticuloendothelial System
RPSE	Reverse Phase Solvent Evaporation Method
RSM	response surface methodology
RTCA	Real-Time Cell Analyzer
SB	silibinin
SEM	scanning electron microscopy
siRNA	small interfering ribonucleic acids
SPC	soybean phosphatidylcholine
SPION	superparamagnetic iron oxide nanoparticles
SRB	sulforhodamine B
SSM	sterically stabilized micelles
TEM	transmission electron microscopy
VEGF	vascular endothelial growth factor
VIP	vasoactive intestinal peptide

CHAPTER 1

AN OVERVIEW OF OVARIAN CANCER, RATIONALE AND MOTIVATION FOR THIS STUDY

"However far modern science and technics have fallen short of their inherent possibilities, they have taught mankind at least one lesson: Nothing is impossible!" – Lewis Mumford (1895-1990)

1.1 Introduction

Cancer has, for centuries, been the bane of the medical fraternity and the last century has seen an alarming rise in incidence of cancer globally, with over 12 million new cases of cancer being diagnosed annually (World Health Organization (WHO), 2013). Large financial aid has been dedicated to research in the field of cancer etiology, detection and treatment, but up to date, we remain at the losing end of the battle against cancer. Cancer is the second leading cause of death worldwide and accounted for 7.6 million deaths in 2008 (Jemal *et al.*, 2011; WHO, 2013). The burden of cancer in the African setting paints an increasingly dismal picture, with approximately 715 000 new cases of cancer diagnosed and 542 000 mortalities reported on the continent in 2008, against the backdrop of the financial burdens of this disease on the health systems of a developing continent (McCormack and Schüz, 2012). Figure 1.1 presents the global distribution of cancer incidence, highlighting the magnitude of cancer burden across different regions (GLOBOCAN, 2008). The WHO has projected cancer-related mortalities to rise to over 11 million by 2030 (WHO, 2013; Bray *et al.*, 2012; Cancer Research UK, 2013).

Cancer, as defined by the National Cancer Institute (NCI) in the United States, is an uncontrollable division and proliferation of abnormal cells and the invasion of these cells into surrounding tissue (NCI, 2012). This is a generic term and encompasses a multitude of malignancies that can affect numerous bodily systems (NCI, 2012). Carcinogenesis is a multistep process, involving a distorted expression of the transcriptional factors involved in cell replication (Ramasamy and Agarwal, 2008). The accumulation of sufficient alterations leads to mutations in the genes regulating cellular growth and differentiation and inhibit programmed cell death. Genetic alteration may also lead to the activation of oncogenes and deactivation of tumour suppressor genes (Macklin and Lowengrub, 2007). The cumulative effect is malignant transformation of cells, rapid growth and proliferation of these malignant cells, amplified angiogenesis, invasion into organs and body cavities and subsequent metastasis (Vogelstein and Kinzler, 2004).

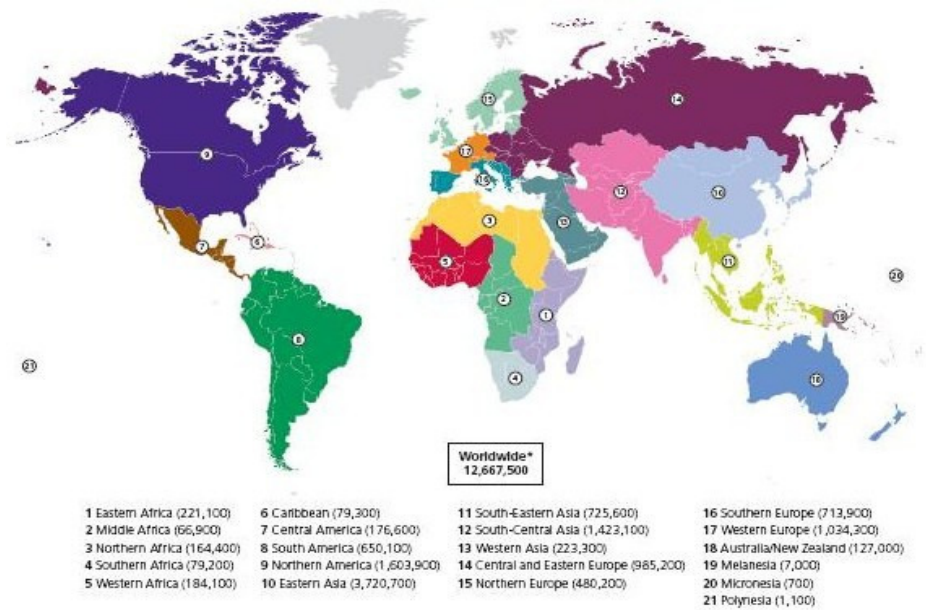


Figure 1.1 A comprehensive view of the estimated number of new cancer cases diagnosed worldwide in 2008 (Source: GLOBOCAN, 2008). *Region estimates do not do not add up to the world estimate due to calculation method.

Ovarian cancer is the most aggressive of, and the foremost cause of death from, all gynecological cancers (Chien *et al.*, 2007; Cirstoiu-Hapca *et al.*, 2010; Kim *et al.*, 2011). The primary factors contributing to the poor prognosis and high mortality rate associated with ovarian cancer is a combination of non-specific symptoms and a lack of early detection modalities, leading to advanced disease, and often significant metastasis, at time of diagnosis (Ferrandina *et al.*, 2006; Chien *et al.*, 2007; Cirstoiu-Hapca *et al.*, 2010; Kim *et al.*, 2011). In addition, ovarian cancer has also displayed a high degree of recurrence, leading to a deplorable overall 5-year survival rate of between 30%-45% (Spentzos *et al.*, 2004; Ferrandina *et al.*, 2006). Table 1.1 highlights the disparity between 5-year survival rates for ovarian cancer relative to that of other gynecological cancers and breast cancer.

Table 1.1 Comparison of approximate 5-year survival rates for breast and gynecological cancers, highlighting the poor outcome, and critical need, for improvement in the treatment of ovarian cancer (American Cancer Society, 2012; Cancer Research UK, 2013).

Cancer Type	5-year survival rate*
Breast	>80%
Uterine	69%
Cervical	67%
Ovarian	30-45%

*Age standardized, overall statistics (not tumour stage-specific)

Ovarian cancer can be classified as epithelial tumours, germ cell tumours, sex cord stromal tumours and tumours not otherwise specified, with over 90% of cases being of

epithelial origin (John Hopkins Pathology, 2001). A system of classification of epithelial ovarian carcinoma's (EOC's) as endorsed by the WHO, the International Federation of Gynecology and Obstetrics (FIGO) and the Society of Gynecologic Oncologists denotes the following subtypes based on histological presentations: (i) serous, (ii) mucinous, (iii) endometrioid, (iv) clear cell and (v) poorly differentiated tumours, as illustrated in Figure 1.2 (Modugno *et al.*, 2001; Cloven *et al.*, 2004; Nagle *et al.*, 2008, Köbel *et al.*, 2010; Su *et al.*, 2013). Furthermore, ovarian cancer is classified as either invasive or of low malignant potential (Modugno *et al.*, 2001).

Elucidating the subtype of ovarian cancer may have significance in determining appropriate chemotherapeutic regimens, since different subtypes have shown differing sensitivity to specific antineoplastic drugs. Clear cell carcinoma of the ovary has been found to have poor prognosis, in terms of initial response and overall 5-year survival rate, despite its earlier detection due to chemoresistance to platinum-based therapies, which are used as first-line agents (Fujiwara *et al.*, 2003; Itamochi *et al.*, 2008). Clear cell EOC did however display lower extreme drug resistance to the antineoplastic drug paclitaxel compared to the serous subtype (Cloven *et al.*, 2004). Hess and co-workers (2003) found a difference in response to first-line platinum based chemotherapy in patients with the mucinous subtype of ovarian cancer (Hess *et al.*, 2003). Investigations conducted by Cloven and team (2004) highlighted a significant resistance to the antineoplastic agent cisplatin by mucinous EOC's while the resistance to doxorubicin was lower for the mucinous subtype compared to serous EOC (Cloven *et al.*, 2004). However, these findings have not transcended into the clinical domain, where adjuvant chemotherapy selection is usually based on stage and grade of tumours as well as standardized drug-formulary based treatment regimens (Cloven *et al.*, 2004). Nevertheless, it facilitates our understanding of factors affecting treatment outcomes and may shape the direction of future therapy towards increasingly individualized therapy with greater effectiveness.

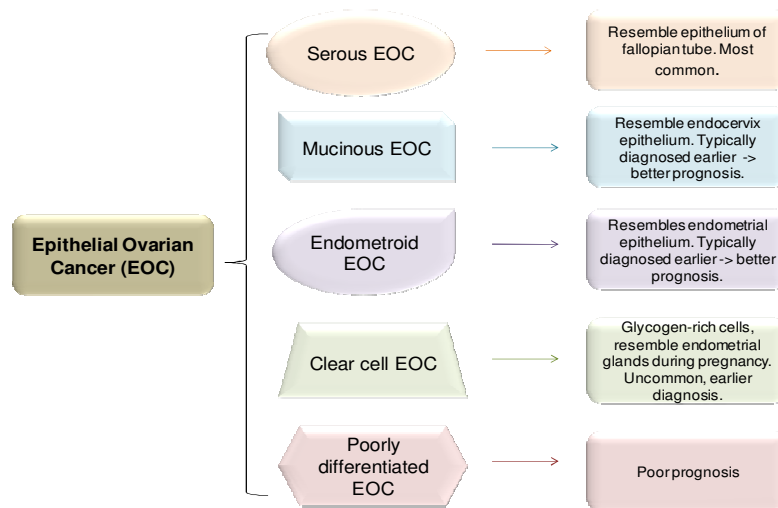


Figure 1.2 Brief histological classification of EOC and primary features of each subtype (Adapted from Cloven *et al.*, 2004).

Clinical observations have shown ovarian cancer to be particularly chemosensitive with 80% of patients responding to initial treatment (Chien *et al.*, 2007). However, the high incidence of recurrence also results in chemoresistant malignancies (Chien *et al.*, 2007). Despite a 70-80% response rate to initial therapy, ovarian cancer has exhibited a relapse rate of up to 75% in 18 to 28 months (Stuart, 2003). A case-controlled study conducted by Modugno and co-workers (2001) confirmed the role of nulliparity and a familial history of defects in the *BRCA1* and *BRCA2* genes in increasing the risk of developing ovarian cancer, while risk is lowered with each additional pregnancy, as well as with the use of oral contraceptives and tubal ligation (Modugno *et al.*, 2001; Sellers *et al.*, 2005). These findings were consistent with the results of other studies (Kurian *et al.*, 2005; Nagle *et al.*, 2008).

There is a strong trend of increasing risk of developing ovarian cancer as age progresses, with the median age of diagnosis approximating 60 years of age as indicated in Figure 1.3. Diagnosis in older women also occurs at a later stage of the disease, since these women are usually postmenopausal and hence, the symptoms of dysfunctional ovaries may be less distinct (Tew and Lichtman, 2008; O’Cearbhaill *et al.*, 2012). Equi-staged tumours are also associated with a poorer prognosis in older women compared to a younger population (Koroukian *et al.*, 2012). The aging global population indicates that the problem could become progressively distressing over time if a solution is not developed soon (O’Cearbhaill *et al.*, 2012).

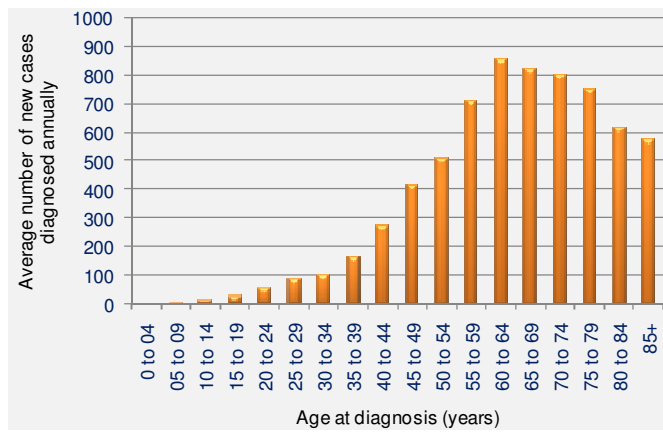


Figure 1.3 Age-specific incidence rates per 100 000 population in the UK, diagnosed annually between 2002 and 2006. Whilst the absolute values are specific to the UK region for a specified time period, the trend is globally representative. (Adapted from Cancer Research UK, 2013)

1.2 Detection and diagnosis of ovarian cancer: The initial problem

The lack of early detection mechanisms for ovarian cancer is perhaps the primary determinant of the poor therapeutic outcomes and overall 5-year survival rate associated with this condition. The intimate correlation between the stage of ovarian cancer at the time of diagnosis and the corresponding 5-year survival rates is widely documented and clearly illustrated in Figure 1.4 (Jacobs and Menon, 2004; Chu and Rubin, 2006; Köbel *et al.*, 2010; Bamias *et al.*, 2011; Rauh-Hain *et al.*, 2011; Maringe *et al.*, 2012).

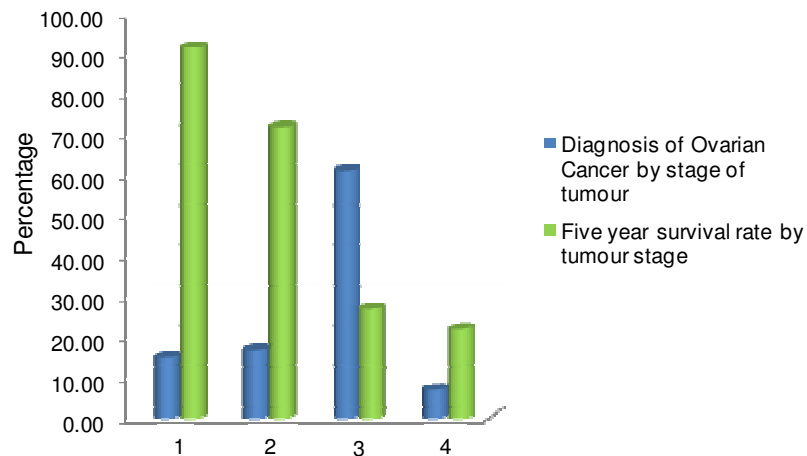


Figure 1.4 General trend in correlation of tumour stage at the time of diagnosis and the corresponding 5-year survival rate adapted from the latest statistics available from SEER for the USA (Howlader *et al.*, 2012). This trend is significant and representative of current global trends. 1) localized tumour; 2) Spread to regional lymph nodes; 3) Distant metastasis; 4) Unknown stage. The proportion of ovarian cancer diagnoses made after metastasis outside the peritoneal region is in stark contrast to the portion of early diagnoses. The radical decline in 5-year survival rate (expressed as a percentage) as tumour stage progresses, is distinct and accounts for the poor prognosis associated with this condition.

The obstacles in the development of screening tests for the early detection of ovarian cancer present feasibility challenges as well as economic challenges, complicated further by the experience of non-specific symptoms. Ovarian cancer lacks detectable histological

lesions which could be considered a precursor to tumour development and, as such, monitored regularly for early tumour detection (Jacobs and Menon, 2004; Chu and Rubin, 2006). Cancer biomarkers that have been identified are predominantly from patients with advanced disease, providing a questionable reference for early stage disease (Jacobs and Menon, 2004; Rauh-Hain *et al.*, 2011). The underlying molecular biology of ovarian cancer appears to differ between tumours that are detected early and have good treatment outcomes, and the more common late-stage tumours. Data highlighting these differences intimate that development of a screening test for early detection may not be successful in the detection of tumours with the later biological make-up, which is in fact the predominant form (Rauh-Hain *et al.*, 2011). There exists no conclusive evidence related to the time required for tumour development and progression. Hence, a suitable interval between screening tests will be difficult to ascertain. Moreover, prevalence of ovarian cancer in the general population is low (Rauh-Hain *et al.*, 2011). Determining the efficacy and applicability of developed screening tests will thus require a very large test population in order to obtain significant quantities of positive screening results, to be defined adequately sensitive and specific (Chu and Rubin, 2006).

1.3 Micro-environmental tumour physiology: Barrier and potential in drug delivery

The micro-environmental physiology of solid tumours has exhibited distinctions from normal healthy tissue which has complicated and compromised successful treatment, as illustrated in Figure 1.5. The significance of dissecting these differences became implicit in the 19th century when Steven Paget explicated his 'seed and soil' theory, which acknowledges the importance of tumour cells as well as the surrounding environment in the initiation and progression of cancer (Witz, 2009; Weber and Kuo, 2012). The foremost distinction exists between the vasculature of tumour tissue and the vasculature present in normal tissue. Tumoural blood vessels exhibit a higher proliferation rate with the resultant vasculature being convoluted with disorganized branching and structure, which creates inconsistency and unpredictability with regards to drug delivery and absorption through the tumour (Fukumura and Jain, 2007). Basement membrane formation is compromised, enlarged inter-endothelial junctions and an increase in vesicles, fenestrations and vesico-vacuolar channels collectively result in hyperpermeability of tumoural vasculature. Transport of macromolecules via these inter-endothelial spaces has been widely exploited as a passive targeting mechanism. Diffusion is considered the primary mechanism by which molecules extravasate into tumour tissue. The size, shape, surface charge and structural integrity of a molecule determines the diffusivity of the molecule, and hence the extent and efficiency of extravasation into tumour tissue. Tumoural interstitial pressure is significantly higher. This combined with the absence of a fully functional lymphatic system,

alters transport of molecules through tumour tissue and has consequently been widely cited to result in the accumulation of macromolecules within tumour tissue. Expansion of tumour mass with spatial confinement creates mechanical stress, which compresses the lymphatic vessels rendering them non-functional. Moreover, tumoural pH is inclined to a more acidic nature. Tissue hypoxia due to the rapid tumour growth and the insufficiency of tumour vasculature to sustain the oxygen requirements has been attributed to the lower pH of tumour tissue (Fukumura and Jain, 2007; Weber and Kuo, 2012). Tumour tissue also displays altered metabolic patterns, with glycolysis being the predominant mechanism of energy production. The ultimate production of hydrogen cations (H^+) in the glycolytic process contributes significantly to the lower tumoural pH (Ward *et al.*, 2013). This change in pH can alter the ionization characteristic of drug molecules, thereby affecting their solubility within tumour cells and absorption across membranes. The uptake of weak basic drugs such as doxorubicin is diminished by lower extracellular pH, hindering the efficacy thereof (Fukumura and Jian, 2007). The hypoxic and acidic environment impedes immunologic function and perpetuates metastasis and invasion (Macklin and Lowengrub, 2007).

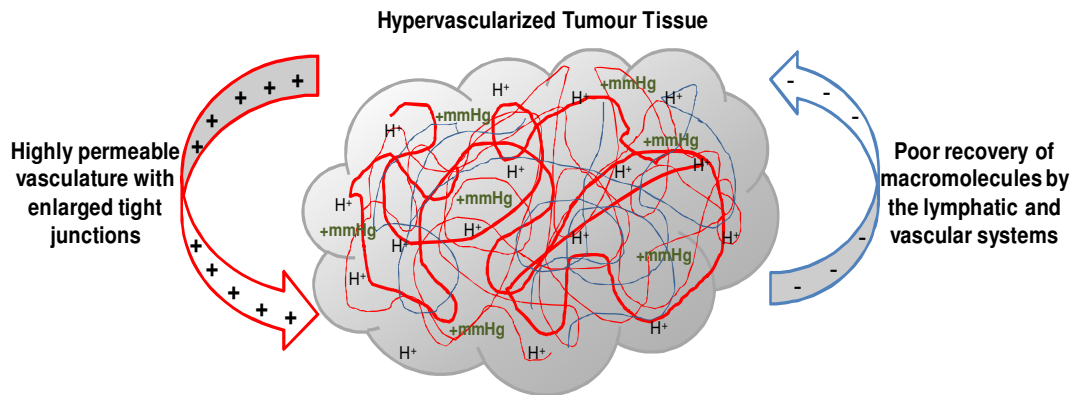


Figure 1.5 Visual illustration of the tumour micro-environmental factors influencing therapeutic efficacy.

1.4 Current treatment protocol for ovarian cancer

The current Gold Standard of treatment for ovarian cancer is surgical debriement followed by intravenously administered chemotherapy of a combination of paclitaxel and cisplatin or carboplatin (taxane/platinum compound combination) (Stuart, 2003; Spentzos *et al.*, 2004; Cirstoiu-Hapca *et al.*, 2010; Kim *et al.*, 2011; Chang *et al.*, 2012). However, many factors compromise the efficacy of available treatment for ovarian cancer. The strongly lipophilic nature of antineoplastic drugs complicates the formulation, administration and delivery of these drugs to target sites, which enhances the appeal of drug delivery vehicles. Paclitaxel, one of the first line drugs in the treatment of ovarian cancer requires solubilization by Cremophor EL, a vehicle that has displayed intense side-

effects such as acute hypersensitivity reactions, hyperlipidaemia and peripheral neuropathy at the high doses required for antineoplastic therapy, which compromises its clinical usefulness (Gelderblom *et al.*, 2001; Cirstoiu-Hapca *et al.*, 2010).

Antineoplastic drugs also exhibit limited specificity for tumour tissue, and a tendency to act indiscriminately, particularly on rapidly dividing tissue. This indiscriminate activity results in deleterious, dose-limiting and often life-threatening side-effects, such as cardiovascular complications, severe myelosuppression, compromised immunity, altered gastric function, myalgia and neurotoxicity, among others (Vauthier *et al.*, 2003; Cho *et al.*, 2007; Cirstoiu-Hapca *et al.*, 2010; Mohanty and Sahoo, 2010; Guo *et al.*, 2011; Shapira *et al.*, 2011). Cisplatin, the other first line agent used in the treatment of ovarian cancer, is associated with severe dose-limiting side-effects, the foremost being nephrotoxicity which has limited the use of cisplatin in 25-30% of patients (Chirino and Pedraza-Chaverri, 2009; Rjiba-Touati *et al.*, 2013). Approaches to alleviate or limit nephrotoxicity commonly involve the administration of rehydration fluids and diuretics in order to decrease renal accumulation of cisplatin. The concomitant administration of compounds with various functionalities, such as antioxidants, nitric oxide modulators and anti-apoptotic drugs have been investigated to reduce cisplatin-induced nephrotoxicity (Rjiba-Touati *et al.*, 2013). Cisplatin demonstrates significant (<90%) protein binding with an initial plasma half-life shorter than 1 hour (Chirino and Pedraza-Chaverri, 2009).

Antineoplastic drugs are known to have a substantially narrow therapeutic window (Cai *et al.*, 2011). Maintaining drug concentrations within the therapeutic window is particularly challenging. Specificity for cancer cells will therefore be a principal criterion in determining the success of new cancer therapies.

1.5 Statement of the problem

The poor aqueous solubility of antineoplastic drugs poses an initial formulation challenge. The intravenous route of administration remains the most feasible route of administration of antineoplastic chemotherapy due the patient acceptance, limited patient involvement such as that requiring the consumption of oral medication regimens, ease of administration and reduced risk of infection (as associated with the insertion of administration ports). Formulation of strongly lipophilic antineoplastic drugs as an intravenous preparation is significantly challenging, necessitating the use of a delivery vehicles, the shortfalls of which are explicated in Section 1.6. Various attempts to develop more hydrophilic derivatives usually resulted in a decrease in cytotoxic efficacy.

The unfavorable biodistribution of antineoplastic agents remains one of the most significant drawbacks of chemotherapy. Firstly, the critical side-effects resulting from activity at inappropriate target sites are dose-limiting and hence, can compromise successful therapeutic outcomes. Myelosuppression in particular can result in prolongation of intervals between cyclical drug administration's allowing cancer cells to replicate and perhaps develop mechanisms of resistance. Other severe toxicities such as cardiotoxicity, neurotoxicity and nephrotoxicity may be fatal. The significance of severe gastrointestinal maladies should not be underestimated, as the patients' nutritional status and electrolyte balance may be severely compromised. Secondly, unfavorable biodistribution of antineoplastic drugs reduces the concentration of drug available at the site of action to exert the desirable antineoplastic effect.

The antineoplastic drug camptothecin (CPT) has exhibited tremendous cytotoxic activity against a wide range of tumours. However, pharmaceutical development and clinical application of this potent drug has been severely hampered due to the poor aqueous solubility and deleterious side-effect profile of CPT, as well as conversion to a significantly less biologically active carboxylate form under physiological conditions. Furthermore, the high affinity of the carboxylate form of CPT for human serum albumin (HSA) unfavorably drives the equilibrium from the active lactone form to the inactive carboxylate form.

1.6 Approach to the problem

This study proposes the development of a novel intravenously administered nano-lipobubble drug delivery system (NLB-DDS) containing the antineoplastic drug CPT, with a size range below 200 nm. The shell of the NLB will be comprised of lipids, enabling the solubilization of the lipophilic model drug. A gaseous core will be introduced to impart bubble characteristics to the DDS. Polymeric coating of the NLB's will further be employed to prolong drug release.

Formulation as a nano-DDS allows for enhanced solubilization of the strongly lipophilic drug. This is further augmented by the presence of a lipoidal NLB shell. The use of phospholipids for the NLB shell, which are characterized by a polar head region as well as a non-polar tail region, facilitates incorporation of the lipophilic drug, whilst conferring aqueous compatibility characteristics on the formulation. This enables intravenous administration, barring the use of a delivery vehicle. The nano-scale size range (<200 nm) also has applicability to passive targeting in tumour tissue by the Enhanced Permeability and Retention (EPR) phenomenon, which favorably alters the biodistribution of antineoplastic drugs. The circulation half-life of nano-DDS is superior to micro-DDS due to evasion of the reticulo-endothelial system (RES).

The incorporation of CPT within the NLB has a dual function. Firstly, the physiologically labile drug, CPT, is protected from the unfavorable physiological environment prior to reaching the target tissue. Conversion to the inactive carboxylate form and subsequent association with HSA is thus prevented. Secondly, retardation of drug release from the NLB allows for adequate accumulation of the DDS within the target tumour tissue before significant drug is released in the systemic circulation. Combined with the passive targeting characteristics, prolonged drug release has the potential to tremendously improve the side-effect profile associated with CPT and other antineoplastic drugs. The favorably revised CPT biodistribution further results in higher concentration of drug within tumour tissue and significantly enhanced therapeutic effect.

1.7 Rationale and Motivation for the study

Angiogenesis occurs at a considerably elevated rate in tumour tissue compared to normal tissue (Rapoport, 2007). The tight junctions that are present in normal endothelial cells are in the region of 7 nm, while the tight junctions present in tumour tissue can manifest as large as 400 nm. Formulation of the proposed nano-DDS with a size range below 200 nm will allow passive targeting of the DDS to the tumour site and extravasation through the leaky vasculature (Gao *et al.*, 2007; Rapoport, 2007; Abu-Lila *et al.*, 2009). Figure 1.6 demonstrates the preferential accumulation of the intended NLB-DDS at the tumour site. NLB behave as macromolecules *in vivo* and their uptake by the lymphatic system in tumour tissue is impaired. Following intravenous infusion of NLB, distribution throughout the systemic circulation will be minimized due to the passively targeted nature of the NLB on account of the EPR phenomenon, as discussed in greater detail in Chapter 2. Diffusion of the gaseous core out of the NLB over time will result in drug release through NLB cavitation.

The advantages of passive tumour targeting are several-fold. Tumour targeting will enable the attainment of augmented levels of CPT at the tumour site by favorably altering biodistribution of the drug following intravenous administration, whilst preserving the state of healthy tissue. Hence, anti-tumour efficacy will be substantially increased while the side-effects associated with conventional chemotherapy will be dramatically reduced. Furthermore, the existence and concurrent treatment of co-morbidities will pose less of a challenge in the realm of cancer treatment due to site-specific release of chemotherapeutic drugs, which will minimize drug-disease and drug-drug interactions with co-existing morbidities and their treatment.

Poor aqueous solubility is an inherent characteristic of most antineoplastic drugs. The utilization of solubilizing agents has proven useful to a certain degree however these reagents demonstrate their own shortfalls such as side-effects and toxicity (Rapoport, 2007). Formulation as nanosystems has resulted in improved solubilization, and subsequently enhanced absorption, of these drugs due to the high surface area:volume ratio afforded by the size and architecture of the nano-DDS's as well as the presence of the lipid component in the proposed NLB formulation, which facilitates incorporation and solubilization of lipophilic drugs (Tirelli, 2006). NLB thus have the potential to enhance the bioavailability of antineoplastic drugs.

Studies undertaken by Abu-Lila and co-workers (2009) highlighted the functionality of liposomes to deliver low molecular weight chemotherapeutic drugs to solid tumour sites by alteration of the biodistribution of these antineoplastic drugs (Abu-Lila *et al.*, 2009). However, liposomes do not display significant stability and their size range often includes a large proportion of micron-sized particles. In addition, preparation steps have to be carefully controlled in order to achieve reproducibility in terms of size and entrapment efficiency (Koo *et al.*, 2005). Since these factors could compromise the use of liposomes in intravenous drug delivery due to risks such as embolism and treatment failure due to instability, approaches will be instituted for stability enhancement, size control and improvement of drug loading. The employment of polymeric materials in combination with the liposomal structure for the NLB formulation will be instituted.

The high cost of antineoplastic drugs and the rising incidence of malignancies will undoubtedly place a burden on the healthcare system, which most developing countries cannot afford. Enhanced drug efficacy will significantly reduce the quantity of antineoplastic drug required to eliminate tumour cells, thus allowing for a reduction in cost. Targeted therapy that displays increased mean residence time (MRT) in tumour tissue, will allow for reduced frequency and duration of therapy, which will provide psychological and physiological benefits for the patient.

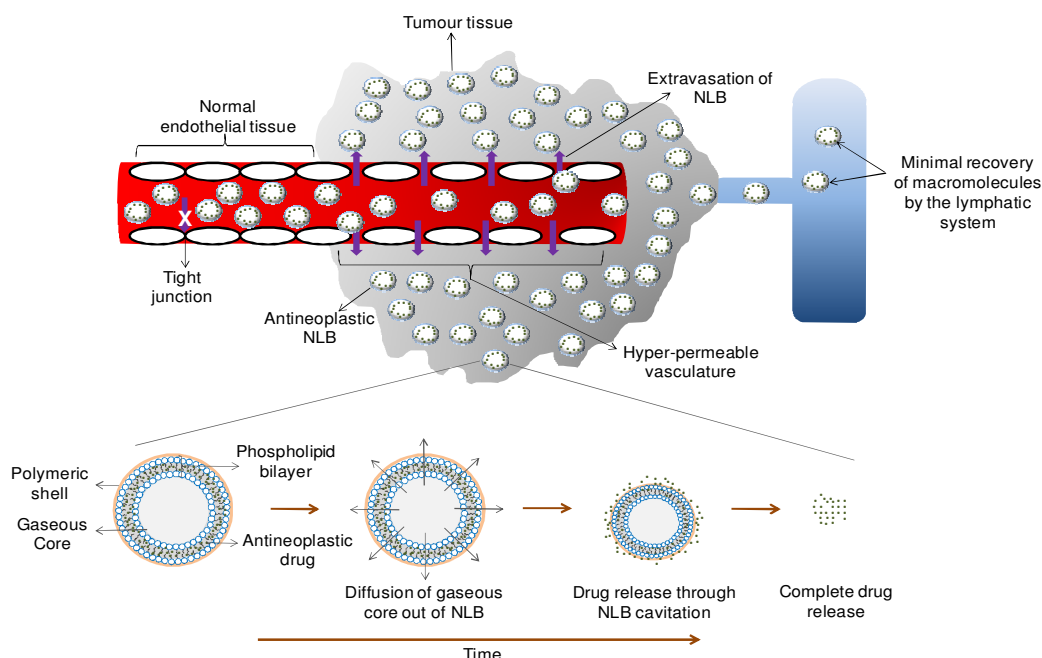


Figure 1.6 Schematic illustration of the components of the NLB-DDS, the passive targeting, extravasation and resultant accumulation of the NLB-DDS within tumour tissue and the mechanism of antineoplastic drug release from the NLB.

1.8 Aim and Objectives of this study

The aim of this study was to design, optimize and characterize a camptothecin-loaded NLB-DDS exhibiting passive targeting to tumour tissue following intravenous administration. The passively targeted nature of the DDS will result from capitalization, by the nano-scale dimensions of the DDS, on the EPR phenomenon displayed by tumour tissue, thereby leading to concentrated release of drug at, and accumulation within, tumour tissue, enhancing antineoplastic efficacy and significantly reducing side-effects. Polymeric coating was instituted to retard drug release in the systemic circulation prior to reaching the tumour site, thereby altering the unfavorable biodistribution responsible for the devastating side-effects which have compromised the clinical use of CPT. The proposed DDS is intended to drastically improve the therapeutic outcome of ovarian cancer therapy, shorten duration of therapy, improve the health-related quality of life of the patient during therapy and increase the overall 5-year survival rate.

In order to achieve these aims the following objectives were identified:

1. To gain a thorough understanding of the pathophysiology of the disease state and considerations for effective drug delivery.
2. To review the current research ideologies and systems intended to improve treatment of ovarian cancer, from a novel drug delivery perspective.
3. To investigate formulation methods of NLB preparation and identify a single effective and industrially viable method to be employed.

4. To conduct extensive preformulation studies on various biocompatible and biodegradable formulatory components and delineate independent variables, and the minima and maxima thereof, for successful NLB formulation.
5. To experimentally synthesize variants of NLB formulations according to an appropriate experimental design followed by a systematic physicochemical and physicommechanical analysis of the variants.
6. To statistically optimize formulation parameters for the synthesis of CPT-loaded, passively targeted NLB.
7. To elucidate the physicochemical and physicommechanical dynamics of the optimized NLB formulation.
8. To investigate the potential and feasibility of phytochemical incorporation into the NLB formulation, as well as, polymer coating of the NLB-DDS and the influence thereof on the physicochemical and physicommechanical properties of the formulation.
9. To undertake *ex vivo* studies on a human ovarian cancer cell line to determine the uptake, efficacy and safety of the NLB-DDS.

1.9 Novelty of this study

Nanobubbles have been extensively investigated for their tumour imaging potential as a result of their inherent echogenicity. In addition, the use of ultrasound in conjunction with nanobubbles has displayed potential for combined imaging and destruction of tumour tissue (i.e. therapy). This study aims to extend this paradigm to antineoplastic therapeutics by loading NLB with an antineoplastic agent. These NLB will be passively targeted to tumour tissue, thereby favorably altering the biodistribution, and hence the efficacy and side-effect profile, of the antineoplastic agent. The incorporation of a phytochemical with anti-tumour activity will be explored to attain synergistic therapeutic activity.

1.10 Overview of this dissertation

Chapter 1 of this dissertation provides a concise introduction into ovarian cancer as a disease state. Furthermore, this chapter provides a detailed description of the intended nano-DDS and rationalizes the undertaking of this study by outlining the challenges in current clinical therapy that can potentially be overcome by the development of this nano-enabled DDS. A diagrammatic illustration of the NLB-DDS is provided to better demonstrate the mechanism of passive targeting and drug release. The aim, and the objectives outlined to achieve this aim are presented herein.

Chapter 2 focuses on the potential and current application of nanotechnology to imaging, detection, diagnosis and treatment of various tumours, with particular reference to ovarian cancer. The potential of nanotechnological approaches in addressing the shortfalls of

several antineoplastic compounds is explored, corroborated by research data from particular studies, further highlighting the vast potential of nanotechnology in reducing the burden attached to this morbidity. A brief insight on currently available and pre-clinical nanosystems is provided to demonstrate the clinical relevance of nanomedicine research.

Chapter 3 delves into the rational selection of formulation materials for preliminary investigation as well as the step-wise approach adopted in the ultimate formulation of the NLB-DDS. The investigations involved in the delineation of a single, effective method of nano-liposomal preparation are expounded. In addition, the preformulation studies undertaken in the identification of key formulation variables affecting the size, zeta potential and efficiency of drug incorporation of the nano-liposomes will be explicated.

Chapter 4 explores the generation of a Face-Centered Central Composite Design for each of the two lipid combinations delineated from preformulation studies described in Chapter 3, to strategically elucidate the effect of independent variables on measured response parameters. In addition, this chapter expounds the selection of relevant measured responses and the effects of independent variables on these measured responses. Finally, the optimal formulation parameters with respect to the desired measured responses are described.

Chapter 5 presents the measured responses of candidate formulations predicted through statistical optimization whilst providing a comparison to the results derived experimentally. Conversion of nano-liposomes to NLB is described, as well as modifications of formulated NLB in the form of phytochemical incorporation and polymeric coating. Physicochemical and physicomechanical characterization of the formulated NLB formulations is explored to determine the feasibility of the modifications undertaken as well as generate a tangible evaluation of the formulation in relation to the aim of the study.

Chapter 6 explores the undertaking of *ex vivo* analyses on a human epithelial ovarian cancer cell line and blood products. Cellular uptake, the degree of cytotoxicity and the hemolytic activity of formulated DDS is evaluated through qualitative and quantitative investigations.

Chapter 7 highlights the conclusions of this study and the recommendations for future work in this potentially revolutionary research area.

CHAPTER 2

INNOVATIVE NANOTECHNOLOGICAL APPROACHES TO THE DETECTION AND TREATMENT OF OVARIAN AND OTHER SOLID TUMOURS

2.1 Introduction

Nanomedicine refers to research into and development of technologies, devices and drug delivery systems for prevention, diagnosis and treatment of disease at the nano-scale (Khosravi-Darani *et al.*, 2007, Rai *et al.*, 2010). Strictly speaking, nanostructures are defined as varying geometrical configurations with at least one dimension in the range of 10-100 nm. However, nanostructures up to 250 nm have found applicability in the medical setting by the Enhanced Permeability and Retention (EPR) effect, active targeting, enhanced residence time and increased cellular uptake (Bawarski *et al.*, 2008; Bawa *et al.*, 2012; Etheridge *et al.*, 2013). Nanosystems combine the fields of medicine, chemistry, pharmacology, biology, mathematics and engineering to provide unique properties that are yet to be fully explored (Farokhzad and Langer, 2006; Rai *et al.*, 2010). Nanosystems with biomedical application are currently a highly researched field and have exhibited immense potential, particularly in the diagnostic, imaging and therapeutic domains (Dominguez and Lustgarten, 2010). Numerous benefits of nanosystems are related to the augmented surface area:volume ratio, which has the potential to favorably influence the solubility, bioavailability, pharmacokinetic and biodistribution profile of drugs, as well as, their inclination toward modification and functionalization (Khosravi-Darani *et al.*, 2007; Chen *et al.*, 2011; Vizirianakis, 2011, Ji *et al.*, 2012). Nanomaterials have been shown to exhibit properties vastly different from the bulk material from which they are synthesized (Chen *et al.*, 2010(a); Chen *et al.*, 2011). In addition, the vast array of structural arrangements make nanosystems incredibly versatile, while their minute dimensions often belie an astonishing robustness. These devices offer the unequivocal advantage of interacting with cells, biological processes and other targets at a molecular level, allowing for inter- and intra-cellular manipulation and monitoring, the benefits of which are beyond our full comprehension at this point. The continued development of novel nanosystems is expected to have extensive applicability at all levels of healthcare, including disease initiation, progression, treatment and monitoring.

Nanosystems are envisaged to:

- Enable superior detection of molecular changes that precede pathogenesis, thereby enabling early detection, pro-active treatment and monitoring as well as expanding the knowledge base on mechanisms of disease progression.

- Enhance selectivity and sensitivity for pathological states to advance disease diagnosis and imaging.
- Transform drug delivery and therapy by capitalizing on the unique properties of the nano-scale size range.
- Effectively combine diagnostic, therapeutic and efficacy monitoring applications in a multi-functional nanosystem.
- Contribute to, and perhaps transform, scientific approaches to all of the above as well as the processes involved in drug discovery, purification and modification (Farokhzad and Langer, 2006).

Research and development into nanosystems applicable to cancer diagnosis, imaging and therapy has emerged as one of the largest fields in nanomedicine (Etheridge *et al.*, 2013). The substantial burden of cancer on the global population and the indiscriminate nature of the condition underscores the considerable interest of governmental, industrial, healthcare and academic entities in exploring and developing the applicability of this technology to the oncology field. This chapter aims to discuss the exciting role and immense potential of nanotechnology in the diagnosis, imaging and treatment of solid tumours, with particular focus on ovarian cancer as a backdrop to the study undertaken. For the purpose of this dissertation the terms nanosystem and nano-enabled drug delivery system shall be used interchangeably and will encompass nanoparticles, micelles, liposomes, quantum dots, nanotubes and all other drug delivery and imaging systems where at least one dimension is of the nano-scale.

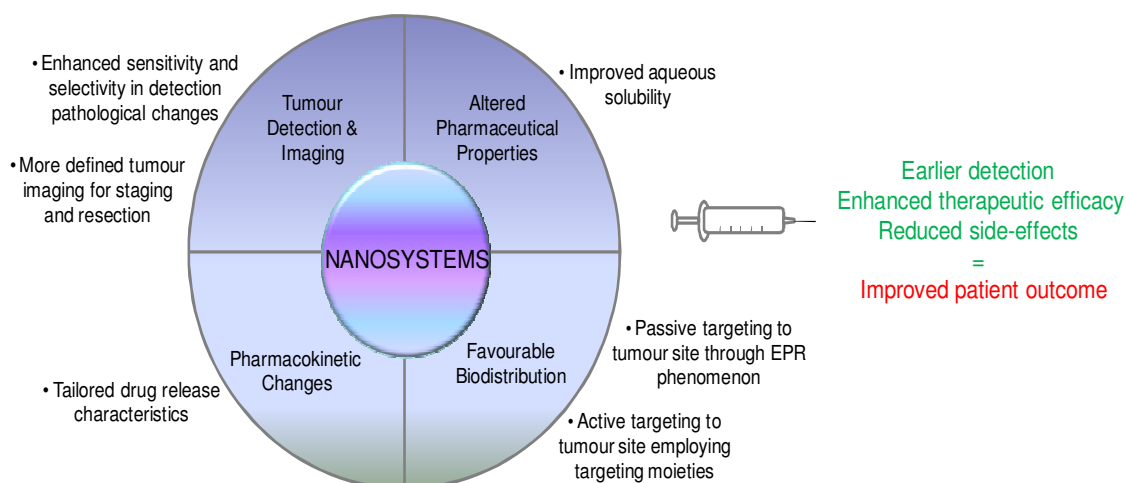


Figure 2.2 Illustrative summary of the potential benefits that nanosystems may offer with regards to tumour diagnosis and treatment.

2.2 Application of nanotechnology in tumour diagnostics and imaging

Early diagnosis and precise imaging of carcinogenesis is critical to successful therapeutic outcomes. However, highly sensitive and specific technologies are required to detect slight biological changes that may characterize early stage disease, as well as to accurately classify the stage and dissemination of tumours. One of the major setbacks in the early detection of ovarian cancer is lack of suitable detection technologies and imaging techniques. Accurate imaging techniques will assist in the early diagnosis of ovarian cancer, accurate staging of the tumour as well as monitoring the efficacy of treatment and early determination of resistance to therapy being used. Recurrence is an enormous problem in ovarian cancer, resulting in atrocious 5-year survival rates, as well as the emergence of resistance to antineoplastic drugs. However, when ovarian cancer is diagnosed in the early stages (when it is confined to the ovary), the 5-year survival rate is approximately 90% (Fishman *et al.*, 2005).

Current systems employed in the detection of tumour cells or cancer biomarkers include surface plasmon resonance, nuclear magnetic resonance, quartz crystal microbalance resonators and polymerase chain reaction, amongst others, which require augmentation of the signal, the expression of fluorescent protein biomarkers and antibodies in the cell or the enhancement of target cells in the sample (Wu *et al.*, 2010). Transvaginal sonography is currently the imaging modality utilized in the imaging detection of ovarian cancer (Fishman *et al.*, 2005; Kim *et al.*, 2011). However, views on the sensitivity and accuracy of this technique in the detection of early stage ovarian cancer have been incongruent (Fishman *et al.*, 2005). In view of this, a detection system that is minimally invasive, sensitive and does not require augmentation or labeling of the sample would be highly beneficial (Wu *et al.*, 2010). Nano-scale detection and imaging devices have the capacity to demonstrate substantial sensitivity and specificity, which could revolutionize the clinical course of cancers. The nano-scale offers the advantage of interacting and detecting changes at intra- and intercellular levels and is thus unsurpassed in analyzing most biological moieties such as cells, viruses, proteins and nucleic acids (Chen *et al.*, 2011).

2.2.1 Biosensors in cancer detection

Biosensors consist of a bioreceptor that interacts with specific analytes within the body, producing a change which is detectable through conversion by a transducer (constituent of biosensor) to a measurable signal (Vo-Dinh *et al.*, 2001). Figure 2.2 outlines the interactions that are responsible for changes that occur and the types of signals that are measured after transduction.

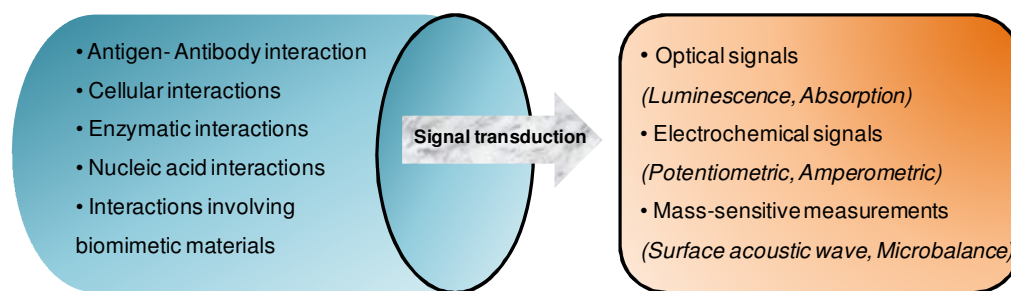


Figure 2.2 Illustrative representation of the various types of interactions between bioreceptors and analytes, as well as the measurable signals that are produced.

Nanofibers have been applied to the field of biosensors, coining the term nano-biosensors (Vo-Dinh *et al.*, 2001). The initial application of nanofibers to biosensors was an antibody-based system for the detection of benzo[a] pyrene tetrol in the body, which indicates exposure to benzo[a]pyrene (BaP) (Vo-Dinh *et al.*, 2001). BaP, a common environmental pollutant, as well as a component of tobacco smoke, is a known human carcinogen (Vo-Dinh *et al.*, 2001; Wu *et al.*, 2010). Early detection of exposure to BaP could have remarkable implications in the detection and treatment of, particularly, lung cancer, which is a leading cause of cancer death worldwide (Wu *et al.*, 2010).

Wu and colleagues (2010) combined biocompatible and biodegradable poly(lactic acid) (PLA) nanofibers with gold (Au) nanoparticles, which have been applied extensively in the field of biosensors, to form nanocomposites (Wu *et al.*, 2010). These nanocomposites were subsequently used on modified indium tin oxide (ITO) electrodes and investigated for their ability to detect drug-sensitive and drug-resistant leukemia cells. These Au/PLA nanocomposite modified ITO electrodes exhibited promising sensitivity in detection of the leukemia cells as well as differentiating between the cell types (Wu *et al.*, 2010). This nano-biosensor has potential for the rapid and early detection of cancer cells, which will be of considerable value in clinical practice.

Angiogenesis (the development of new blood vessels in the human body) is essential to the growth and preservation of living tissue (Kwon *et al.*, 2010). However, this process occurs at an elevated rate in tumour tissue and is related to proliferation and metastasis of cancer cells (Kwon *et al.*, 2010). Vascular endothelial growth factor (VEGF) is a potent pro-angiogenic agent, pivotal to the angiogenic process and thus an attractive target for cancer therapy as well as a useful means for early cancer detection (Kwon *et al.*, 2010). Current methods for the detection and quantification of VEGF include enzyme-linked immunosorbent assay (ELISA), VEGF receptors and field-effect transistor biosensors (Kwon *et al.*, 2010). There, however, exists a room for improvement in the sensitivity and ease of use of these tests. To this end, Kwon and fellow researchers (2010) combined conducting polymer (polypyrrole) nanotubes with aptamers (nanosize molecules with a

great degree of sensitivity and specificity for target molecules) bonded to the nanotubes, in a modified biosensor for the detection of VEGF (Kwon *et al.*, 2010). Two carboxylated polypyrrole carbon nanotubes (CPNT) were synthesized (CPNT 1=190-220 nm; CPNT 2=100-130 nm), attached to biosensors and evaluated. Although both CPNT's displayed a high degree of sensitivity in detecting VEGF, CPNT 2 exhibited approximately two-fold higher sensitivity, highlighting the significance of size in this detection method. The increased sensitivity of the transducer with CPNT 2 was attributed to increased conductivity as a result of the augmented surface area exposed in CPNT 2, a consequence of the smaller dimensions (Kwon *et al.*, 2010). The presence of aptamer on CPNT 2 produced superior sensitivity compared to non-aptamer based biosensors and the larger size of CPNT 1 (Kwon *et al.*, 2010). In addition, the rapid real time detection adds another favorable dimension to this system, since biological events detected can be converted directly into a measurable signal and no labeling of samples is required (Kwon *et al.*, 2010; Chen *et al.*, 2011). Kwon and team (2010) were successful in detecting previously unprecedented low levels of VEGF, which could have enormous implications for the early detection of several cancers. Furthermore, the modified biosensor system developed is reusable, enhancing the practicality and attractiveness of this detection device (Kwon *et al.*, 2010).

Telomerase is regarded as a general biomarker for cancer due to a significant up-regulation (85-90%) in its expression in human tumour cells. The detection of this biomarker, thus, has enormous potential in early cancer detection, as well as monitoring the efficacy of chemotherapeutic interventions (Zheng and Li, 2010). Telomerase is located in trace amounts within cell nuclei, therefore the ideal detection of telomerase will involve ultrasensitive single cell analysis of living cells. Nanofiber biosensors conjugated with anti-telomerase antibody are capable of intracellular detection of telomerase on account of its size and direct interaction between conjugated anti-telomerase and telomerase by penetration of the cell nucleus (Zheng and Li, 2010). The significance of the nanoscale was once again highlighted in this study, whereby detection of telomerase was attempted by employing the cytoplasm of cancer cells. There was no significant detection of telomerase, emphasizing the importance of nucleus penetration for telomerase detection (Zheng and Li, 2010). This would be impossible with larger devices. Furthermore, fluorescence was significantly reduced when cells expressing low levels of telomerase were assayed. The nanofiber biosensor is thus able to differentiate normal cells from telomerase over-expressing cancer cells, making telomerase detection by nanosystems a superior detection technique.

2.2.2 Quantum dots for tumour detection and imaging

Quantum dots (QD) are semiconductor, fluorescent nanocrystals that have received considerable attention in the biomedical field, particularly for their potential as imaging agents (Geszke *et al.*, 2001; Schroeder *et al.*, 2007; Pan and Feng, 2009). The advantages of quantum dots over the conventional dyes employed for imaging include:

- The spectrum of emission can be altered by changes in the size and composition of QD (Geszke *et al.*, 2001; Schroeder *et al.*, 2007; Pan and Feng, 2009).
- QD exhibit a high quantum yield of fluorescence and superior brightness (Geszke *et al.*, 2001; Pan and Feng, 2009; Papagiannaros *et al.*, 2009).
- A high degree of photostability and resistance to photobleaching (Geszke *et al.*, 2001; Schroeder *et al.*, 2007; Pan and Feng, 2009; Papagiannaros *et al.*, 2009).
- A broader spectrum of excitation (Pan and Feng, 2009).
- More rapid imaging (Papagiannaros *et al.*, 2009).

However, use has been restricted as a consequence of toxicity from semiconductor QD (particularly cadmium based QD) and inadequate *in vivo* and physical stability profiles, partly due to their hydrophobic nature (Geszke *et al.*, 2001; Pan and Feng, 2009; Setua *et al.*, 2010). Modifications to QD have therefore been attempted in the form of surface coating and entrapping QD in water soluble nanoparticles and lipid micelles (Geszke *et al.*, 2011). These methods have shown potential in increasing the stability of QD as well as improving the biocompatibility, biodistribution and reducing toxicity (Pan and Feng, 2009). As outlined with previously discussed nanosystems, biocompatible and stable QD can then be functionalized for selectivity and site-specific targeting (Chin *et al.*, 2010). This will prove beneficial in the early detection and diagnosis of cancer, which forms the basis of successful therapeutic interventions. Furthermore, QD have shown promise in the detection of sentinel lymph nodes, which is exceptionally beneficial in rapidly metastasizing cancers, such as ovarian cancer.

Encapsulation of QD in lipid micelles has been investigated as a means of addressing the drawback of instability, as well as investigating the efficacy of targeting, by further functionalization of these micelles (Schroeder *et al.*, 2007). The aforementioned preparation formulated by Schroeder and co-workers (2007) proved non-toxic to cells when compared to cells incubated in the absence of the formulation and cells that were incubated with a non-targeted formulation, as well as highly selective for target cells (80-90%) (Schroeder *et al.*, 2007). As a practical consideration, entrapped quantum dots displayed impressive stability over a prolonged period of time with preservation of fluorescent capacity, making them viable for clinical use. Analysis of pegylated lipid

micelles entrapping quantum dots one year after preparation by Schroeder and co-workers (2007), displayed no difference in structure, optical properties and physical stability (aggregation or precipitation) (Schroeder *et al.*, 2007). This favorable stability profile was demonstrated in other studies for variable periods (3 months) (Papagiannaros *et al.*, 2009). Differing results on fluorescence intensity was reported by Schroeder and team (2007) and Papagiannaros and team (2009) after encapsulation of QD in micelles (Schroeder *et al.*, 2007; Papagiannaros *et al.*, 2009). The first group observed a decrease in fluorescence intensity of encapsulated QD compared to single QD, which was attributed to a quenching effect by adjacent QD. However, the stability of the formulation acted to counter this effect and ultimately the fluorescent capacity was sufficient for the intended *in vivo* application (Schroeder *et al.*, 2007). In contrast, the second group reported a greater intensity in fluorescence of QD-encapsulating-micelles (Papagiannaros *et al.*, 2009). Despite this disparity, both research groups demonstrated clear and precise tumour imaging. Hence the systems described by Schroeder and co-workers (2007) and Papagiannaros and co-workers (2009) addressed many of the *in vivo* shortfalls established by previous work on QD and served to further highlight the feasibility of this nanosystem in the domain of cancer detection and imaging.

The nanoscale of QD is essential to the imaging function, since it affects biodistribution. Larger QD may be confined to the blood vessels, thereby producing diffuse fluorescence and poorly differentiated tumour tissue and organs. By contrast, the nano-size will allow extravasation from blood vessels and accumulation of the QD in tumour tissue, resulting in clearly contrasted and delineated tumoural images, with high intensity fluorescence and reduced background noise (Papagiannaros *et al.*, 2009). Furthermore, differential QD accumulation in organs has the potential to highlight distant metastasis.

In the domain of cancer, imaging techniques are utilized to stage tumours as well as to aid surgeons undertaking cytoreductive surgery. For this application, emission spectra should be between 400-650 nm to enable visibility without the use of specialized equipment (Chin *et al.*, 2010). Currently, imaging in the near infra-red region is widely used as it is a minimally invasive process that enables clear, detailed imaging at a molecular level (Papagiannaros *et al.*, 2009). This technique has been applied in tumour imaging, as well as mapping of tumour biomarkers, and sentinel lymph nodes as an aid in surgical resection. Furthermore, this technique has been utilized to monitor the response of tumours to chemotherapy. However, tissue penetration is limited (Papagiannaros *et al.*, 2009). The emission spectrum of nanosystems such as QD can be tailored for specific applications. However, the imaging of tumours and metastatic tissue requires sufficient tissue penetration, which usually occurs at emission wavelengths that are out of the

visible spectrum. Therefore modifications are required to satisfy the two requirements pivotal to successful tumour and metastatic tissue imaging.

Multispectral imaging is an emerging technique that involves the splitting of signals for the detection of different moieties by a single excitation (Chin *et al.*, 2010). This will allow simultaneous superficial as well as deep tissue imaging, while minimizing the photo-damage of surrounding tissue (Chin *et al.*, 2010; Geszke *et al.*, 2011). Indium phosphide/zinc sulphide QD have been formulated with an exciton emission and a defect emission which allows for simultaneous superficial imaging and deep tissue penetration (Chin *et al.*, 2010).

2.3 A nanotechnological approach to cancer therapy

Challenges to successful antineoplastic therapy are several-fold. Firstly, poor aqueous solubility poses significant formulatory and delivery challenges. Secondly, the physiological environment presents barriers to high drug bioavailability. Serum proteins can attach to drug molecules, rendering them unavailable for absorption and cellular internalization to exert their antineoplastic activity. Physiological instability, metabolic degradation and renal clearance may further compromise drug concentration at the site of action. However, it is the indiscriminate activity of antineoplastic drugs and the resultant side-effects that portray possibly the greatest challenge. These side-effects can be dose-limiting, thereby compromising therapeutic efficacy and outcome, or may themselves prove fatal.

The potential of nanosystems in addressing and overcoming the aforementioned drawbacks associated with current antineoplastic therapy reside in their ability to, firstly, encapsulate lipophilic drugs within the nanosystem or employ a nanovehicle to successfully deliver these drugs *in vivo* (Kim *et al.*, 2011). Formulation as nanosystems, particularly encapsulation within a nanosystem, serves a protective function from inactivation and metabolic degradation (Kim *et al.*, 2011). Secondly, nanosystems below 300 nm are able to circumvent the reticuloendothelial system (RES), thereby increasing the circulation half-life and improving the pharmacokinetic profile of antineoplastic drugs. Thirdly, and one of the foremost benefits in the application of nanomedicine to cancer therapeutics lies in the passive targeting and accumulation attributes of nanosystems to tumour tissue due to the EPR phenomenon displayed by tumour tissue. In addition, the large surface area:volume ratio of nanosystems facilitates the attachment of targeting moieties for active targeting to tumour sites. Active and passive targeting favorably alter the biodistribution of antineoplastic drugs, simultaneously reducing side-effects and increasing the concentration of drug within tumour tissue for the augmentation of

therapeutic antineoplastic effect (Cirstoiu-Hapca *et al.*, 2010; Kim *et al.*, 2011). Finally, formulation as nanosystems have enabled direct uptake of the nanosystems into tumour cells by endocytic pathways and by-passing of the cellular efflux pump, thereby overcoming a mechanism of drug resistance (Lei *et al.*, 2011; Kim *et al.*, 2011).

The potential of nanotechnological engineering and manipulations in addressing the various challenges limiting the success of antineoplastic therapy will be herein addressed with reference to poor aqueous solubility of antineoplastic drugs, passive and active targeting of nanosystems in enhancing therapeutic efficacy and the increasing problem of emergent drug resistance.

2.3.1 Poor aqueous solubility: A cascading pharmaceutical challenge

Considering water constitutes over 50% of the human body, administered drugs are bound to encounter an aqueous environment on their path to the site(s) of interest (Guyton, 1997). Furthermore, most routes of administration, particularly intravenous administration, require solubilization in an aqueous medium. However, the problem of administering poorly aqueous soluble drugs continues to plague scientists. Approximately 40% of new chemical entities are poorly aqueous soluble or aqueous insoluble, hindering formulation development and the use of potent drug molecules (Merisko-Liversidge *et al.*, 2003; Beig *et al.*, 2012; Buckley *et al.*, 2012). Moreover, new drug development has been stifled due to unsatisfactory biopharmaceutical properties, not least of all being problems related to aqueous solubility (Savić *et al.*, 2003; Pathak *et al.*, 2006). Poor aqueous solubility is one of the fundamental problems of antineoplastic drugs and has thus been the stimulus for the development of carrier systems for these drug molecules, among other modifications.

The aforementioned augmented surface area:volume ratio exhibited by nanosystems has drastic effects on aqueous solubility (Pathak *et al.*, 2006, Lu and Park., 2012). This approach has been widely exploited, particularly in the realm of drug administration in cancer therapeutics. In addition to improving aqueous solubility of antineoplastic drug molecules, the nano-size range allows for more rapid dissolution of the drug within the body allowing for easier absorption and greater propensity to exert its effect (Pathak *et al.*, 2006; Lu and Park, 2012). These favorable effects of nano-sizing can be succinctly explained by the Noyes-Whitney and Ostwald-Freundlich principles, which associates the nano-scale size range to an amplified particle dissolution velocity as well as saturation solubility, ultimately favoring increased drug bioavailability (Ganta *et al.*, 2009; Lu and Park 2012).

2.3.2 Targeted therapy: The future of medicine

The idea of targeted therapy was first postulated by Paul Ehrlich (1906), with the objective being the attainment of therapeutically effective doses while preserving the state of healthy tissue (Rapoport, 2007; Hernot and Klibanov, 2008; Husseini and Pitt, 2008). As previously highlighted, the path to effective drug delivery to tumour tissue and successful treatment outcomes is marred by a multitude of factors, not least of all being compromised bioaccessibility and thereby poor bioavailability of antineoplastic drugs at tumour sites (Shapira *et al.*, 2011).

2.3.2.1 Passive targeting of cancer nanotherapeutics

Nano-drug delivery systems (nano-DDS) have the capacity for passive targeting to tumour sites by nature of their size and the exceptional qualities this size range confers on the system itself (Lei *et al.*, 2011). Characteristic of tumour tissue is a phenomenon termed the EPR effect. Of particular significance are the structural differences in the microvasculature of tumour tissue relative to that of vessels found in normal tissue. Tumours grow at an accelerated pace, rendering their demand for nutrients supplied via the vascular system greater than that of normal, healthy cells. In an effort to satisfy this amplified demand, rapid and hyper-vascularization occurs within tumour tissue (Cho *et al.*, 2007; Geusens *et al.*, 2009; Pan and Feng, 2009). However, this microvasculature lacks the structural organization of normal blood vessels, exhibiting irregular diameters and branching patterns that compromise the integrity of the vessels (Brannon-Peppas and Blanchette, 2004; Cho *et al.*, 2007). The endothelial cells found in the blood vessels of normal tissue may have spaces between them that are approximately 7-10 nm in size, and are thus referred to as tight junctions. In tumour microvasculature however, these spaces can range up to a few hundred nanometers, allowing the preferential extravasation of nanosystems into tumour tissue (Cho *et al.*, 2007; Geusens *et al.*, 2009; Pan and Feng, 2009; Lei *et al.*, 2011). Moreover, recovery of macromolecules via the vascular and lymphatic systems is severely reduced in tumour tissue, effectively resulting in retention of these macromolecules within tumour tissue (Cho *et al.*, 2007; Geusens *et al.*, 2009; Pan and Feng, 2009). Passive targeting is thus a very efficient means of targeting with regards to tumour site-specific drug delivery and nano-DDS are able to capitalize on this phenomenon.

2.3.2.2 Enhancing therapeutic efficacy through active targeting

Nanosystems are particularly amenable to the attachment of targeting moieties as a result of their augmented surface area:volume ratio. The targeting nature of nanosystems can be tailored for specific targets and functions by the inclusion of targeting moieties such as peptides, antibodies and carbohydrates (Cirstoiu-Hapca *et al.*, 2010; Guo *et al.*, 2011; Kim

et al., 2011; Lei *et al.*, 2011; Shapira *et al.*, 2011). These functionalized nanosystems are thereby able to capitalize on the presence of receptors that are over-expressed, or expressed specifically, on the surface of the specific cancer subtype that is being targeted, by the formation of a ligand-receptor complex (Brannon-Peppas and Blanchette, 2004; Cho *et al.*, 2007; Cirstoiu-Hapca *et al.*, 2010; Kim *et al.*, 2011; Viziranakis, 2011). Ideally, the target for antineoplastic drugs should be essential to the survival of tumour cells as well as specific to tumour cells (Blagosklonny, 2003; Cho *et al.*, 2007). However, targets that fulfill these characteristics are scarce and immensely difficult to isolate. The formulation constituents of the nanosystem, such as polymers, can also add to the targeting nature, by responding to micro-environmental conditions or other physiological stimuli in tumour tissue. These are termed “smart” or stimuli-responsive polymers and are able to modulate drug delivery in response to physiological changes that characterize the pathological tissue, such as the lower pH (~pH 6.5) of tumour tissue (Lehner *et al.*, 2012; Meng *et al.*, 2012). Substantial research has been concentrated on isolating receptor targets specific to tumours, in general and for specific tumour subtypes, which can be utilized for drug delivery and imaging agents.

2.3.2.2.1 Folate receptor- α

Folate is a low molecular weight vitamin essential to cellular function through its role in mitochondrial protein synthesis, amino acid metabolism and the synthesis of nucleic acid precursors (Leamon and Low, 2001). Animals are unable to synthesize this micronutrient, hence, the absorption of folate from exogenous sources is essential to satisfactory cellular function. Folate receptors, ubiquitously present throughout the body, facilitate cellular uptake of folate by endocytosis.

Folate receptor- α has been one of the most prevalent receptors investigated for targeting, despite its ubiquitous presence in the body, as a result of the significant over-production and presence of this receptor on the surface of a wide spectrum of tumours (Geszke *et al.*, 2001; Vauthier *et al.*, 2003; Pan and Feng, 2009; Rastogi *et al.*, 2011). Folic acid, the ligand responsible for binding to this receptor, is a popular ligand as it is smaller, non-immunogenic and hardly problematic to procure (Setua *et al.*, 2010). Table 2.1 briefly outlines different nanosystem configurations that have been functionalized for targeting to the folate receptor.

Table 2.1 Tabulated nanosystems functionalized for folate receptor targeting in cancer therapeutics.

Type of Nanosystem	Brief Description	Reference
Magnetic nanoparticles	Superparamagnetic nanoparticles coated with temperature sensitive polymer and folic acid, for tumour imaging and treatment.	Rastogi <i>et al.</i> , 2011
Quantum dots	Stabilized core/shell ZnS:mNZnS QD, functionalized with folic acid for tumour imaging.	Geszke <i>et al.</i> , 2011
Nanocrystals	Rare-earth oxide nanocrystals functionalized with folic acid, for bi-modal tumour imaging.	Setua <i>et al.</i> , 2010
Thermosensitive magnetic liposomes	Folate targeted liposomes that respond to induced localized hyperthermia, for biological and physical tumour targeting.	Pradhan <i>et al.</i> , 2010
Supramolecular vesicle aggregates	A self-assembling polymeric system containing gemcitabine, conjugated to folic acid for targeted cancer therapy. <i>In vivo</i> studies highlighted superior activity of the targeted system relative to a non-targeted system.	Paolino <i>et al.</i> , 2012
Targeted nanoparticle	A nanoparticle consisting of a heparin-folate-paclitaxel conjugate with paclitaxel in the core of the nanoparticle. This system was designed to minimize P-glycoprotein mediated tumour resistance to therapy and demonstrated promising results in the treatment of head and neck cancers in an animal model.	Wang <i>et al.</i> , 2009

2.3.2.2.2 Heat shock protein 90 (Hsp90)

Hsp90, an intracellular molecule involved in signal activation, is widely present throughout the body, yet over-expressed in several cancers, such as ovarian cancer, head and neck cancers, esophageal cancers and leukemia (Önyüksel *et al.*, 2009; Landriscina *et al.*, 2010). This pro-carcinogenic molecule is thus an attractive target as a treatment modality for cancer. 17-allylamino-17-demethoxy geldanamycin (17-AAG) has been identified as an inhibitor of Hsp90, due to binding to the ATP-binding site on the N-terminus of Hsp90, thereby blocking the activity of this compound and, in turn, preventing tumour cell proliferation (Önyüksel *et al.*, 2009). Yet again, poor aqueous solubility and hepatotoxicity renders this compound clinically non-viable. The favorable characteristics that define nanosystems, though, augur well for the future use of this compound in cancer therapy.

It was this aim that drove the study by Önyüksel and fellow researchers (2009), which formulated 17-AAG in long-circulating, sterically stabilized phospholipid nanomicelles (SSM) (Önyüksel *et al.*, 2009). These SSM were further functionalized with vasoactive intestinal peptide (VIP), the receptor for which is over-expressed on the tumour membrane of many cancers (Önyüksel *et al.*, 2009). Firstly, the successful solubilization of therapeutically significant concentrations of 17-AAG was achieved with the SSM.

Secondly the functionalized SSM's displayed superior toxicity as a result of increased cellular uptake (Önyüksel *et al.*, 2009). Unexpectedly, targeted nanosystems displayed sub-optimal cytotoxic properties in the testing period, compared to free 17-AAG. However, this may be due to delayed release of SSM-associated 17-AAG. It must be borne in mind though that *ex vivo* cytotoxicity was not the challenge with 17-AAG, rather stability and toxicity challenges needed to be overcome. The nanosystem addressed these shortcomings, while the functionalized system retained the cytotoxic capacity. The size range achieved (~16 nm) allowed this DDS to escape clearance by the RES, while the properties of PEG contributed to the long circulation lifespan, which cumulatively allowed greater chance for interaction with, and internalization into, target cells (Önyüksel *et al.*, 2009). In addition to the above-mentioned ATP-binding site, a second ATP-binding site is present on the C-terminus. This site has displayed affinity for other antineoplastic agents such as cisplatin, novobiocin and epigallocatechin-3-gallate (Landriscina *et al.*, 2010).

2.3.2.2.3 Human epidermal growth factor receptor (HER)-2

HER-2 has emerged as a prominent receptor target over-expressed in breast and ovarian cancer. Breast cancer is one of the most prevalent tumour types among women, with 20-30% presenting with HER-2 positive tumours which demonstrate chemoresistance to some antineoplastic agents, and an overall poor prognosis (Mi *et al.*, 2012). Trastuzumab® is a humanized monoclonal antibody developed by Genentech in the late 1980's to target HER-2 and has been successfully used clinically in the treatment of HER-2 positive breast cancer (Bazell, 1998; Mi *et al.*, 2012).

Lei and co-workers (2011) highlighted the increased uptake of functionalized nanoparticles containing doxorubicin by ovarian cancer cell lines (Lei *et al.*, 2011). These nanoparticles were conjugated with an anti-HER-2 ligand to form a complex with the HER-2 receptor that displays preferential expression on the surface of ovarian cancer cells. The functionalized nanoparticles exhibited increased uptake by the cancer cells, due to a receptor-mediated endocytosis, compared to their non-functionalized counterparts (Lei *et al.*, 2011).

Several other receptors have also been identified as potential targets in cancer chemotherapy. Epithelial cell adhesion molecule (EpCAM) is a transmembranous glycoprotein that is over-expressed on the surface of solid tumours, but not on normal tissue (Das and Sahoo, 2011). Upon binding, the receptor-ligand complex is rapidly internalized, which is particularly advantageous for the delivery of drugs with intracellular targets (Das and Sahoo, 2011). Vasoactive intestinal peptide (VIP) is over-expressed on the tumour membrane of many cancers and is therefore a possible target (Önyüksel *et al.*,

2009). Other potential targets that have been identified include TAG 72 glycoprotein, luteinizing hormone-releasing hormone receptor, follicle stimulating hormone receptor, transferrin receptor and heparin-binding glycoprotein's such as VEGF (Schroeder *et al.*, 2007; Cirstoiu-Hapca *et al.*, 2010; Kim *et al.*, 2011; Paszko *et al.*, 2011).

2.3.2.2.4 Aptamer-based targeted nanosystems

Aptamers are a class of oligonucleotides comprising synthetic single-stranded DNA or RNA molecules that can be incorporated into DDS for highly specific targeting to various molecular targets present on tumour cells (Li *et al.*, 2013). Aptamers may be conjugated to drug molecules or DDS by intercalation of covalent bonding. Various nano-constructs have been assessed for aptamer functionalization, such as nanorods, nanoparticles and carbon nanotubes, to improve targeting and uptake of the DDS by tumour cells.

AS1411 was the first DNA aptamer to enter clinical oncology trials (Soundararajan *et al.*, 2009). This aptamer has demonstrated extraordinary specificity as well as binding affinity for its plasma membrane target receptor, nucleolin, which is over-expressed in tumour cells. Yang and co-workers (2012) formulated a gold nanorod DDS with a mesoporous, AS1411 surface-functionalized silica framework (Yang *et al.*, 2012). This photothermal DDS is activated by illumination in the near infra-red region resulting in structural changes and consequent drug release. *In vitro* results highlighted versatility of the DDS, as well as biocompatibility, high tumour specificity and appropriate drug release for intracellular targets (Yang *et al.*, 2012).

Functionalization of a liposomal DDS with the sgc8 aptamer which is specifically targeted to protein tyrosine kinase present on CEM-CCRF leukemia cells was undertaken by Kang and team (Kang *et al.*, 2010). The high aptamer load resulted in increased binding affinity to target tumour cells with no compromise on formulation stability. *In vitro* studies confirmed the selectivity of the functionalized liposomal DDS for the target cell as well as intracellular delivery of the drug to tumour cells (Kang *et al.*, 2010). However, this system did not include *in vivo* studies, which is essential to the critical assessment of targeting efficacy of DDS.

2.3.3 Tumour drug resistance: A progressive challenge

Multidrug resistance (MDR) has emerged as an acute problem contributing to the already diverse and significant challenges compromising the success of cancer chemotherapy (Lo Y-L, 2000; Vauthier *et al.*, 2003). MDR can manifest as a failure of initial treatment protocols to adequately reduce tumour size or, as is the case most often with ovarian cancer, as a relapse/recurrence after successful therapy (Vauthier *et al.*, 2003; Kim *et al.*,

2011). The high rate of recurrence in ovarian cancer is the primary contributing factor to the poor prognosis associated with ovarian cancer and the low 5-year survival rate. MDR currently accounts for treatment failure in over 90% of patients presenting with metastasis which, in the case of ovarian cancer, is the majority of patients (Gao *et al.*, 2012).

Drug resistance displayed by tumours can be classified as follows (Shapira *et al.*, 2011; Gao *et al.*, 2012):

- Decreased drug influx into tumour cells.
- Increased drug efflux out of tumour cells.
- Activation of DNA repair.
- Metabolic degradation of antineoplastic drugs.
- Simultaneous inactivation of apoptotic pathways and activation of protective mechanisms of cellular anti-apoptotic pathways.

The application of nanotechnology has shown immense potential in overcoming or circumventing the extra- and intra-cellular mechanisms associated with drug resistance. The most significant application has been to overcome the resistance to doxorubicin, which has displayed substantial success and will be discussed later. Among the extra-cellular resistance mechanisms that nanosystems will find applicability in, is the inactivation of drug molecules prior to their reaching the site of action. Several nanosystems offer protection from unsuitable environments and metabolic and enzymatic degradation, as well as protection against early clearance from the body. Coating with compounds such as poly(ethylene glycol) (PEG) allows nanosystems to navigate the body undetected by clearance systems, thereby increasing the circulation half-life (Vauthier *et al.*, 2003).

The internalization of free drug into tumour cells is primarily through passive diffusion, whilst the mechanism of nanosystem entry into tumour cells involves non-specific endocytosis (Gao *et al.*, 2012). A primary mechanism of resistance in cancer cells is increased drug efflux out of cells by efflux pumps. The passive diffusion of free drug allows for recognition by and activation of efflux pumps, reducing cellular drug concentration and compromising antineoplastic therapy (Gao *et al.*, 2012). However, the mechanism of nanosystem internalization facilitates undetected entry into cells, bypassing the increased drug efflux mechanism of drug resistance in tumour cells, as illustrated in Figure 2.3 (Gao *et al.*, 2012).

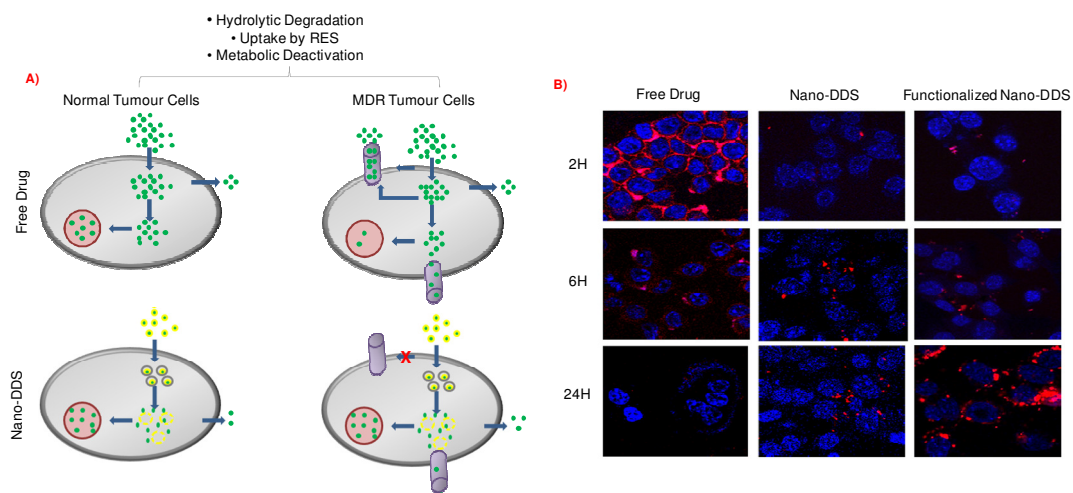


Figure 2.3 A: is a diagrammatic comparison of the internalization mechanisms of free drug and nano-DDS's in normal tumour cells and MDR tumour cells (Adapted with permission from Gao *et al.*, 2012). B: confocal micrographs highlighting the cellular internalization mechanisms of free drug, a nano-DDS and a functionalized nano-DDS. In this image the drug is indicated in red while the cell nuclei are highlighted in blue. The distinct difference is drug concentration within the cell after incubation for 2 hours denotes a difference in mechanism of cellular uptake. The significant reduction of free drug after 6 hours and complete absence of free drug after 24 hours indicates efflux of the drug out of the cell. However, drug administered in nanosystems persist within the cell for over 24 hours, indicating a by-pass of the cellular efflux mechanism. Moreover, functionalized nanosystems display superior cellular drug concentration (Source 2.3B: Wate *et al.*, 2012).

Small interfering ribonucleic acids (siRNA) provide an interesting alternative therapeutic strategy for MDR tumours, however successful *in vivo* delivery presents a challenge to clinical application, due to the size, molecular weight and poor stability profile of these compounds (Ganesh *et al.*, 2013). Ganesh and co-workers (2013) synthesized hyaluronic acid based, self assembling, CD44 targeting nanostructures with outstanding siRNA encapsulation as well as appreciable stability (Ganesh *et al.*, 2013). CD44 is a glycoprotein that is over-expressed on the surface of various tumours and stem cell tumour precursors, is a recognized biomarker in non-small cell lung cancer (NSCLC) and hence, provides an attractive target in cancer therapy (Ganesh *et al.*, 2013). This extensive study demonstrated high cellular uptake of the nanosystem by receptor mediated endocytosis in a tumour cell line over-expressing CD44, contrasted by severely reduced uptake in a control tumour cell line expressing low levels of this glycoprotein (Ganesh *et al.*, 2013).

2.4 Antineoplastic drug challenges: Innovative nanotechnological solutions

2.4.1 Doxorubicin

Doxorubicin (DOX), an anthracycline antibiotic is one of the most efficacious drugs in the treatment of several solid tumours, including breast and ovarian cancers (Brannon-Peppas and Blanchette, 2004; Dreis *et al.*, 2007; Cai *et al.*, 2010; Lei *et al.*, 2011).

However, clinical application of DOX has been severely hindered as a result of the critical toxicity profile, the foremost of which being cardiotoxicity (Brannon-Peppas and Blanchette, 2004; Dreis *et al.*, 2007). Formulation as nanoparticles has been investigated as a possible means of reducing detrimental side-effects, as well as increasing the efficacy of DOX, in order to preserve the use of this potent, widely applicable antineoplastic agent (Dreis *et al.*, 2007). Several materials have been examined for their potential in this application, with DOX being incorporated into, or bound to the nanoparticles. Among these materials are poly(butyl cyanoacrylate), poly(lactic-co-glycolic acid) (PLGA), poly(isohexyl cyanoacrylate) and gelatin (Wartlick *et al.*, 2004; Dreis *et al.*, 2007). Formulation of DOX as nanoparticles has been immensely successful, with formulations displaying passive targeting on account of the nano-scale sizing, ability to cross the blood-brain-barrier for the treatment of brain tumours, as well as success against several lines of drug-resistant cancer cells (Dreis *et al.*, 2007). Human serum albumin (HSA) has also been explored as a nanoparticulate carrier for DOX, with appreciable success (Dreis *et al.*, 2007). Currently there are two commercially available, registered HSA-based formulations, namely Albutex and Abraxane, which drove research into the viability of this material as a nanocarrier (Dreis *et al.*, 2007).

The development of multi-drug resistance in cancer cells has further compromised the feasibility of DOX utilization (Vauthier *et al.*, 2003; Lei *et al.*, 2011). MDR is most often due to the over-expression of the transmembranous protein, P-glycoprotein (P-gp), which compromises the therapeutic efficacy of DOX (Das and Sahoo, 2011; Lei *et al.*, 2011). Increasing the dose of DOX to overcome this drawback is not viable due to the above-mentioned dose-related side-effects (Lei *et al.*, 2011). Lei and team (2011) developed DOX-encapsulated nanoparticles and observed a significant increase in cellular uptake of the nanoparticulate DDS compared to free DOX which was attributed to a difference in the mechanism of cellular uptake. The free form of DOX passes into the cell via diffusion, while the nano-enabled DDS was taken up via endocytosis, which proved more favorable in cells displaying an over-expression of P-gp (Lei *et al.*, 2011).

The capacity of targeted nano-enabled DDS's to accumulate in target tissue has further proved beneficial with regards to the administration of DOX in P-gp-negative cells. Drug resistance can also be a consequence of alteration of the intracellular pH-gradient, which results in drugs being trapped in cellular components from where they cannot exert their action (Lei *et al.*, 2011). Cytotoxic studies undertaken by Lei and team (2011) highlighted the increased cytotoxic effect of functionalized and non-functionalized DOX-containing PLGA nanoparticles compared to free DOX at higher concentrations (Lei *et al.*, 2011). The research team rationalized that the DOX-containing nanoparticles were entrapped in

lysosomes or endosomes within the cell and the release of DOX into the cytosol was limited by an unfavorable pH-gradient. The DOX was therefore unable to reach the site of action, the cell nucleus. This resulted in limited cytotoxicity at low concentrations. However, at elevated concentrations, the concentration of the DOX from the nanoparticles surpasses the cells lysosomal and endosomal capacity, resulting in increased DOX in the cytosol of the cell, with uninhibited movement to the cell nucleus, where it can exert its effect (Lei *et al.*, 2011).

Poly(alkyl cyanoacrylate) (PACA) nanoparticles have also shown tremendous potential in overcoming MDR to DOX. However, the mechanism to overcome drug resistance appears to differ from that of PLGA nanoparticles, in that PACA nanoparticles are not endocytosed into cells, but rather adhere to the surface of tumour cells (Vauthier *et al.*, 2003). The drug is subsequently released and combines with the degradation products of the nanoparticles, forming an ion-pair that diffuses into the tumour cell undetected by P-gp (Vauthier *et al.*, 2003).

Yet another attempt at overcoming tumour cell resistance to DOX was the co-encapsulation of DOX and, the chemo-sensitizing agent, Cyclosporin A within a single nanoparticle (Vauthier *et al.*, 2003). DOX formed the core of the nanoparticle, covered by the Cyclosporin A. This configuration allowed for the rapid release of Cyclosporin A and resulting sensitization, followed by the release of DOX. Formulation as a nanoparticle ensured both agents reached the desired site of action via passive targeting, thereby potentiating the activity of the individual agents and their synergistic activity, while reducing harmful effects on healthy tissue (Vauthier *et al.*, 2003).

2.4.2 Camptothecin

Camptothecin (CPT) is a potent antineoplastic drug which has demonstrated antineoplastic activity against a vast array of solid tumours including ovarian, gastric, breast, cervical, melanoma, skin and lung cancers (Koo *et al.*, 2005; Mu *et al.*, 2005; Fang *et al.*, 2009). CPT inhibits and stabilizes the topoisomerase I enzyme which is required for cell replication and transcription and is over-expressed in certain cancer cells but not in normal tissue, thereby inducing apoptosis of the cancer cells (Shenderova *et al.*, 1997; Ertl *et al.*, 1999; Koo *et al.*, 2005; Zhang *et al.*, 2007). However, use of this drug in clinical practice has been diminished due to its poor aqueous solubility and insolubility in most biocompatible organic solvents, instability under physiological conditions and severe toxicity profile (Hafeti and Amsden, 2002; Koo *et al.*, 2005; Zhang *et al.*, 2007; Fang *et al.*, 2009). The chemical composition of CPT contains an active lactone group, which is responsible for its insolubility and physiologically-labile properties, yet crucial to its

antineoplastic activity (Shenderova *et al.*, 1997; Ertl *et al.*, 1999; Koo *et al.*, 2005; Ziolkowska *et al.*, 2010). It is therefore essential to protect this lactone group in the formulation and delivery of CPT preparations. Although derivatives of camptothecin are utilized, they lack the potency of CPT (Zhang *et al.*, 2007; Fang *et al.*, 2009). Furthermore, camptothecin and its derivatives usually require continuous infusion over a period of time, or multiple injections over a short period, which is a great disadvantage with regards to patient comfort and acceptability (Cortesi *et al.*, 1997). In addition, prolonged administration results in intolerable side-effects, including neutropenia, anemia and other related hematologic manifestations, altered gastric function and dermatological manifestations (Cortesi *et al.*, 1997).

Several methods have been investigated to improve the solubility profile of CPT (Zhang *et al.*, 2007). Whilst formulation of CPT as liposomes, microemulsions and polymeric microspheres have enjoyed a degree of success, incorporation into a nano-DDS may hold greater potential for the clinical use of this drug (Cortesi *et al.*, 1997; Shenderova *et al.*, 1997; Zhang *et al.*, 2007). An emphasis has also been placed on the development of controlled release DDS's, as it is hypothesized that the properties of these systems will be able to adequately address the factors limiting CPT utilization clinically (Cortesi *et al.*, 1997).

Micelles are composed of amphiphiles that take on a spherical form spontaneously in aqueous conditions, above the critical micellar concentration (Koo *et al.*, 2005). These moieties consist of a hydrophobic core and hydrophilic corona, thereby enabling the solubilization of poorly aqueous soluble drugs and their delivery in an aqueous medium, the likes of which will be required for intravenous delivery (Savić *et al.*, 2003; Mu *et al.*, 2005). In addition, the nano-dimensions of micelles allow for their easy passage through the more permeable vasculature that predominates in cancer tissue, making them valuable in cancer therapy (Mu *et al.*, 2005). The ease of manufacture, reproducibility and stability of micelles make them attractive systems for drug delivery.

Aiming to investigate methods of safely and effectively delivering CPT to the intended site of action, i.e. tumour tissue, Koo and colleagues (2005) developed SSM of distearoylphosphatidylethanolamine (DSPE) conjugated to polyethylene glycol 2000 (PEG-2000) (Koo *et al.*, 2005). This study demonstrated, firstly, an approximately 25-fold increase in solubility of CPT in the optimized formulation, compared to free CPT, as well as increased aqueous stability with preservation of the active lactone moiety as a result of drug encapsulation within the hydrophobic core of the SSM, rather than being exposed to the aqueous environment where hydrolytic degradation can occur (Koo *et al.*, 2005).

Since CPT acts on cells in the S-phase of the cell-cycle, formulations with a longer half-life will have a greater cytotoxic effect. The SSM formulation, due to its increased stability and circulation half-life, displayed three-fold greater cytotoxicity than free CPT after 24 hours when tested against breast cancer cells, due to a larger proportion of tumour cells being exposed to CPT. The augmented cytotoxicity may also be attributable to increased cellular uptake and accumulation of the nanosystem within tumour tissue (Koo *et al.*, 2005). The aforementioned findings were supported by results obtained by Mu and team (2005), which produced mixed micelles as CPT delivery systems (Mu *et al.*, 2005). In addition to demonstrating ease of preparation and favorable pharmacokinetic properties, Koo and colleagues highlighted the potential of this DDS for practical application in a clinical setting. The SSM developed displayed negligible alterations in size, solubility and the wavelength of peak fluorescence emission after lyophilization and reconstitution (Koo *et al.*, 2005). This has significant implications for storage and use in a clinical setting. The incorporation of PEG was attributed to the stability to freeze-drying, since PEG has cryoprotectant and lyoprotectant properties (Koo *et al.*, 2005). The CPT-loaded SSM prepared in this study displayed immense potential for application in clinical practice due to superior efficacy and practicality of use.

To address the above-mentioned shortfalls of CPT, Fang and co-workers (2009) formulated a camptothecin-containing nanoemulsion DDS (Fang *et al.*, 2009). Although the primary focus of this study was investigation of physicochemical properties of the nanoemulsions prepared, their *in vitro* and *ex vivo* studies delineated promising results. Varying cytotoxic profiles were obtained for the nanoemulsions prepared, as a function of changes in formulatory composition. In addition, the study did not take into account the effect of metabolism, enzymatic degradation and other processes, which the system will undergo in the body and which will greatly affect the nature of the DDS that ultimately reaches the target site. However, the superior drug-loading capacity (90%) and low hemolytic destruction highlights the potential of a nano-enabled DDS to effectively deliver CPT.

CPT-containing nanoparticles have been vigorously investigated in the quest to develop an efficacious DDS (Miura *et al.*, 2004; Kunii *et al.*, 2007; Zhang *et al.*, 2007; Martins *et al.*, 2012). This nanosystem flaunts prolonged vascular circulation, particularly when coated with PEG, allowing for greater interaction between tumour tissue and antineoplastic drug, as well as superior cellular uptake of CPT resulting in tumour cells being bombarded, thereby having enhanced cytotoxic effect (Zhang *et al.*, 2007). However, CPT loading capacity of nanoparticles remains the limiting factor in successful formulation (Zhang *et al.*, 2007).

2.4.3 Paclitaxel

Paclitaxel (PTX) is a microtubule-stabilizing agent, which acts to disrupt cell division, causing cell death (Brannon-Peppas and Blanchette, 2004; Vergara *et al.*, 2012). It is currently considered first line treatment for ovarian cancer. PTX is a strongly hydrophobic compound, which poses significant formulation problems for intravenous administration (Fonseca *et al.*, 2002; Cirstoiu-Hapca *et al.*, 2010). Solubilization in Cremophor EL has been successful, with the only currently available PTX formulation being the intravenously administered Taxol® (Fonseca *et al.*, 2002). However, this compound causes significant side-effects, making the development of delivery systems not requiring solubilisation in Cremophor EL appealing (Vergara *et al.*, 2012). Nanoparticles have been the most widely explored nanosystem for the delivery of paclitaxel, with a variety of materials and functionalization techniques having been explored (Fonseca *et al.*, 2002; Xu *et al.*, 2005; Akhlaghi *et al.*, 2010; Cirstoiu-Hapca *et al.*, 2010; Lee *et al.*, 2012). PTX nanoparticles have been widely successful in addressing the problems associated with PTX administration and efficacy, that is (Cirstoiu-Hapca *et al.*, 2010):

- The nanoparticles have successfully solubilized PTX and displayed adequate drug loading capacity.
- Drug delivery is more targeted, even in non-functionalized NP's due to passive diffusion.
- Increased therapeutic efficacy *in vivo*, as a result of targeted delivery, increased cellular uptake, protection of PTX from enzymatic degradation and inactivation and an increase in circulation half-life.

The immense allure of PTX incorporation into nanoparticles is attributed to the favorable outcomes, particularly with regards to the biodistribution and pharmacokinetic profile of PTX associated with nanosystems, relative to that of free PTX and Taxol® (Fonseca *et al.*, 2002). PLGA nanoparticles have been successfully prepared in an appropriate size range (117-160 nm) for extravasation into tumour tissue, with extremely high loading efficiencies (Fonseca *et al.*, 2002; Brannon-Peppas and Blanchette, 2004). Furthermore, when tested against human small cell lung cancer cell lines, this nanosystem displayed an approximately 70% loss of cell viability (Fonseca *et al.*, 2002). The ability of nanoparticles to overcome resistance mediated by P-gp is particularly beneficial to its application in PTX delivery, since there is already evidence of acquired resistance to this drug (Fonseca *et al.*, 2002).

2.4.4 Nutlin-3a

Nutlin-3a, a promising antineoplastic drug currently under investigation, acts to inhibit the inactivation of the p53 tumour suppressing protein (Sonnemann *et al.*, 2011; Das and Sahoo, 2011). A significant fraction of tumours display altered or inactivated p53 genes, which results in loss of the tumour suppressing function (Das and Sahoo, 2011). Inactivation of the p53 protein is also via attachment by human double minute 2 (HDM2) oncoprotein, which causes inactivation of p53 (Das and Sahoo, 2011). Nutlin-3a shares a binding site with p53 on the HDM2 oncoprotein, thereby preventing the attachment and inactivation of p53 (Das and Sahoo, 2011). The potential of this drug in restoring the tumour suppressing capacity of p53, and hence in treating cancer, is vast.

However, there are also many shortfalls limiting the use of this drug, such as poor solubility, non-specific targeting, systemic toxicity, low bioavailability in tumour tissue, efflux by transmembranous proteins and degradation by cellular lysosomes, resulting in decreased cellular concentration (Das and Sahoo, 2011). Nanosystems have the propensity to overcome the above-mentioned shortfalls, allowing for the optimal use of this potentially valuable drug. Das and Sahoo (2011) formulated non-functionalized nutlin-3a-containing PLGA nanoparticles (nutlin-PLGANP) and EpCAM-functionalized nutlin-PLGANP for the treatment of colon and lung cancer (Das and Sahoo, 2011). The effectiveness of nanosystems is a function of the drug loading efficiency, target cell uptake and release of drug in the target cell. The functionalized and non-functionalized nanoparticles prepared by Das and Sahoo (2011) exhibited a high loading efficiency of nutlin-3a (~78% and 81%, respectively) as well as significantly increased cellular uptake, compared to free Nutlin-3a. This team reported a 5-fold and 16-fold increase in cellular uptake of nanoparticulate nutlin-3a and the functionalized counterparts, respectively, compared to the free form (Das and Sahoo, 2011). Finally, Das and Sahoo (2011) demonstrated augmented cytotoxicity by the unconjugated nanoparticles and a further increase by the conjugated nanoparticles, compared to native nutlin-3a (Das and Sahoo, 2011). Although non-drug-loaded nanoparticles were not used as a control in this study to ascertain the effect of the system itself on cytotoxicity, other studies have demonstrated non-cytotoxic activity by PLGA nanoparticles. This work requires further *in vivo* analysis, however the presented *in vitro* results are indeed promising.

2.4.5 Indisulam

Indisulam is a sulphonamide drug that interrupts the cell cycle at the G1/S phase (Cesur *et al.*, 2009). The cytotoxic effects have been established, particularly against breast cancer. However, upon reaching clinical trials, dose-related toxicities unfavorably tipped the risk:benefit scale, rendering the drug unsuitable for clinical use (Cesur *et al.*, 2009).

Aqueous indisulam formulations extravasate freely from the vascular system, resulting in toxicity to healthy tissue. Furthermore, they bind to erythrocytes and plasma proteins, causing haemotoxicity (Cesur *et al.*, 2009). Thus, indisulam requires a delivery vehicle to prevent interaction with plasma proteins and erythrocytes, as well as, ideally, to promote preferential accumulation in tumour tissue.

To this end, Cesur and team (2009) formulated a nanomicellar DDS incorporating indisulam for targeted delivery to breast cancer tissue. This simple, cost-effective method of preparation resulted in uniform, reproducible and stable nanomicelles of ~15 nm in size (Cesur *et al.*, 2009). This size range will allow for preferential accumulation of the DDS in tumour tissue as a result of extravasation from leaky vasculature. Solubility of indisulam in aqueous medium was substantially increased (~8-fold), allowing for the intravenous delivery of a greater concentration of drug. Cytotoxicity against the chosen breast cancer cell line was augmented in the nanomicellar DDS compared to indisulam in dimethyl sulphoxide (DMSO). In addition, the prepared formulation could be lyophilized to facilitate long-term storage, without significant alteration of the properties (Cesur *et al.*, 2009). In spite of these promising results, this DDS will have to be subjected to *in vivo* evaluation and clinical trials before the full potential and safety can be ascertained.

2.4.6 Curcumin

An emerging alternative in antineoplastic therapy is the utilization of phytochemicals, either as a therapeutic modality on its own, or in conjunction with commercially available antineoplastic drugs as a means of sensitizing tumour cells to conventional treatment (Mohanty and Sahoo, 2010). Curcumin, a hydrophobic polyphenol derived from the *Curcuma longa* herb, is one such entity that has displayed antineoplastic activity, among its wide range of therapeutic applications, as a result of interaction with the cell cycle process, angiogenesis, apoptosis and metastasis (Das *et al.*, 2010; Mohanty and Sahoo, 2010; Anitha *et al.*, 2011). Furthermore, the clinically established safety profile of this phytochemical favor its use in cancer chemotherapy, with large doses proving tolerable (Mohanty and Sahoo, 2010). However, several pharmacokinetic challenges plague the successful clinical use of curcumin. Poor aqueous solubility poses formulatory and administration challenges, while degradation, poor tissue penetration and absorption, as well as rapid systemic elimination culminate in severely reduced bioavailability (Das *et al.*, 2010; Mohanty and Sahoo, 2010; Anitha *et al.*, 2011).

Since the obvious potential of this compound cannot be disregarded, particularly in the face of growing exigency for successful antineoplastic treatment, efforts to overcome the above-mentioned challenges to curcumin use have produced nanosystems incorporating

curcumin (Tiyaboonchai *et al.*, 2007; Das *et al.*, 2010; Mohanty and Sahoo, 2010; Anitha *et al.*, 2011). PLGA nanoparticulate DDS's have shown variable yet significant increases in curcumin bioavailability, whilst other approaches have included incorporation in a phospholipid complex as well as bioadhesive DDS (Mohanty and Sahoo, 2010). A particularly outstanding study conducted by Mohanty and Sahoo (2010) formulated highly stable glycerol monooleate (GMO) based curcumin nanoparticles that displayed a highly favorable pharmacokinetic profile (Mohanty and Sahoo, 2010). These nanoparticles displayed approximately 90% curcumin entrapment, as well as biphasic release (~46% in 24 hours and ~66% over 10 days) the characteristic of which would be favorable in cancer therapy. The nanoparticulate system exhibited greater aqueous solubility and stability than native curcumin, indicating the protection from hydrolytic degradation conferred on curcumin by the nanosystem (Mohanty and Sahoo, 2010). Nanoparticulate curcumin showed augmented cellular uptake compared to free curcumin (5.9-7.7 times greater), substantially greater antiproliferative effect on tested cancer cell lines as well as 3.8 times greater induction of apoptosis (Mohanty and Sahoo, 2010). Toxicity studies of non-drug-loaded nanoparticles proved the safety of this carrier system and the materials employed. The study was further extended to *in vivo* analysis, where higher levels of systemic curcumin were detected for longer periods of time after the administration of nanoparticulate curcumin (Mohanty and Sahoo, 2010). The findings by Mohanty and Sahoo (2010) were far superior to those from previous studies on PLGA nanoparticulate curcumin. This was attributed to the controlled and prolonged manner of release from GMO nanoparticles.

Anitha and colleagues (2011) employed a straight-forward, easily up-scalable method to formulate modified chitosan nanoparticles (<200 nm) incorporating curcumin to address the aforementioned shortfalls of curcumin bioavailability (Anitha *et al.*, 2011). The substantially favorable drug entrapment was comparable to that achieved by Mohanty and Sahoo (2010) (87% versus 90%), with controlled drug release achieved over several days. Furthermore cell viability studies indicated the retention of anti-tumour activity by curcumin despite loading into nanoparticles, whilst fluorescence spectroscopy confirmed the release of curcumin within cancer cells with resultant apoptosis. The results of the studies presented above have been corroborated by several other studies reporting on various nano-DDS's which successfully addressed the challenges limiting the use of curcumin and highlighted the feasibility of nano-enabled curcumin as an antineoplastic agent (Tiyaboonchai *et al.*, 2007; Anand *et al.*, 2010; Das *et al.*, 2010; Dhule *et al.*, 2012; Kundu *et al.*, 2012; Liu *et al.*, 2012).

As the annals of nanomedicine research expand, it is the translation of nanosystems from bench-top to bed-side that substantiates the clinical relevance of this field of research. Although currently small in number, the nanosystems that have received approval by the United States Food and Drug Administration (FDA) have demonstrated considerable clinical success and are now firmly embedded in the treatment protocol of specific tumour subtypes. Moreover, the significant number of nanosystems undergoing pre-clinical investigations inspires an expectation of the imminent approval and clinical availability of more innovative nanosystems for cancer treatment. Table 2.2 provides a brief overview of currently available as well as pre-clinical nanosystems for cancer therapy.

2.5 Nano-enabled antisense oligonucleotides in cancer therapeutics

Antisense oligonucleotides are fragments of deoxynucleotide that are complementary in sequence to a defective portion of mRNA, and acts to interrupt the translation of defective proteins from mRNA (Bogunia-Kubik and Masanori, 2002). Hence, antisense oligonucleotides have potential in cancer therapeutics, by blocking the expression of defective genes. However, these moieties are labile and display poor cell penetration, necessitating a suitable carrier system for their successful clinical application (Bogunia-Kubik and Masanori, 2002; Fattal and Bochot, 2008). Formulation as nanoparticles and liposomes has been investigated to address these shortcomings of antisense oligonucleotides. Furthermore, the capacity of nanosystems for targeting aids in the utilization of antisense nucleotides, as it will prevent non-specific binding

Table 2.2 A brief outline of commercially available and pre-clinical nanosystems with application in the oncology field.

In Clinical Use					
Product	Type of Nanosystem	Manufacturer, Year of FDA Approval	Indication	Notes	References
Doxil[®]	Liposome (~100 nm)	Alza Corporation (1995)	Refractory ovarian carcinoma, Kaposi's sarcoma,	First marketed product employing stealth technology. Significant reduction in cardiotoxicity associated with DOX.	Barenholz, 2001; Nishiyama and Kataoka, 2006
DaunoXome[®]	Liposome (60-80 nm)	NeXstar Pharmaceutical (1996)	Kaposi's sarcoma	Intravenous liposomal formulation of anthracycline daunorubicin exhibiting reduced cardiotoxicity <i>in vivo</i> , due to a passive targeting mechanism.	Bellot <i>et al.</i> , 2001
Emend[®]	Nanocrystal	Merck and Co., Inc. (2003)	Chemotherapy-associated nausea	Nanocrystals of the substance P antagonist, aprepitant, formulated as such to enhance the water solubility and maximize bioavailability from the narrow absorption window of this drug.	Junghanns and Müller, 2008
Abraxane[™]	Albumin nanoparticle (~130 nm)	American Pharmaceutical Partners Inc. And American BioScience (2005)	Refractory metastatic breast cancer, NSCLC	Injectable formulation containing paclitaxel, employing innovative nanoparticle albumin bound technology to achieve tumour targeting.	Nijhara and Balakrishnan, 2006; Hawkins <i>et al.</i> , 2008; Kratz, 2008
Undergoing Pre-Clinical Investigations					
Product	Drug	Size	Company	Description	References
NK911	DOX	40 nm	Nippon Kayaku	Polymeric micellar system consisting of a block copolymer of PEG and poly(aspartic acid).	Nakanishi <i>et al.</i> , 2001; Tsukioka <i>et al.</i> , 2003
Genexol[®]	PTX	<50 nm	Samyang	Micellar DDS formulated with the amphiphilic polymer monomethoxy-PEG- <i>b</i> -poly(D,L-lactide). Response rate of metastatic breast cancer to Genexol [®] was superior to Abraxane [®] and Taxol [®] in Phase II and III clinical trials. Efficacy against NSCLC and pancreatic ductal adenocarcinoma has also established in clinical trials.	Shea <i>et al.</i> , 2011; Lu and Park 2012
SP1049C	DOX	30 nm	Suprateck	A non-ionic surfactant-based micellar DDS comprising Pluronic [®] L61 and F127. This nanosystem has demonstrated efficacy against multi-drug resistant cells and is currently in Phase III clinical trials.	Alakhov <i>et al.</i> , 1999; Danson <i>et al.</i> , 2004

2.6 Nano-theranostics

Nano-theranostics, an area of research still in its infancy, refers to the simultaneous use of one nanosystem for diagnostic and therapeutic purposes (Rai *et al.*, 2010; Veisheh *et al.*, 2010; Vizirianakis, 2011). One of the primary benefits of these systems is the individualization of treatment (Rai *et al.*, 2010; Vizirianakis, 2011). Therapeutic regimens can be designed and assessed according to the disease presentations of individual patients, thereby achieving optimized treatment outcomes with regards to safety and efficacy (Rai *et al.*, 2010). Furthermore, invasive procedures are minimized by the combination of diagnosis and therapy. Various nano-constructs have been created and investigated for potential theranostic application in solid tumours, such as liposomes, nanoparticles, micelles and emulsions (Shiraishi *et al.*, 2011). Thus far, ultrasound has been largely investigated in combination with the nano-constructs since it allows for the safe and effective imaging of solid tumours as well as being capable of disrupting the nano-constructs resulting in targeted drug release (Shiraishi *et al.*, 2011).

2.6.1 Magnetic nanoparticles

Magnetic nanoparticles (MNP) have received considerable attention for application in the field of biomedical imaging and therapy, particularly with regards to cancer (Veisheh *et al.*, 2010; Mahmoudi *et al.*, 2011; Rastogi *et al.*, 2011). At room temperature these nanoparticles undergo strong magnetization in the presence of a magnetic field, which is reversed at the removal of the magnetic field (Rastogi *et al.*, 2011). This allows for external manipulation to achieve a specific result, be it imaging of a specific region or body system or stimuli-responsive drug release. In addition, the high surface area:volume ratio makes them ideal for the conjugation of targeting moieties to tailor the application (Mahmoudi *et al.*, 2011). *In vivo*, biological barriers pose a significant challenge to the accessibility of imaging and drug delivery systems to the target site (Veisheh *et al.*, 2010). MNP are particularly adept at overcoming this challenge. The well-controlled narrow size range of MNP formulations allow them to traverse physiological barriers on their path to the intended site, aided by the application of the external stimulus. However, agglomeration due to dipole interaction of these nanoparticles poses a problem. Several modifications have been investigated to overcome this problem, such as polymer coating. Moreover, the chosen polymers often had properties that were advantageous to the function of the MNP, such as increasing circulation life-span *in vivo* (PEG) and temperature- and pH-responsiveness (poly(N-isopropylacrylamide), Chitosan) (Rastogi *et al.*, 2011). Modification of MNP attempted by Rastogi and co-workers (2011) included the use of thermo-sensitive polymers for hyperthermia-induced drug release, as well as folic acid conjugation for active tumour targeting (Rastogi *et al.*, 2011). Magnetic resonance imaging conducted with the formulation attested to its applicability to *in vivo* use, while

drug-release was determined to be site-specific due to folic acid targeting, the nanosize capitalizing on the EPR effect, and an externally applied thermal stimulus.

Superparamagnetic iron oxide nanoparticles (SPION) are a popular subtype of magnetic NP's that have been widely studied due to their targeting ability via the application of an external stimulus, as well as the favorable safety profile (Veiseh *et al.*, 2010). SPION consist of an iron oxide core that is responsible for the magnetic targeting ability, which is either coated with a biocompatible polymer or is precipitated into the pores of a porous polymer (Mahmoudi *et al.*, 2011). Superparamagnetic nanoparticles are localized by i) passive targeting as a result of their size, which is only applicable in certain conditions such as solid tumours, ii) active targeting through the attachment of ligands and iii) by the process of the externally applied magnetic force over-coming the force exerted on the NP by blood flow. The NP are then able to extravasate out of the blood vessel and accumulate at the intended site of action, where imaging can be conducted or drug release can occur (Mahmoudi *et al.*, 2011). SPION formulations of note is the commercially available Combidex®, that finds application in the imaging of lymph node metastasis, as well as Lumiren® for bowel imaging which will be useful in the detection of colonic and colorectal tumours (Veiseh *et al.*, 2010).

2.6.2 Photodynamic therapy

Photodynamic therapy (PDT) involves the administration of a non-toxic agent that acts as a photosensitizer (PS). Photo-excitation of the PS leads to the generation of free radicals, which destroy tumour tissue (Tsay *et al.*, 2007; Spyratou *et al.*, 2012). An alternative method of PDT involves the transition of the PS from a singlet to an excited triplet state. Transfer of energy from the excited PS to oxygen molecules results in the production of singlet oxygen species, which destroy cellular components, causing cell death (Tsay *et al.*, 2007). The irradiation of tumours with light of a pre-determined wavelength ultimately causes the generation of cytotoxic products through the interaction of the PS and light in the presence of oxygen, as illustrated in Figure 2.4 (Rai *et al.*, 2010). These cytotoxic products result in tissue destruction and cell death (Paszko *et al.*, 2011). The chosen wavelength of irradiating light should ideally be one that is absorbed to a greater degree by the tumour tissue relative to the surrounding healthy tissue.

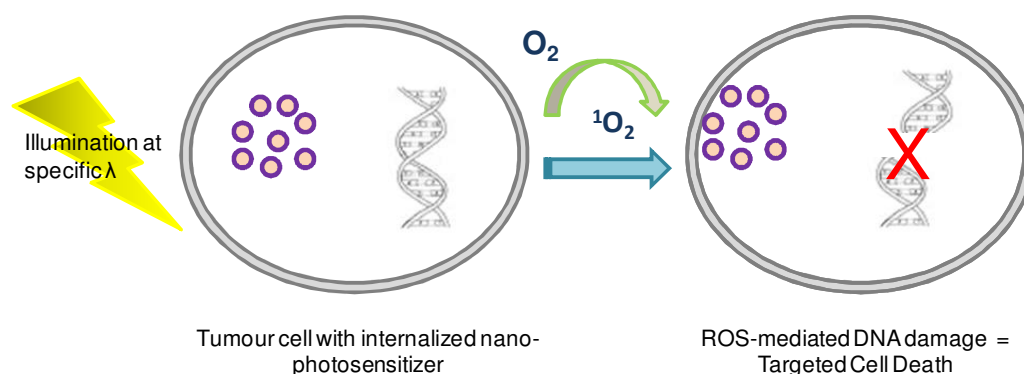


Figure 2.4 Illustrative representation of the mechanism of PS cytotoxicity for PDT (Adapted with permission from Spyrtou *et al.*, 2012).

PS have been extensively investigated for application in cancer imaging and therapy (Tsay *et al.*, 2007; Rai *et al.*, 2010; Spyrtou *et al.*, 2012). One such PS is hypericin, which has gained attention for its potential in the diagnosis of bladder and oral tumours as well as in combination with bevacizumab for the treatment of bladder cancer (Rai *et al.*, 2010). When combined with other imaging techniques, PDT can also be used as an aid in cytoreductive surgery. However the potential for clinical application of these agents is marred by pharmacokinetic problems such as non-selective distribution of PS, which may prove dangerous in widely disseminated tumours, as is often the case with ovarian cancer by the time of diagnosis (Rai *et al.*, 2010; Paszko *et al.*, 2011). The hydrophobic nature of most PS result in a tendency to aggregate in biological environments, consequently altering the optical properties of PS, as well as oxygen production (Rai *et al.*, 2010; Paszko *et al.*, 2011). The solubility profile also poses challenges to delivery of PS (Rai *et al.*, 2010). PS display sub-optimal tissue half-life *in vivo*, and the possibility of toxicity in the absence of irradiation, i.e. dark toxicity (Allison *et al.*, 2008). In addition, PS exhibit a limitation on the targeting depth due to attenuated intensity of irradiation following propagation through skin and tissue (Allison *et al.*, 2008).

It is the above-mentioned shortcomings that have triggered the emergence of nanoparticulate-based PDT. Formulation of PS in a nanosystem can greatly influence its activity by altering the pharmacokinetic properties, localization and cellular uptake of the PS (García-Díaz *et al.*, 2012). Selectivity for tumour tissue is pivotal to the safety and efficacy of PDT. As previously highlighted, the preferential distribution of nanosystems into tumour tissue is advantageous as a method of targeting. Furthermore, nanosystems are amenable to the attachment of targeting moieties, which will facilitate a greater targeting capacity. Incorporation of the hydrophobic PS into nanosystems that exhibit outward hydrophilicity will stabilize the formulation in physiological environments and minimize the challenges associated with PS administration. Table 2.3 highlights a few examples of nanosystems that have been investigated for PDT.

An investigation undertaken by García-Díaz and co-workers (2012) succinctly illustrates the unprecedented influence of nanotechnological manipulation may have on the effectiveness of PDT in cancer therapy (García-Díaz *et al.*, 2012). Determining the *in vitro* and *in vivo* activity of novel PS, temocene, in relation to drug delivery vehicles containing the active molecule, this team was able to demonstrate the enhanced safety and *in vivo* activity of temocene incorporated into liposomes and micelles (García-Díaz *et al.*, 2012). This work also emphasized the stability of liposomal and micelle drug delivery vehicles, with respect to lyophilization and aggregation. A highlight of this study to be noted was the toxic effects of free temocene *in vivo*, as a result of vascular aggregation of the PS. This resulted in the discontinuation of *in vivo* studies on free temocene. Liposomal temocene, however demonstrated greatest tumour selectivity and cell internalization. Micellar temocene, although lacking in activity *in vitro*, was the most effective *in vivo* when combined with a short drug-to-light interval, due to targeting of tumour vasculature that is absent in cell cultures used for *in vitro* analysis (García-Díaz *et al.*, 2012).

A particularly fascinating study by Ling and team (2012) describes the formulation of a nuclei targeting lipid-nanocarrier for PDT (Ling *et al.*, 2012). Whilst PDT has become a widely accepted diagnostic and therapeutic mechanism for certain tumours, there remains some challenges with regards to larger and more deeply located tumours, namely the dependence of PDT efficacy on light dose, which is compromised for larger and deeper tumours (Ling *et al.*, 2012). Since the mechanism of action of the singlet oxygen generated in PDT is DNA damage and inactivation of enzymes responsible for DNA repair, the logical cellular target for PS in PDT would be the nucleus (Sobolev *et al.*, 2000; Ling *et al.*, 2012). The generation of these cytotoxic singlet oxygen species beyond the cell and the ultimate target, the nucleus, leads to reduced efficacy due to the short diffusion range of the singlet oxygen (Ling *et al.*, 2012). Hence, intracellular delivery, distribution and accumulation of the PS are fundamental to the efficacy of PDT (Sobolev *et al.*, 2000). To address this challenge, Ling and co-workers (2012) formulated a lipid nanoparticle coated with folate-containing pullulan, which would be stable in plasma and targeted to the over-expressed folate receptor on tumour cells, thereby accumulating preferentially in tumour cells following endocytosis (Ling *et al.*, 2012). Enzymatic degradation of the pullulan-folate coating releases lipid and drug, which form lipid-drug complexes, the lipophilicity of which facilitates transport into the nucleus of the cell. A focal point of this study was the demonstration of enhanced nuclei accumulation of the model and other drugs, indicative of the potential for enhanced PDT that is more widely applicable in clinical cancer therapy, as well as the versatility of this nanosystem. Furthermore, augmented cytotoxicity was exhibited at low irradiation intensity, highlighting applicability to treatment of deeply-located tumours (Ling *et al.*, 2012).

Table 2.3 Nanosystems investigated for use in PDT, with therapeutic and/or imaging potential.

Nanosystem		Imaging potential	Therapeutic potential	<i>In vitro/ Ex vivo/ In vivo study</i>	Features
Mesoporous nanoparticles	silica	X	X	<i>In vitro; Ex vivo</i>	Drug and imaging molecules can be incorporated into the pores of the NP's. <i>In-vitro</i> studies demonstrated successful tumour cell uptake and cytotoxicity (Roy <i>et al.</i> , 2003).
Foslip®, liposomal preparation			X	<i>In vitro; Ex vivo</i>	Liposomal preparation containing Foscan (temoporfin). Has exhibited enhanced efficacy and reduced dark toxicity relative to Foscan (Kiehlisch <i>et al.</i> , 2007; Paszko <i>et al.</i> , 2011).
Zinc(II)phthalocyanine (ZnPc) containing micelles		X	X	<i>In vitro</i>	Micellar formulation proved more stable with an enhanced lifetime of the triplet oxygen excited state (cytotoxic), augmented fluorescence quantum yield and protection of the hydrophobic compound ZnPc (Sibata <i>et al.</i> , 2004).
Peptide coated-Quantum dots conjugated to PS's		X	X	<i>In vitro</i>	Water soluble QD that retains the photo-physical properties of the QD and PS. Efficient generation of singlet oxygen through Fluorescence Resonance Energy Transfer (Tsay <i>et al.</i> , 2007).
Aerosol nanoparticles containing doxorubicin and PS methylene blue.	OT-alginate		X	<i>In vitro; Ex vivo</i>	Combination of PDT with chemotherapy by incorporating methylene blue, a PS, into DOX-containing nanoparticles displayed enhanced <i>in-vitro</i> cytotoxicity in a resistant tumour cell line (Khdair <i>et al.</i> , 2009).
Pullulan-folate coated lipid nanoparticles			X	<i>In vitro; Ex vivo</i>	Pullulan-folate coated lipid nanoparticles demonstrated enhanced nuclei targeting and accumulation, the desired site for enhanced PDT efficacy, and enhanced efficacy at low intensity irradiation, for treatment of deep-seated tumours. In addition, DOX substitution highlighted the versatility of the system, enhancing the already present nuclei accumulation DOX (Ling <i>et al.</i> , 2012).
Organically modified silica (ORMOSIL) nanoparticles			X	<i>In vitro; Ex vivo; In vivo</i>	ORMOSIL nanoparticles covalently linked to a PS, to avoid release of the PS in systemic circulation. Spectroscopic and functional properties were retained by this system. This system has the potential for bi-functional diagnostic and therapeutic value with slight modification (Ohulchanskyy <i>et al.</i> , 2007).

2.7 Concluding Remarks

Successful nanotechnological innovations that transcend medical ideologies decades ahead of time demand the amalgamation of several individual specialties including, but not limited to, biology, chemistry, engineering, mathematics and pharmacology. Nano-scale dimensions have demonstrated characteristics that are vastly different from identical compounds at micro- and macro-scale. Exploitation of these characteristics has been extensively investigated for application in the detection and treatment of ovarian and other solid tumours. The potential of nanotechnology highlighted during these studies brings forth innovations that could revolutionize the incidence, prognosis, mortality and burden of ovarian cancer. Nanosystems have exhibited potential at the pathophysiological level in terms of passive targeting to tumour tissue, transportation into tumour cells and bypassing mechanisms of tumour resistance, as well as at the biopharmaceutical level, by enhancing drug solubilization, efficacy and hence clinical relevance. In addition, nanosystems have proven to be immensely feasible in addressing the shortfalls of therapeutically active phytochemicals whose cost-effectiveness and ease of procurement render them invaluable treatment options.

The escalating incidence of cancer worldwide and the increased exposure to carcinogens necessitates radical advancements in cancer detection and treatment to improve therapeutic outcomes as well as reduce the burden on healthcare systems. Hence, this disease state has dominated nanotechnological investigations. Commercially available nanosystems for the detection and treatment of ovarian cancer, as well as those in late stage clinical trials validate the feasibility of research in the field of nanotechnology for ovarian cancer. Moreover, the development of drug delivery systems to improve the pharmacokinetics, biodistribution, bioavailability, and safety profiles of existing drug molecules is particularly attractive as it is usually a shorter, more economical process relative to that involved in the identification and registration of new drug compounds.

Nanosystems elevate the paradigm of targeted therapy to another echelon, surpassed only by the potential to combine tumour detection, therapy and monitoring mechanisms into one system. While the current outlook on the role of nanotechnology in addressing cancer detection and treatment shortfalls that plague medical experts is promising, our understanding on the mechanisms, fate and impact of nanosystems and their development is far from absolute. These issues will need to be intensely investigated for the responsible development of widely employed nanosystems to thrive. With that said, we may indeed be only a few nanometers away from comprehensive, multimodal solutions to the 'cancer plague'.

CHAPTER 3

PRELIMINARY STUDIES FOR THE DESIGN AND DEVELOPMENT OF A PARENTERAL ANTINEOPLASTIC NANO-LIPOBUBBLE FORMULATION

3.1 Introduction

Liposomes and nanobubbles have been intensely researched particularly for their application in the oncology field (Tardi *et al.*, 2007; Bawarski *et al.*, 2008; Allen and Cullis, 2013; Etheridge *et al.*, 2013). The resemblance of liposomal membranes to biological phospholipid membranes and their ability to deliver poorly aqueous soluble drugs (which constitutes a large proportion of new drug compounds) as well as aqueous soluble drugs, validates the appeal of this drug delivery system (DDS) (Mertins *et al.*, 2005; Lesoin *et al.*, 2011; Zalba *et al.*, 2012). However, storage and *in vivo* stability as well as premature drug leakage have presented major challenges to their clinical use and addressing these drawbacks has been the focus of several studies (Mertins *et al.*, 2005).

Doxil[®], the first United States Food and Drug Administration (FDA) approved nano-drug delivery system (nano-DDS), is a pegylated liposomal formulation containing the broad-spectrum antineoplastic drug doxorubicin. First approved in 1995, during the largely infantile stage of nanomedicine, the development of this revolutionary therapeutic formulation validated the potential of nanotechnology in medical applications and instigated greater resource investment toward research in this field. This was rapidly followed by the approval of Optison[™] (1998), a microbubble diagnostic imaging agent utilized mainly in cardiology. As understanding of the *in vivo* mechanistic of nanosystems evolved, the potential to confer nanotechnological ingenuity to a similar diagnostic modality that could be used in the imaging of solid tumours became apparent (Wang *et al.*, 2010). The preferential accumulation of nano-scale echogenic bubbles (nanobubbles) within tumour tissue, as a result of the Enhanced Permeability and Retention (EPR) phenomenon, enhances accurate visualization of solid tumours for the purposes of tumour diagnosis, staging and resection. However, challenges with regards to *in vivo* persistence of the nanobubbles soon presented, compelling research into modifications such as polymeric coating and pegylation to increase the lifespan of the nanobubbles.

When discussing advancements in translational oncology nanomedicine one would be amiss not to mention Abraxane, an albumin-bound nanoparticulate formulation approved by the FDA in 2005 for the treatment of metastatic breast cancer and recurring ovarian cancer (Bawarski *et al.*, 2008). The novel mechanism of action of Abraxane and resultant

clinical success was substantiated by expansion of the FDA approved indications to include non-small cell lung cancer in 2012 (FDA, 2012). It is on this meticulous foundation the paradigm dictating the development of the proposed novel nano-lipobubble drug delivery system (NLB-DDS) was established.

3.2 Preliminary Studies in the Development of the NLB-DDS

The extensive range of pharmaceutical materials currently available makes investigation of all pharmaceutical excipients a counter-productive undertaking, with respect to cost and time implications. A comprehensive literature review to identify a narrower range of materials that are pertinent to the intended application is, thus, a viable undertaking preceding the initiation of pre-formulation studies. The intention of pre-formulation studies was to investigate material and methodology variations that result in a successful formulation and that have significant effect on measured responses, as this can be manipulated to tailor the properties of the intended DDS.

Successful formulation of a DDS and subsequent drug delivery compels a comprehensive understanding of, firstly, the desired properties of the DDS and, secondly, the fundamental properties of the drug to be delivered and thus the materials to be employed in the formulation of the DDS. Intravenously administered DDS demand stringent biocompatibility of materials employed in the formulation process and this consideration presents the focal point in the selection of materials for investigation. The demand for a successful formulation that can be employed clinically will be substantial, hence a further consideration in material selection was the source (natural, naturally derived or synthetic) as well as ease of procurement and cost of the materials. Figure 3.1 represents a concise illustration of the key considerations in developing the NLB-DDS, as well as the ideal properties of the intended system.



Figure 3.1 Illustrative representation of the ideal properties and key considerations of the intended NLB-DDS

This Chapter highlights the initial stages of the study, including the processes involved in and the rationale behind 1) the choice of formulatory components, 2) methodology design for the NLB-DDS and 3) the preliminary tests conducted on formulated NLB. Moreover, the effects of each of the formulation components, and their interactions, on the physicochemical and physicomachanical properties of the NLB are elucidated in the quest to ascertain the optimal formulation parameters for the DDS.

3.2.1 Rational Selection of Materials

3.2.1.1 Lipid Components

As previously highlighted, an inherent property of most antineoplastic drugs, not least of all, the model drug in this study, is vastly poor aqueous solubility. A fundamental formulation challenge was to incorporate these hydrophobic compounds into a suitable carrier, whilst ensuring hematological compatibility of the DDS (i.e. compatibility with, and stability in, an aqueous environment) for intravenous administration. Hence, the use of amphiphilic compounds as an initial structural component of the intended NLB-DDS was a rational choice. Phospholipids are amphiphilic compounds ubiquitously present in the body, as major components of biological membranes and pulmonary surfactant (Lo, 2000; Kent, 2005). Furthermore various phospholipids, such as egg phosphatidylcholine, soybean phosphatidylcholine, phosphatidylserine, and phosphatidylethanolamine have been extensively highlighted in the literature as critical components in the successful formulation of intravenously administered lipid emulsions, micelles, non-drug-loaded nanobubbles, as well as nanoliposomes - an initial stage to the preparation of the NLB-DDS in this study (Shimizu *et al.*, 2005; Chou *et al.*, 2006; Wang *et al.*, 2006). The different properties of each phospholipid can be used to tailor the desired physical and

chemical properties of the DDS. The ratio of the polar:non-polar components can have a notable influence on the drug loading capacity of the DDS, depending on the affinity of the drug. One of the major formulation considerations is the predilection of lipid-based drug carriers for uptake by the reticuloendothelial system (RES). The presence of phospholipids has been highlighted to reduce the propensity of DDS for phagocytosis by decreasing the adsorption of opsonic proteins (Hadinoto *et al.*, 2007). Phospholipids are biocompatible and biodegradable materials, the metabolic breakdown products of which will not have adverse biological effects. In addition, phospholipids have been investigated for their role in overcoming resistance in some tumour cell lines, a property that will prove tremendously beneficial to the intended DDS (Lo, 2000). A study by Lo (2000) highlighted the physicochemical similarities between some zwitterionic phospholipids, such as phosphatidylcholine and phosphatidylethanolamine, and hydrophobic cationic drugs. The aforementioned drugs are rendered ineffective in resistant cells due to efflux by P-glycoprotein (P-gp) present on the cell membrane. The study proceeded to successfully exploit these similarities to employ phospholipids as a substrate for P-gp, thereby saturating this efflux pump. The antineoplastic drugs are subsequently able to exert their effects, due to the modulatory effects of phospholipids on tumour cell resistance (Lo, 2000). To this end, two phospholipids, namely distearoylphosphatidylcholine (DSPC) and distearoylphosphatidylethanolamine (DSPE), were investigated as primary components of the NLB-DDS. In addition, the use of cholesterol (CHO) and coconut oil were also explored for their potential as components of the NLB membrane.

3.2.1.1.1 Distearoylphosphatidylcholine

Phosphatidylcholines (PC) are a class of phospholipids that possess a choline head group and are widely available from natural sources such as egg-yolk and soy beans (Kawaguchi *et al.*, 2008; Patil *et al.*, 2010; Cole *et al.*, 2012). This neutral or zwitterionic phospholipid is located in the exoplasmic leaflet of mammalian cell membranes and functions in membrane-mediated cell signaling (Kent, 2005; Fernández-Murray and McMaster, 2007; Aktas *et al.*, 2010). Furthermore, PC is the principle phospholipid present in plasma lipoproteins, highlighting the safety of this lipid in intravenously administered formulations (Cole *et al.*, 2012). PC has been vastly explored in drug delivery applications with noteworthy success with regards to solubilization of poorly aqueous soluble drugs, enhanced cell permeation and drug absorption as well as characterization and classification of new drug entities (Kapitza *et al.*, 2007). A study by Kapitza and co-workers (2007) further established the immense safety and compatibility of PC to cells, by highlighting the maintenance of cell membrane integrity following exposure to high concentrations of PC-containing liposomes (Kapitza *et al.*, 2007). The tolerability of

such excessive PC concentrations can have remarkable consequences on the quantity of drug successfully deliverable by PC-containing DDS. DSPC has been cited extensively for incorporation into DDS, particularly liposomes (Santos *et al.*, 2002; Shimizu *et al.*, 2005; Kawakami *et al.*, 2006; Suzuki *et al.*, 2008; Haeri *et al.*, 2011; Hossann *et al.*, 2012). Clinical studies of a pegylated liposomal doxorubicin formulation containing DSPC exhibited favorable characteristics such as low clearance rate, enhanced stability and longer half-life when compared to a similar formulation containing hydrogenated soybean phosphatidylcholine (Chou *et al.*, 2006; Hsiao *et al.*, 2009). This formulation (Lipo-Dox[®]) is used extensively in Taiwan in the treatment of recurrent ovarian cancer, metastatic breast cancer and Kaposi's sarcoma (Hsiao *et al.*, 2009)

3.2.1.1.2 Distearoylphosphatidylethanolamine

Phosphatidylethanolamine (PE) is a zwitterionic molecule (between pH 2-7) present in the inner leaflet of biological membranes in mammalian cells, however to a lesser degree than PC (Marconescu and Thorpe, 2008). PE is associated to a larger extent with nervous tissue and neural cells in humans and is the primary phospholipid present in bacterial cells, such as E.coli (Wang *et al.*, 2000; Welti *et al.*, 2007). From a chemistry perspective, PE is a combination of glycerol esterified with two fatty acids, in the 1,2 or 1,3 positions, and phosphoric acid, with a small ethanolamine head group resulting in a cone-shaped molecule. DSPE-methoxy-polyethylene glycol (DSPE-m-PEG) is a highly beneficial amphiphilic conjugate that is regularly employed in the formulation of liposomes due to the ability to circumvent opsonization by plasma proteins and immunoglobulins, thus achieving prolonged circulation lifespan of the liposomes *in vivo*, and enhanced pharmacokinetics of the drugs being delivered (Santos *et al.*, 2002; Chou and Chu, 2003; Ishida *et al.*, 2005; Shehata *et al.*, 2008; Hossann *et al.*, 2010; Hossann *et al.*, 2012). In chemotherapeutic studies the popularity of this compound can be attributed to its ability to carry poorly aqueous soluble antineoplastic drugs and release the drug load in a controlled manner, due to the long fatty acyl chains which minimizes mobility of entrapped drug molecules (Gill *et al.*, 2011; Wang *et al.*, 2012).

In this study DSPE-m-PEG was employed for the steric benefits it may provide to liposomal systems. Steric stabilization describes the inhibition of opsonization of the liposomes, thereby extending the *in vivo* residence time of the liposomes (Song *et al.*, 2002). As previously described, increased *in vivo* residence time enables greater accumulation of the envisaged DDS within tumour tissue, favorably altering the biodistribution of the drug and hence, the therapeutic efficacy and side-effect profile (Song *et al.*, 2002). A study conducted by Sezgin and co-workers (2008) demonstrated the

successful development of a DSPE-micellar intravenous DDS containing poorly aqueous soluble porphyrins commonly used in photodynamic therapy of solid tumours (Sezgin *et al.*, 2008). In addition, comparative analysis with Pluronic micelles highlighted a more favorably negative zeta potential for the DSPE micelles (Sezgin *et al.*, 2008). Several other studies have demonstrated the value of DSPE incorporation in micellar and liposomal DDS displaying effective loading and controlled release of hydrophobic drugs (Ishida *et al.*, 2001; Charrois and Allen, 2004; Sawant *et al.*, 2008; Gao *et al.*, 2009; Gill *et al.*, 2011; Katragadda *et al.*, 2011).

3.2.1.1.3 Cholesterol

Cholesterol (CHO), a primary lipid component of mammalian plasma cell membranes, has been widely cited for use in various DDS, particularly those employed in cancer therapy (Róg and Pasenkiewicz-Gierula, 2006; Jia *et al.*, 2008; Cai *et al.*, 2011; Haeri *et al.*, 2011; Sato *et al.*, 2012). Ease of procurement also favorably influenced the choice of this material. The addition of CHO to formulations has been noted to have a stabilizing effect on liposomes *in-vitro* and upon storage as well as a substantial decrease in drug leakage out of liposomes, particularly when combined with DSPE (Chou and Chu, 2003; Evjen *et al.*, 2010). Furthermore, the presence of CHO may favorably affect the mechanism and efficiency of DDS internalization and ultimately enhance drug delivery. Combination with phospholipids may result in more ordered packing of the phospholipid chains and consequently a more rigid liposomal/NLB membrane (Zalba *et al.*, 2012). Moreover, the presence of CHO may reduce activation of the complement pathway of the immune system, thereby enhancing retention of the NLB *in vivo* (Vonarbourg *et al.* 2006). Incorporation of CHO into liposomal structures contributed to decreased aggregation of liposomes and preservation of the size characteristics when exposed to serum, which could favorably impact the *in vivo* stability and biodistribution of passively targeted nanostructures (Zalba *et al.*, 2012). Tardi and co-workers (2007) demonstrated the versatility of CHO combined with phospholipids in the formulation of liposomes by tailoring the ratios of these components to maximally encapsulate two antineoplastic agents as well as co-ordinate their release *in vivo* (Tardi *et al.*, 2007). Suzuki and co-workers (2008) established the applicability of CHO in liposomes exhibiting active and passive targeting to tumour tissue (Suzuki *et al.*, 2008).

3.2.1.1.4 Coconut oil

Coconut oil is a vegetable oil, constituted primarily of capric acid and lauric acid (Wang *et al.*, 2006). Vegetable oils are widely considered safe for intravenous use, with coconut oil in particular being a source of essential medium-chain fatty acids employed in parenteral

nutrition (Tamilvanan, 2009). The addition of coconut oil to formulations has resulted in exceptionally high drug encapsulation efficiency of antineoplastic drugs and phytochemicals (Fang *et al.*, 2007). Fang and co-workers also demonstrated a significant retardation in drug release with increasing concentrations of coconut oil in formulated lipospheres (Fang *et al.*, 2007). Moreover, the addition of oil components such as coconut oil to intravenous formulations has been associated with reduced hemolytic activity (Fang *et al.*, 2007).

3.2.1.2 The model drug: Camptothecin

Camptothecin (CPT) is a naturally occurring plant indole alkaloid with a highly unsaturated pentacyclic ring structure, initially isolated in 1966 from the bark of the Chinese tree *Camptotheca accuminata* (van Hengel *et al.*, 1992; Hatefi and Amsden, 2002; Ishii *et al.*, 2004; Liu *et al.*, 2009). The cellular target of CPT is DNA topoisomerase I, an enzyme vital to the process of DNA replication (Yurkovetskiy and Fram, 2009). The double helical structure of DNA causes supercoiling during the transcription, replication and repair processes, which is counter-productive to these processes and can damage the DNA strands. Topoisomerase I transiently severs the phosphate backbone of DNA and forms a cleavable complex with DNA, thereby relieving the torsional stress caused by supercoiling and enabling effective transcription. The enzyme is subsequently cleaved and the severed DNA strand is annealed. However, the binding of CPT to topoisomerase I stabilizes the enzyme-DNA complex, inhibiting cleavage of the enzyme and ultimately arresting DNA replication (Lee *et al.*, 2009; Yurkovetskiy and Fram, 2009). CPT activity is thus more pronounced at the S-phase of the cell cycle.

The potent antineoplastic activity of the drug has found application against a wide spectrum of solid tumours, including small cell lung cancer, cervical, colorectal, and ovarian tumours (Hatefi and Amsden, 2002; Koo *et al.*, 2005; Lee *et al.*, 2009; Liu *et al.*, 2009; Jó *et al.*, 2010). Native CPT, however, displays very poor aqueous solubility (~2µg/mL) as well as poor solubility in most organic solvents, which poses an initial challenge with regards to pharmaceutical formulation and administration (Hatefi and Amsden, 2002; Liu *et al.*, 2009, Martins *et al.*, 2012). Additionally the high degree of protein binding *in vivo* compromises the achievement of therapeutically significant levels of CPT at the site of action (Yurkovetskiy and Fram, 2009). Furthermore CPT displays a short half-life approximating 1 hour in PBS (pH 7.4), which can be extrapolated to *in vivo* conditions (Kang *et al.*, 2002). Moreover, CPT exhibits a deleterious side-effect profile as well as physiological instability (Jó *et al.*, 2010). Hence, the challenge to successfully employ this potent drug clinically is a significant yet relevant one, in an era where ovarian

cancer and other solid tumours are responsible for significant morbidity and mortality globally.

Structure-activity relationship studies have highlighted an active lactone group which is responsible for the insolubility and physiologically-labile properties of CPT, yet crucial to its antineoplastic activity (Hatefi and Amsden, 2002). At and above physiological pH, ring-opening of this lactone group occurs, resulting in reversible conversion to an inactive carboxylate form as illustrated in Figure 3.2 (Hatefi and Amsden, 2002). This compromises the bioavailability of the active lactone form. Moreover, human serum albumin (HSA) has a particular affinity for the carboxylate form of CPT. Binding to HSA unfavorably affects the lactone-carboxylate equilibrium, further compromising the bioavailability of the active lactone form of CPT (Liu *et al.*, 2009). Thus an essential consideration in the development of DDS for successful CPT delivery is preservation of the lactone form of CPT from hydrolytic and pH-dependant degradation.

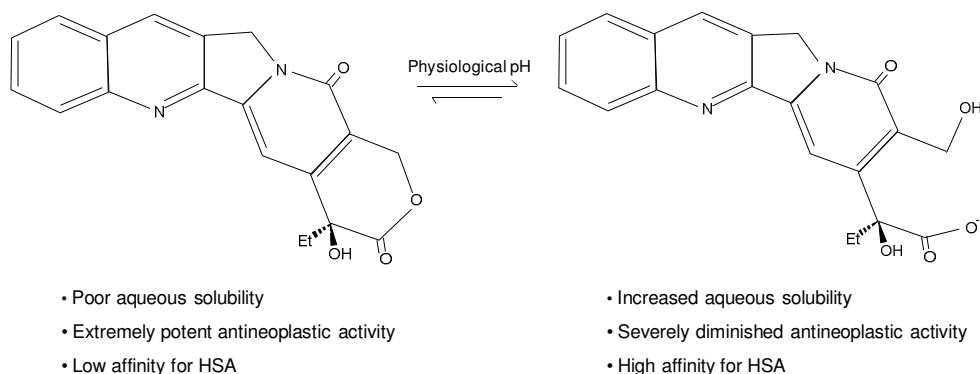


Figure 3.2 Structural illustration of the reversible chemical degradation of CPT from the active lactone form to the poorly active carboxylate form, under physiological conditions.

3.2.1.3 Emulsifiers/Surfactants

The inclusion of an emulsifier/surfactant was critical in the formulation of a stable NLB-DDS since the shape and size of the intended DDS is influenced largely by surface tension characteristics, which can be modulated by the inclusion of surfactants (Pilkington and Briscoe, 2012). Stability of the initial emulsion prepared, as outlined later in Section 3.3.2.2, is dependent on adequate interaction between aqueous and organic phases and is a significant contributor to the desired properties of the final formulation. The inclusion of a surfactant reduces the surface tension which was significant in the facilitation of particle partitioning during the ultrasonication processes outlined below in Sections 3.3.2.1 and 3.3.2.2, thereby reducing the size of formulated nano-liposomes (NLS) and subsequently NLB. The merits of employing ionic and non-ionic surfactants, and their effect on the ultimate surface charge of formulations, have been widely explicated in the literature, with respect to physical stability and size of formulations, effects of the

physiological environment, cellular adsorption, cellular internalization, and haemocompatibility. Hence, this study investigates the inclusion of non-ionic and ionic surfactants, the properties of which are outlined in Table 3.1, in formulating the NLB-DDS.

3.2.1.3.1 Non-ionic Surfactants: Tween 80™ and Span 80™

Tween 80™, from the polysorbate group of surfactants, is a non-ionic surfactant commonly employed in the food and pharmaceutical industries due to its low cost and excessive tolerability (Simões *et al.*, 2005; Wang *et al.*, 2008; Weiszár *et al.*, 2012). Tween 80™ is the foremost surfactant used in FDA-approved parenteral formulations (Alvarez-Núñez and Yalkowsky, 2000; Weiszár *et al.*, 2012). Pharmaceutically, the wide ranging applications of Tween 80 include stabilization of formulations such as liposomes, emulsions and micelles, enhancing oral drug absorption and skin permeation of topical preparations as well as protein delivery (Simões *et al.*, 2005; Wang *et al.*, 2008).

Span 80, sorbitan monooleate, is a low HLB, biodegradable, sorbitan ester derived from sugars and vegetable oils. Span 80 has proven highly effective in the production of water-in-oil emulsions as well as a dispersion and wetting agent (Kumar and Rajeshwarrao, 2011). However, combination with polysorbates enables tailoring of emulsification properties for the formulation of oil-in-water or double emulsion systems. This lipophilic compound is routinely employed as a food additive, as well as in the cosmetic and pharmaceutical industries, due to the safety profile and easily accessible nature (Kumar and Rajeshwarrao, 2011).

3.2.1.3.2 Ionic surfactant: Dioctyl sulfosuccinate

As an anionic surfactant, the incorporation of dioctyl sulfosuccinate, (DOS) has the capacity to provide electrostatic stabilization of the intended NLB-DDS against agglomeration (Cerqueira *et al.*, 2010; George and Ghosh, 2013). DOS has demonstrated stability in neutral as well as acidic medium (Dai *et al.*, 2010). Contrasting results have been reported on the adsorption of cationic and anionic molecules to cellular membranes. The larger anionic domains present on cellular surfaces dictates an electrostatic repulsion to anionic molecules. However, some studies have reported the non-specific adsorption of anionic DDS's, and enhanced cellular internalization, which was attributed to reduced tendency of anionic molecules for opsonization (Wilhelm *et al.*, 2003; Xiao *et al.*, 2011). Use of surfactants in parenteral dosage forms is subject to stringent control. Negatively charged nanosystems have demonstrated haemocompatibility following intravenous administration, whilst a dose-dependent hemolysis has been observed for cationic DDS's.

Table 3.1 Tabulated summary of the properties of surfactants investigated.

Surfactant	Molecular Weight	HLB	Solubility
Tween 80™	1310	15	Freely soluble in water
Span 80™	428.61	4.3	Insoluble in cold water. Soluble in organic solvents, mineral and vegetable oils
DOS	444.56	10.2	Soluble in water and less polar solvents

3.3 Materials and Methods

3.3.1 Materials

Camptothecin (CPT) ($\geq 90\%$; Mw=348.35), 1,2-distearoyl-sn-glycero-3-phosphocholine (DSPC) ($\geq 99\%$ purity; Mw=790.15), L- α -distearoylphosphatidylethanolamine-methoxy-polyethylene glycol conjugate (DSPE-m-PEG) ($\geq 98\%$; Mw=2748.1), cholesterol (CHO) ($\geq 99\%$ purity, Mw=386.65), dioctyl sulfosuccinate sodium salt (DOS) ($\geq 99\%$ purity; Mw=444.56), polysorbate 80 (Tween 80™) and sorbitan monooleate (Span 80™) were procured from Sigma Chemical Company (St Louis, MO, USA). Dimethyl sulphoxide (DMSO) was purchased from Merck Chemicals. Coconut oil was of BP grade and obtained from a pharmacy. Millipore filters (pore size=0.22 μ m) were procured from Micro Filtration cc. (KZN, South Africa). De-ionized water was obtained from a Milli-Q water purification system (Milli-Q, Millipore, Billerica, MA, USA). Chloroform, methanol, buffer salts and all other reagents were of analytical grade and used without further modification. In addition, all A-grade glassware was employed in the preparation and analyses of formulations.

3.3.2 Methods

A step-wise approach was adopted in the preparation of drug-loaded NLB. Since NLS are a formulation precursor to NLB, two methods of nano-liposomal preparation were initially investigated, namely the Film Hydration Method (FHM) and a modified Reverse Phase Solvent Evaporation Method (RPSE). Following delineation of the most suitable method, NLS were initially formulated employing the various materials outlined in Section 3.2.1 to identify suitable independent variables and the maxima and minima parameters for each variable. These parameters were central to the generation of an experimental design. The NLS of this design were prepared and further characterized for optimization. Gas incorporation was performed on optimized NLS formulations, to formulate NLB. These optimized NLB were subsequently subjected to physicochemical and physicomachanical characterization. In addition, the feasibility of further modifications such as polymeric coating and phytochemical incorporation were investigated on the NLB-DDS, with further characterization ensuing. All formulations were prepared and analyzed in triplicate (n=3).

3.3.2.1 Preparation of Nano-liposomes by the film hydration method

The FH method is perhaps the most widely employed method in the formulation of liposomes, as has been described extensively in the literature (Sadzuka *et al.*, 2002; Lesoin *et al.*, 2011; Sakai *et al.*, 2008; Zalba *et al.*, 2012). Briefly, varying quantities and combinations of synthetic phospholipids, CHO and coconut oil were simultaneously dissolved in a chloroform:methanol (9:1; 10mL) solvent system under constant agitation employing a magnetic stirrer. CPT was then added to the solution, under continued stirring. This organic solution was subjected to rotary evaporation (Multivapor™, Buchi Labortechnik AG, Switzerland) under vacuum at 60°C-65°C, until the formation of a uniform thin lipid film. The film was maintained under a fume hood overnight to ensure complete evaporation of organic solvents. The lipid film so formed was subsequently hydrated with phosphate buffered saline (PBS) (pH 7.4; 25°C) with the incorporation of a surfactant under ultrasonication employing a Vibracell probe ultrasonicator (Sonics and Materials Inc., Newtown, CT, USA). The resultant NLS suspension was subjected to three cycles of freezing (at -70°C) and thawing (at 37°C), to convert multilamellar NLS to unilamellar NLS with filtration through 0.22µm millipore filters after each freeze-thaw cycle. All analyses were undertaken in triplicate (n=3)

3.3.2.2. Preparation of Nano-liposomes by the reverse phase solvent evaporation method

NLS formulations were formulated by an adapted reverse-phase solvent evaporation method, as described elsewhere (Cortesi *et al.*, 2002; Guinedi *et al.*, 2005; Mertins *et al.*, 2005; du Toit *et al.*, 2011; García-Jimeno *et al.*, 2011; Zalba *et al.*, 2012). Briefly, organic solutions of lipids and drug were prepared as outlined in section 3.3.2.1 (Preparation of NLS by the Film Hydration Method). PBS (pH 7.4, 25°C; 10mL) and the relevant surfactant were subsequently added to the organic solution under ultra-sonication (Amplitude=80%; 90 seconds), over an ice-bath, employing a Vibracell probe ultrasonicator (Sonics & Materials Inc, Newtown, CT, USA). This culminated in the formation of a stable emulsion which was subsequently subjected to evaporation under vacuum (60-65°C) for 2-3 hours, employing a Multivapor™ (Buchi Labortechnik AG, Switzerland). PBS (pH 7.4, 25°C; 5mL) was then added periodically during the evaporation process and the formulation was subjected to ultra-sonication as previously outlined for 30 seconds, following each addition. Complete evaporation of the solvent resulted in an aqueous NLS suspension. The resultant NLS suspension was subjected to three cycles of freezing (at -70°C) and thawing (at 37°C), to convert multilamellar NLS to unilamellar NLS with filtration through 0.22µm millipore filters after each freeze-thaw cycle. All ensuing modifications and analyses were conducted on these unilamellar NLS.

In both methods described above (Sections 3.3.2.1 and 3.3.2.2) preset rotary evaporation parameters were maintained, as outlined in Table 3.2.

Table 3.2 Fixed conditions of rotary evaporation undertaken in the formation of NLS

Parameter:	Setting:
Temperature	60°C-65°C
Heating Medium	Water
Rotational speed setting	5
Pressure	~360mBar
Evaporation time	2-3 hours

3.3.2.3 Morphological characterization of nano-liposomal formulations

The shape of formulated NLS was confirmed by Transmission Electron Microscopy (TEM). Briefly, formvar-coated copper grids were coated with the nano-liposomal suspension, employing a micro-pipette and allowed to dry for approximately one hour. The grids were then inserted into the loading chamber of a Transmission Electron Microscope (TEM-100S, Jeol Ltd., Japan). TEM employs energized electron beams to produce high resolution images at significantly high magnifications, which is essential in the imaging of nanostructures. Photomicrographs were obtained at different magnifications to illustrate the structure of individual NLS.

3.3.2.4 Construction of a standard curve for the photospectroscopic quantification of camptothecin

Due to the solubility characteristics of CPT, serial dilutions of CPT were prepared in DMSO:PBS (pH7.4; 37°C) (1:1). A stock solution of CPT (3mg) in DMSO (200mL) was prepared. Dilutions were prepared as outlined in Table 3.3. Following a UV wave-scan to determine the optimal wavelength for CPT detection, vortexed aliquots of the above serial dilutions were analyzed at the appropriate wavelength, employing a Cecil CE 3021 spectrophotometer (Cecil Instruments Ltd., Milton, Cambridge, UK). Analyses were undertaken in triplicate on two consecutive days to determine the reproducibility of results.

Table 3.3 Serial dilutions of CPT in DMSO:PBS (pH 7.4; 37°C) (1:1) for the construction of a standard curve

Dilution	Stock Solution (mL)	DMSO (mL)	PBS (mL)
1	1	4	5
2	2	3	5
3	3	2	5
4	4	1	5
5	5	0	5

3.3.2.5 Determining favorable camptothecin loading

The substantial cost of antineoplastic drugs dictates the relevance of attaining a balance between achieving maximal drug loading and minimizing drug wastage. Moreover, the quantity of CPT added to all formulations should remain constant. Therefore establishing the most suitable quantity of CPT to be added to formulations was an initial consideration. An investigation of increasing quantities of CPT between 3mg to 10mg, determined suitable from previous studies, was added to the formulation, and the resulting drug incorporation was determined on several preliminary formulations (Hatefi *et al.*, 2004; Fang *et al.*, 2009; Liu *et al.*, 2009).

The efficiency of drug incorporation into the DDS was determined by a novel method derived for this DDS. The NLS formulated by both methods described in sections 3.3.2.1 and 3.3.2.2 were ultimately suspended in an aqueous phase. Hence, it was hypothesized that the NLS would orientate with the non-polar group of the phospholipids directed inward in the liposomal bi-layer of the NLS and the polar head group directed outwards, towards the aqueous suspending medium. CPT will therefore either be incorporated within the NLS bi-layer, or will precipitate out. Unincorporated drug, due to insolubility in the suspending medium, will be present primarily as a precipitate. Therefore, it was rationalized that the unincorporated precipitated drug could be removed by double filtration through a 0.22µm filter.

Formulated NLS suspensions were double filtered through 0.22µm filters to remove free drug. The filtrate was subsequently sonicated (Amplitude = 80%, 5 minutes) and, thereafter, dissolved in DMSO (1:1) to prevent precipitation of CPT. Drug incorporation efficiency was elucidated, in triplicate, by UV photospectroscopy with reference to a constructed standard curve of CPT in PBS (pH7.4; 37°C). Equation 3.1 was employed to determine the drug incorporation efficiency (DIE) as a percentage of the quantity of drug (CPT) incorporated into the NLS relative to the total quantity of drug (CPT) initially added during formulation:

$$\text{where, DIE (\%)} = \frac{\text{Quantity of incorporated drug}}{\text{Quantity of total drug added}} \times 100 \quad (\text{Equation 3.1})$$

Whilst a greater quantity of CPT (by weight) was determined to be incorporated in the NLS following the addition of 8mg-10mg CPT, the optimal drug incorporation efficiency was demonstrated for an initial CPT quantity of 5mg. All other formulation parameters remained constant during these investigations. Eight formulations (in triplicate) were employed during this study which were representative of all the initial materials investigated during pre-formulation studies. Henceforth, the quantity of CPT added to all formulations will be a fixed parameter (5mg).

3.3.2.6 Size and size distribution characterization of nano-liposomes

The aqueous NLS suspensions were analyzed for size and size distribution data employing a Zetasizer NanoZS (Malvern Instruments Ltd, Malvern, Worcestershire, UK). Samples were filtered through a 0.22 μ m filter into a suitable cuvette and analyzed by dynamic light scattering, enhanced by a non-invasive back scatter technology. Size and size distribution profiles were elucidated based on the diffusional velocity of particles in the sample by Brownian motion. Particle size is represented by the hydrodynamic diameter, calculated by application of the Stokes-Einstein equation (Equation 3.2):

$$d(H) = \frac{kT}{3\pi\eta D} \quad (\text{Equation 3.2})$$

where $d(H)$ represents the hydrodynamic diameter of the particle, k is the Boltzmann's constant, T represents the absolute temperature of the sample, η is the viscosity of the sample and D is the translational diffusion coefficient.

Measurements were derived from two different angles, thereby increasing accuracy of the measurements. All size measurements were conducted in triplicate at 37°C over a three hour period, whilst being maintained at 37°C in an orbital shaker bath (20rpm).

3.3.2.7 Investigating the influence of ultrasonication on the size characteristics of nano-liposomes

Initial investigations intimated the noteworthy effect of duration and amplitude of ultrasonication during the emulsification process in the RSPE method on the stability of resultant emulsions and size characteristics of NLS formulated. Ultrasonication undertaken during the hydration of films formed by the FH method appeared to be of equal relevance in terms of resultant NLS size and size distribution characteristics. The effect of a range of ultrasonic amplitudes (40-80%) and durations (1-10 minutes) was investigated to determine the ultrasonication conditions that achieved the optimum

balance between formulation stability and size characteristics of the formulation. Resultant emulsions were initially observed macroscopically to determine formulation stability as a function of phase separation of the emulsion. Stable formulations were characterized for size and size distribution patterns as outlined in Section 3.3.2.6.

3.4 Results and Discussion

3.4.1 Morphological analysis of nano-liposomes

Transmission electron microscopy proved to be a suitable means of imaging the intimate structure of the NLS and proved the formation of regular, consistent NLS as illustrated in Figure 3.3.

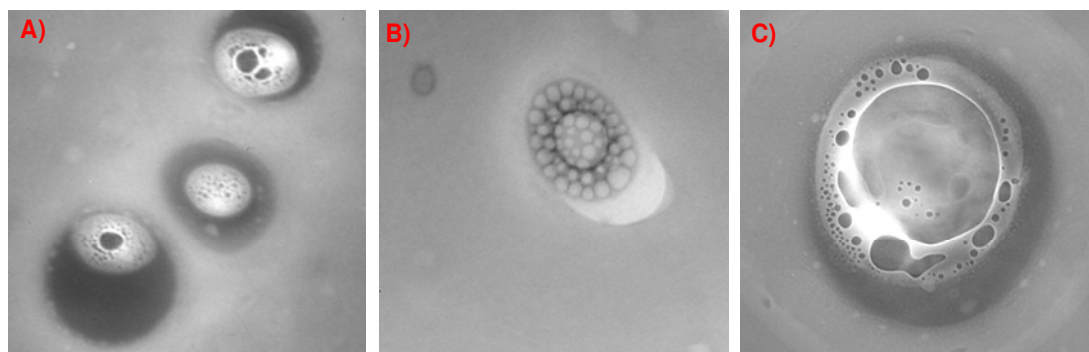


Figure 3.3 Transmission Electron Micrographs of NLS at A) 30000x magnification, B) 40000x magnification and C) 50000x magnification.

3.4.2 Generation of a standard curve for quantification of camptothecin

A UV wave-scan was initially performed between 250-600 nm to determine the optimum wavelength at which CPT was detected. The spectrum represented in Figure 3.4 highlighted 366 nm as the wavelength of maximal CPT detection, which was employed for the ensuing photospectroscopic quantification of CPT.

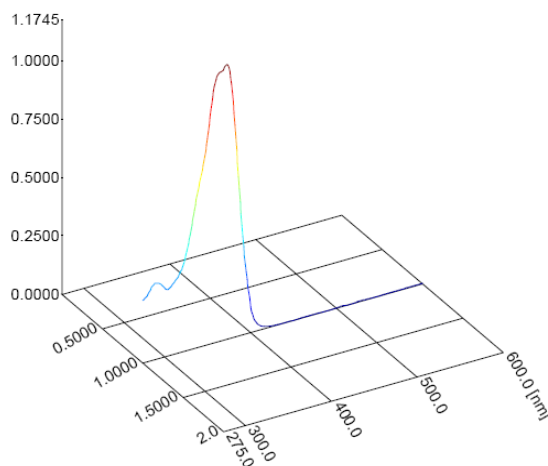


Figure 3.4 Three dimensional absorption spectrum of CPT in DMSO:PBS (pH 7.4; 37°C) (1:1)

Displayed in Figure 3.5 below is the calibration curve of CPT in DMSO:PBS (pH 7.4; 37°C) (1:1) at 366 nm, which was used for the quantification of CPT for DIE determinations, as well as the corresponding regression co-efficient and y-value. In addition 95% confidence and prediction bands are depicted. The standard deviation for each of the serial dilutions was <0.025 on the first day and <0.03 on the second day, confirming the precision of the instrument and the reproducibility of results.

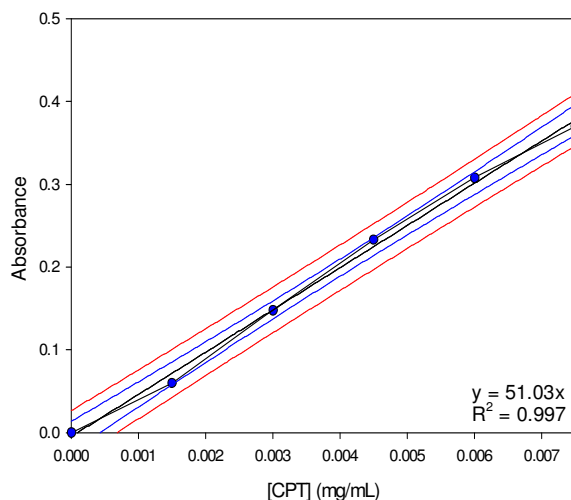


Figure 3.5 Standard curve of the absorbance of CPT in DMSO:PBS (pH 7.4; 37°C) (1:1), as well as 95% confidence and prediction bands (in all cases n=3 and SD<0.02).

3.4.3 Delineation of the most feasible method of nano-liposome preparation

The FH method, also known as the Bangham method, is perhaps the most widely used method of liposomal preparation. However, in this study the RPSE method proved most beneficial as it was less time consuming since samples did not require overnight evaporation. The most significant disparity, however, was noted in the DIE of formulations prepared by both methods. NLS formed by the RPSE method exhibited significantly higher (~15-20%) DIE than those formed by the FH method. This is congruent with results from other studies employing different drugs (Xia and Xu, 2005; Zhang *et al.*, 2012). The size distribution of NLS formed by the FH method also appeared to be greater than those formed by the RPSE method. However, this distinction was only marginally significant. Moreover, a principal aim of this study was the formulation of a clinically relevant DDS. With the consideration of taking this formulation from bench-top to bedside, it was concluded that a lyophilized powder that could be reconstituted as and when needed, would be the most feasible form of presenting this DDS. Employing the FH method would thus involve two drying steps (film formation and lyophilization) which makes for protracted preparation, in relation to the RPSE method. Consequent to the above-mentioned findings and considerations, the RPSE method was determined the preferred

method of NLS formulation and was the method used for fabrication of further NLS formulations.

3.4.4 Influence of ultrasonication on the properties of formulated nano-liposomes

Initially ultrasonication during the emulsification step of the RPSE method was undertaken for 5-10 minutes at amplitudes of 40-80%. However, most formulations were negatively affected as evidenced by the macroscopic examination of the formulations post-ultrasonication. The resultant emulsions separated rapidly, indicative of instability. Upon zeta sizing, large size distributions ($PDI > 0.5$) were observed. Radical shortening of the ultrasonication time as well as undertaking ultrasonication over an ice bath had a substantial effect on the stability of the formulation as well as the size and size distribution characteristics. However, decreasing sonication amplitude ($\leq 65\%$) resulted in marginally larger NLS. Extensive investigation in this respect culminated in the delineation of ultrasonication duration of 90 seconds initially, followed by 45 seconds following PBS addition in the RPSE method, at an amplitude of 80%.

A similar trend was observed in the influence of ultrasonication parameters during the hydration of lipid membranes formed by the FH method. An amplitude of 80% was determined feasible for successful NLS formation. Ultrasonication duration below 3 minutes resulted in NLS larger than 200 nm, whilst prolonged ultrasonication resulted in unstable formulations with high PDI values. Investigations culminated in the determination of 5 minutes as the most feasible duration of ultrasonication for the formulations under investigation.

3.4.5 Establishment of the influence of formulation variations on nanoliposomes characteristics for the selection of favorable parameters

The use of single lipids was ruled out early in the study, due to inconsistent, poorly reproducible NLS. A review of literature further highlighted the beneficial effects of combining lipids in achieving the desired characteristics of DDS's. Varying combinations of each of the four lipid phases, i.e. DSPC, DSPE-m-PEG, CHO and coconut oil produced NLS of vastly different characteristics. The combination of coconut oil with all other lipids proved unsuccessful, mainly due to large NLS size and wide size distribution, the likes of which were unsuited to the intended application of the DDS, as indicated in Figure 3.6 (A-D). Furthermore, the change in NLS size was measured over time, as a measure of NLS stability. Coconut oil-containing formulations exhibited drastic and inconsistent size changes over the analysis period. Fang and team (2007) also demonstrated an increase in size of formulated lipospheres with increasing coconut oil concentration. However their

observations were of more consistent, reproducible size increases. The increase in liposphere size with increasing coconut oil concentration in this study was attributed to smaller emulsifier-to-oil ratio, which is largely responsible for reducing interfacial tension (Fang *et al.*, 2007). Notably, the higher viscosity of coconut oil in comparison to the other formulatory components, which bear similarity to the materials used in the present study, resulted in higher viscosity of the emulsion preceding liposphere (and NLB) formation, and hence was identified as a contributor to increased liposphere size. The combinations of DSPC and CHO as well as DSPE-m-PEG and DSPC proved promising for the achievement of suitable NLS size and size distributions, which were the central focus of pre-formulation studies, due to the dependence of passive targeting efficacy on the nano-scale size range of the intended DDS. In addition NLS formulations employing both these lipid combinations displayed adequate DIE (>40%). However, it was observed that total lipid concentrations above 0.4%^{w/v} resulted in wider size distributions. This was postulated to result from the precipitation of lipid during the transition from organic to aqueous solvent phase. Therefore a total lipid concentration of 0.4%^{w/v} was a further fixed parameter maintained during NLS formulation.

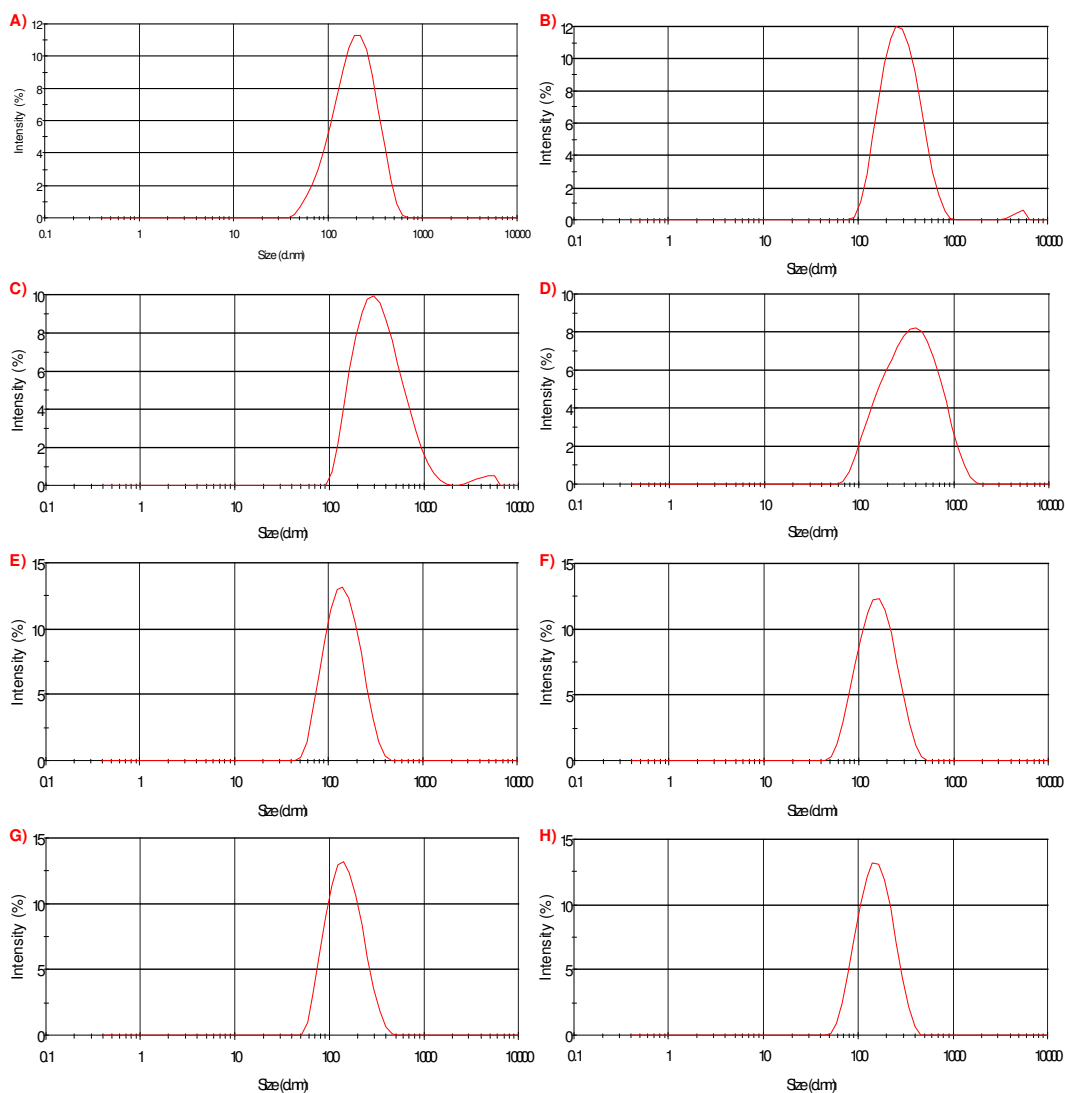


Figure 3.6 Typical Size/Intensity profiles for varying ratios of the following lipid combinations, DSPC-coconut oil NLS: **A** and **B**; CHO-coconut oil NLS: **C** and **D**; DSPC-CHO NLS **E** and **F**; DSPC-DSPE-m-PEG NLS **G** and **H**.

Variation in surfactants had a considerable influence on every aspect of NLS formulation. The addition of Tween 80TM and Span 80TM individually to formulations resulted in unstable emulsions that separated rapidly, produced NLS with large size distributions and poor reproducibility. This is analogous to the results achieved by Simões and co-workers (2005) in their investigations relating to the effect of Tween 80TM on model soybean phosphatidylcholine (SPC) bi-layer vesicles, where significant size inconsistency was observed (Simões *et al.*, 2005). Combining Tween 80TM and Span 80TM proved considerably beneficial, as was immediately apparent upon the achievement of a stable emulsion and adequate sizes approximating 160-217 nm. The addition of DOS resulted in appreciably stable formulations of a significantly smaller size range (125-145 nm) and narrow size distributions. In addition, formulations containing DOS demonstrated superior

DIE. These factors concluded in the selection of DOS as a qualitative fixed parameter for NLS formulation.

3.5 Concluding Remarks

The initial consideration of pre-formulation studies was the selection of the most advantageous method for NLS formulation with the considerations of formulation time, simplicity, NLS size and DIE. The RSPE method was deemed the most feasible method of NLS preparation for this study.

A thorough literature review culminated in the selection of suitable materials for investigation. Preliminary studies provided a framework for formulation variables to be chosen. The consistent, reproducible formulation of nanostructures can be affected by minute changes in several formulation parameters. It was thus essential to highlight the variations in methodology and formulation constituents that had significant effect on the measured outcomes and those which could be optimized and maintained during formulation. Hence, fixed formulation parameters were outlined so as to minimize the extent of formulation variables under investigation. Fixed method parameters included total phospholipid concentration, amplitude and time for ultrasonication, quantity of CPT added to the formulation and rotary evaporation conditions. The combinations of DSPC-CHO and DSPC-DSPE-m-PEG were highlighted as the main lipid components of the NLS. The relative ratios of these phospholipids were quantitative parameters the will be statistically optimized through the formulation of NLS variants of the experimental design. The ultimate selection of DOS as the surfactant was also a fixed parameter, however the concentration to be employed in the candidate formulations was a quantitative parameter that was subjected to statistical optimization, as outlined in Chapter 4.

CHAPTER 4

FORMULATION AND STATISTICAL OPTIMIZATION OF A CAMPTOTHECIN-LOADED INTRAVENOUS NANO-LIPOSOMAL DRUG DELIVERY SYSTEM

4.1 Introduction

The estimated average time from drug discovery to development and registration of a clinically relevant product spans over 10-12 years (Pien *et al.*, 2005; Amir-Aslani, 2008). The substantial risk of failure of new drug compounds is exceptionally costly and does not go unnoticed by pharmaceutical companies in their research endeavours. Studies demonstrate on average only 1 in 5000 compounds initially investigated will result in a pharmaceutically viable product (Curry, 2008). Maximizing profitability and return on the investment in R&D involves capitalization on the protection offered by patents during the 20 year lifespan of the patent. Extended developmental stages result in shorter marketable periods before expiration of the patent which may negatively impact profitability of the drug compound.

The formulation of a drug delivery system (DDS) that enhances the clinical usefulness of existing drug compounds has proven to be a shorter, less risky undertaking with the requirements for these DDS being less stringent than those for new drug molecules. The propagation of research and development demands substantial consideration and appreciation of the economic viability of this undertaking as industrial and governmental financial investment is a pivotal enabling factor in pharmaceutical research and development.

In general, the requirements for the intended DDS include (Petрак, 2005; Murday *et al.*, 2009):

- Biocompatibility and biodegradability of the formulated nano-lipobubble-DDS (NLB-DDS).
- Stability of the NLB-DDS under physiologic conditions.
- Ability of the NLB-DDS to reach the tumour tissue in order to increase the concentration of drug in target cells.
- Controlled release of the incorporated drug/s in accordance with the requirements of the drug being delivered, in order to maximize therapeutic efficacy of the drug/s.

- Prevention or minimization of the pharmacological action of camptothecin (CPT) at sites other than the target site so as to minimize the undesirable side-effects that have compromised the clinical viability of CPT.
- Resistance to premature degradation and immunologic reactions of CPT and the NLB-DDS.
- Rate of elimination < rate of delivery to tumour tissue site.
- Rate of CPT release at target site should result in sufficient drug concentration to exert its pharmacological action.

'Intelligent' DDS have been gaining momentum exponentially since inception of the concept, due to the therapeutic and financial advantages of these innovative DDS to patients and the pharmaceutical industry, respectively. The complexity of innovation of these specialized DDS has been accompanied by the influence of wide ranging experimental and formulation parameters that need to be evaluated and understood. With the growth of this competitive market, the need to obtain maximal and precise information by expending the least resources and time became a pivotal factor. Hence, the development of experimental designs has been a major advancement in the development of DDS. The application of an experimental design allows for the arrangement of investigations in a manner that maximizes the acquisition of relevant data in the most efficient manner, thereby reducing the materials and time involved in acquiring the information. The development of an experimental design requires firstly, an intimate understanding of the formulation and experimental variables that affect the formulation. Secondly, the measured outcomes that are pertinent to the specific DDS should be identified, as the effect of variables will be analyzed relative to the effect on measured outcomes. Moreover, the choice of experimental design chosen is dictated by the number and type of variables under investigation, since the confidence level of predicted responses may vary accordingly.

4.2 Statistical modeling employing a Face-Centered Central Composite Design

Following preliminary studies outlined in Chapter 3, independent variables were delineated, as well as the minima and maxima parameters of these independent variables. A two-factor three-level Face-Centered Central Composite Design (FC-CCD) was generated by Minitab[®], V15 (Minitab[®] Incorporated, PA, USA), for each of the two lipid combinations, i.e. an experimental design for the combination of DSPC-CHO and DSPC-DSPE-m-PEG. Central Composite Design (CCD) has proved to be a relevant and invaluable tool in pharmaceutical dosage design, particularly in the design of

nanoparticulate formulations (Hao *et al.*, 2012). Analysis of independent variables is undertaken at three levels, designated as -1; 0; and 1, which are equidistant from the center point creating a rotatable design.

The independent variables in each of the experimental designs generated were quantitative in nature. Table 4.1 outlines the three levels at which each independent variable was assessed. These levels are further illustrated in Figure 4.1. Each experimental design consisted of 13 experimental runs, the compositions of which are outlined in Tables 4.3 and 4.4. Generation of these experimental runs aims to minimize the number of formulations required to generate maximum significant information to enable prediction of the measured responses and statistically optimize the intended DDS.

Table 4.1 Summary of the minima and maxima of independent variables established from pre-formulation studies and the translation to three analyses levels employed in the experimental design.

Independent Variable	Levels		
	-1	0	1
Lipid Ratio (DSPC:CHO or DSPE)	1:3	2:2	3:1
DOS concentration	0.1% ^{w/v}	0.2% ^{w/v}	0.3% ^{w/v}

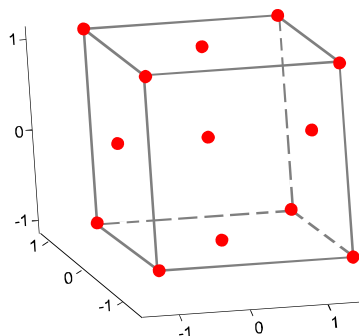


Figure 4.1 Schematic representation of the experimental runs designated at each of the three levels of the FC-CCD.

4.3 Determination of suitable measured responses

As previously stated, the nanometer size range is pivotal to the desired characteristics of this intravenous formulation. To achieve successful extravasation and accumulation within tumour tissue for effective passive targeting, an average size range below 160 nm was initially delineated for pre-formulation of the nano-liposomes (NLS). In addition, size distribution had to be controlled within a very narrow range. Polydispersity relates the standard deviation to the mean NLS size and is an indication of the size uniformity of formulated NLS. Hence, low polydispersity indices (PDI) denote high size uniformity of the

formulated NLS. A PDI ≤ 0.2 was considered favorable. Nano zeta-sizing was, therefore, defined as a pivotal measured response (dependent variable).

Ensuring formulation stability of intravenous DDS's, with particular regard to minimizing NLS aggregation, is an essential consideration during the fabrication process. Zeta potential is an indication of the surface charge of the formulated NLS and, as such, signifies the propensity of the NLS for aggregation. A highly charged (positive or negative) surface displays an aversion to NLS aggregation due to stronger electrostatic repulsive forces surmounting the attractive van der Waals forces, thereby having a stabilizing effect on the formulation. This concept was succinctly described by Derjaguin, Verwey, Landau and Overbeek in the DLVO theory. Formulation constituents can have a significant effect on zeta potential. Thus zeta potential was identified as a pertinent measured response.

The efficacy of a DDS is strongly associated with the concentration of drug at the site of action, which in turn is highly influenced by the quantity of drug initially incorporated into the DDS. The nanoscale of the proposed DDS may influence the capacity for drug incorporation into the DDS. However, the achievement of appreciably high concentrations of drug incorporated into the nano-DDS is central to the efficacy and viability of the proposed DDS. Low drug incorporation will necessitate the administration of larger quantities of the DDS in order to achieve therapeutically significant drug concentrations. This may limit the therapeutic, manufacturing, and financial benefits of the DDS. Therefore, drug incorporation efficiency (DIE) was denoted a critical response for evaluation during pre-formulation studies.

Lastly, the success of any DDS cannot be fully established without assessing drug release patterns. Drug release patterns provide an indication of undesirable premature drug release, as well as whether a therapeutically effective concentration of drug will be achievable at the site of action as a result of the release pattern of drug from the DDS. To this end, drug release, and subsequently mean dissolution time (MDT), was evaluated.

Table 4.2 presents the upper and lower limits of measured responses, as derived from pre-formulation studies, for each of the 2 experimental designs, as well as the objective in this study with respect to each of the measured responses.

Table 4.2 Delineation of the lower and upper limits of the chosen measured responses, and the objective for optimization with respect to each measured response.

Dependent Variable	Lower Limit	Upper Limit	Objective
DSPC/CHO-NLS			
Size (d.nm)	125	135	Minimize
Zeta Potential (mV)	-42	-32	Minimize
DIE (%)	65	75	Maximize
MDT (hours)	7.5	21	Maximize
DSPC/DSPE-NLS			
Size (d.nm)	85	95	Minimize
Zeta Potential (mV)	-8	-5	Minimize
DIE (%)	37	44	Maximize
MDT (hours)	7	18	Maximize

4.4 Materials and Methods

4.4.1 Materials

Camptothecin (CPT) ($\geq 90\%$; Mw=348.35), 1,2-distearoyl-sn-glycero-3-phosphocholine (DSPC) ($\geq 99\%$ purity; Mw=790.15), L- α -distearoylphosphatidylethanolamine-methoxy-polyethylene glycol conjugate (DSPE-m-PEG) ($\geq 98\%$; Mw=2748.1), cholesterol (CHO) ($\geq 99\%$ purity, Mw=386.65), dioctyl sulfosuccinate sodium salt (DOS) ($\geq 99\%$ purity; Mw=444.56), polysorbate 80 (Tween 80TM) and sorbitan monooleate (Span 80TM) were procured from Sigma Chemical Company (St Louis, MO, USA). Dimethyl sulphoxide (DMSO) was purchased from Merck Chemicals. Coconut oil was of BP grade and obtained from a pharmacy. Millipore filters (pore size=0.22 μ m) were procured from Micro Filtration cc. (KZN, South Africa). De-ionized water was obtained from a Milli-Q water purification system (Milli-Q, Millipore, Billerica, MA, USA). Chloroform, methanol, buffer salts and all other reagents were of analytical grade and used without further modification. In addition, all A-grade glassware was employed in the preparation and analyses of formulations.

4.4.2 Methods

4.4.2.1 Formulation of camptothecin-loaded nano-liposomes

Two sets of NLS formulations were prepared in accordance with the experimental designs generated, as previously discussed. The formulation components of these experimental designs are outlined in Tables 4.3 and 4.4, whilst the formulation parameters that were maintained across all formulations are outlined in Table 4.5. Henceforth, NLS from these two experimental designs will be referred to as CHO-NLS and DSPE-NLS, respectively, a reference to the major compositional difference distinguishing these two sets of experimental designs.

Table 4.3 Composition of formulations for each experimental run of the CHO-NLS experimental design

Experimental Run	Independent Variables		
	DSPC (% ^w / _v)	CHO (% ^w / _v)	DOS (% ^w / _v)
A1	0.2	0.2	0.1
A2	0.1	0.3	0.3
A3	0.2	0.2	0.2
A4	0.3	0.1	0.3
A5	0.1	0.3	0.2
A6	0.2	0.2	0.3
A7	0.3	0.1	0.1
A8	0.2	0.2	0.2
A9	0.3	0.1	0.2
A10	0.1	0.3	0.1
A11	0.2	0.2	0.2
A12	0.2	0.2	0.2
A13	0.2	0.2	0.2

Table 4.4 Composition of formulations for each experimental run of the DSPE-NLS experimental design.

Experimental Run	Independent Variables		
	DSPC (% ^w / _v)	DSPE (% ^w / _v)	DOS (% ^w / _v)
B1	0.1	0.3	0.1
B2	0.2	0.2	0.3
B3	0.2	0.2	0.2
B4	0.2	0.2	0.1
B5	0.2	0.2	0.2
B6	0.1	0.3	0.3
B7	0.1	0.3	0.2
B8	0.2	0.2	0.2
B9	0.3	0.1	0.3
B10	0.2	0.2	0.2
B11	0.3	0.1	0.1
B12	0.2	0.2	0.2
B13	0.3	0.1	0.2

Table 4.5 Fixed formulation parameters maintained during the preparation of NLS.

Fixed Formulation Parameters	
CPT concentration	0.05% ^{w/v}
Total initial lipid concentration	0.4% ^{w/v}
Solvent system	chloroform:methanol (9:1)
Evaporation temperature	60-65 °C
Ultrasonication amplitude	80

4.4.2.2 Determination of the size, size distribution and surface charge characteristics of formulated nano-liposomes

Size and size distribution characterization was undertaken as previously described in Chapter 3, Section 3.3.2.6. Zeta potential of the NLS suspensions were also analyzed employing the Zetasizer NanoZS (Malvern Instruments Ltd, Malvern, Worcestershire, UK). Briefly, this system employs a laser doppler micro-electrophoresis technique to determine the velocity of the particles in the sample in response to an applied electric field. This enables the elucidation of electrophoretic mobility and consequently zeta potential of the sample. As outlined above, all zeta potential measurements were conducted in triplicate at 25 °C over a three hour period, whilst the sample was maintained at 37 °C in an orbital shaker bath (20rpm).

4.4.2.3 Elucidation of camptothecin incorporation efficiency

Systematic investigation of the efficiency of CPT incorporation of the formulations in each of the two experimental designs was conducted as detailed in Chapter 3, Section 3.3.2.5. Briefly, the formulated NLS suspended in phosphate buffered saline (PBS) was double filtered through 0.22µm filters to remove unincorporated CPT. Ultrasonication was employed to breakdown the NLS, followed by the addition of DMSO to the NLS suspension (1:1) to dissolve the hydrophobic drug. Elucidation of DIE ensued in triplicate by UV spectroscopy with reference to the previously generated standard curve of CPT in DMSO:PBS (pH 7.4; 37 °C) (1:1).

4.4.2.4 *In vitro* camptothecin release analysis

Following removal of free drug from the NLS suspension, 5mL samples were enclosed in treated dialysis tubing (Mw cut-off=12000Da) and suspended in PBS (pH 7.4; 37 °C; 500mL). The receptacle was maintained at 37 °C in an orbital shaker bath rotating at 20rpm. At pre-determined intervals, 5mL aliquots were removed from the external PBS phase and added to DMSO (5mL), creating a 1:1 ratio, to prevent precipitation of the drug. Fresh buffer (5mL) was replaced to the external phase to maintain sink conditions.

Vortexed samples were analyzed by UV spectroscopy at 366nm, against previously constructed standard curves of CPT in DMSO:PBS (pH7.4; 37 °C) (1:1).

4.4.2.5 Micro-ultrasound imaging of formulated nano-liposomes

In addition to the aforementioned TEM imaging technique described in Chapter 3, micro-ultrasound imaging employing a Vevo[®] 2100 (Visualsonics, Toronto, Ontario, Canada) was employed to confirm the overall appearance of the NLS. This technique, further, highlights behavioral characteristics such as aggregation of the NLS, which is a vital indicator of stability. A 10%^{w/v} carrageenan hydrogel was prepared, onto which ultrasound gel was applied. The NLS were injected into the hydrogel and an ultra-sound beam was applied, producing images of the NLS as they dispersed through the hydrogel.

4.5 Results and Discussion

In an attempt to facilitate understanding of the data obtained and the mathematical modeling thereof, the experimental results will initially be simultaneously represented for both experimental designs. The ensuing sections, presenting the process of mathematical modeling and statistical optimization of the NLS formulations, will be divided into CHO-NLS and DSPE-NLS.

4.5.1 Experimental results

4.5.1.1 Size and size distribution analysis of fabricated nano-liposomes

As previously outlined, the benefits of the DDS presented rely largely on the nano-scale size of the NLS. The nano-size scale will be principally responsible for the passively targeted nature of the DDS and the efficiency thereof. Furthermore, nano-sizing enables the solubilization of poorly aqueous soluble antineoplastic drugs, such as the model drug CPT. Hence, assessment of NLS size was fundamental in this study. A benchmark size of 160 nm was established. Figure 4.2 typifies the size-intensity profiles obtained for the smallest and largest NLS from each design. The experimental size data for CHO-NLS and DSPE-NLS is represented in Table 4.6, along with the PDI for each experimental run.

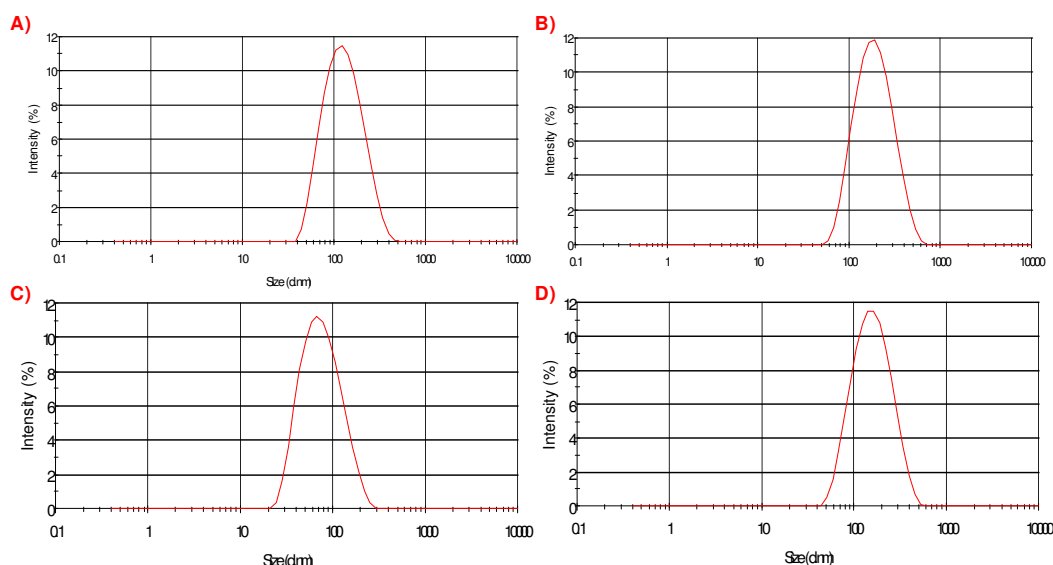


Figure 4.2 Typical size profiles representing CHO-NLS at the minimal (A) and maximal (B) presenting sizes and DSPE-NLS at the minimal (C) and maximal (D) presenting sizes.

Table 4.6 Tabulated representation of the average size of NLS for each of the two experimental designs

CHO-NLS	Average Size (d.nm)	Average Pdl	DSPE-NLS	Average Size (d.nm)	Average Pdl
A1	162.79	0.223	B1	89.75	0.265
A2	125.06	0.167	B2	80.24	0.166
A3	144.88	0.197	B3	94.59	0.173
A4	132.88	0.136	B4	100.86	0.202
A5	120.04	0.200	B5	94.59	0.173
A6	118.53	0.147	B6	100.36	0.187
A7	131.31	0.212	B7	92.61	0.214
A8	144.88	0.197	B8	94.59	0.173
A9	142.95	0.185	B9	72.14	0.154
A10	137.13	0.215	B10	94.59	0.173
A11	144.88	0.197	B11	136.2	0.251
A12	144.88	0.197	B12	94.59	0.173
A13	144.88	0.197	B13	144.1	0.198

All formulations fell within the desired size range. The foremost contributor to size variations between the various formulations was concentration of DOS. Higher concentrations of DOS resulted in a reduction of NLS size as well as a narrower size distribution, indicated by the lower Pdl. In addition, CHO-containing NLS formulations were generally of a larger size than DSPE-containing NLS formulations, as indicated in Figure 4.2 and Table 4.6. This was attributed to firstly, the bulkiness on the CHO molecule and secondly, the lateral stabilization mechanism of DSPE. Moreover, strong hydrogen

bonding and electrostatic interaction exists between the head groups of PE molecules, creating reduced volume in the region of the head group (Borba *et al.*, 2009).

4.5.1.2 Surface charge characterization of formulated nano-liposomes

Zeta potential is an indication of the surface charge of the NLS formulated, and hence the propensity of these NLS for aggregation. Zeta potential is thus considered a suitable indicator of formulation stability. All NLS formulations displayed negative zeta potential, which may be attributed to the anionic nature of the surfactant (DOS). This observation was corroborated with the evident favorable decrease in zeta potential with increasing concentration of DOS, whilst all other formulatory components remained the same, as illustrated in Figure 4.3.

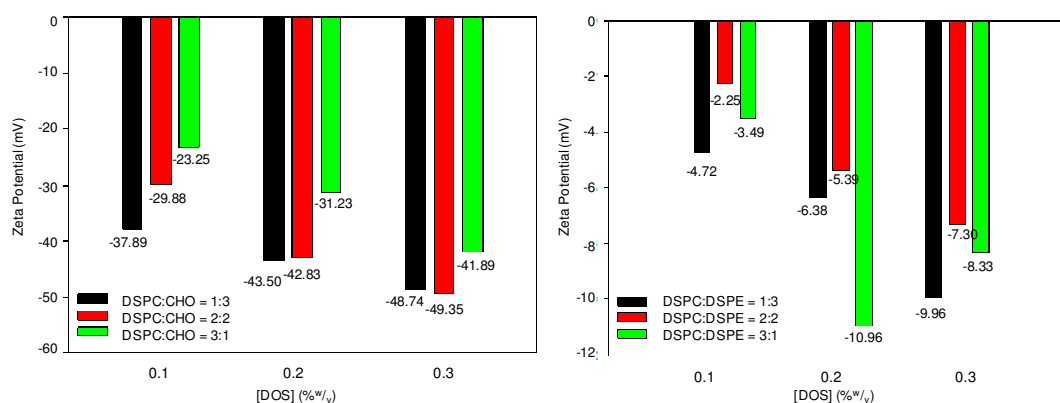


Figure 4.3 Graphical illustration of the relationship between [DOS] and zeta potential. Each set of bars represents formulations containing a particular [DOS].

However, a significant difference was noted between DSPE- and CHO-containing formulations. NLS formulated from the combination of DSPE and CHO exhibited significantly more strongly negative zeta potentials compared to NLS formulated from DSPE and DSPE combinations (~-45mV and ~-7mV respectively). CHO has an enormous stabilizing effect on phospholipid bilayers, being cited for creating a more organized arrangement of acyl chains on phospholipids as well as tighter packing of atoms in the hydrophobic core (Róg and Pasenkiewicz-Gierula, 2006;). Xia and Xu (2005) observed similar effects on the zeta potential of liposomes following the incorporation of CHO. This favorable effect on the zeta potential was also attributed to the interaction between the hydroxyl group on CHO and the choline group present in the phospholipid (Xia and Xu, 2005).

4.5.1.3 Quantification of camptothecin incorporation efficiency

The achievement of adequately high levels of drug incorporation into nano-enabled drug delivery systems is particularly challenging due to the nano-scale size range of these DDS. Table 4.7 provides a comprehensive view of the DIE determined for formulations in each of the two experimental designs, arranged so as to facilitate an understanding of the effect of independent variables on the DIE.

Table 4.7 Tabulation of the DIE percentages obtained for formulations in Designs 1 and 2, highlighting the significant distinction between CHO- and DSPE-NLS.

DSPC (% ^{w/v})	CHO (% ^{w/v})	DSPE (% ^{w/v})	DOS (% ^{w/v})	DIE (%)
			0.1	55.50
	0.3		0.2	62.79
0.1			0.3	64.42
		0.3	0.1	28.45
			0.2	32.46
			0.3	76.31
	0.2		0.1	39.21
			0.2	62.59
0.2			0.3	75.84
		0.2	0.1	37.95
			0.2	36.72
			0.3	37.02
	0.1		0.1	60.94
			0.2	64.85
0.3			0.3	81.47
		0.1	0.1	28.35
			0.2	44.19
			0.3	43.16

DSPC:CHO NLS demonstrated favorably high DIE, with all, except two, formulations displaying DIE>60%. The maximum reproducible DIE achieved was 81.47%. DSPE-NLS exhibited DIE ranging between 28%-45%, with only one formulation displaying a DIE of 76.31%. Reproducibility of DIE presented a challenge, particularly with regards to DSPE-NLS. The bulky nature of the CHO molecule, as opposed to the di-branched appearance of the DSPE molecule, resulted in the formation of larger NLS, thereby allowing more generous accommodation of CPT. Increasing DOS concentration within each phospholipid ratio resulted in increasing DIE for CHO-NLS. This effect could be attributed to the stabilizing effect of DOS on the NLS.

4.5.1.4 Assessment of the release characteristics of camptothecin from nano-liposomes

The achievement of adequate passive targeting of the DDS to tumour tissue was a fundamental objective in this study. Ideally, a formulation exhibiting a favorable stability profile coupled with a reduced rate of drug release from the DDS has the potential to extensively enhance the preferential accumulation of drug within tumour tissue, thereby reducing the adverse effects associated with non-specific distribution of antineoplastic drugs. Since CPT acts on the S-phase of the cell cycle, prolonged release of CPT will be particularly beneficial, enabling CPT to exert its antineoplastic effect on a greater proportion of tumor cells. The half-life of CPT in PBS was determined to approximate 1 hour (Kang *et al.*, 2002). Extension of this half-life is fundamental to improving the pharmacokinetic properties of CPT.

The fractional drug release profiles of CHO-NLS in Figure 4.4, illustrate a somewhat bi-phasic pattern of CPT release across all formulations. CPT release over the first 6 hours of analysis was generally slightly faster than that over the next 18 hours, as demonstrated by the steeper gradient of the curve over this initial period. The absence of a significant burst release of CPT suggests adequate incorporation of the drug into the NLS-DDS, with no surface adsorption. This characteristic is particularly beneficial with regards to intravenously administered formulations, indicating minimal drug will be released in the systemic circulation prior to accumulation within the target tissue. Formulation as CHO-NLS resulted in a prolongation of the half-life of CPT to approximately 4 hours. Cumulative drug release from CHO-NLS over the course of the 24 hour analysis period was between 70%-100%. Quantification of drug release was undertaken by determination of the MDT of each experimental run. The calculated MDT's extended over quite a large range, from 7.5-21. Formulations A1 and A6 exhibited the shortest and longest MDT, respectively. Formulation A10 appeared to be somewhat of an outlier when the pattern of fractional drug release was observed graphically. However, the MDT was almost a midpoint value in the range of MDT values obtained for this experimental design.

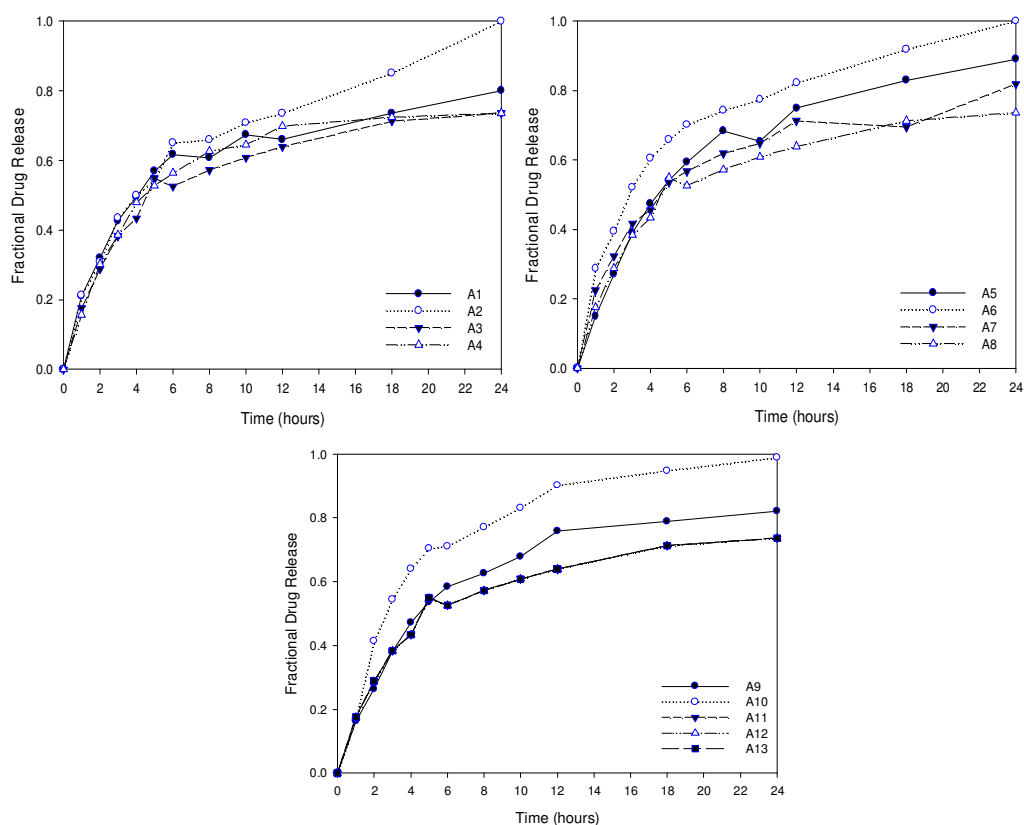


Figure 4.4 Fractional drug release profiles for CHO-NLS in PBS (pH 7.4; 37°C) (Design 1) undertaken over a 24 hour period (in all cases n=3 and SD \leq 0.03).

The observed fractional drug release patterns for DSPE-NLS, presented in Figure 4.5, were more erratic than that observed for CHO-NLS. In general, drug release in the first hour of analysis was noticeably more rapid, relative to that of CHO-NLS, suggestive of a slight burst release. This burst release was attributed to association of CPT with the outer membrane of the NLS, perhaps through association with PEG. All formulations in this experimental design demonstrated >90% release of CPT within the 24 hours analysis period, with maximal drug release being observed at approximately 18 hours for a large proportion of the formulations. The faster rate of CPT release observed could be related to the poor stability of DSPE-NLS, indicated by the mildly negative zeta potential. Formulation as DSPE-NLS did not exhibit a significant increase in the half-life of CPT. The MDT's established from this experimental design was of a narrower range than that of the CHO-NLS, with the exception of formulation B6 which was somewhat of an outlying value. The shortest and longest MDT was exhibited by formulations B11 and B6, respectively. Interestingly, formulation B11 also demonstrated the largest average size of NLS in this experimental design, as well as the most unfavorable zeta potential. Formulation B6 had the highest DIE, which may have impacted the concentration of CPT released from the NLS and consequently the MDT. Formulations with a higher DSPE concentration (B1, B6, B7) produced very similar and consistent patterns of drug release. This was attributed to

the stabilization afforded to the formulations by the increased concentration of PEG associated with DSPE molecules.

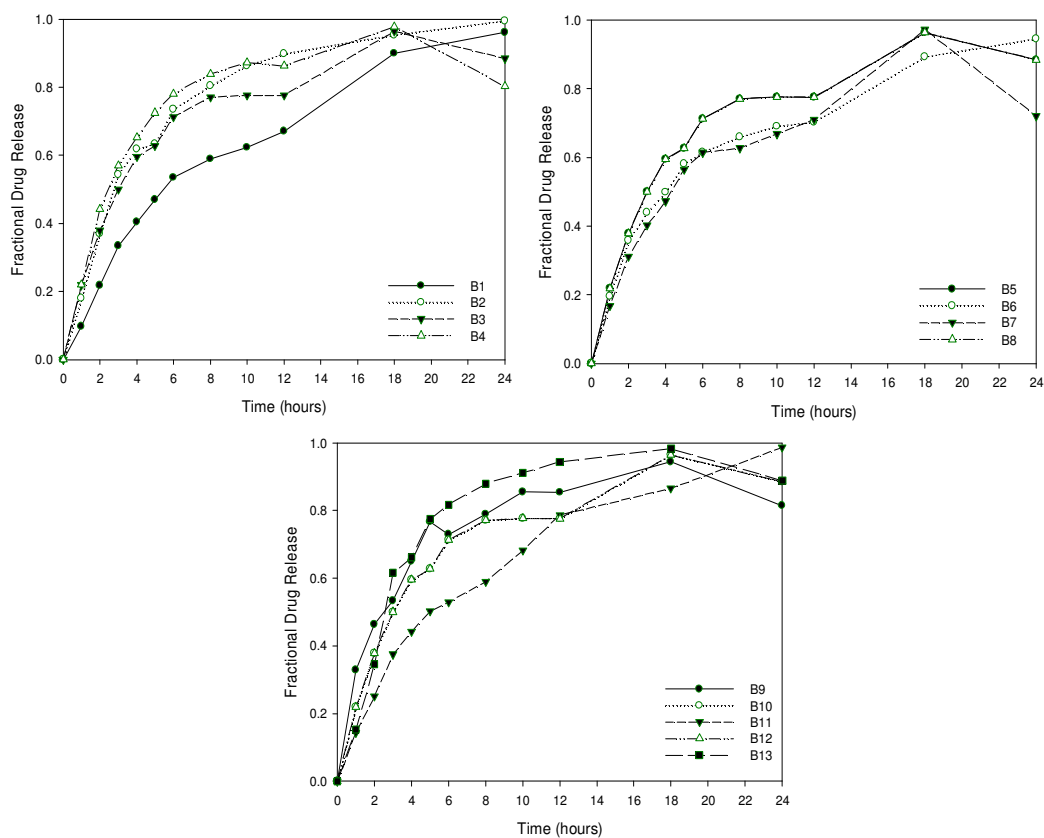


Figure 4.5 Fractional drug release profiles for DSPE-NLS (Design 2) in PBS (pH 7.4; 37°C) undertaken over a 24 hour period (in all cases n=3 and SD ≤ 0.03).

Table 4.8 Calculated MDT values for each experimental run designated for each of the two experimental designs.

CHO-NLS	MDT (Hours)	DSPE-NLS	MDT (Hours)
A1	7.513	B1	7.608
A2	20.911	B2	12.075
A3	10.189	B3	9.912
A4	18.574	B4	10.937
A5	13.981	B5	9.912
A6	21.278	B6	17.707
A7	11.018	B7	7.819
A8	10.189	B8	9.912
A9	13.901	B9	10.575
A10	13.523	B10	9.912
A11	10.189	B11	7.403
A12	10.189	B12	9.912
A13	10.189	B13	10.514

4.5.1.5 Behavioral characterization of formulated nano-liposomes through micro-ultrasound imaging

Macroscopic visual assessment of the general behavioral characteristics of CHO-NLS demonstrated even and adequate distribution through the prepared medium, with the marked absence of aggregation. The micro-ultrasound images in Figure 4.6 highlight the distribution of CHO-NLS following injection into a stiff carrageenan hydrogel. This behavior suggests high stability of the formulation, even in the presence of resistance to motion, and augurs well for *in vivo* stability.

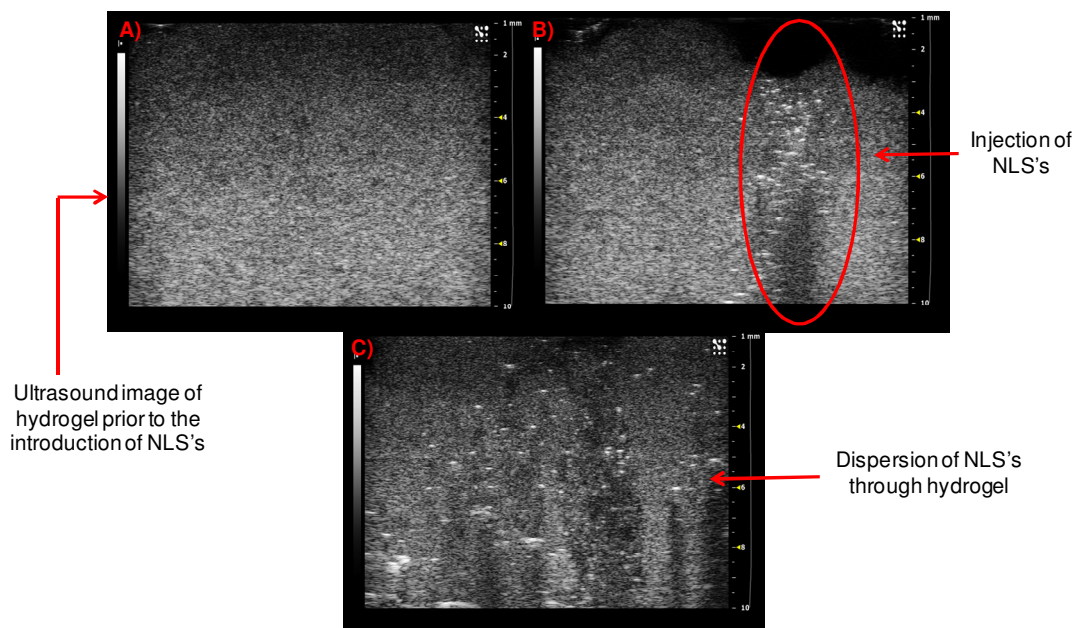


Figure 4.6 Micro-ultrasound images of CHO-NLS following injection into a carrageenan hydrogel.

4.5.2 Computational modeling of experimental data

Response surface methodology (RSM) is an effective tool for mathematical modeling of experimental data, particularly for systems where numerous factors can influence the properties of the system. RSM enables simultaneous evaluation of multiple significant parameters, thereby reducing the experimental runs required to obtain adequate data for optimization (Balachandran *et al.*, 2012). Results obtained from the experimental runs were processed using RSM. Employment of this statistically relevant approach resulted in the generation of second order polynomial equations (Equations 4.1-4.8). Each equation highlights the significance of the effect of each independent variable on the measured response, as well as the relationship/interaction between the independent variables (Balachandran *et al.*, 2012). Analysis of variance (ANOVA), data correlation determination and regression analysis were utilized for data processing and in the assessment of the statistical relevance of the proposed models.

4.5.2.1 Experimental design and statistical optimization of CHO nano-liposomes

4.5.2.1.1 Validation of statistical optimization through data correlation

The relevance and robustness of the experimental design to accurately predict the most optimal formulation composition for the desired measured responses can be assessed by the intensity of the correlation between experimentally determined and statistically predicted measured responses. The outstanding correlation demonstrated between the measured responses obtained experimentally and the fitted responses predicted by computational modeling as presented in Figure 4.7A-D, particularly for zeta potential, serves to validate the applicability of this FC-CCD to the optimization of this nano-sized pharmaceutical formulation. The correlation established between the experimental and predicted outcomes with regards to average size, though significantly lower ($R^2=62.6\%$) than those of the other measured outcomes ($\sim 80-97\%$), was still adequate. In addition, the very close correlation between experimental and predicted average size data of particular formulations is noteworthy. The strongest correlation of experimental and fitted responses was achieved for zeta potential with a correlation coefficient of 97.3%.

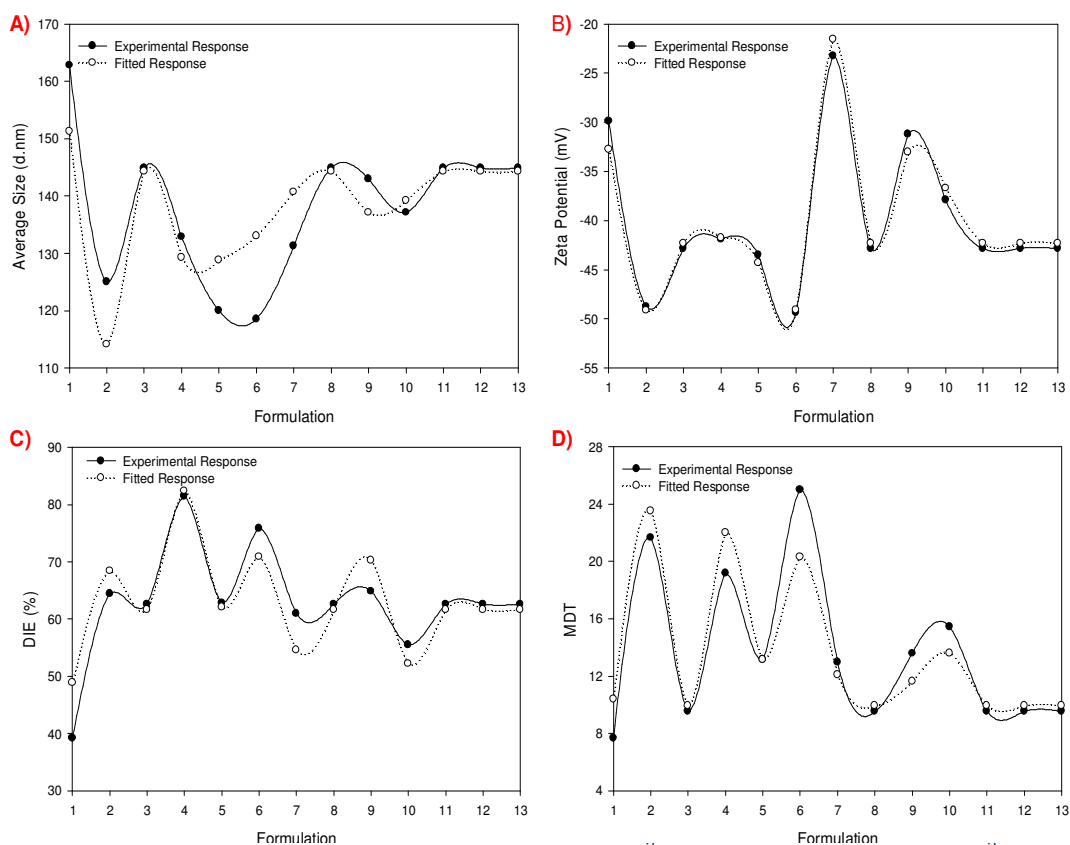


Figure 4.7 Correlation scatter plots of A) Average size ($R^2=62.6\%$); B) Zeta potential ($R^2=97.3\%$); C) DIE ($R^2=80.7\%$) and D) MDT ($R^2=85.7\%$) for the determination of correlation between the experimental and fitted measured responses for CHO-NLS.

4.5.2.1.2 Characterization of the relationship of independent variables relative to measured outcomes

The measured outcomes were influenced by each of the two independent variables in different manners and to varying extents, such that thorough formulation optimization demanded adequate consideration and assimilation of this data. RSM enables the construction of contour plots and 3-dimensional response surface plots which graphically illustrate the inter-relationship of formulations variables (independent variables) and their individual and collective effect on measured outcomes. The generation of second order polynomial regression equations represents a central outcome in the analysis of the relationships between independent variables and is critical to the process of formulation optimization.

Presented herein, Figures 4.8 and 4.9, are the contour and response surface plots for CHO-NLS highlighting the influence of lipid ratio (DSPC:CHO) and surfactant concentration ([DOS]) on each of the measured outcomes, average size, zeta potential, DIE and MDT in turn.

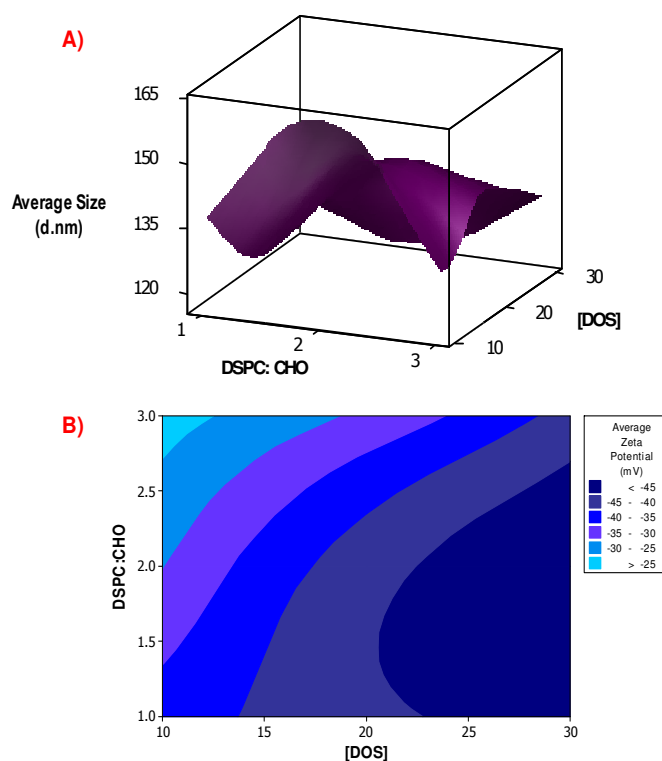


Figure 4.8 Graphical illustrations employing A) a 3-D response surface graph and B) a contour plot to depict the influence of independent variables on the average size and zeta potential, respectively, of CHO-NLS.

The ratio of DSPC to CHO had a variable effect on the average size of CHO-NLS as depicted in Figure 4.8A. An increase in DSPC or CHO within the ratio had a mirror effect

on the average size of the NLS, until the ratio of the lipids approximated 1:1, where the largest average sizes were noted. The increase in average size as a consequence of increased CHO was attributed to the bulkiness of the CHO molecule. There was a noteworthy inverse relationship between DOS concentration and the resultant average size of CHO-NLS. Increasing surfactant concentration resulted in a progressive reduction in the surface tension of the emulsion prior to NLS formation, thereby facilitating the formation of smaller NLS.

The zeta potential of formulations was evidently influenced by the surfactant concentration in the formulation. Increase in DOS concentration resulted in a favorably heightened anionic surface charge, which is illustrated in the contour plot in Figure 4.8B. Moreover, this effect exhibited a consistent trend across all formulations, irrespective of the lipid ratio. Statistically, the effect on zeta potential was only partially significant ($p=0.054$). Theoretically, the presence of CHO was expected to contribute significantly to the negative zeta potential of CHO-NLS. Experimentally, formulations at each of the three levels of DOS concentration analyzed generally demonstrated a favorable decrease in zeta potential with increasing CHO concentration. Formulation A6 was the sole exception, being 0.61mV less than A2 (-49.35mV and -48.74mV respectively). In addition, the wide disparity in zeta potential between CHO-NLS and the significantly less negative DSPE-NLS further corroborated this theory.

There was a clear direct relationship between DOS concentration and DIE, although this was determined to be statistically insignificant. The contour plot (Figure 4.9A) depicting the influence of each of the two independent variables on DIE demonstrates a pattern of increasing DIE as the concentration of DOS increases, which is independent of the ratio of phospholipids. Formulation A4 exhibited the highest DIE.

The shape of the MDT response surface plot in Figure 4.9B showed an inverse, although less distinct, pattern to the average size plot with regards to the effect of DSPC:CHO. Hence, the larger CHO-NLS exhibited the shortest MDT. Generally, higher DOS concentrations resulted in longer MDT. This could be attributed to the high stability of formulations with high DOS concentrations, which resulted in slower release of incorporated CPT. A general trend was observed whereby higher DIE resulted in longer MDT.

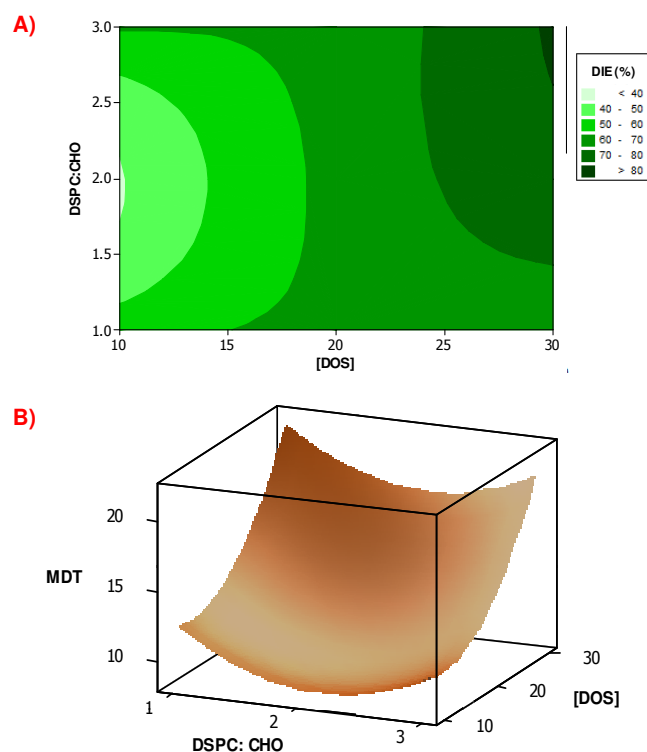


Figure 4.9 Graphical illustrations employing A) a contour plot and B) a 3-D response surface plot to depict the relationship of independent variables to the measured outcomes DIE and MDT respectively, of CHO-NLS

Consideration of the relationships of independent variables and their influence on the measured outcomes culminated in the derivation of the following regression equations (Equations 4.1-4.4). These equations facilitate accurate prediction of each measured outcome under consideration as a function of varying independent variables.

$$\text{Average size} = 14.4 + 42.53(X_1) + (-0.74)(X_2) + (-11.30)(X_1)^2 + (-0.02)(X_2)^2 + 0.341(X_1)(X_2) \quad (\text{Equation 4.1})$$

$$\text{Zeta potential} = (-24.96) + (-5.01)(X_1) + (-0.98)(X_2) + 3.63(X_1)^2 + 0.01(X_2)^2 + (-0.19)(X_1)(X_2) \quad (\text{Equation 4.2})$$

$$\text{DIE} = 54.08 + (-19.82)(X_1) + 1.23(X_2) + 4.53(X_1)^2 + (-0.18)(X_2)^2 + 0.29(X_1)(X_2) \quad (\text{Equation 4.3})$$

$$\text{MDT} = 32.99 + (-10.56)(X_1) + (-1.67)(X_2) + 2.45(X_1)^2 + 0.05(X_2)^2 + (-0.0002)(X_1)(X_2) \quad (\text{Equation 4.4})$$

where $X_1 = \text{DSPC:CHO}$, and $X_2 = [\text{DOS}]$

4.5.2.1.3 Analysis of the fit of the derived model

Residual plots are employed to provide an indication of the suitability and integrity of the model. Four different residual plots are depicted in Figure 4.10 for each of the measured outcomes. A well fit model will exhibit a normal distribution of points for each of the measured outcomes, with constant variance. The distribution of points in the normal probability of residuals for each of the measured outcomes lies in close proximity to the

straight line, indicating a normal distribution. The assumption of constant variance is tested by analysis of the plot of residuals versus fitted values. A random distribution of points above and below the zero line with no discernible pattern is indicative of a constant variance and the applicability of the model to all values of independent variables within the defined parameters. Each of the four plots of residual versus fitted values exhibited an arbitrary distribution of points, with only a few outlying points. Histograms prove particularly useful as they provide an insight into the overall characteristics of the model. Whilst the ideal bell-shaped histogram was not achieved for any of the measured outcomes, the generated histograms were, nevertheless, congruent with the previous conclusions of normal distribution and constant variance of data. The fourth graph is a plot of the residuals in the order that the data was collated (order of experimental runs) and provides an indication of the effect of other variables on the measured outcomes which may not have been identified and analyzed as well as errors that may have a pattern and cannot be overlooked. This plot somewhat rounds off the applicability of the model by confirming the comprehensiveness of the analytical process. The residuals versus order of data plot for each of the measured outcomes for CHO-NLS displayed slight clustering of consecutive points, as well as a few infrequent inversions of signs of consecutive data points.

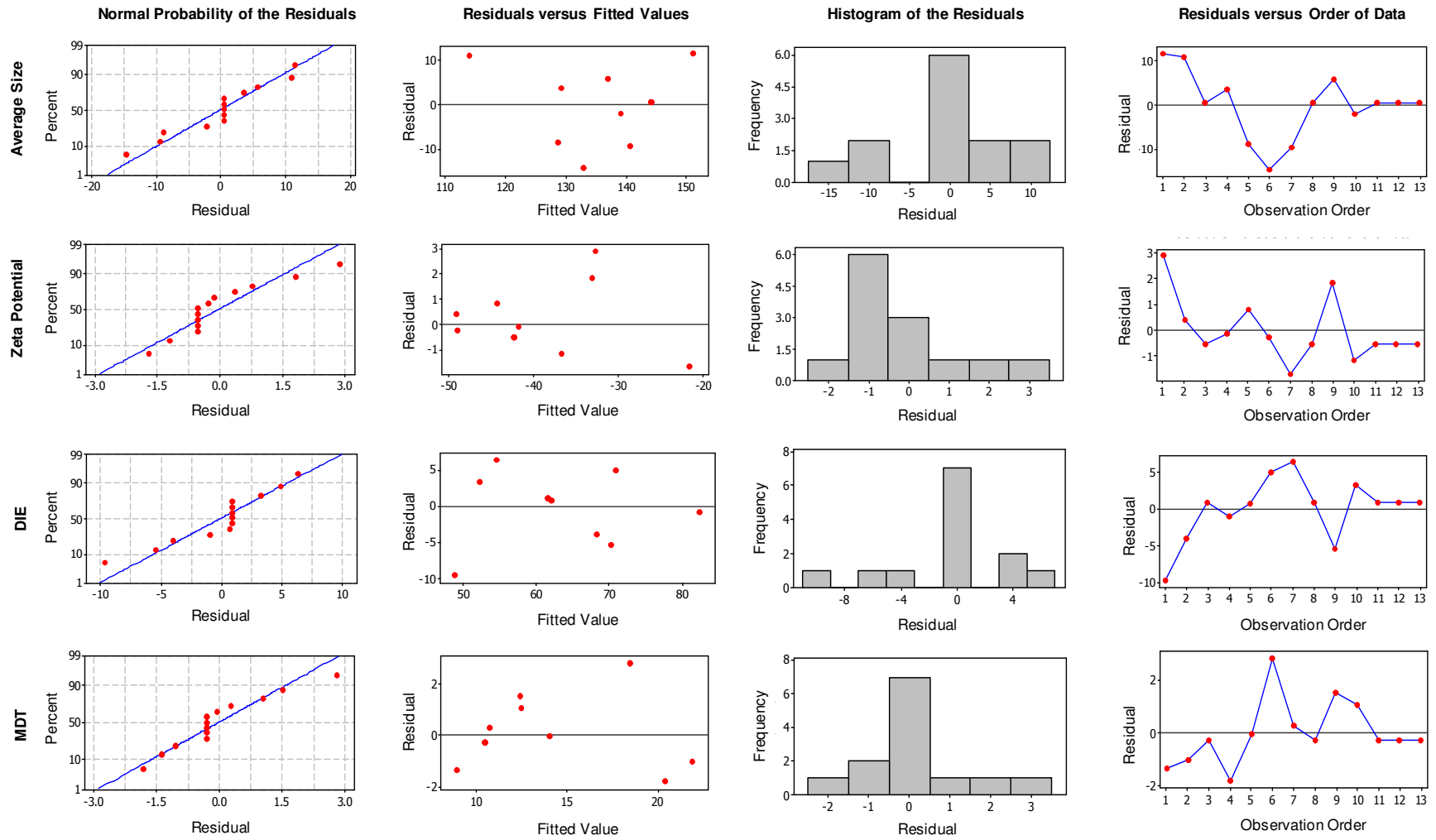


Figure 4.10 Summary of the Residual Plots generated for the measured outcomes of CHO-NLS.

The application of ANOVA revealed a paucity of statistical significance of the independent variables on the measured outcomes ($p \leq 0.05$), with the exception of [DOS] which had a statistically significant effect on MDT, as highlighted in Table 4.9. However, the concentration of DOS had a noteworthy effect on the zeta potential of the formulation.

Table 4.9 Summary of the p -values for each of the independent variables relative to the measured outcomes.

Measured Response	DSPC:CHO	[DOS]
Average Size	0.146	0.784
Zeta Potential	0.276	0.054
DIE	0.222	0.434
MDT	0.177	0.049

4.5.2.1.4 Constrained optimization of the CHO nano-liposomal drug delivery system

Comprehensive optimization of a formulation with regards to all four measured outcomes requires consideration of the significance of each of the measured outcomes and the range of each outcome that is considered feasible and that which is the most desirable. Computational modeling by Minitab[®], V15 software (Minitab[®] Incorporated, PA, USA) following the application of a FC-CCD concluded in the determination that CHO-NLS consisting of DSPC:CHO in a 3:1 ratio and 0.3%^{w/v} DOS would produce the greatest individual and collective optimization of measured responses. The predicted size and zeta potential of this candidate formulation were 129.29 d.nm and -41.77mV respectively. A substantial DIE of 82.41% and MDT=20.382 was forecast for this formulation. The desirability of each of the individual outcomes exceeded 0.7, with an outstanding overall desirability=0.91 predicted for the optimized CHO-NLS. The optimal parameters of the CHO-NLS formulation are depicted in Figure 4.11.

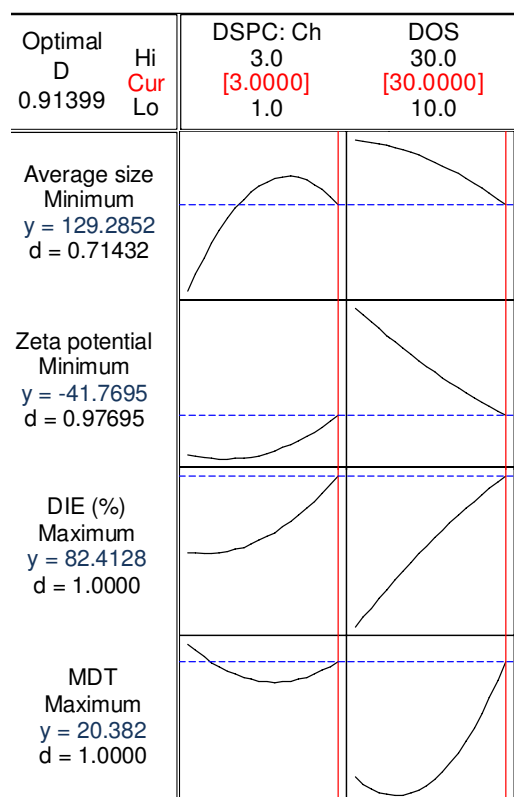


Figure 4.11 Optimization plots for CHO-NLS, indicating optimal levels of independent variables, the predicted outcomes based on these independent variables as well as the desirability of the predicted outcomes.

4.5.2.2 Experimental design and statistical optimization of DSPE nano-liposomes

4.5.2.2.1 Validation of statistical optimization through data correlation

Suitability of the derived model for DSPE-NLS was assessed through analysis of correlation of the regression plots for each of the measured outcomes as outlined in Figure 4.12A-D. Correlation of the measured response data obtained experimentally to the modeled fitted responses for average size and zeta potential was exceptionally strong with correlation coefficients of 83.9% and 81.1%, respectively. Although marginally lower, the correlation of experimental and fitted data for DIE and MDT was highly satisfactory. Correlation of experimental and fitted data for DSPE-NLS validated the applicability and robustness of the derived model for optimization of DSPE-NLS.

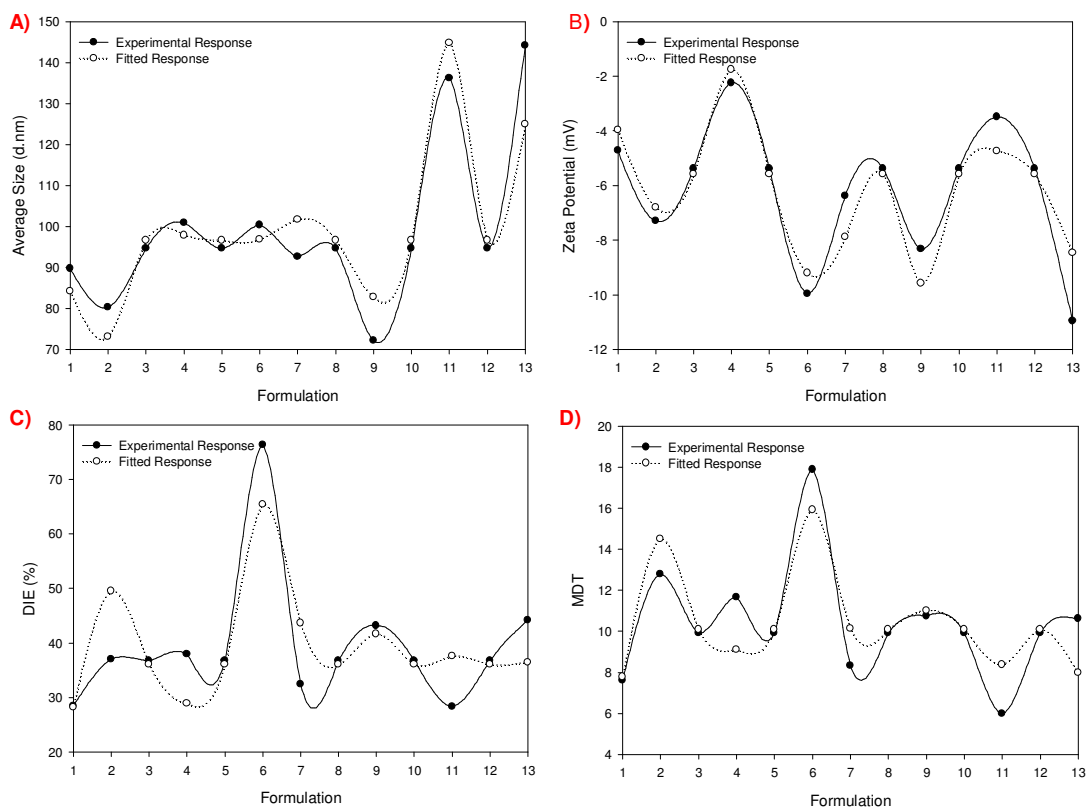


Figure 4.12 Scatter plots of A) Average size ($R^2=83.9\%$); B) Zeta potential ($R^2=81.1\%$); C) DIE ($R^2=63.5\%$) and D) MDT ($R^2=69.3\%$) for the determination of correlation between the experimental and fitted measured responses for DSPE-NLS.

4.5.2.2.2 Characterization of the relationship of independent variables relative to measured outcomes

RSM was employed to characterize the individual and collective effect of phospholipid ratio and DOS concentration on the measured outcomes under investigation for DSPE-NLS. The construction of 3-D response surface graphs and contour plots provided visual representations of these relationships. Presented in Figure 4.13 are the response surface graphs and contour plots generated to conceptualize the inter-relationships of independent variables of DSPE-NLS and the influence of these variables on the average size, zeta potential and MDT of DSPE-NLS. There was no observable relationship between either of the independent variables and DIE

The average size of DSPE-NLS was discernibly affected by both the ratio of phospholipids in the formulation as well as surfactant concentration. The simultaneous increase in DSPC concentration and reduction in DSPE concentration resulted in an increase in the average size of NLS. DSPC tends to be a bulkier molecule than DSPE, however the presence of PEG attached to DSPE increases the size of the DSPE molecule. Hence, resultant increase in the average size was ascribed to the mechanism and strength of intercalation

of phospholipid chains during formation of the double membrane of the NLS. The presence of PEG conjugated to DSPE facilitated stronger binding and closer association of the phospholipid tails, thereby resulting in NLS of smaller average sizes. Moreover, the lateral stabilizing effect provided by DSPE resulted in reduced average sizes of NLS with increasing DSPE concentration. Analogous to the relationship observed in CHO-NLS, there appeared to be an inverse relationship between DOS concentration and the resultant average size of DSPE-NLS. Reduction in average size of NLS as a function of increasing DOS concentration was determined to be a consequence of the stabilization effect of the surfactant on the NLS as well as decreased surface tension in the emulsion that precedes NLS formation.

The zeta potential of DSPE-NLS was favorably influenced by increasing DOS concentration. Since DSPC and DSPE are neutral phospholipids, the marginally negative zeta potential was attributed to the anionic surfactant. The contour plot in Figure 4.13B illustrates the predominant influence of DOS concentration on zeta potential relative to that of varying phospholipid ratio. Formulations at the 0 level of the experimental design exhibited the most unfavorable, almost neutral, zeta potential.

The phospholipid constitution of DSPE-NLS, when considered alone, appeared to have minimal effect on the MDT of CPT. However, the formulation (B6) comprising of the highest concentration of DSPE and DOS produced the longest MDT. Whilst increasing DOS concentration evidently resulted in longer MDT of CPT, the MDT resulting from formulation B6 could not be entirely attributed to the DOS concentration. Higher DSPE concentration involves a higher concentration of PEG that is attached to DSPE. PEG has a substantial stabilizing effect on liposomes and appears to retard and control drug release from the DSPE-NLS. Hence, the longest MDT achieved was a cumulative effect of high DSPE-m-PEG concentration as well as increasing DOS concentration. A noteworthy observation was the trend of increased MDT of formulations with higher DIE. Overall, the MDT of DSPE-NLS was significantly shorter than that of CHO-NLS.

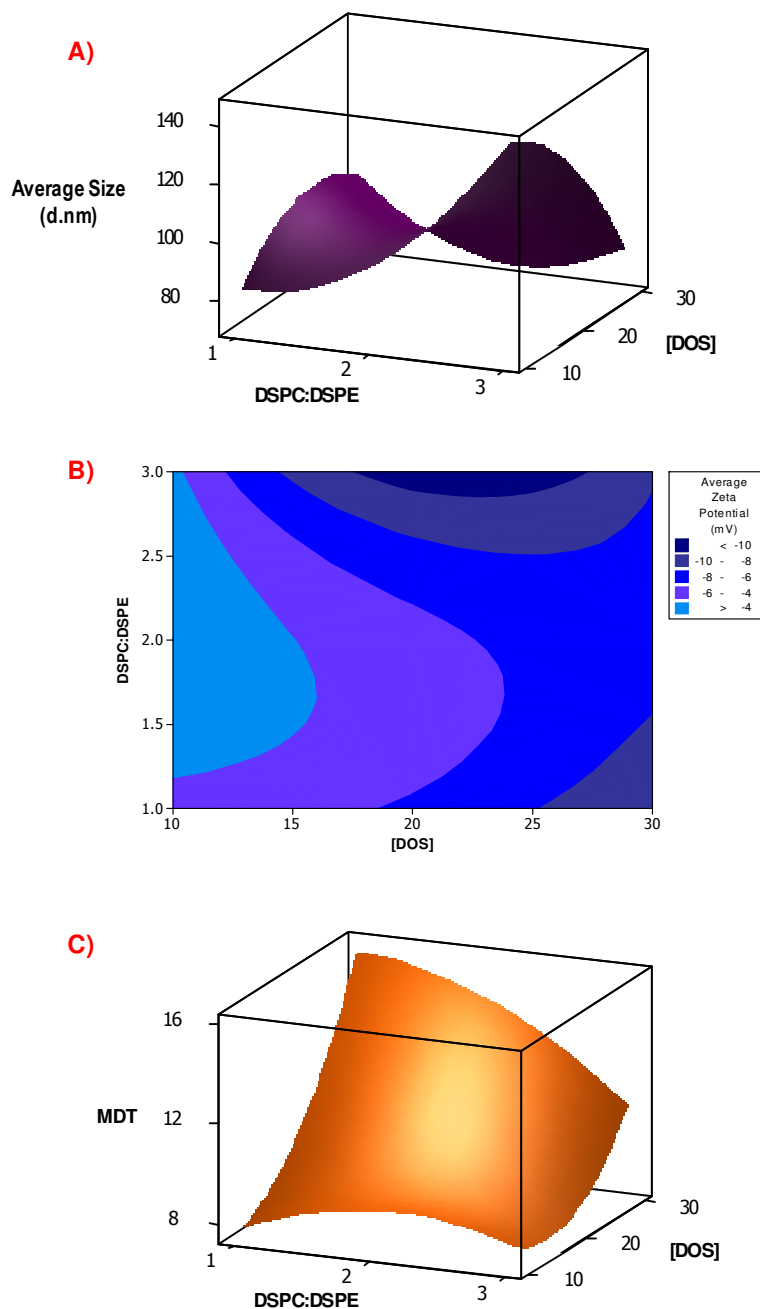


Figure 4.13 Graphical illustration employing 3-D response surface graphs (A and C) and a contour plot (B) to depict the influence of independent variables on the average size, zeta potential and MDT of DSPE-NLS.

Accurate and in-depth analysis of the relationship between independent variables and their influence on measured outcomes facilitated the derivation of regression equations 4.5-4.8. These equations enable accurate determination of the average size, zeta potential, DIE and MDT that will result from variation of either or both of the independent variables and are thus crucial to determining the constitution of the optimal formulation with respect to the desired objective of each measured outcome.

$$\text{Average size} = 45.51 + (-17.71)(X_1) + 6.95(X_2) + 16.66(X_1)^2 + (-0.11)(X_2)^2 + (-1.86)(X_1)(X_2) \quad (\text{Equation 4.5})$$

$$\text{Zeta potential} = (-4.71) + 9.87(X_1) + (-0.79)(X_2) + (-2.59)(X_1)^2 + 0.01(X_2)^2 + 0.01(X_1)(X_2) \quad (\text{Equation 4.6})$$

$$\text{DIE} = 18.28 + (-3.09)(X_1) + 1.41(X_2) + 4.01(X_1)^2 + 0.03(X_2)^2 + (-0.83)(X_1)(X_2) \quad (\text{Equation 4.7})$$

$$\text{MDT} = 4.07 + 5.83(X_1) + (-0.14)(X_2) + (-1.04)(X_1)^2 + 0.02(X_2)^2 + (-0.14)(X_1)(X_2) \quad (\text{Equation 4.8})$$

where X_1 = DSPC:DSPE, and X_2 = [DOS]

4.5.2.2.3 Analysis of the fit of the derived model

Analysis of the fit of the model derived for DSPE-NLS was undertaken through evaluation of four residual plots for each outcome, presented in Figure 4.14. Each residual plot illustrates different characteristics of the model, thereby collectively allowing a comprehensive assessment of the model.

The data points of each of the normal probability plots are closely associated with the straight line, indicating normal distribution of the residuals. No observable pattern was noted on the plots of residuals versus fitted values, thereby verifying the assumption of constant variance. The histograms of residuals for each of the measured outcomes produced plots that were bell-shaped or almost bell-shaped, which further corroborated the favorable distribution and constant variance of data points. Finally, the plot of residuals versus order of the data was employed to determine the presence of other variables that had not been assessed as well as to identify errors that were non-random. These plots displayed no clustering of data points and the alternating of positive and negative data points was suggestive of negative correlation. Analysis of the residual plots intimated a well fit model was generated for DSPE-NLS.

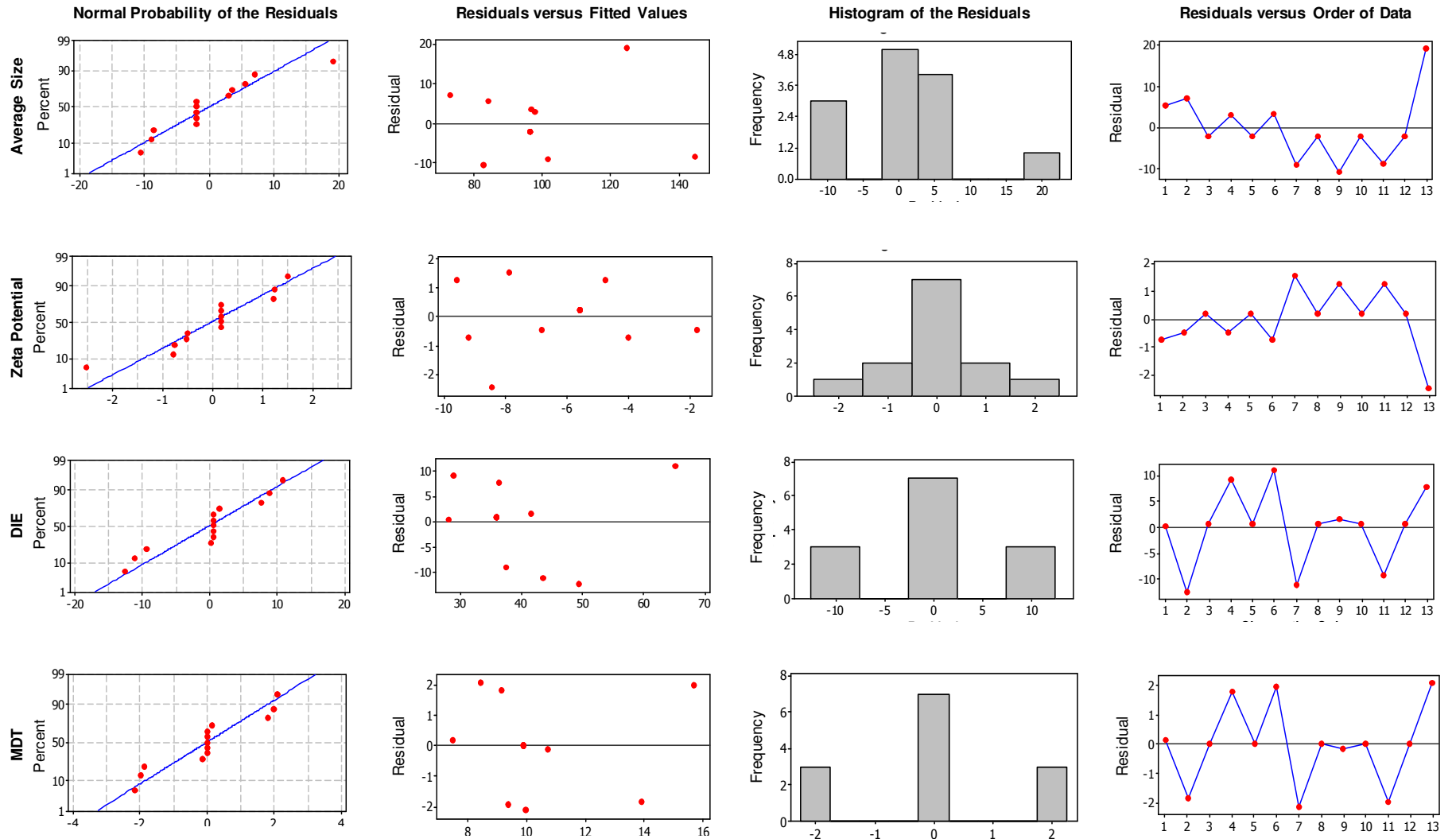


Figure 4.14 Summary of the Residual Plots generated for the measured outcomes of DSPE-NLS.

The application of ANOVA of the data obtained for DSPE-NLS highlighted the definitive and statistically significant effect of DOS concentration on the average size of formulated NLS ($p=0.039$). Phospholipid ratio proved significant on the resultant zeta potential, whilst DOS concentration can be considered to have also had a significant influence on measured zeta potential. Statistically neither phospholipid ratio nor DOS concentration was deemed to impact significantly on DIE or MDT.

Table 4.10 Summary of the p -values for each of the independent variables relative to the measured outcomes.

Measured Response	DSPC:DSPE	[DOS]
Average Size	0.540	0.039
Zeta Potential	0.031	0.066
DIE	0.905	0.590
MDT	0.318	0.800

4.5.2.2.4 Constrained optimization of the DSPE nano-liposomal drug delivery system

The interplay of independent variables on measured responses was optimized employing Minitab®, V15 software (Minitab® Incorporated, PA, USA). Ultimately, a formulation constituting of 0.13%^{w/v} DSPC, 0.27%^{w/v} DSPE and 0.3%^{w/v} DOS was determined to provide the optimal measured responses, as illustrated in Fig 4.15. The desirability for each measured response exceeded 0.9, with an exceptional overall desirability of the formulation=0.979. The predicted average size and MDT of this optimized DSPE-NLS formulation was particularly appealing. Whilst the predicted zeta potential is not indicative of a pharmaceutically acceptable stability profile, post-optimization modifications may simply and adequately address this drawback.

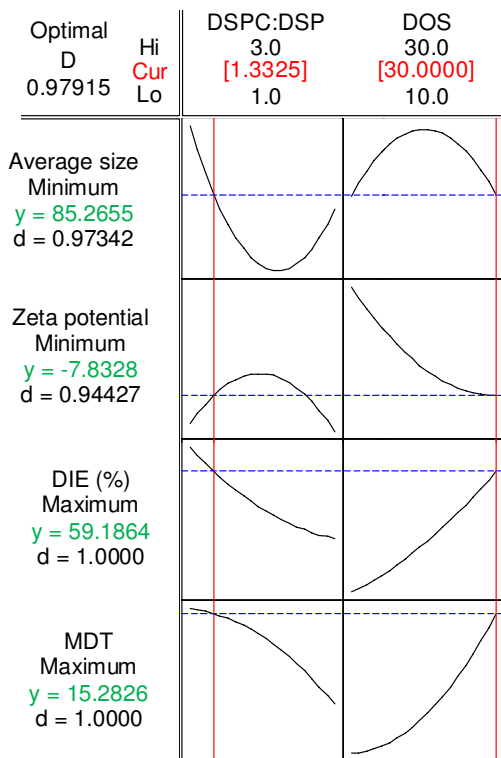


Figure 4.15 Optimization plots for DSPE-NLS, indicating optimal levels of independent variables, the predicted outcomes based on these independent variables and the desirability of the predicted outcomes.

4.6 Concluding Remarks

This chapter provided a systematic and in-depth exploration of the process of statistical optimization by experimental design. The experimental design of each NLS formulation was delineated so as to simultaneously maximize the data obtained and minimize the formulations required to obtain this data. The influence of independent variables and the intensity of this influence on the measured outcomes proved different for each of the two experimental designs. RSM facilitated the comprehensive assessment of the relationships between independent variables and measured responses. Mathematical modeling enabled the generation of regression equations that can be employed to accurately predict measured outcomes as a function of varying independent variable input.

The independent variables determined to produce the optimal responses for CHO-NLS were lipid ratio DSPC:CHO=3:1 and a DOS concentration=0.3%^{w/v}. The desirability of each of the measured responses predicted for this candidate formulation ranged between 0.7 and 1.0, with a composite desirability for the formulation exceeding 0.91. For DSPE-NLS a phospholipid ratio DSPC:DSPE=1.33:2.67 and DOS concentration of 0.3%^{w/v} was determined to produce the most desirable measured responses. The measured responses predicted for this candidate formulation had desirability's ranging between 0.94 and 1, with an overall desirability=0.98. The outstanding composite desirability predicted

for each of the candidate formulations validates the choice and range of independent variables investigated and bodes well for the achievement of formulations that bear clinically relevant characteristics, through the achievement of stable formulations in the nanoscale range for passively targeted drug delivery to tumour sites.

CHAPTER 5

MODIFICATION AND PERFORMANCE EVALUATION OF THE OPTIMIZED NANO-LIPOBUBBLE DRUG DELIVERY SYSTEM

5.1 Introduction

Statistical optimization, as outlined in Chapter 4, culminated in the delineation of the optimal compositions for the formulation of cholesterol-containing nano-liposomes (CHO-NLS) and distearoylphosphatidylethanolamine-containing nano-liposomes (DSPE-NLS) as well as the predicted measured responses for each of these candidate formulations. Physicochemical and physicochemical characterization of these candidate formulations was pivotal in assessing the viability of the formulation and, ultimately, whether the aim of the study was achieved. Moreover, the aim of this study was the formulation of antineoplastic-loaded nano-lipobubbles (NLB) for intravenous administration. Hence, conversion of NLS to NLB and characterization thereof will be the focal point of this chapter.

Further modifications were undertaken on candidate NLB formulations in an attempt to augment the antineoplastic activity, physicochemical, and physicochemical properties of the NLB drug delivery system (NLB-DDS). The employment of phytochemicals for therapeutic purposes has garnered considerable attention due to a deeper understanding of traditional and complementary medicine (D'Incalci *et al.*, 2005; Sun and Liu, 2006; Lee *et al.*, 2013). In line with this, the incorporation of a phytochemical with established antineoplastic properties was explored. Phytochemicals may exhibit diverse mechanisms of antitumour activity such as sensitization of tumour cells to augment the activity of conventional antineoplastic drugs, synergistic activity with antineoplastic drugs or may even act as preferential substrates to enable the antineoplastic drug to exert its effect at the site of action (D'Incalci *et al.*, 2005; Nabekura *et al.*, 2010). However, the achievement of adequate systemic bioavailability often presents a challenge when therapeutic applications are intended. Hence, the incorporation of phytochemicals into DDS for individual or adjuvant therapy to conventional treatment regimens represents a viable concept (Aqil *et al.*, 2013). This approach capitalizes on inexpensive, highly tolerable products that may enhance the efficacy of antineoplastic drugs when used in combination (D'Incalci *et al.*, 2005).

One of the fundamental drawbacks of liposomes and lipobubbles is limited life-span *in vivo* (Madrigal-Carballo *et al.*, 2010; Chun *et al.*, 2013). Moreover, drug leakage from

liposomes during storage compromises drug delivery applications. Layer-by-layer (LBL) polymeric coating is a widely adopted approach to enhance the stability profile and tailor the drug release characteristics of liposomes (Ciobanu *et al.*, 2007; Madrigal-Carballo *et al.*, 2010; Chun *et al.*, 2013). Electrostatic attraction between the charged liposomal surface and an oppositely charged polymer underscores the mechanism of sequential polymeric layering (Volodkin *et al.*, 2007; Chun *et al.*, 2013). The application of polymeric coating can also be employed to facilitate targeted drug release in response to micro-environmental conditions that characterize the pathophysiology of the condition/site, such as changes in pH or temperature.

This chapter delves into the in-depth physicochemical and physicomechanical characterization of each of the candidate NLS determined through statistical optimization, as well as conversion to NLB and the modifications undertaken thereupon, as illustrated in Figure 5.1. Sequential characterization will provide a basis for comparison of changes in NLB characteristics resulting from each modification and the contribution of each modification to ultimately attaining NLB formulations demonstrating the pre-determined characteristics of a clinically viable antineoplastic nano-DDS.

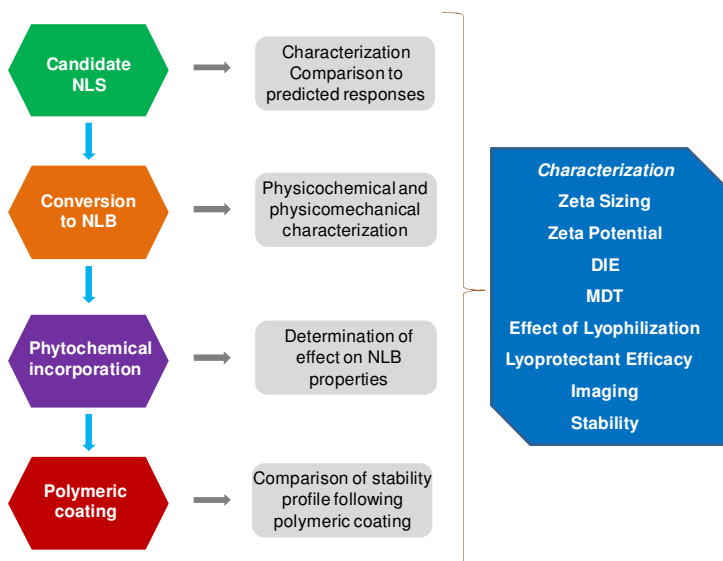


Figure 5.3 Schematic summary of the modifications undertaken on candidate NLS formulations and the analytical characterization involved.

5.2 Phytochemicals in antineoplastic therapy: Silibinin

Interest into naturally occurring phytochemicals for tumour therapy have been increasing exponentially and investigation into these compounds has intensified over the years due to the demonstration of tumour prevention and growth inhibition properties in several studies (Gallo *et al.*, 2003; Yang *et al.*, 2003; Hogan *et al.*, 2007; Ramasamy and Agarwal,

2008; Nair *et al.*, 2010). Silibinin (SB) is a naturally occurring polyphenol antioxidant extracted from the crude seed extract of the plant milk thistle (*Silybum marianum*) (Bhatia *et al.*, 1999; Gallo *et al.*, 2003; Hogan *et al.*, 2007; Cao *et al.*, 2012). The mechanism of anti-tumour effect of SB has been attributed to factors such as the promotion of cellular antioxidant defense mechanisms, angiogenesis antagonism by a reduction in VEGF secretion, induction of apoptosis, and antiproliferative effects due to cell cycle arrest (Bhatia *et al.*, 1999; Yang *et al.*, 2003; Hogan *et al.*, 2007; Ramasamy and Agarwal, 2008). Different mechanisms of activity and combinations of the aforementioned mechanisms appear to predominate in different tumour models, attributing anti-tumour potential against a wide range of tumours such as colon, breast, prostate, ovarian, lung, bladder, cervical, and hepatocellular carcinomas (Ramasamy and Agarwal, 2008).

Initially marketed widely for its hepatoprotective properties, the naturally occurring flavanoid SB has a remarkable safety profile, being well tolerated at considerably high doses following different routes of administration (Gallo *et al.*, 2003). However, absolute oral bioavailability of SB is poor due to gastric degradation, metabolism by phase II conjugation, and limited aqueous solubility (0.43mg/mL) - leading to a slow absorption rate (Wu *et al.*, 2009; Parveen *et al.*, 2011; Cao *et al.*, 2012). Classification as a Class II drug according to the Biopharmaceutical Classification System highlights a high degree of permeability of SB, despite the poor aqueous solubility. Hence incorporation into DDS that have the capacity to improve the aqueous solubility of SB could prove highly beneficial to the clinical utility of this flavonolignan. Furthermore, complexation of SB to phosphatidylcholine, creating silipide, has proven a successful means of improving the solubility and bioavailability of SB (Wu *et al.*, 2009). This further rationalizes the incorporation of SB into phospholipid-based nanosystems.

5.3 Materials and Methods

5.3.1 Materials

Materials employed during NLB formulation and the analyses that ensued were unchanged from those outlined in Chapter 4, Section 4.4.1. In addition, the phytochemical silibinin ($\geq 98\%$ purity; Mw=482.44), sulphur hexafluoride gas (Mw=146.06), gelatin (\sim Mw=20000-25000), poly-L-lysine (PLL) (\sim Mw=30000-70000), polyethyleneimine (PEI) (50%^{w/v} in H₂O; Mw=750000), commercial grade carrageenan (Mw= \sim 200000), poly(acrylic acid) (PAA) (Mw=1800), sodium alginate (Mw=216), lactose (Mw=360.32), fructose (Mw=180.16), fluorescein isothiocyanate (FITC) ($\geq 90\%$ purity; Mw=389.38) and foetal bovine serum (FBS) were acquired from Sigma Chemical Company (St Louis, MO, USA). Chitosan (CHT) (food grade) was obtained from Wellable Group Marine Biological &

Chemical Co., Ltd. (Shishi City, Fujian, China) and pectin (LM-105-AS) was obtained from CP Kelco (Lille Skensved, Denmark).

5.3.2 Methods

5.3.2.1 Preparation of candidate CHO nano-liposomes and DSPE nano-liposomes

DSPC, DOS and either CHO or DSPE (concentrations as per Table 5.1) were simultaneously dissolved in a chloroform:methanol (9:1; 10mL) solvent system under continuous stirring at 400rpm for 5 minutes, employing a magnetic stirrer. Camptothecin (CPT) (0.05%^{w/v}) was added to the organic solution under continuous agitation. Phosphate buffered saline (PBS) (pH 7.4, 25°C; 10mL) was subsequently added to the organic solution under ultra-sonication (amplitude = 80%; 90 seconds), over an ice-bath, employing a Vibracell probe ultrasonicator (Sonics & Materials Inc., Newtown, Connecticut, USA). This culminated in the formation of a homogenous, single-phase emulsion. This emulsion was subsequently subjected to evaporation under vacuum (60-65°C) for 2-3 hours, employing a Multivapor™ (Buchi Labortechnik AG, Switzerland). PBS (pH 7.4, 25°C; 10mL) was added periodically during the evaporation process and the formulation was subjected to ultra-sonication as previously outlined for 30 seconds, after each addition. Complete evaporation of the solvent resulted in an aqueous NLS suspension. The resultant NLS suspension was subjected to three cycles of freezing at -70°C and thawing at 37°C, to convert multilamellar NLS to unilamellar NLS with filtration through a 0.22µm millipore filter after each freeze-thaw cycle. All ensuing modifications and analyses were conducted in triplicate (n=3) on these unilamellar NLS.

Table 5.1 Composition of the candidate NLS systems obtained by statistical optimization.

Materials	CHO-NLS (% ^{w/v})	DSPE-NLS (% ^{w/v})
DSPC	0.3	0.133
DSPE	-	0.267
CHO	0.1	-
DOS	0.3	0.3

5.3.2.2 Conversion of formulated nano-liposomes to nano-lipobubbles: Effect of sonication duration

Based on previously reported methods for conversion of NLS to NLB, NLS suspensions (10mL) prepared as described in Section 5.3.2.1 above were filtered and injected into 20mL vials. SF₆ gas was introduced into the headspace of the vials, which were subsequently sealed. Sonication of the vials was undertaken in a bath type sonicator causing the SF₆ gas to penetrate the lipid membrane of the NLS, and form a gaseous core, thereby creating NLB (du Toit *et al.*, 2011).

Sonication was undertaken for 2, 3 and 5 minutes to determine the effect of sonication duration on the ultimate size and stability of the NLB. The variation in size and zeta potential was insignificant after sonication for 2 and 3 minutes. However, following sonication for 5 minutes, the Pdl was unfavorably higher due to the formation of a small proportion (<5%) of NLB below 25nm. The zeta potential of the NLB sonicated for 5 minutes exhibited an unfavorable deficit of ~10mV for CHO-NLB and ~4mV for DSPE-NLB. Hence, sonication duration of 3 minutes was delineated for all further formulations.

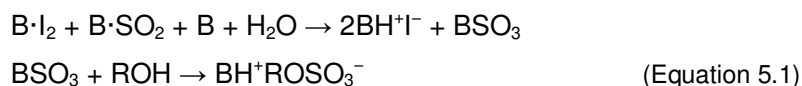
5.3.2.3 Investigating the effect of lyophilization on nano-lipobubble size and stability

To determine the effect of lyophilization on the stability of formulated NLB, the average size, size distribution and zeta potential of formulated NLB prepared pre- and post-lyophilization with and without a lyoprotectant was determined. CHO-NLS and DSPE-NLS were formulated as outlined in Section 5.3.2.1 and converted to NLB as outlined in Section 5.3.2.2. The formulated NLB were subjected to size, size distribution and zeta potential analysis in triplicate as described in Chapter 3, Section 3.3.2.6 and Chapter 4, Section 4.4.2.2, respectively, over a 3 hour period whilst being maintained at 37°C in an orbital shaker bath rotating at 25rpm.

Simultaneously, unmodified NLS suspensions (15mL), as well as NLS suspensions containing lactose or fructose (~0.05%^{w/v}) as lyoprotectants were frozen at -70°C for 48 hours. The samples were subsequently lyophilized (Labconco, Kansas City, MO, USA) and the products were re-suspended in PBS (pH 7.4; 25°C; 10mL) to a concentration of 0.5%^{w/v}. The resultant NLS suspensions were subjected to three freeze-thaw cycles with filtration through 0.22µm millipore filters undertaken after each cycle. Conversion of NLS to NLB was undertaken according to the methodology outlined in Section 5.3.2.2. Average size, size distribution and zeta potential analysis ensued over a 3 hour period, whilst the NLB suspensions were maintained at 37°C in an orbital shaker bath rotating at 25rpm.

5.3.2.4 Assessment of lyoprotectant efficacy through water content determination

Determination of water content was undertaken by volumetric Karl Fischer (KF) titration on the lyophilized powder (10mg) of plain, fructose-containing and lactose-containing formulations employing a Karl Fischer titrator (Mettler Toledo, Columbus, Ohio, USA). Volumetric KF titration involves the solubilization of a sample in a KF standard titrant solution containing alcohol, a base, SO₂ and a known concentration of I₂. The reaction proceeds as illustrated in Equation 5.1. Water quantification is based on the oxidation of SO₂ by I₂. One mole of I₂ is consumed for each mole of H₂O present.



5.3.2.5 Generation of standard curves for the photospectroscopic quantification of silibinin

Due to the poor aqueous solubility of SB, serial dilutions of SB were prepared in DMSO:PBS (pH 7.4; 37°C and pH 6.0; 37°C) (1:1) analogous to those prepared in Chapter 3, Section 3.3.2.4 from a stock solution of SB in DMSO (0.002%_{v/v}). Following a UV scan to determine the optimum wavelength for SB detection, vortexed aliquots of the abovementioned serial dilutions were analyzed at 334nm for pH 7.4 and 290nm for pH 6.0, employing a Cecil CE 3021 photospectrometer (Cecil Instruments Ltd., Milton, Cambridge, UK). Analyses were undertaken in triplicate on 2 consecutive days to confirm reproducibility of results.

5.3.2.6 Determining the efficacy of phytochemical incorporation

The addition of SB to NLB preparations initially involved the addition of 15-200mg SB dissolved in acetone (5mL) during the emulsification process. The ensuing methodology remained unchanged from that outlined in Section 5.3.2.1. The effect of SB incorporation on the size profile and surface charge of formulated NLB was initially investigated as outlined in Chapter 3, Section 3.3.2.6 and Chapter 4, Section 4.4.2.2, respectively. The efficiency of SB incorporation following the addition of the aforementioned range of SB quantities, as well as the effect of SB incorporation on the incorporation efficiency of CPT was subsequently determined.

Quantification of SB incorporated into the NLB followed the principles of CPT quantification as outlined in Chapter 3, Section 3.3.2.5, due to the poor aqueous solubility of SB. Following double filtration through 0.22µm filters to remove unincorporated SB, NLB suspensions were ultra-sonicated to disrupt the structural integrity of the NLB. DMSO was added to the suspensions, creating a 1:1 dilution, to solubilize the SB. SB incorporation efficiency was determined in triplicate by UV photospectroscopy, against a constructed standard reference curve of SB in DMSO:PBS (pH 7.4; 37°C) (1:1).

5.3.2.7 Evaluating polymeric coating by layer-by-layer self-deposition

LBL polymeric coating is based on the principle of electrostatic attraction between oppositely charged molecules, resulting in the alternate deposition of polymers onto charged surfaces. Candidate NLS exhibited an overall anionic surface charge, with CHO-NLS possessing a more strongly negative zeta potential, which facilitated the

establishment of a polycationic primary polymeric layer, followed by the alternate deposition of polyanionic and polycationic polymeric layers.

Summarily, unilamellar NLS suspension as prepared in Section 5.3.2.1 were added drop-wise to a cationic polymer solution under constant agitation employing a magnetic stirrer. Coating was allowed for periods of 3-12 hours under ambient condition, with zeta potential analysis, as described in Chapter 4, Section 4.4.2.2, undertaken at regular intervals to determine successful polymer coating. The cationic NLS suspension was subsequently added drop-wise to an anionic polymeric solution under constant stirring and adsorption of the polymer was allowed under ambient conditions for periods of 6-18 hours, with periodic zeta potential analysis. Two or four polymeric layers were applied. Lactose, a lyoprotectant, was added to the polymer coated-NLS suspension and the suspension was frozen at -70 °C for 48 hours, followed by lyophilization. The lyophilized powder was re-suspended in PBS (pH 7.4; 25 °C) to form polymer coated NLS, and converted to polymer coated NLB as outlined in Section 5.3.2.3. Table 5.2 summarizes the polymers and concentrations thereof investigated as suitable NLS coating materials.

Table 5.2 Cationic and anionic polymers investigated for application in NLS coating by the LBL self deposition methodology.

Cationic Polymers	Concentration (% ^w / _v)
Gelatin	0.5 – 2
PEI	1 – 3
PLL	0.5 – 3
CHT	0.1 – 1.0
Anionic Polymers:	Concentration (% ^w / _v)*
Carrageenan	0.2 - 0.4
Pectin	0.5 – 1
Sodium alginate	0.5 – 2
PAA	0.5 – 2.0

5.3.2.8 Determining chemical structural transitions resulting from polymeric coating of nano-liposomes

Fourier Transform Infra-Red (FTIR) spectrophotometric analysis was employed to assess the changes in chemical structure of the CHO- and DSPE-NLS following polymeric coating with CHT and PAA. Lyophilized samples of uncoated CHO- and DSPE-NLS, optimized CHO- and DSPE-NLS, native CHT and native PAA, were analyzed under ambient conditions employing a Perkin Elmer Spectrum BXII FTIR spectrometer (Perkin Elmer Life and Analytical Sciences Inc., Shelton, CT, USA). The FTIR spectrum of each sample was recorded at a wavelength range of 650-4000cm⁻¹ with a resolution of 2cm⁻¹.

Changes in vibrational frequencies were used to confirm the successful adsorption of CHT and PAA onto the NLS surface.

5.3.2.9 Elucidating the size characteristics of formulated nano-liposomes and nano-lipobubbles

The nano-scale size range is central to the clinical relevance and feasibility of the intended DDS. Variation in average size and size distribution were also highlighted as key indicators of formulation stability. Hence, all modifications investigated were initially assessed from the standpoint of the effect the modification had on the resultant size profile of the formulation. Average size and size distribution was examined as discussed in Chapter 3, Section 3.3.2.6. During initial investigations to assess the effect of each modification on the size profile on the formulation, analysis was undertaken over a 3 hour period whilst the NLB was maintained at physiological temperature in an orbital shaker bath rotating at 25rpm. Table 5.3 succinctly summarizes the modifications investigated for their effect on the average size and size distribution characteristics of the NLS and NLB.

Table 5.3 Summary of average size and size distribution assessments undertaken on candidate NLS and NLB formulations and the modifications that ensued.

Modifications Assessed by Average Size and Size Distribution Analyses
<ul style="list-style-type: none">• Candidate NLS from experimental design• Impact of gas incorporation to create NLB• Effect of sonication time• Influence of lyophilization (with and without lyoprotectants)• Effect of phytochemical incorporation• Bearing of polymeric coating

5.3.2.10 Surface charge characterization of formulated nano-liposomes and nano-lipobubbles

As denoted under the discussion regarding the emphasis on size characteristics, surface charge characteristics are of equal essence in this study due to the intravenous nature of the formulated DDS and the severe implications of NLB aggregation *in vivo*. In addition, the high cost of antineoplastic drugs warrant the need for a stable formulation with lengthened shelf-life. Consequently zeta potential determination was undertaken in conjunction with size analysis as described in Chapter 4, Section 4.4.2.2. In addition variation in zeta potential was a distinct indicator of successful polymeric coating with oppositely charged polymers.

5.3.2.11 Morphological characterization of formulated nano-lipobubbles

Scanning electron microscopy (SEM) was undertaken on the lyophilized products following polymeric coating, employing a Phenom™ scanning electron microscope (FEI Company, Hillsboro, OR, USA) to qualitatively assess the resulting morphological structures of lyophilized products. Samples were fixed as a monolayer to a sampling stub and coated with gold-palladium for 30 seconds before photomicrographs were acquired.

Furthermore, lyophilized powders of formulated NLS were reconstituted with PBS (pH 7.4; 25°C) in the presence of FITC dye and subsequently converted to NLB, as outlined in Section 5.3.2.3. The NLB suspension was allowed to dry onto a cover-slip covered with a slide for 1 hour, followed by imaging employing an inverted immunofluorescence microscope (Olympus IX71, Olympus, Tokyo, Japan) after 100mS exposure.

5.3.2.12 Investigating the efficiency of camptothecin incorporation

Determination of the efficiency of CPT incorporation was undertaken on candidate NLS for comparison to predicted values, on formulated NLB, following SB incorporation and the application of polymer coating to NLB. Drug incorporation efficiency (DIE) of CPT was undertaken as described in Chapter 3, Section 3.3.2.5.

5.3.2.13 Generation of a standard curve for the photospectroscopic quantification of camptothecin

In addition to physiological pH, drug release was also undertaken at approximate tumoural pH (6.0; 37°C) to determine the effect of lower pH on CPT release characteristics. The analysis of CPT release characteristics at approximate tumoural pH (6.0) necessitated the construction of a standard curve of CPT in PBS (pH 6.0; 37°C) to enable photospectroscopic quantification of CPT. Preparation of a stock solution of CPT in DMSO and subsequent serial dilutions were undertaken analogous to the method outlined in Chapter 3, Section 3.3.2.4. Following a wavescan to delineate the optimal wavelength for CPT determination at pH 6.0, the aforementioned serial dilutions were analyzed at 345nm.

5.3.2.14 Elucidation of camptothecin and silibinin release characteristics

Drug release investigations were undertaken analogous to that outlined in Chapter 4, Section 4.4.2.4, at approximate tumoural and physiological pH, following reconstitution of lyophilized powder and conversion to NLB as explicated in Section 5.3.2.3. Quantification of drug release was undertaken with reference to the relevant standard curves for CPT and SB. Adjustment of the concentration and volume of NLB suspension was undertaken

in order to accommodate for the inclusion of SB and maintain sink conditions for both compounds.

5.3.2.15 Delineation of the stability characteristics of optimized nano-lipobubbles

The clinical feasibility and usefulness of formulations is influenced in large part by the stability of formulations under various conditions. Whilst surface charge was denoted as the initial indicator of formulation stability, other conditions that have the potential to affect or be affected by stability of the formulation required further consideration. Hence, stability of formulations was determined through exposure to serum, behavioral changes following reconstitution and long term storage stability.

5.3.2.15.1 Determining stability of nano-lipobubbles in the presence of serum

For intravenously administered formulations, establishment of the characteristics of the formulation in the presence of serum is a vital determination. Coated and uncoated CHO- and DSPE-NLB (10mL) were incubated at 37°C for 1 hour with FBS (50%^{v/v}), which is regarded as an appropriate concentration to adequately mimic physiologic conditions. At 15 minute intervals, 100µL of the NLB-FBS combination was diluted with 10mL PBS (pH 7.4, 37°C) and average size, size distribution and surface charge characterization ensued, employing a Zetasizer NanoZS (Malvern Instruments Ltd, Malvern, Worcestershire, UK), as previously outlined in Chapter 3, Section 3.3.2.6 and Chapter 4, Section 4.4.2.2, respectively.

5.3.2.15.2 Assessing stability of the formulation after reconstitution

Assessing the stability of NLB suspensions post-reconstitution is critical to delineate pre-administration storage conditions and the provision period that can be allowed between reconstitution of the formulation and administration to the patient. A Turbiscan™ LAB (Formulaction, L'Union, France) was employed to qualitatively analyze the behavioral characteristics of formulated NLB suspensions. The relevant NLB suspensions (20mL) were introduced into specialized vials and analyzed at pre-determined intervals over a 12 hour period at 25°C.

The Turbiscan™ LAB consists of a pulsed near infra-red light source which moves vertically along the sample acquiring data every 40µm, as well as 2 detectors. The transmission detector, positioned at 180°, detects light that is transmitted through the sample, whilst the backscattering detector, positioned at 45°, detects the light that is rebounded by the sample. Data obtained by the Turbiscan™ LAB is based on multiple light scattering whereby the photons are repeatedly scattered by the suspended material

before detection. The Turbiscan™ LAB is very sensitive to detect changes in the formulation such as creaming, sedimentation, flocculation and changes in particle size which may be indicative of coalescence. Backscatter data was employed in the analysis of formulation stability in this study. The intensity of the light that is detected by the backscattering detector is influenced by:

- The diameter of the suspended particulate matter.
- The volume fraction of particles.
- The respective refractive indices of the suspended and continuous phases.

5.3.2.15.3 Determining the effect of long-term storage on physicochemical characteristics of formulated nano-lipobubbles

The long-term stability of formulated NLB was determined as a function of change in average size, zeta potential, CPT content, and SB content over the analysis period of 3 months. Lyophilized NLS were sealed in transparent vials with SF₆ gas filled into the headspace and stored at 4 °C and 25 °C. At weekly intervals PBS was introduced into the vials and sonication in a bath-type sonicator was undertaken to form NLB, as outlined in Section 5.3.2.2. Drug content, zeta sizing, and zeta potential determinations were undertaken as outlined in Chapter 3, Sections 3.3.2.5, 3.3.2.6 and Chapter 4, Section 4.4.2.2, respectively.

5.4 Results and Discussion

5.4.1 Size and surface charge characterization of candidate formulations

The average size of CHO-NLS was 2.41% larger than predicted by statistical optimization which, given the nano-scale of the formulation, is quite satisfactory. In addition, the average size obtained was still adequately below the benchmark size of 160nm that was initially delineated for favorable passive targeting to tumour tissue, as indicated in Figure 5.2A. The PDI (result not shown) was 0.151, indicating the narrow size distribution of NLS within the formulation. Conversion of NLS to NLB resulted in a slight decrease in average size, illustrated in the size profile in Figure 5.2B. This may be attributed to replacement of the aqueous core with a gaseous core which occupied a smaller volume. In addition, ultrasonication employed in creating the gaseous core may have caused a reduction in the average size of the CHO-NLB.

The zeta potential obtained experimentally for the candidate CHO-NLS formulation was 9.26% less negative than that predicted for this formulation by statistical optimization. There was a further unfavorable decrease in surface charge following conversion of the CHO-NLS to CHO-NLB. This may be attributed to slight destabilization of the lipid

membrane during the conversion process. However, the zeta potential of formulated CHO-NLB remained highly favorable, designating a stable formulation that is not inclined to aggregation.

The average size and zeta potential of candidate NLS, as well as the average size and zeta potential following conversion of these NLS to NLB is outlined in Table 5.4. In addition, a comparison to the measured responses predicted by statistical optimization for each of the candidate NLS is highlighted through the percentage deviation value.

Table 5.4 Experimentally determined average size and zeta potential of candidate CHO- and DSPE-NLS and NLB, as well as the percentage deviation from the values predicted for NLS by computational modelling.

Formulation	Average Size (d.nm)	% Deviation	Zeta Potential (mV)	% Deviation
CHO-NLS	132.4	2.41	-37.9	9.26
CHO-NLB	125.6	-	-28.1	-
DSPE-NLS	83.41	2.18	-7.74	1.18
DSPE-NLB	84.20	-	-7.44	-

The average size of candidate DSPE-NLS was 2.18% smaller than predicted for this formulation by statistical optimization, as illustrated in Figure 5.2C. Conversion to DSPE-NLB demonstrated an insignificant increase in the average size of the formulation, depicted in Figure 5.2D. The exceptional size characteristics of DSPE-NLB greatly favors passive targeting of the DDS to tumour tissue by the Enhanced Permeability and Retention (EPR) effect and, hence, may tremendously improve the safety and efficacy of CPT delivered by this DDS *in vivo*.

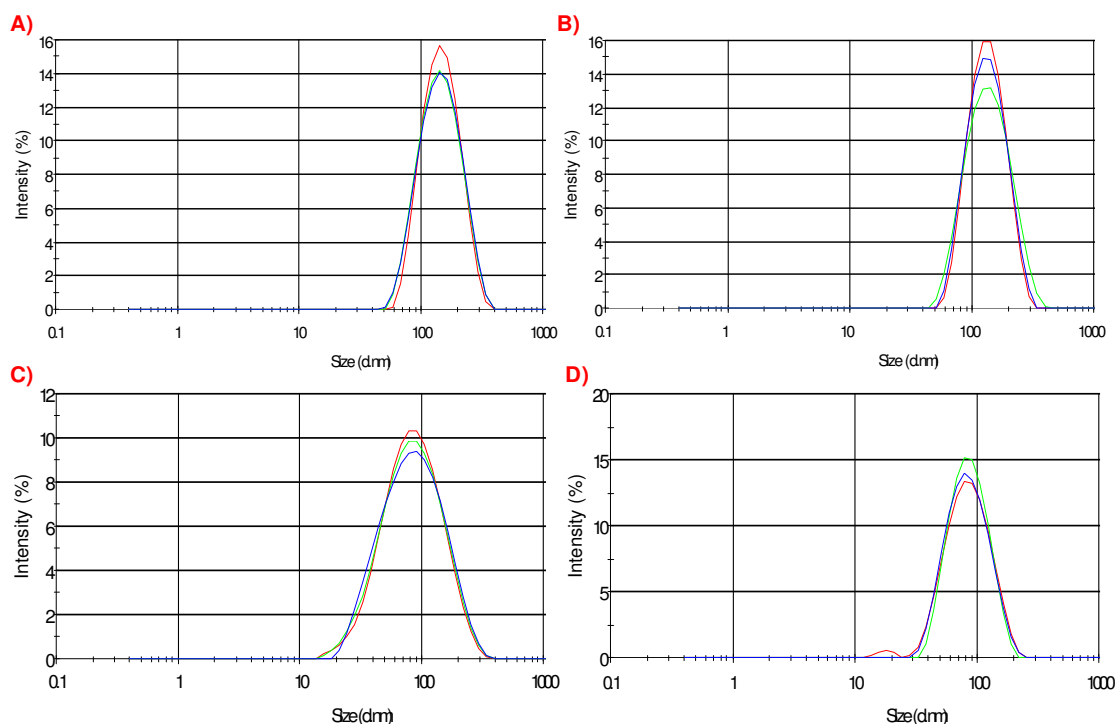


Figure 5.4 Size-Intensity profiles of A) candidate CHO-NLS, B) CHO-NLB, C) candidate DSPE-NLS and D) DSPE-NLB (in all cases $n=3$ and $SD < 0.02$).

The zeta potential achieved experimentally for the candidate DSPE-NLS was very closely correlated with the zeta potential predicted for this DDS by statistical optimization, deviating by only 1.19%. Conversion of the DSPE-NLS to DSPE-NLB resulted in a marginal decrease in surface charge, analogous to that observed for CHO-NLB. Despite the stabilizing effect of PEG in the formulation, the zeta potential of DSPE-NLS was not adequately negative to be pharmaceutically acceptable. Hence, manipulation of DSPE-NLB to enhance the surface charge and the stability of the formulation was considered critical.

5.4.2 Determination of the effect of lyophilization on formulated nano-lipobubbles

The clinical merits of NLS, precursors to the formation of NLB, has been widely described and further validated by the NLS formulations that have gained the approval of regulatory bodies for clinical use (Chen *et al.*, 2010 (b); Chaudhury *et al.*, 2012). However, long term storage stability has presented a constant challenge, leading to a growing interest in stabilization mechanisms for liposome storage (Chaudhury *et al.*, 2012). This consideration was also relevant in the present study, whereby the storage form of the proposed DDS was envisaged to be NLS in the presence of SF₆, which would form the gaseous core upon conversion to NLB. Hence, lyophilization was investigated as a means of creating a formulation that demonstrates long-term storage viability.

The effect of lyophilization on the formulated CHO- and DSPE-NLB was determined as a function of changes in the average size, zeta potential, and DIE of formulations pre- and post-lyophilization and in the absence and presence of a lyoprotectant. Under all conditions, lyophilization appeared to have a destabilizing effect on formulated CHO-NLB. This was more distinctly evident in the resultant zeta potential of formulations following lyophilization, which was markedly less favorable, as highlighted in Table 5.5. The decrease in surface charge allowed aggregation and coalescence of the NLB, which was evident in the fluctuating average size over the analysis period. Moreover, the ~9% decrease in DIE observed with CHO-NLB post-lyophilization attested to the instability of the formulation. The structural integrity of the lipid membrane was compromised during the freezing and lyophilization processes, as outlined in Figure 5.3, leading to reduced incorporation of the lipophilic drug molecule into the NLB-DDS. The addition of suitable lyoprotectants had an immensely favorable effect on the average size of CHO-NLB determined post-lyophilization. The zeta potential of lyophilized and reconstituted products was comparable to that of pre-lyophilized formulations. The presence of lactose enhanced the DIE of CHO-NLB, demonstrating an insignificant (<2%) decrease relative to that of the DIE achieved prior to lyophilization.

Table 5.5 Tabulation of the physical characteristics of CHO- and DSPE-NLB formulations highlighting the effect of lyophilization and lyoprotectant incorporation on the resultant NLB properties.

	Average Size (d.nm)	Zeta Potential (mV)	DIE (%)
Pre-lyophilization			
CHO-NLB	125.60	-28.10	80.10
DSPE-NLB	84.20	-7.44	59.21
Post-lyophilization (no lyoprotectant)			
CHO-NLB	278.21	-22.70	71.31
DSPE-NLB	91.62	-7.32	57.17
Post-lyophilization (with lactose)			
CHO-NLB	129.40	-27.90	78.65
DSPE-NLB	85.17	-8.20	57.20

By contrast, the effect of lyophilization on DSPE-NLB was distinctly less unfavorable relative to that on CHO-NLB, even in the absence of a lyoprotectant. The presence of the PEG molecule conjugated to DSPE was credited for the stability of this formulation to lyophilization. PEG exhibits cryoprotectant as well as lyoprotectant properties, which facilitated stability of the formulation under freezing and lyophilization conditions. The addition of a lyoprotectant demonstrated comparable size and a marginal improvement in the resultant surface charge characteristics of DSPE-formulations.

The water replacement hypothesis suggests the mechanism of lyoprotection of sugars involves interactions between sugars and the head groups of phospholipids, resulting in maintenance of the spacing of the phospholipid head groups (Chen *et al.*, 2010 (b)). Moreover, the sugars also act to reduce the van der Waals forces between the acyl chains of phospholipids, collectively maintaining the structural integrity of the lipid bi-layer membrane. Figure 5.3 schematically illustrates the underpinnings of the water replacement hypothesis. Briefly, Figure 5.3A represents the aqueous NLS suspension. Freezing and lyophilization in the absence of a lyoprotectant sugar would follow the path from 5.3A-D. Figures 5.3B and 5.3C illustrate the slight disorganization that will occur with the phospholipid bilayers and water molecules during the freezing and drying processes, respectively. Reconstitution of the formulation shows a disruption of the structural integrity of the lipid bi-layer membrane, the effect of which may be demonstrated through alteration of the size distribution and zeta potential of the formulation as well as increased leakage of encapsulated drug compound out of the NLS. In comparison, lyophilization employing a sugar as a lyoprotectant would follow the pathway from 5.3A directly to 5.3E and 5.3F. The lyoprotectant sugar molecules gradually replace the water molecules, thereby maintaining the space between the polar head groups of the phospholipids in the lipid bi-layer, whilst also reducing the interactions between the non-polar chains of the phospholipids. Upon reconstitution, the structural integrity of the lipid membrane is restored, resulting in maintenance of the pre-lyophilization size and surface charge properties of the formulation as well as the drug loading capacity.

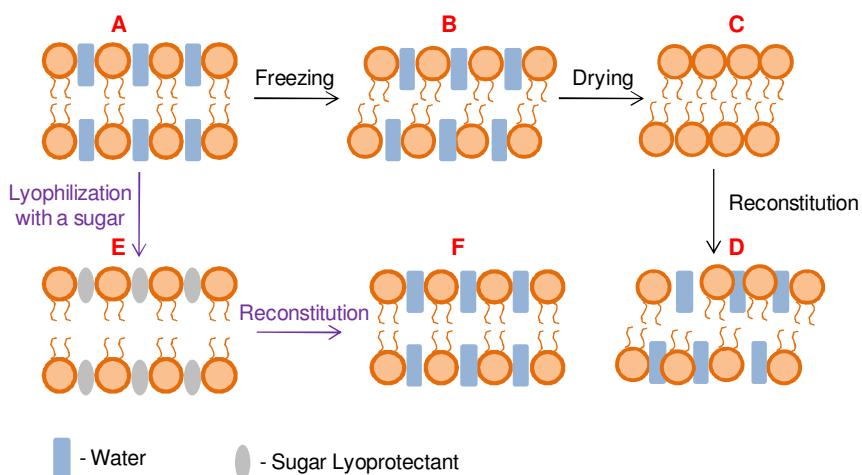


Figure 5.3 Schematic representation of the mechanism of lyoprotection afforded by sugar molecules in the lyophilization of liposomes. (Recreated from Chen *et al.*, 2010 (b))

5.4.3 Determination of lyoprotectant efficacy on formulated nano-liposomes and nano-lipobubbles

As previously explicated, the process of lyophilization is undertaken to enhance the storage stability of formulations, particularly with regards to NLS. Thorough removal of moisture from the formulation reduces the propensity for hydrolytic degradation and other chemical reactions associated with the presence of water. The maximal water content of lyophilized products deemed acceptable is 3%^{w/w} (Chaudhury *et al.*, 2012).

In the absence of a lyoprotectant the lyophilized products of CHO-NLS tended to aggregate, requiring slight agitation for loosening. In addition, formulations appeared to be more hygroscopic, showing greater moisture absorption after 48 hours, as was evidenced by the macroscopically observed clumping of the lyophilized powder. Two sugars, fructose and lactose, were investigated for their efficiency as lyoprotectants in the formulations. The presence of fructose in the formulations resulted in a post-lyophilization product that tended to aggregate with a somewhat spongy appearance and texture, particularly in CHO-NLS, as illustrated in Figure 5.4. Alteration of the concentration of fructose had no significant effect on the texture of the lyophilized product. However, the addition of lactose as a lyoprotectant to CHO-NLS resulted in a more freely flowing powder post-lyophilization. DSPE-NLS showed only very slight aggregation of the lyophilized powder, due to the cryoprotectant and lyoprotectant properties of the PEG molecule. Macroscopic observation of lyophilized DSPE-NLS containing fructose or lactose as lyoprotectants revealed similar, though less pronounced, effects to that observed with CHO-NLS. KF titration corroborated these macroscopic findings, with formulations containing fructose exhibiting approximately 2-4% higher water content on a 10mg sample size. Lactose-containing NLS samples displayed acceptable water content (<3%^{w/w}), hence lactose was employed as the lyoprotectant in all ensuing formulations.



Figure 5.4 Digital images of the post lyophilization products of CHO-NLS A) in the absence of a lyoprotectant, B) with fructose and C) with lactose.

5.4.4 Generation of a standard curve for the photospectroscopic quantification of silibinin

A wavescan was undertaken between 250-600nm to determine the optimum analytical wavelength at which SB is detected at physiologic and tumoural pH. The wavescans depicted in Figures 5.5A and B represents the absorption spectra of SB over the aforementioned wavelength range at pH 7.4 and pH 6.0, respectively. The optimal wavelength for the detection of SB at physiologic pH was deemed to be 334nm. The absorption spectrum of SB at pH 6.0 displayed a double peak, however the intensity was greatest and the peak sharpest at 290nm. Hence, UV-photospectroscopic analysis of SB at pH 6.0 was undertaken at 290nm.

The standard curves generated for the photospectroscopic quantification of SB in DMSO:PBS (pH 7.4 and 6.0; 37°C) (1:1) as well as the regression co-efficients and y-values are depicted in Figures 5.6A and B, respectively. Moreover, the 95% prediction and confidence bands are depicted. The standard deviation between absorbance data on day 1 and day 2 were <0.025, highlighting the precision of the instrument, accuracy of analysis and reproducibility of results.

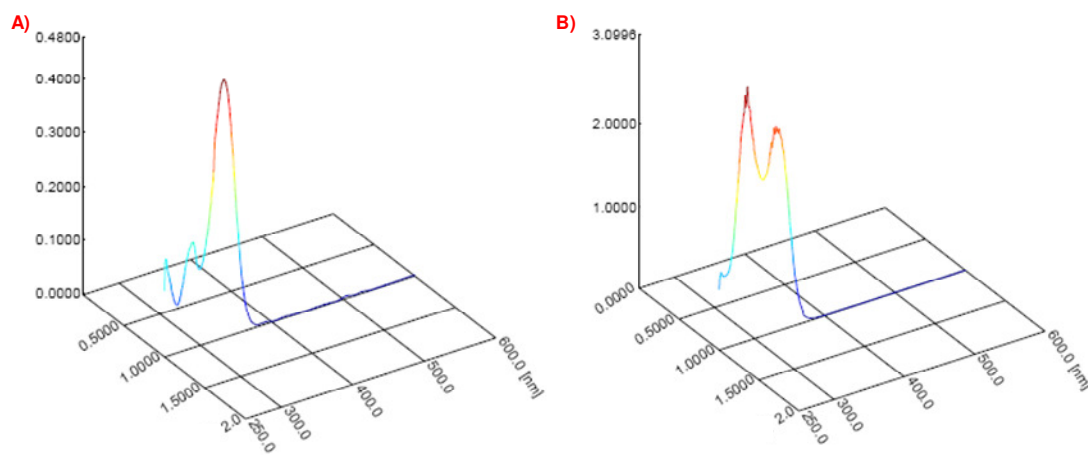


Figure 5.5 Three dimensional absorption spectrum of SB in A) DMSO:PBS (pH 7.4; 37°C) (1:1) and B) DMSO:PBS (pH 6.0; 37°C) (1:1).

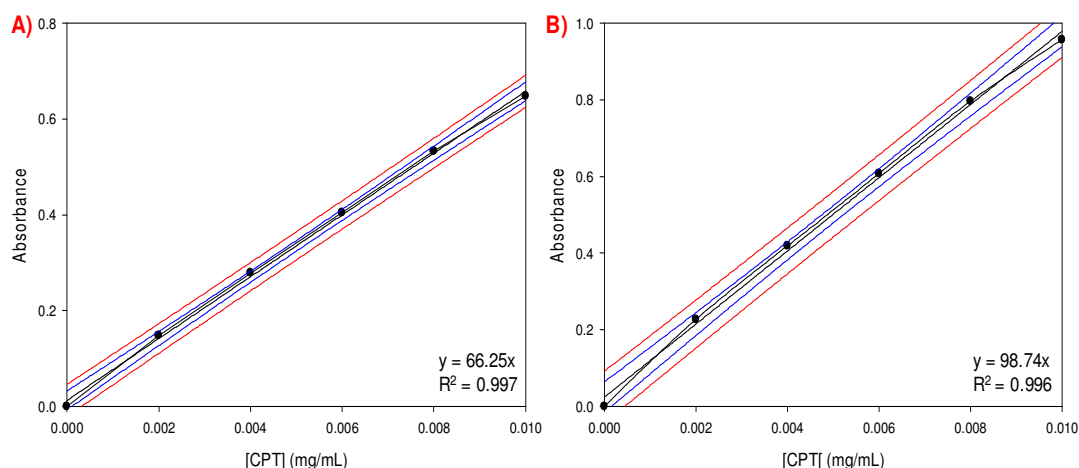


Figure 5.6 Standard curves of the absorbance of SB in A) DMSO:PBS (pH 7.4; 37°C) (1:1) and B) DMSO:PBS (pH 6.0; 37°C) (1:1), as well as the 95% confidence and prediction bands for the respective curves (in all cases $n=3$ and $SD < 0.02$).

5.4.5 Silibinin incorporation and the effect thereof on the physical characteristics of formulated nano-lipobubbles

The incorporation of SB in the formulated NLB-DDS was undertaken to enhance the cytotoxic activity of the formulations and provide a means of effective delivery of this poorly soluble phytochemical. However, the maintenance of the nano-scale of the formulation was the focal point of the study and could not be compromised by the addition of a second antineoplastic compound. Moreover, this modification preceded the intended polymeric coating of the NLB. Hence, only size increments up to 20 nm could be accommodated for CHO-NLB and that of ~50 nm could be allowed for DSPE-NLB.

The initial incorporation of 100-200mg of SB resulted in large average sizes and erratic changes in size over time for CHO-NLB. The size distribution was also very broad with $Pdl > 0.6$. The size profiles of CHO-NLB obtained following the addition of 15-50mg SB were notably more favorable. The disparity in the physical characteristics and DIE of CHO-NLB upon the addition of 15mg and 30mg SB was marginal. Increasing the quantity of SB to 50mg resulted in ~22 nm increase in average of the CHO-NLB, which in turn would not allow for adequate polymeric coating whilst remaining below the 200 nm benchmark size. Furthermore, the concurrent decrease in surface charge and efficiency of SB incorporation proved unfavorable. The tremendously favorable size profile obtained for DSPE-NLB allowed the DDS to remain within a suitable size range following the addition of 15-200mg SB. However, the already unfavorable surface charge was further diminished as the quantity of SB was increased within the defined range, as was the efficiency of SB incorporation. DIE of SB above 50% was identified following the addition of 15mg and 30mg SB only. The disparity in average size of DSPE-NLB to which 15mg and 30mg SB had been added was insignificant, whilst the zeta potential of the formulations was

marginally more favorable following the addition of 30mg SB. Hence, 30mg of SB was delineated for incorporation into both CHO- and DSPE-NLB. Table 5.6 summarizes the resultant average size and zeta potential of CHO- and DSPE-NLB resulting from the addition of a range of SB quantities, as well as the respective efficiency of SB incorporation.

Table 5.6 Physical characteristics of formulated NLB-DDS and efficiency of SB incorporation relative to quantity of SB added to the formulation.

SB Added (mg)	CHO-NLB			DSPE-NLB		
	Average Size (d.nm)	Zeta Potential (mV)	SB Incorporation (%)	Average Size (d.nm)	Zeta Potential (mV)	SB Incorporation (%)
15	137.32	-27.26	66.89	91.57	-8.13	54.63
30	137.56	-27.58	65.59	93.65	-8.24	52.75
50	159.30	-21.23	61.72	93.09	-7.02	43.03
100	246.30	-18.70	50.28	99.84	-6.10	36.21
150	249.73	-18.90	46.77	132.14	-6.46	30.14
200	267.80	-16.30	43.00	143.10	-6.29	24.28

5.4.6 Investigating the feasibility of polymeric coating of nano-lipobubbles: Macroscopic and microscopic evaluation

The application of successful polymeric coating was assessed through inversion of the zeta potential through positive and negative values following the introduction of an oppositely charged polymer. Despite the simplicity of achieving successful polymer coating by this method, as described in the literature, this proved particularly challenging in this study. Coating of CHO- and DSPE-NLS with PLL was discontinued following coating with concentrations up to 3%^{w/v}, as well as increasing the volume ratio of polymer to NLS suspension. The zeta potentials obtained after coating with PLL for CHO-NLS ranged between -7mV and -3.6mV and that obtained for DSPE-NLS ranged between -2.1mV and +0.003mV following coating for 24 hours. Hence, an adequate cationic surface to enable the electrostatic attraction and deposition of an anionic polymer was not achieved.

The deposition of gelatin onto the anionic CHO- and DSPE-NLS surfaces appeared to be incomplete after 18 hours, as evidence by the lack of a positive zeta potential. The zeta potentials acquired were close to neutral, despite varying the concentration of the cationic polymer. The indication of instability and lack of a positively charged surface did not augur well for the deposition of an anionic polymeric layer by electrostatic attraction.

Following coating with the various polymers and combinations of polymers employed, the lyophilized products exhibited varied macroscopic appearances, most of which were incongruent with the uniform powder that was expected. Coating of NLS with alternating layers of PEI and pectin or carrageenan produced a fine network structure (depicted in Figure 5.7A), reconstitution of which required prolonged stirring times (~3 hours) at elevated temperatures of approximately 40°C. PEI, when used alone and in combination with alginate, produced uniformly spongy products with a micro-spindle appearance, as displayed in Figure 5.7B. Reconstitution of the sponges also necessitated extended stirring periods and was incomplete after continuous agitation for 4 hours at physiologic temperature. This is unsuitable to clinical application and will result in release of drug from the DDS prior to administration.

Coating with CHT and carrageenan proved unsuccessful with separation into 2 distinct layers being observed following the addition of carrageenan. Variation in the concentration of each of these polymers did not prove to have an adequately favorable effect. Coating of formulated CHO- and DSPE NLS alternately with CHT and pectin produced spongy products (highlighted in Figure 5.7C), the reconstitution of which was incomplete after stirring for 8 hours at ~37°C.

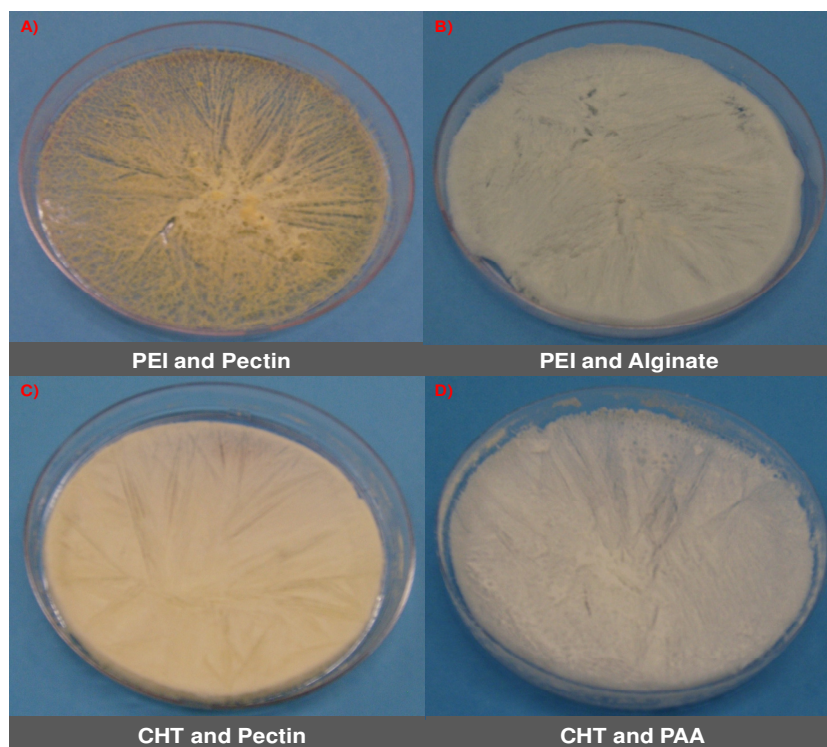


Figure 5.7 Digital images of typical post-lyophilization products of CHO-NLS coated with A) PEI and pectin, B) PEI and alginate, C) CHT and pectin, D) CHT and PAA.

The sequential layering of CHO- and DSPE-NLS with CHT and PAA proved extremely beneficial, displaying adequate inversion of zeta potential following the adsorption of each layer, as illustrated in Figure 5.8. This change in zeta potential manifested over a shorter period with CHO-NLS. This was attributed to the initially more highly charged nature of the formulated NLS, which resulted in swifter and more complete adsorption of the oppositely charged polymeric layer. Increasing the concentration of PAA from 0.5%^{w/v} to 2%^{w/v} resulted in an overall strongly anionic surface with no significant polymer precipitation in the suspension. Similarly, decreasing the concentration of CHT from 0.5%^{w/v} to 0.1%^{w/v} facilitated the establishment of the desired overall anionic zeta potential. Lyophilization of the NLS following the successful application of four polymeric layers, in the presence of lactose, resulted in a somewhat flaky powder (as illustrated in Figure 5.7D), which could be rapidly and easily re-dispersed under ambient conditions. Moreover, the average size of resultant polymer coated-NLB following reconstitution and the introduction of a gaseous core, remained well below 200 nm (CHO-NLB=189.81 nm; DSPE-NLB=141.62 nm), which was the benchmark size delineated for the stabilized nanosystem. The resultant surface charge of polymer-coated CHO-NLB following the application of four polymeric layers was -32.47mV and that of DSPE-NLB was -24.27mV. The institution of polymeric coating had a more pronounced favorable effect on the surface charge of DSPE-NLB than on CHO-NLB. The strongly anionic surface achieved for both formulations had propitious consequences on the stability of NLB formulations. Moreover, anionic surfaces have been reported to have advantageous implications with regard to haemocompatibility and cellular internalization, as expounded in Chapter 3, Section 3.2.1.3.2.

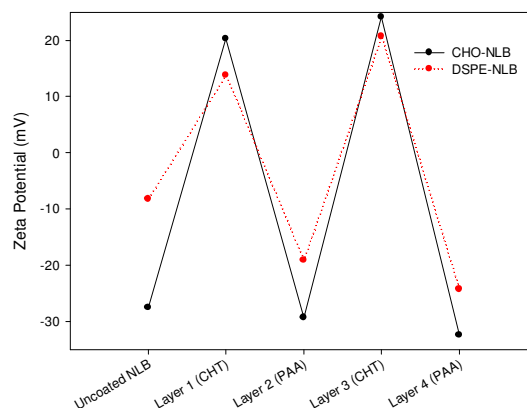


Figure 5.8 Effect of the sequential deposition of alternating layers of CHT and PAA on the zeta potential of CHO- and DSPE-NLB.

Qualitative assessment of the morphological characteristics of lyophilized polymer coated CHO- and DSPE-NLS, employing scanning electron microscopy, provided a deeper understanding of the macroscopic appearance and behavior of the formulations. The network structure observed macroscopically following coating of CHO-NLS with PEI and

pectin or carrageenan was identified as a polyelectrolyte complex (PEC) embedded with NLS as illustrated in Figures 5.9A and 5.9B. The NLS were well distributed through the PEC and there was a distinct absence of aggregation. However, the tight network structure may be responsible for the prolonged time required for complete solubilization of the product.

The spongy macroscopic presentation of CHO-NLS coated with CHT and pectin was confirmed by the scanning electron micrograph in Figure 5.9C. The surface appears uneven with shallow contusions. CHO-NLS are fairly evenly scattered throughout the sponge, however, the concentration of NLS is distinctly lower than that observed with other formulations. This trend was consistent following assessment of representative sections from three samples. The reduced concentration was attributed to NLS being trapped in the shallow contusions of the sponge as well as partial aggregation of the NLS due to entrapment within the spongy environment. The micrograph in Figure 5.9D of DSPE-NLS coated sequentially with CHT and PAA revealed well defined NLS with the absence of a significant matrix. This substantiates the ease of reconstitution of the samples. The microscopic appearance of CHO-NLS coated with the same polymer combination exhibited comparable characteristics to that observed with coated DSPE-NLS.

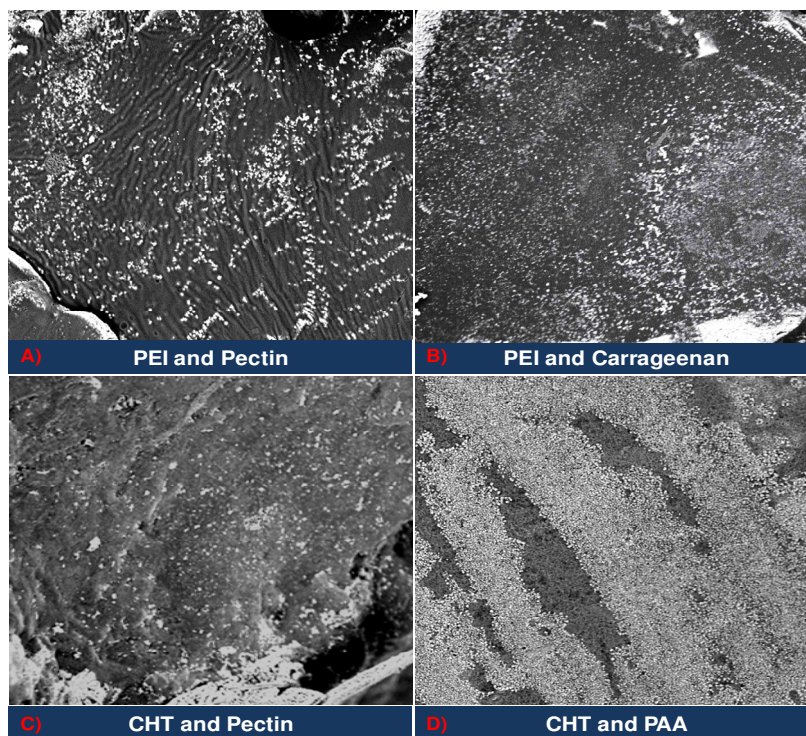


Figure 5.9 Scanning electron micrographs of post-lyophilization products of CHO-NLS coated with A) PEI and pectin (4200x magnification); B) PEI and carrageenan (2800x magnification); C) CHT and pectin (3200x magnification) and D) CHT and PAA (4800x magnification).

5.4.7 Confirmation of polymeric coating through chemical structural transition analyses

The undertaking of FTIR analysis was intended, in conjunction with the results of zeta potential analysis, to confirm the adsorption of oppositely charged polymers to the surface of formulated CHO- and DSPE-NLS. The FTIR spectra of uncoated and optimized CHO- and DSPE-NLS as well as that of the native polymers (CHT and PAA) employed in polymeric coating of the NLS are depicted in Figures 5.10A and 5.10B. There is a distinct difference between the FTIR spectrum of uncoated and optimized NLS which is related to the adsorption of CHT and PAA. The appearance of a prominent peak at 1702cm^{-1} in the spectrum of optimized CHO-NLS and at 1705cm^{-1} was the most outstanding difference relative to the spectra of uncoated CHO- and DSPE-NLS. These peaks corresponded to the carboxyl group of PAA, which manifested at 1695cm^{-1} in the spectrum of native PAA. There was a clear change in the appearance of minor peaks between uncoated and optimized CHO-NLS at the region of $1200\text{-}1660\text{cm}^{-1}$, due to CH_2 bending and $\text{C}=\text{C}$ bands in PAA. A broad band was observed from approximately $2800\text{-}3500\text{cm}^{-1}$ with optimized CHO- and DSPE-NLS, which was ascribed to the stretching hydroxyl band in PAA. The marked similarity in the spectra of optimized CHO- and DSPE-NLS to PAA is evident of successful and complete PAA adsorption. The high degree of PAA adsorption suggests a strong attraction to a cationic surface, which can be ascribed to successful CHT adsorption prior to the introduction of PAA, since the surface of uncoated NLS was of an anionic nature. These results corroborate the changes in zeta potential following the application of sequential polymeric layers and confirm the achievement of a robust polyelectrolyte coating of formulated NLS.

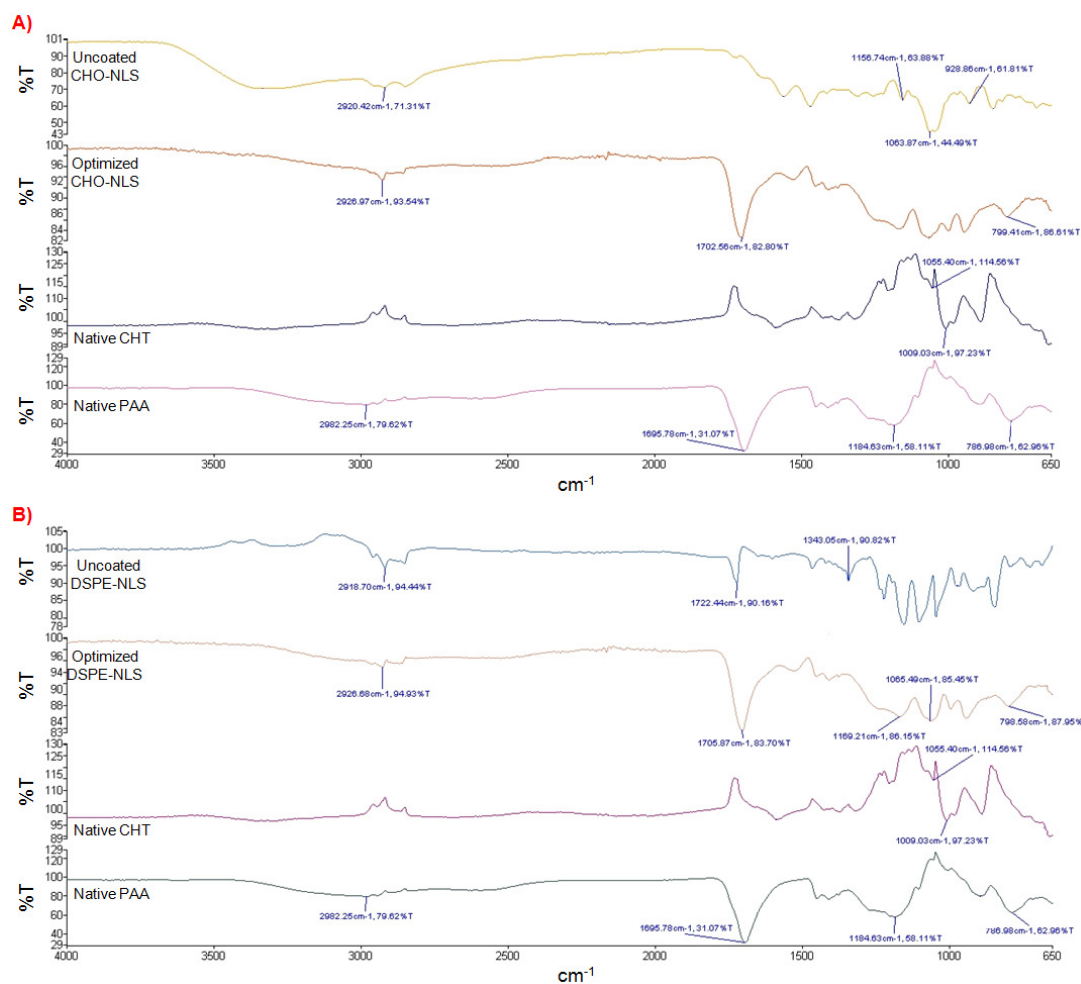


Figure 5.10 FTIR spectra highlighting the chemical structural transitions of optimized A) CHO-NLS and B) DSPE-NLS following polymeric coating, relative to uncoated CHO- and DSPE-NLS and the native polymers employed in the polyelectrolyte coating.

5.4.8 Determining the restoration of nano-lipobubble structure employing fluorescence microscopy

Fluorescence microscopy was employed to confirm the restoration of NLS structure and subsequent conversion to NLB, following reconstitution of the lyophilized powder. The fluorescence micrographs of CHO-NLB and DSPE-NLB displayed in Figures 5.11A and B, respectively, highlight the resilience of the bi-layer lipid membrane structure and the restoration of the spherical NLB structure. Moreover, there is a distinct absence of aggregation of the NLB.

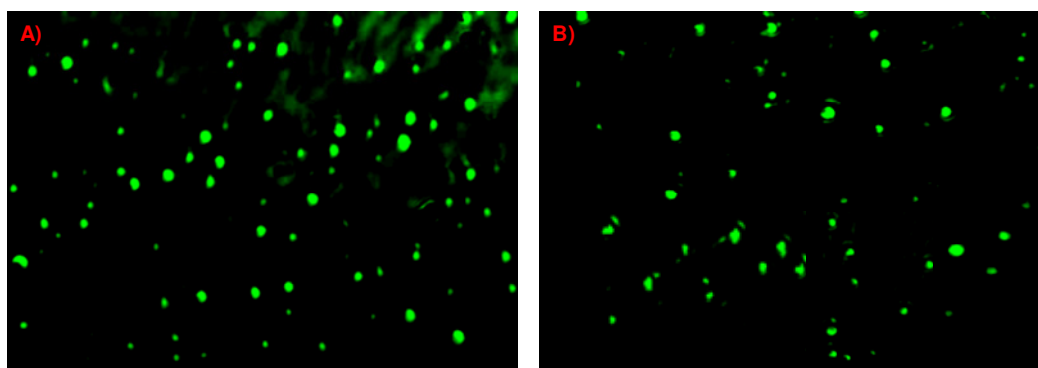


Figure 5.11 Fluorescence micrographs of A) CHO-NLB and B) DSPE-NLB labelled with FITC dye confirming the restoration of NLB structure following lyophilization, reconstitution and SF₆ gas introduction.

5.4.9 Establishing the efficiency of camptothecin incorporation

The efficiency of CPT incorporation for candidate CHO- and DSPE-NLS demonstrated exceptionally close correlation to those predicted by statistical optimization, as outlined in Table 5.7. Conversion of NLS to NLB did not result in significant change in DIE. However, lyophilization followed by reconstitution resulted in ~2% decrease in DIE for CHO-NLB and DSPE-NLB.

Table 5.7 Experimentally derived and statistically predicted DIE of CPT for CHO- and DSPE-NLB.

Formulation	DIE		
	Experimental (%)	Predicted (%)	Variance (%)
CHO-NLS	81.86	82.4128	0.007
DSPE-NLS	59.11	59.1864	0.001

The introduction of SB to the NLB formulations bore the potential to affect all physical and physicochemical characteristics of the formulations, not least of all being CPT incorporation. The considerations, with regards to drug incorporation, following this modification were two-fold. Firstly, the efficiency of SB incorporation was analyzed, since this directly influenced the synergistic antineoplastic effect desired from the introduction of this phytochemical. Secondly, the effect of SB incorporation on the efficiency of CPT incorporation was pertinent to the feasibility of this modification. CPT and SB are both lipophilic compounds and hence were expected to compete for incorporation within the NLB-DDS. The quantity of SB (30mg) determined to be the most feasible for incorporation into CHO- and DSPE-NLB displayed >65% incorporation into CHO-NLS with an insignificant decrease in CPT incorporation. DSPE-NLB exhibited a satisfactory incorporation efficiency of SB (~53%) following the addition of 30mg SB. However, this formulation repeatedly exhibited a concurrent increase in CPT incorporation of ~2.5%.

The final modification undertaken on formulated CHO- and DSPE-NLB was the application of sequential layers of polymeric coating. The extended hours required for the

complete adsorption of polymeric coats presented a concern with respect to the leakage of drugs from the NLB-DDS. Coating time was minimized by regular analysis of zeta potential to determine successful coating with the respective polymer in the shortest period. CPT and SB content were assessed before and after the application of polymeric coating.

The robustness of CHO-containing bi-layer NLB membranes was again evident by the marginal decrease in CPT and SB content following complete polymeric coating. Moreover, the high surface charge of CHO-NLB perhaps contributed to swifter adsorption of polymers on to the surface, thereby further hindering drug leakage out of the NLB. DSPE-NLB, however, suffered higher drug leakage during the process of polymeric coating. Preliminary studies had displayed more rapid release of drug from DSPE-NLB as opposed to CHO-NLB hence this observation was not entirely unexpected. Nevertheless, CPT content of DSPE-NLB following polymeric coating was only ~4.5% lower and that of SB was ~2.7% lower than that achieved prior to the initiation of polymeric coating. Figure 5.12 summarizes the final DIE of CPT and SB following polymeric coating, lyophilization and reconstitution in the presence of lactose.

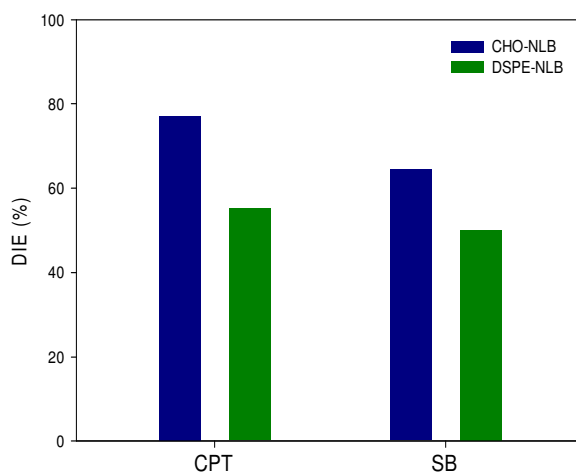


Figure 5.12 Graphical illustration of the post-modification DIE's of CPT and SB in CHO-NLB and DSPE-NLB.

5.4.10 Generation of a standard curve for the photospectroscopic quantification of CPT at tumoural pH

The evaluation of CPT release characteristics at approximate tumoural pH of 6.0 (37°C) necessitated the development of a standard curve to quantify CPT release at the relevant time intervals. A wave-scan was fundamental in delineating the optimal wavelength at which CPT was detected and is illustrated in Figure 5.13.

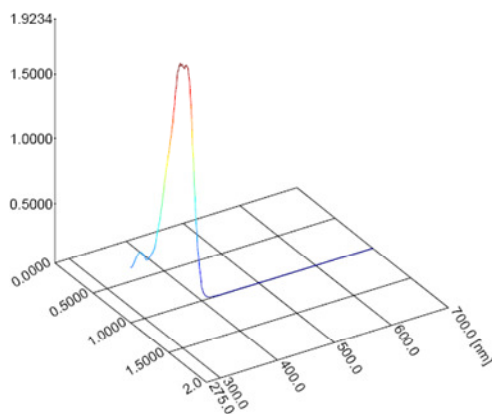


Figure 5.13 Three dimensional absorption spectrum of CPT in DMSO:PBS (pH 6.0, 37°C) (1:1).

A standard curve of CPT absorbance was subsequently prepared at 345nm based on serial dilutions of CPT in DMSO:PBS (pH 6.0; 37°C) (1:1). Figure 5.14 illustrates the standard reference curve of CPT in DMSO:PBS (pH 6.0; 37°C) (1:1) as well as the regression co-efficient, y-value, and 95% confidence and prediction bands. Absorbance values obtained on each of the two days the measurements were conducted exhibited a standard deviation of <0.02, validating the precision of the instrument and accurate reproducibility of data.

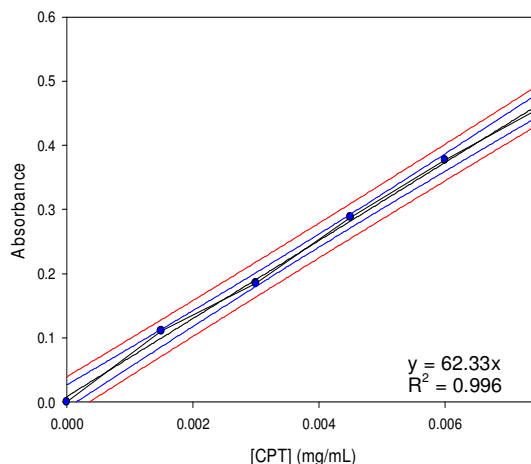


Figure 5.14 Standard curve of the absorbance of CPT in DMSO:PBS (pH 6.0; 37°C) (1:1), as well as the 95% confidence and prediction bands (in all cases n=3 and SD<0.02).

5.4.11 Establishment of drug release characteristics and the effects of modifications on candidate formulations

The observed pattern of CPT release from candidate NLS was analogous to the general trend observed with formulations in each of the experimental designs. Candidate NLS and NLB displayed a somewhat bi-phasic CPT release pattern, which was most prominent for CHO-NLS, as illustrated in Figures 5.15A and 5.15B. The disparity between release of CPT from CHO-NLS and DSPE-NLS, depicted in Figure 5.15A, was once again a central

feature noted with the candidate NLS. The difference in CPT release may be directly attributed to the average size and surface charge characteristics of each of the candidate NLS. The lower average size of DSPE-NLS provides a greater surface area-to-volume ratio, thereby increasing the area of diffusivity for CPT out of the DDS. Moreover, the substantially more negative surface charge of CHO-NLS diminishes the tendency for agglomeration of the NLS, thus enhancing the stability of the formulation. CHO-NLS demonstrated a slightly more rapid CPT release than DSPE-NLS over the first 6 hours of analysis. Thereafter the rate of CPT release appeared to decrease. The bi-phasic pattern of DSPE-NLS exhibited faster CPT release for approximately the first 12 hours of the analytical period, followed by a slight decrease in CPT release. Hence the fractional release of CPT from DSPE-NLS exceeds that from CHO-NLS from 10 hours onwards. Complete release of CPT from DSPE-NLS was observed at 20 hours. CHO-NLS displayed only ~75% cumulative release of incorporated CPT over the 24 hour analysis period. The more acidic pH employed to represent the tumoural environment appeared to have only a marginal effect on CPT release, that varied over the analytical period, from each of the candidate NLS.

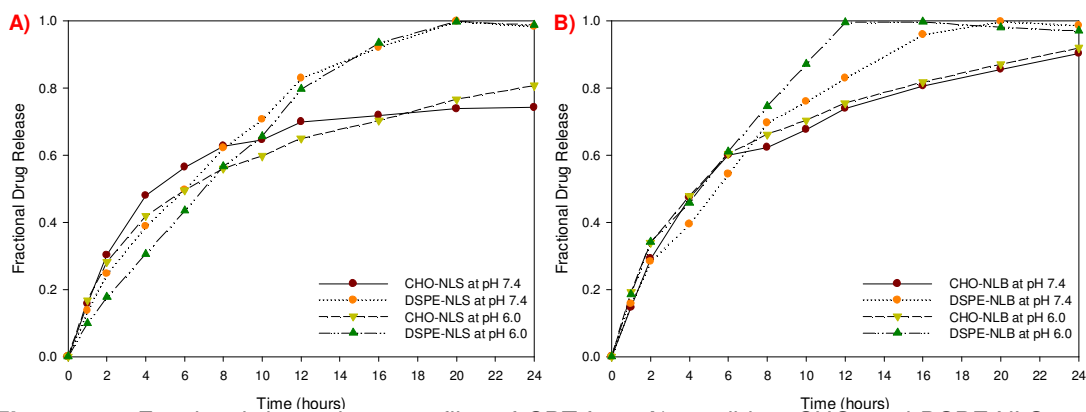


Figure 5.15 Fractional drug release profiles of CPT from A) candidate CHO- and DSPE-NLS and B) candidate CHO- and DSPE-NLB, at tumoural and physiologic pH over 24 hours (in all cases n=3 and SD<0.02).

The introduction of a gaseous core in the conversion of candidate NLS to NLB resulted in a significantly more rapid release of CPT across all formulations, as illustrated in Figure 5.15B. The first 6 hours of analysis demonstrated very similar CPT release from all of the formulations at physiological and tumoural pH, with the exception of DSPE-NLB at physiological pH. Beyond 8 hours, CPT exhibited a somewhat slower release pattern from CHO-NLB, achieving between 90-92% cumulative CPT release over the 24 hour analytical period under both pH conditions. The significant decrease in surface charge that followed the conversion of CHO-NLS to lyophilized and reconstituted CHO-NLB (-37.9mV to -27.9mV) was attributed with the increase in CPT release from the candidate CHO-

NLB. A decrease in the intensity of a charged surface results in a less stable formulation that has a greater propensity for aggregation of the NLB. Notwithstanding the decrease in surface charge of CHO-NLB, the zeta potential achieved following conversion to NLB was highly satisfactory, accounting for the absence of a significant burst release from the NLB formulation as well as the controlled pattern of CPT release. Once again, analysis at the lower pH highlighted no significant consequence on the release of CPT from CHO-NLB.

The release of CPT from DSPE-NLB, illustrated in Figure 5.15B, was notably higher than from DSPE-NLS, particularly at lower pH where complete CPT release was observed by 16 hours. The swifter release of CPT from DSPE-NLB can be attributed somewhat to the low surface charge of the formulation. However, it is postulated that the average size of the formulation as well as permeability of the lipid membrane may further contribute to the pattern of CPT release since the zeta potential of post-lyophilization DSPE-NLB is marginally more favourable than that of DSPE-NLS. The considerably faster release of CPT from DSPE-NLB at pH 6.0 may suggest a higher permeability of the lipid membrane to the SF₆ gas in the core of the NLB at lower pH, resulting in swifter release of the incorporated drug.

The addition of a second active compound SB, constituted a need to assess the release characteristics of SB as well as determine the effect of SB release on the release profile of CPT. The release pattern of CPT from CHO-NLB containing SB (CHO-NLB+SB) demonstrated no outstanding differences to that of SB naïve formulations for the first 10 hours, except for an evident burst release of CPT over the first hour (as illustrated in Figure 5.16A). A similar burst release of SB was observed over this period, displayed in Figure 5.16B, suggesting association of both compounds to a certain degree with the surface of the NLB. Furthermore, the presence of an additional compound may have altered the surface tension of the formulated CHO-NLB, leading to the initial burst release of both CPT and SB. From 10 hours the release of CPT from CHO-NLB+SB is approximately 7-9% higher than that observed for CHO-NLB without SB. An effect of the different pH of release medium (7.4 and 6.0) employed during analysis only became evident after 10 hours, when the release of CPT at pH 6.0 appeared to be slightly higher than that at pH 7.4. However, the effect of tumoural pH on the release characteristics of CPT from CHO-NLB+SB was still considered negligible following this study. A cumulative CPT release of 82-86% was achieved for CPT from CHO-NLB+SB over the 24 hour investigation.

The release pattern of CPT from DSPE-NLB containing SB (DSPE-NLB+SB) was slower relative to that for CHO-NLB+SB for the first 10 hours, thereafter exceeding that of CHO-NLB+SB. The lack of significant burst release of CPT and SB suggests association of CPT and SB with the surface of the NLB was absent or to a far lesser extent than suspected for CHO-NLB+SB. The release of CPT from DSPE-NLB+SB was lower than that from SB naïve DSPE-NLB throughout the period under investigation. The difference in pH of the release medium had no demonstrable effect on the release behaviour of CPT from DSPE-NLB+SB. Complete release of CPT from DSPE-NLB+SB was determined by the completion of the 24 hour assessment period.

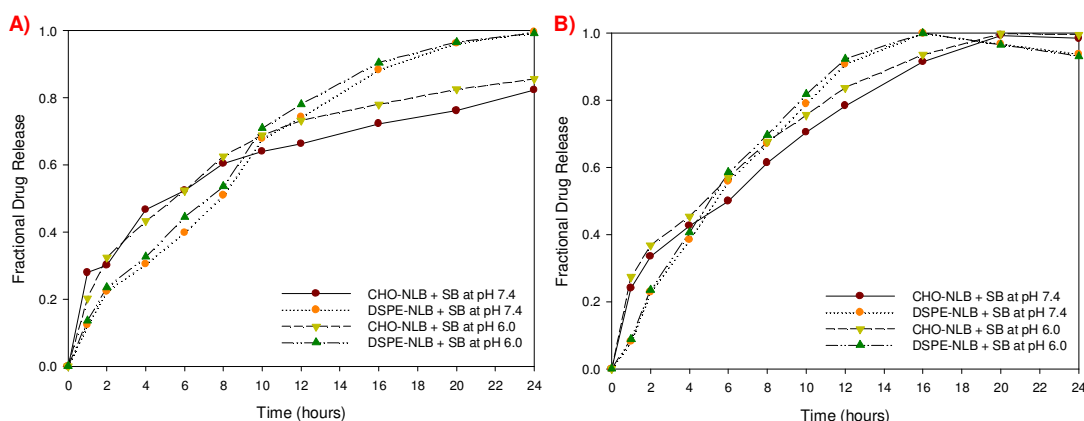


Figure 5.16 Fractional drug release of A) CPT and B) SB, from CHO- and DSPE-NLB containing SB, at tumoural and physiologic pH over 24 hours (in all cases n=3 and SD<0.02).

Following the aforementioned burst release of SB from formulated CHO-NLB during the first hour of analysis, the ensuing pattern, exhibited in Figure 5.16B, highlights a fairly constant release pattern that is considerably faster than that observed with CPT. SB is more aqueous soluble than CPT which may have contributed to retention of CPT within the lipid environment of the NLB to a greater extent than that of SB. SB appeared to release 3-8% faster at lower pH than at physiologic pH over the 24 hour period. Complete release of SB from CHO-NLB was denoted after 20 hours at both physiologic and tumoural pH. The pattern of SB release established from DSPE-NLB was remarkably constant, closely resembling first order release. The steeper gradient of the release profile substantiates the achievement of complete SB release from DSPE-NLB+SB in 16 hours. The pH of the release medium had a marginal influence on the release characteristics of SB. The release of SB from DSPE-NLB+SB was significantly more rapid than that of CPT from the same formulation, after the first hour.

The challenge of delivering a poorly aqueous soluble compound that undergoes extensive metabolism has compromised the utilization of SB to its full clinical potential. This phytochemical has, however, demonstrated high permeability *in vivo*. Incorporation into

the NLB-DDS provides a mechanism of delivery to the tumour tissue where SB can enter tumour cells and exert its antineoplastic activity effectively.

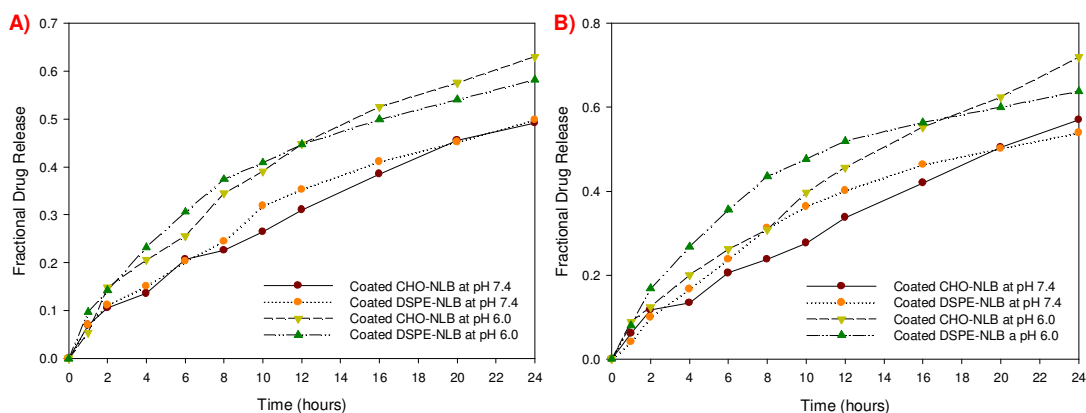


Figure 5.17 Fractional drug release of A) CPT and B) SB, from coated CHO- and DSPE-NLB, at tumoural and physiologic pH over 24 hours (in all cases $n=3$ and $SD<0.02$).

The emphasis placed on delaying the onset and reducing the rate of CPT and SB release was established on the need to reduce the indiscriminate systemic activity of these compounds as well as increasing the concentration of CPT and SB at the tumour site. To achieve this, sufficient time was required to allow for passive accumulation of the formulated DDS at the tumour site before a significant proportion of the incorporated compounds were released. Moreover, extending the release of CPT would be particularly advantageous since the drug acts predominantly in the S-phase of the cell cycle. Hence, extended release facilitates the exposure of a greater quantity of tumour cells in the S-phase to CPT, thereby enhancing the efficacy of CPT. The institution of layered polymeric coating on formulated NLB proved exceptionally advantageous at slowing the release of both CPT and SB from each of the candidate NLB-DDS.

Whilst the application of polymeric coating significantly slowed the release of CPT from CHO-NLB at both physiologic and tumoural pH, the disparity in release characteristics was considerably more acute at pH 7.4. The bi-phasic release pattern observed with uncoated NLB was distinctly absent, with the release profile taking on a more constant linear shape, as demonstrated in Figure 5.17A. The cumulative release of CPT achieved at 24 hours was $<50\%$. This is a considerable extension of the ≤ 1 hour half-life of CPT in aqueous medium as reported in the literature (Yang *et al.*, 1999; Kang *et al.*, 2002). In addition, less than 7% of CPT was released from the NLB-DDS in the first hour of analysis, highlighting the absence of burst release as well as indicating adequately low concentration of CPT released into the systemic circulation. The achievement of the aforementioned release characteristics of CPT from the formulated polymer coated CHO-

NLB has the potential to address the toxicity profile of CPT which is one of the major drawbacks limiting the clinical application of this broad-spectrum antineoplastic agent.

Evaluation of CPT release at a lower tumoural pH of 6.0, presented in Figure 5.17A, also revealed a favorable decrease in the release of CPT over the period of investigation. The release of CPT in the first hour of analysis was lower than that observed for uncoated CHO-NLB at pH 6.0 as well as for polymer coated CHO-NLB at physiologic pH. Moreover, the release profile of CPT from coated CHO-NLB had a notably more linear appearance than uncoated CHO-NLB, suggesting a more controlled manner of release. However, beyond the first hour the release of CPT from the polymer coated NLB-DDS was substantially more rapid than observed at physiological pH. A cumulative release of ~63% CPT was achieved over the 24 hour period, which was more than 14% higher than CPT release attained from coated CHO-NLB over the same period. This was attributed to the pH-responsive property of CHT which was incorporated in the polymeric layers coating the NLB. CHT is a linear polysaccharide that demonstrates aqueous solubility up to pH 6.2, due to the protonation of glucosamine units at this lower pH (Pujana *et al.*, 2012; Chatrabhuti and Chirachanchai, 2013). This alteration in the characteristics of CHT at lower pH facilitates use of this polymer for pH-responsive applications. While the formulated NLB-DDS cannot be considered strictly pH-responsive, increase in the release of CPT at the lower tumoural pH results in increased concentration of the antineoplastic drug within tumour tissue which has the potential to significantly enhance therapeutic efficacy of CPT.

Evaluation of the release characteristics of CPT from coated DSPE-NLB bore a strong resemblance to that obtained from coated CHO-NLB in both a physiologic and tumoural pH release medium. A general trend observed with uncoated DSPE-NLB was more rapid release of active compounds relative to uncoated CHO-NLB. This observation was attributed to lower stability of the DSPE-NLB, due to the less anionic surface charge, as well as the higher permeability of DSPE-NLB lipid membrane. Following polymeric coating, the zeta potential of DSPE-NLB demonstrated a tremendously favorable enhancement of the anionic intensity of the surface charge, to a greater extent than the change observed with coated CHO-NLB. In addition, the polymeric coating considerably decreased permeability of the DDS to the SF₆ gaseous core. The coated DSPE-NLB retained some of the bi-phasic release characteristics at pH 6.0 that was discerned from the uncoated formulations. Release of CPT from DSPE-NLB was faster over the first 8 hours of evaluation. The cumulative release of CPT demonstrated from DSPE-NLB at physiological and tumoural pH approximated 50% and 58%, respectively. This favorable

release pattern combined with the smaller size of coated DSPE-NLB, relative to that of coated CHO-NLB may prove vastly advantageous to the passive targeting capacity of this DDS.

As described for CPT, the release of SB from CHO- and DSPE-NLB was significantly reduced as a consequence of the polymeric coating, as depicted in Figure 5.17B. The burst release of SB from uncoated CHO-NLB was a particular concern. Polymeric coating successfully reduced the release of SB from CHO-NLB by ~19% during the first hour under both pH environments. The influence of pH was tangible, particularly after the first 2 hours of analysis. The release of SB from CHO-NLB was slightly faster than that derived for CPT. The cumulative release achieved for SB from CHO-NLB at pH 7.4 and 6.0 were 57% and ~72%, respectively. Investigation of DSPE-NLB also highlighted considerably slower release of SB following polymeric coating of the DDS. There was a pronounced influence of pH on the release of SB from coated DSPE-NLB, with cumulative release at physiologic pH ~10% lower than that determined at tumoural pH. The reduced release of SB at physiologic pH indicates a lower concentration of SB will be subjected to metabolism in the systemic circulation and clearance prior to reaching the tumour tissue. The quicker release of SB from coated DSPE-NLB at tumoural pH will facilitate the achievement of higher concentrations of SB at the target site, resulting in superior SB efficacy as well as enhanced synergistic antineoplastic effect with CPT.

5.4.12 Defining the stability characteristics of formulated nano-lipobubbles

Stability of pharmaceutical formulations can significantly influence viability of the formulation from cost, production and clinical use standpoints. Formulations that cannot be stored for an acceptable period require production shortly before use which can result in an increase in production and transportation costs, delays in treatment due to unforeseen circumstances and ultimately complicate clinical use. Moreover, post-reconstitution time-dependent stability of lyophilized products, suitable storage conditions, as well as post-administration stability is pivotal to the assessment of the overall feasibility of formulations.

5.4.12.1 Determination of the stability of nano-lipobubbles in serum

The intended intravenous delivery of the NLB formulations demands the establishment of stringent stability parameters, particularly with regards to the size characteristics of administered formulations. The adsorption of serum proteins, or the aggregation of NLB in the presence of serum proteins can significantly affect the feasibility of the formulation. Uncoated CHO-NLB exhibited a <10 nm increase in size in the presence of serum

proteins, over the analysis period, as well as a marginal decrease in surface charge. This was attributed to slight destabilization of the CHO-NLB in the presence of serum proteins which resulted in aggregation of the NLB. The increase in surface charge following polymer coating of the CHO-NLB afforded greater stability to the formulation. Hence the presence of serum proteins had only a marginal effect on the stability of the formulation. The <2 nm increase in size was not attributed to the presence of serum proteins, but rather to normal size variation of the nanosystem over time. Maintenance of the zeta potential was a further indication that aggregation of the CHO-NLB was absent.

Table 5.8 Physical characteristics of uncoated and polymer coated CHO- and DSPE-NLB in the presence of FBS.

CHO-NLB						
Time (min)	Uncoated NLB			Polymer-coated NLB		
	Average Size (d.nm)	PdI	Zeta Potential (mV)	Average Size (d.nm)	PdI	Zeta Potential (mV)
0	137.56	0.19	-27.58	189.81	0.21	-32.47
15	140.02	0.23	-25.83	190.01	0.20	-32.41
30	140.67	0.27	-24.02	190.72	0.23	-31.98
45	143.91	0.24	-24.78	191.06	0.19	-32.42
60	145.32	0.29	-23.35	191.39	0.21	-31.77

DSPE-NLB						
Time (min)	Uncoated NLB			Polymer-coated NLB		
	Average Size (d.nm)	PdI	Zeta Potential (mV)	Average Size (d.nm)	PdI	Zeta Potential (mV)
0	93.65	0.26	-8.24	141.62	0.21	-24.27
15	93.91	0.22	-8.20	141.84	0.19	-24.21
30	93.86	0.21	-7.94	141.91	0.20	-24.00
45	94.27	0.24	-8.17	142.06	0.21	-23.84
60	94.91	0.21	-8.21	142.24	0.21	-23.87

There was a distinct absence of membrane destabilization for uncoated and polymer-coated DSPE-NLB in the presence of serum proteins, as evidenced by the minute variations in size and zeta potential of formulations of the analysis period. The presence of PEG conjugated to DSPE in the membrane of the formulated DSPE-NLB conferred superior stability to the formulation against the effects of serum proteins. The strong anionic charge of polymer-coated DSPE-NLB was accredited for the stability of the formulation against aggregation and interaction with serum proteins.

5.4.12.2 Characterizing the stability of reconstituted nano-lipobubbles

The reconstitution of lyophilized powders or particulate formulations into suspensions is accompanied by a change in the stability of the formulation. Preparation and administration instructions by manufacturers of some cytotoxic preparations define a

period of just 4-6 hours between reconstitution of the product and complete intravenous infusion of the cytotoxic preparation. The stability of formulated NLB-DDS was assessed at ambient temperature employing a Turbiscan™ LAB (Formulaction, L'Union, France). Determination of the light backscattered by the coated and uncoated NLB preparations was employed to define stability characteristics of the formulations. The Turbiscan™ LAB is able to detect minute alterations in the behavior of suspended matter considerably earlier than macroscopic observation will allow.

The backscatter plot of uncoated CHO-NLB (depicted in Figure 5.18A) highlights no localized changes in the behavior of the particulate matter, which would be indicative of sedimentation or creaming of the suspended NLB. However, the change in backscatter across the entire spectrum suggested a change in the size of the NLB. A decrease in size was observed over the first 6 hours post reconstitution, which may have been the result of gradual evaporation of the gaseous core out of the NLB. Thereafter a marginal increase (<2%) in size of the CHO-NLB was observed. The decrease in formulation stability that is associated with time after reconstitution resulted in aggregation, and possibly coalescence, of CHO-NLB thereby causing the increase in size detected by the increase in backscatter. The maximal variation in backscatter determined over the 12 hour period following reconstitution approximated 4%. The change in backscatter was quantified over the analytical period and is depicted in Figure 5.18C. The most distinct change in backscatter, as indicated by the steepest gradient, was observed from 0.5-4.5 hours with a 0.94%/hour change in backscatter.

The backscatter profile for polymer coated CHO-NLB, depicted in Figure 5.18B represents an exemplary display of formulation stability. Similar to the uncoated CHO-NLB, there was no evidence of creaming or sedimentation. A marginal (<2%) variation in size of the CHO-NLB was observed over the 12 hour period. However, unlike with uncoated CHO-NLB, only a uni-directional size variation was observed. The slight reduction in size of coated CHO-NLB was attributed to gradual permeation of SF₆ gas out of the NLB. The enhanced stability of the formulated coated CHO-NLB underlies the absence of aggregation that was observed with the uncoated CHO-NLB from 6 hours post-reconstitution. Figure 5.18D quantifies the change in backscatter referenced to the initial measurement, over the analytical period. The gradient of the graph highlights the exceptional stability of the polymer coated CHO-NLB formulation with a 0.01% change in backscatter per hour.

There is a definitive absence of migrational behavior of uncoated and coated DSPE-NLB, confirming stability of the formulation against sedimentation or creaming. The backscatter

plot of uncoated DSPE-NLB, presented in non-referenced mode in Figure 5.19A, highlights comparable characteristics to uncoated CHO-NLS with regards to a reduction in NLB size observed during the first half of the analysis period, followed by an increase in size of the suspended NLB. This phenomenon was again attributed to the evaporation of the gaseous core from the DSPE-NLB resulting in diminished size of the DDS followed by aggregation of the less stable DSPE-NLB during the latter stages of analysis. The maximal change in backscatter observed over the 12 hour period approximated 2.5%. Whilst DSPE-NLB were less stable than CHO-NLB, as concluded by the zeta potential displayed by each formulation, the change in backscatter was less than the 4% variation observed for CHO-NLB. The smaller initial size of uncoated DSPE-NLB contained a smaller volume of SF₆ gas in the core of the formulation. Consequently, evaporation of the gaseous core out of the formulated DSPE-NLB caused a slighter size variation than that observed with larger CHO-NLB. The change in backscatter was quantified by means of the DeltaBS(t) plot depicted in Figure 5.19C. This plot highlights the largest reduction in backscatter over the 0.5-4.5 hours, followed by alternating increase and decrease in backscatter which suggests insignificant size variation due to reversible aggregation of the suspended NLB in Brownian motion. The slope of the graph between 0.5-4.5 hours indicates a 0.3% change in backscatter per hour.

The backscatter plot of polymer coated DSPE-NLB presented a significantly more favorable scenario with regards to stability characteristics of the DDS. This graph, presented in non-referenced mode in Figure 5.19B, highlighted an almost inconceivable change in backscatter over the 12 hour analysis period. This exceptional stability was confirmed by quantification of the change in backscatter with reference to the initial measurement at the start of the assessment, presented in Figure 5.19D. The virtually horizontal gradient of the graph concludes a 0% change in backscatter per hour over the entire 12 hour period. Hence, the stability profile of DSPE-NLB following reconstitution suggests a highly stable formulation that will allow sufficient time between reconstitution and administration to patients.

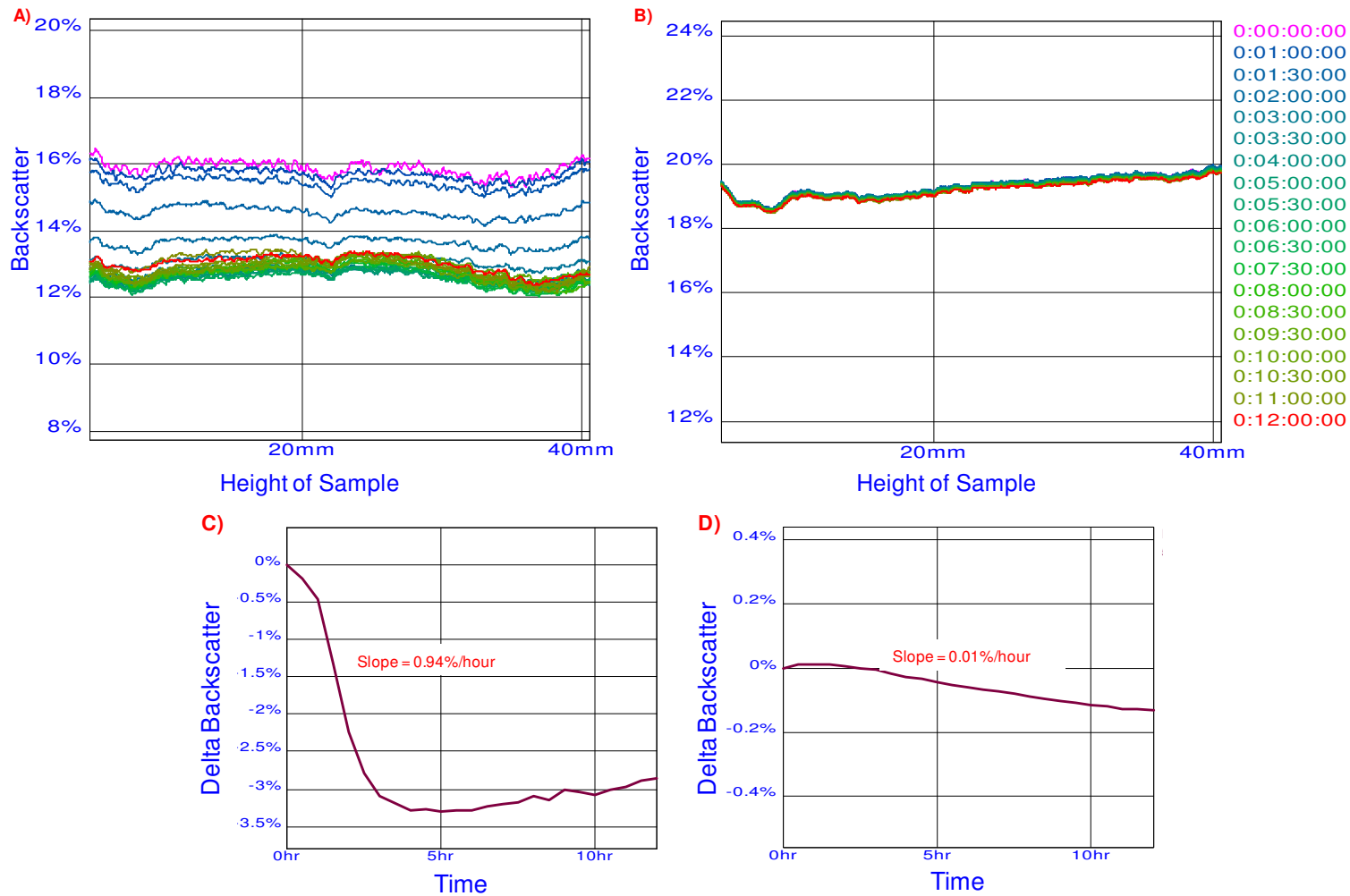


Figure 5.18 Backscatter profiles of A) uncoated CHO-NLB and B) polymer coated CHO-NLB in non-reference mode, up to 12 hours post reconstitution at ambient temperature. Change in backscatter as a function of time of C) uncoated CHO-NLB and D) polymer coated CHO-NLB, with reference to the initial measurement.

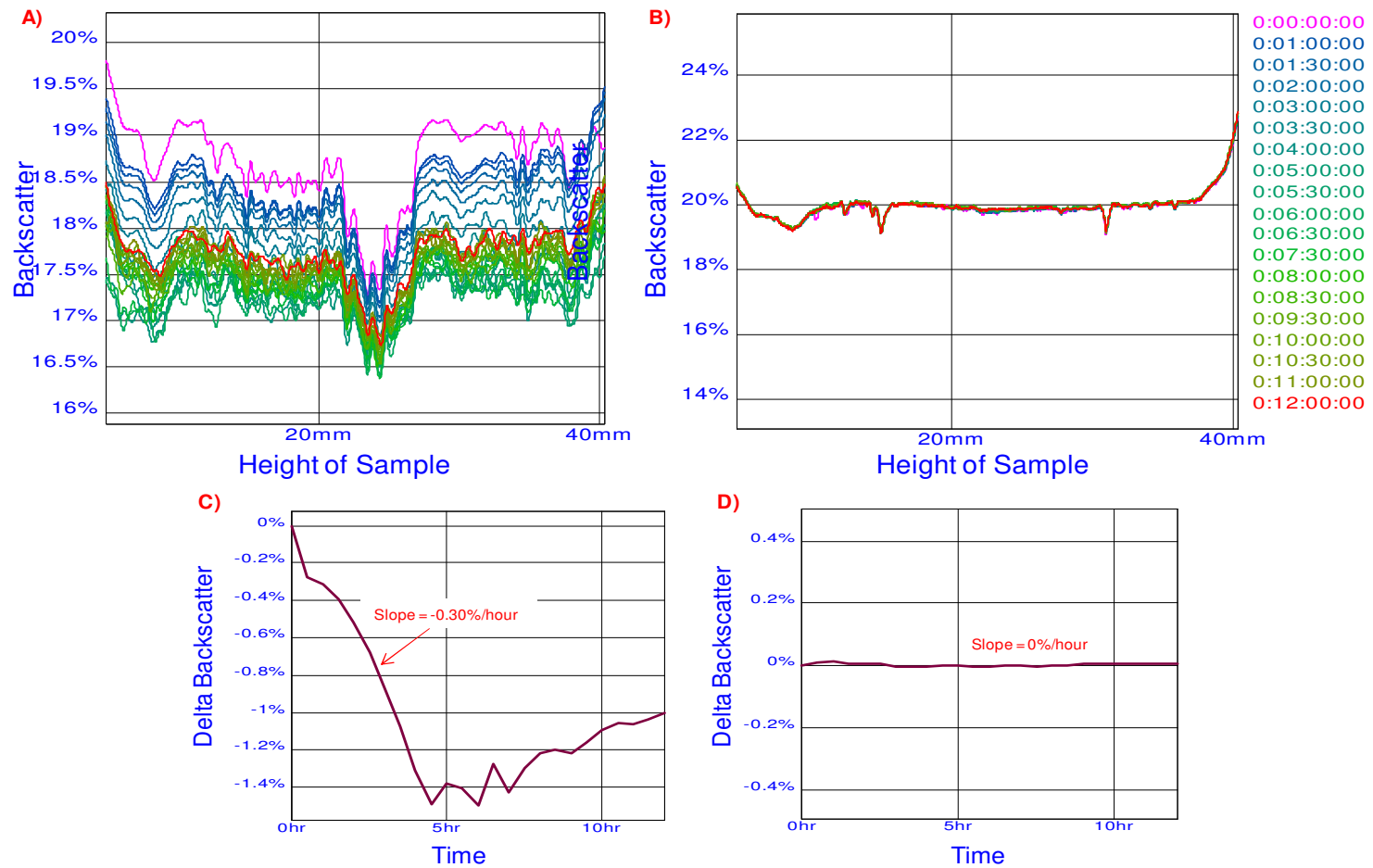


Figure 5.19 Backscatter profiles of A) uncoated DSPE-NLB and B) polymer coated DSPE-NLB in non-reference mode, up to 12 hours post reconstitution at ambient temperature. Change in backscatter as a function of time of C) uncoated DSPE-NLB and D) polymer coated DSPE-NLB, with reference to the initial measurement.

5.4.12.3 Evaluation of the storage stability of nano-lipobubbles

The stability of formulated polymer coated CHO- and DSPE-NLB as a lyophilized product was assessed over a 3 month period under ambient and refrigeration temperatures. At weekly intervals the formulations were reconstituted, converted to NLB and the average size and zeta potential of the formulations as well as DIE of both CPT and SB were determined. The change in size of CHO-NLB was minimal over the first 8 weeks, following which refrigerated formulations maintained their size better than formulations stored at room temperature, as highlighted in Figure 5.20A. However, the difference between refrigerated and non-refrigerated formulations was <2 nm during the third month. At the conclusion of the 12 week study, the CHO-NLB formulations remained below 200 nm. DSPE-NLB displayed an insignificant variation in the average size of formulations stored at both temperatures over the entire study. In addition, the formulations exhibited only a 2-3 nm increase in size by the end of the investigation. Long term storage, as well as the storage temperatures, appeared to have a greater impact on the surface charge of formulations, as illustrated in Figure 5.20B. CHO-NLB stored at ambient temperature demonstrated an unfavorable 7.24mV increase in zeta potential over the assessment period, whilst refrigerated samples bore a 4.17mV increase in zeta potential. The disparity in zeta potential between refrigerated and non-refrigerated samples increased as the study proceeded.

The leakage of incorporated drugs from formulated liposomes and nanobubbles while stored as suspensions presents one of the fundamental stability challenges related to the feasibility of these DDS. Lyophilization has been previously explored and reported as a means of enhancing the storage stability of the aforementioned DDS. Hence, the final presentation of CHO- and DSPE-NLB formulated in this study was lyophilized products. The storage stability of both formulations with regards to the DIE of CPT over the analytical period, presented in Figure 5.20C, was outstanding. CHO-NLB displayed <3% decrease in the DIE of CPT, whilst the decrease was <4% for DSPE-NLB by the conclusion of the analysis. The influence of storage temperature on the incorporation of CPT in both DDS was insignificant. Storage temperature, as depicted in Figure 5.20D, appeared to have a negligible impact on the efficiency of SB incorporation in DSPE-NLB. However, storage time resulted in a gradual decrease in SB incorporation, culminating in a <3% lower DIE for SB at the end of the 3 month study. The storage stability of CHO-NLB with respect to SB incorporation was slightly less favorable than observed with DSPE-NLB, with Figure 5.20D denoting ~4% decrease in SB DIE over the period of investigation. Between weeks 3-8, the influence of refrigeration on the incorporation of SB is evident. However, overall the influence of storage temperature on the incorporation stability of SB was negligible for CHO-NLB.

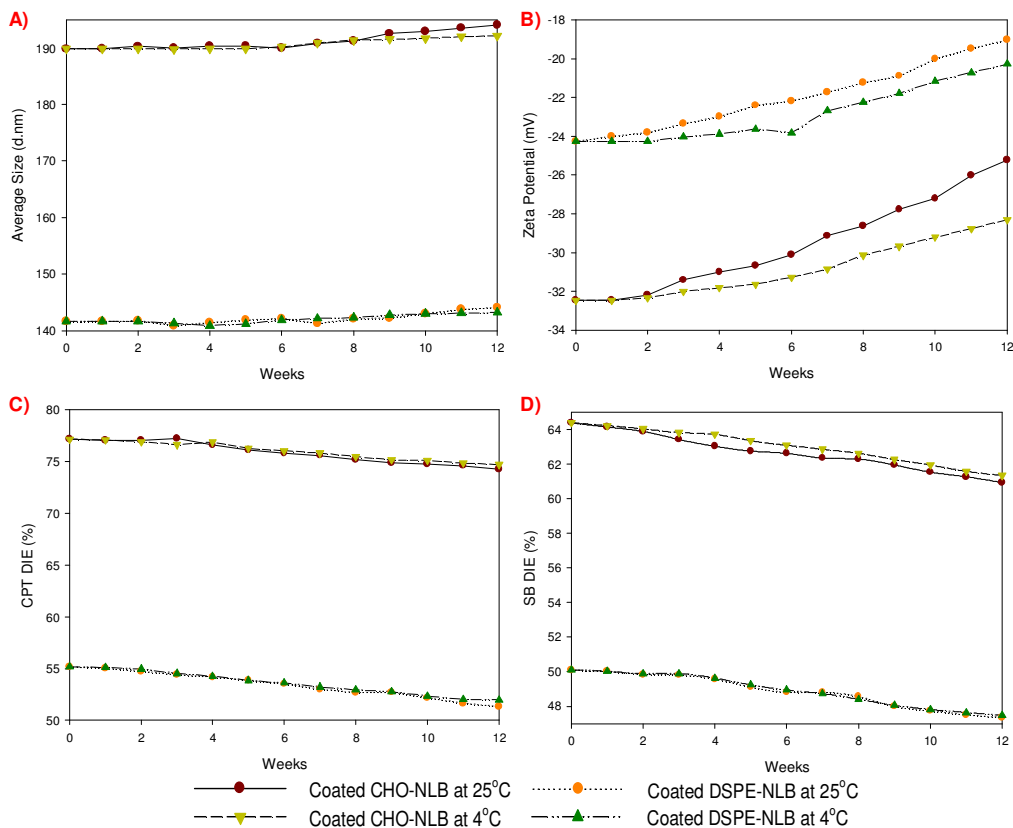


Figure 5.20 Defining the A) average size, B) zeta potential, C) CPT incorporation and D) SB incorporation of polymer coated CHO- and DSPE-NLB stored under ambient and refrigeration temperatures over a three month period (in all cases n=3 and SD<0.03).

5.5 Concluding Remarks

This chapter established a methodical characterization of the candidate nano-liposomal formulations defined by statistical optimization in Chapter 4. Evaluation of the experimentally derived results revealed close correlation to the predicted responses. Conversion to the intended NLB formulation highlighted superior stability, drug incorporation and drug release characteristics of CHO-NLB, whilst the size profile of DSPE-NLB was particularly favorable. The feasibility of lyophilization was investigated as a practical consideration to improve the long term stability of the formulation, thereby enhancing the industrial and clinical viability of the novel DDS. Fluorescence microscopy further confirmed the restoration of the morphological structure of NLB following lyophilization.

Further modifications undertaken on the formulated NLB-DDS included the incorporation of a phytochemical with antineoplastic properties. Maintaining a favorable size profile to facilitate the passively targeted nature of the DDS was a central consideration in determining the optimal concentration of SB to be incorporated into the DDS. Interestingly,

the incorporation of SB into CHO-NLB had a marginal effect on the concurrent DIE of CPT and a slight increase in CPT incorporation into DSPE-NLB. The inclusion of SB into the DDS resulted in a burst release of both CPT and SB from CHO-NLB during the first hour, as well as more rapid release of CPT over the 24 hour assessment period. By contrast, the incorporation of SB into DSPE-NLB resulted in a slower release of CPT. The higher aqueous solubility of SB relative to CPT was attributed with the more rapid release of SB, with complete release of SB being achieved in 20 hours for CHO-NLB and 16 hours for DSPE-NLB.

The application of sequentially layered polymeric coating of the formulated NLB proved challenging. SEM revealed the formation of PEC with the combination of PEI and pectin or carrageenan. The combination of CHT and PAA proved immensely favorable, with lyophilization producing a flaky powder that was easily reconstituted. In addition, the average size of both CHO- and DSPE-NLB remained below the benchmark 200 nm size initially outlined. The significant change in zeta potential observed following the application of the cationic (CHT) and anionic (PAA) polymers, as well as the chemical structural changes determined following polymeric coating confirm the successful application of a robust polymeric coating of formulated NLB. The bearing of polymeric coating had a particularly advantageous impact on the surface charge of DSPE-NLB, with a favorable ~16mV decrease in zeta potential. CHO-NLB displayed incorporation efficiencies of 77.17% and 64.38% respectively for CPT and SB. DSPE-NLB displayed incorporation efficiencies of 55.17% and 50.10%, respectively, for CPT and SB. Moreover, the application of polymeric coating significantly enhanced the release characteristics of both drug compounds and introduced differential release characteristics at physiologic and tumoural pH, thereby improving the passive targeting capacity of the intended DDS.

Stability of formulations is a pivotal consideration for pharmaceutical formulations. The assessment of stability of the formulated NLB-DDS further highlighted the impact of polymeric coating on the stability characteristics of CHO- and DSPE-NLB. Post-reconstitution evaluation of polymer coated CHO- and DSPE-NLB denoted remarkable stability characteristics for the entire 12 hour assessment period, particularly for DSPE-NLB. Marginal changes in size were observed, however, the study concluded adequate time could be allowed between reconstitution of the NLB-DDS and administration to the patient to facilitate ease of use. The evaluation of long term storage stability of the NLB-DDS under ambient and refrigerated temperatures over a 3 month period highlighted excellent stability with regards to the incorporation of CPT and SB with insignificant influence of storage temperature. The increase in size of CHO-NLB was only evident after 8 weeks whilst the non-refrigerated formulation underwent an unfavorable >7mV increase

in zeta potential. The size and zeta potential profiles of DSPE-NLB over the three month assessment period demonstrated superior stability.

Lastly, the formulated polymer-coated CHO- and DSPE-NLB remained below the benchmark size initially outlined, displayed satisfactory incorporation of both CPT and SB and successfully enhanced the drug release characteristics of CPT and SB to facilitate more effective passive targeting and drug efficacy. The stability characteristics of the formulations further denote substantial industrial and clinical feasibility.

CHAPTER 6

EX VIVO EVALUATION OF OPTIMIZED NANO-LIPOBUBBLE FORMULATIONS

6.1 Introduction

This study did not require clearance from the Human Ethics Research Committee of the University of the Witwatersrand (Waiver letter in Appendix D).

The undertaking of *in vitro* analyses provides vital data on the physicochemical and physicomachanical characteristics of formulated drug delivery systems (DDS), thereby creating a basis on which to initially assess the feasibility of the formulation and substantiating further assessment. Subsequently, the undertaking of *ex vivo* investigations enables assessment of formulations under conditions that mimic the *in vivo* environment more closely and provides data under conditions that cannot be adequately simulated *in vitro*. The diverse array of *ex vivo* analyses undertaken on DDS is dictated by the intended application of the DDS, the route of administration of the DDS and the factors that can potentially affect the activity and fate of the DDS *in vivo*. Common *ex vivo* characterization studies include cell cytotoxicity determination on a relevant cell line, cellular uptake of the DDS, permeation studies employing animal tissue, hemolytic assessment and gene transfection efficiency.

Following the feasibility of the optimized nano-lipobubble drug delivery systems (NLB-DDS) determined in Chapter 5, comprehensive systematic characterization compelled pertinent *ex vivo* analyses of formulated cholesterol-containing NLB (CHO-NLB) and distearoylphosphatidylethanolamine-containing NLB (DSPE-NLB). The intended intravenous administration of the NLB-DDS necessitated assessment of the effect of the respective formulations on erythrocytes. This was determined through quantification of hemolysis following treatment with each of the formulations. The A2780 epithelial ovarian cancer cell line was employed for all cellular-based assays. This adherent cell line was originally isolated from the tumour tissue of an untreated patient. The strain employed in the analyses described herein was a non-resistant subtype. The intra-cellular target of the incorporated antineoplastic agent camptothecin (CPT) requires uptake of the DDS by the tumour cells in order for CPT to effectively exert its antineoplastic activity. Hence, qualitative analysis of cellular uptake was conducted. The achievement of enhanced cytotoxic efficiency against tumour cells was a central consideration in this study. Thus, cytotoxic characterization of the optimized DDS will be comprehensively described in this Chapter by deliberating the results achieved by 2 different methods of cytotoxicity determination as well as the merits thereof.

6.2 Materials and Methods

6.2.1 Materials

The materials employed in the formulation of optimized CHO-NLB and DSPE-NLB were unchanged from those described in Chapter 5, Section 5.3.1. In addition a human epithelial ovarian cancer cell line (A2780), from the European Collection of Cell Cultures, cryoprotective medium (15%^{v/v} DMSO) and sulforhodamine B (SRB) dye was procured from Sigma Chemical Company (St Louis, MO, USA). RPMI-1640, foetal bovine serum (FBS), a penicillin-streptomycin antibiotic combination, L-glutamine and Trypsin-EDTA were purchased from Lonza Group Ltd (Basel, Switzerland). Trypan blue (0.4%^{v/v}) and dual chamber cell counting slides were procured from BioRad Laboratories Inc. (Hercules, CA, USA). BD™ Falcon sterile round-bottom polystyrene test tubes (5cm), 7-amino-actinomycin (7-AAD), fluorescein isothiocyanate (FITC), R-phycoerythrin (PE₂), peridinin-chlorophyll proteins (PerCP) and allophycocyanin (APC) stains were purchased from The Scientific Group (Randburg, Gauteng, South Africa). Specialized E-plates 16 were procured from ACEA Biosciences Inc. (San Diego, CA, USA). Sterile porvair cell culture flasks, sterile centrifuge tubes (15mL and 50mL), disposable 10mL pipettes, sterile micro-pipette tips and all other equipment employed in the culturing and analyses of cells were procured from Whitehead Scientific (Pty) Ltd (Cape Town, Western Cape, South Africa). Culturing and treatment of cells were undertaken under a vertical laminar flow unit (Labotec, Midrand, Gauteng, South Africa).

6.2.2 Methods

6.2.2.1 Preparation of optimized and control nano-lipobubbles

The preparation of placebo, uncoated and optimized CHO- and DSPE-NLB were undertaken as described in Chapter 5, Sections 5.3.2.2, and 5.3.2.7. Reconstitution of lyophilized products of the respective formulations and subsequent conversion to NLB was conducted immediately prior to treatment of erythrocytes or tumour cells, as applicable. All formulations were subjected to filtration sterilization employing 0.22µm millipore filters under aseptic conditions.

6.2.2.2 Cell culturing and expansion of the A2780 ovarian cancer cell line

A2780 ovarian cancer cells were cultured in RPMI-1640 medium supplemented with FBS (10%^{v/v}), L-glutamine (0.2%^{v/v}), and a penicillin-streptomycin antibiotic combination (0.2%^{v/v}). Cells were incubated at 37°C in a humidified incubator with 95%O₂ and 5%CO₂ (Afrox, Johannesburg, Gauteng, South Africa) and monitored daily through microscopic observation. Cells were sub-cultured at 80-90% confluence, under sterile conditions with aseptic technique being observed throughout the culturing and analyses of cells. Briefly, cell culture medium was removed from the culture flask and cells were thoroughly rinsed

with phosphate buffered saline (PBS) (pH 7.4; 37°C; 3-5mL) to remove remnants of serum. Trypsin-EDTA (~3mL) was added to the cell culture flask and cells were incubated for 3 minutes in the humidified incubator to facilitate detachment of the cells. Fresh cell culture medium (~3mL) was introduced into the cell culture flask to re-suspend the cells and the entire volume was transferred to a sterile test tube. The suspension was subsequently centrifuged at 800rpm for 3 minutes, the supernatant discarded and the pellet of cells was re-suspended in fresh cell culture medium. The cell suspension was subsequently split into 3 cell culture flasks and allowed to attach and proliferate in the humidified incubator. Following adequate expansion of the cell line, cells were suspended in a combination of cell culture medium and cryoprotectant medium (1:1) and frozen at -70°C until further analysis.

6.2.2.3 Determination of cell concentration and viability

Previously frozen cells were thawed and pipetted into sterile test tubes containing cell culture medium. The total volume was centrifuged at 800rpm for 3 minutes and the supernatant discarded. The cell sediment was re-suspended in cell culture medium (3-5mL). Cell counting was undertaken by the trypan blue assay, according to the manufacturer's specifications. Briefly, the cell suspension (10 μ L) was added to trypan blue (20 μ L) and the combination was introduced into the chamber of a specialized cell counting slide. The concentration of cells was determined employing an automated cell counter (TC10™ Automated cell counter, BioRad Laboratories Inc., Hercules, CA, USA). For each analytical experiment cells of the same passage number were employed and analyses were undertaken in triplicate. Moreover, only cells demonstrating \geq 95% viability after freezing were used for analyses.

6.2.2.4 Delineating experimental controls

Control samples are essential in *ex vivo studies*, to confirm the integrity of the study. Untreated cells and plain cell culture medium incubated without further treatment were employed as positive controls, to confirm the viability of the cell line and the sterility of the medium, respectively. Cells treated with CPT or silibinin (SB) in DMSO, diluted with PBS, were utilized to determine the susceptibility of the cell line to the model drug and phytochemical, respectively, as well as to provide a basis for comparison of the efficacy of formulated DDS. Moreover, cell lines treated with DMSO+PBS or PBS were used to establish the effect of the solvents used for CPT, SB and the NLB-DDS on the cell line. Finally, treatment of the cell line with placebo NLB was utilized to establish the cytotoxic potential of the polymers and lipids employed in the formulation as well as the nanostructure itself.

6.2.2.5 Determination of hemolytic activity of nano-lipobubbles

The intravenous nature of the proposed formulation demands an investigation of the effect of CHO- and DSPE-NLB on red blood cells (RBC) in order to establish hemocompatibility of the formulation. The method employed was analogous to that described by Shen and co-workers (2009), Elmowafy and co-workers (2013) and Sharma and co-workers (2013) (Shen *et al.*, 2009; Elmowafy *et al.*, 2013. Sharma *et al.*, 2013). Sheep blood was employed for this investigation. Briefly, blood was collected into heparinized sterile test tubes and centrifuged at 2000xg for 5 minutes in order to separate the various blood components. The supernatant was discarded in order to isolate the RBC sediment. The RBC were re-dispersed in an anticoagulant preservative, Alserver's buffer, followed by repeated washing and centrifugation, until a clear cell suspension was achieved. The RBC were subsequently divided into six test tubes for analysis. Two of the test tubes were used as controls to enable generation of a standard curve for the quantification of hemolytic activity. Hemolysis results in the disruption of the RBC membrane and subsequent release of hemoglobin, which can be detected by UV-spectroscopy. The RBC were treated as follows:

Test tube 1: RBC incubated with PBS (pH 7.4; 37°C) for 30 minutes at 37°C. The suspension was centrifuged at 2000xg for 5 minutes and the supernatant analyzed by UV-spectroscopy at 546nm. This control was also used as the blank sample and represented no hemolytic activity.

Test tube 2: RBC incubated with excess ammonium chloride (NH₄Cl) for 30 minutes at 37°C, followed by centrifugation at 2000xg for 5 minutes. The supernatant was analyzed by UV-spectroscopy as for test tube 1. This control represented complete hemolysis.

Test tubes 3 and 4: RBC incubated with CHO-NLB (10mg/mL and 20mg/mL; 10mL) for 30 minutes at 37°C, followed by centrifugation at 2000xg for 5 minutes. The supernatant was analyzed by UV-spectroscopy as for test tube 1.

Test tubes 5 and 6: RBC incubated with DSPE-NLB (10mg/mL and 20mg/mL; 10mL) for 30 minutes at 37°C, followed by centrifugation at 2000xg for 5 minutes. The supernatant was analyzed by UV-spectroscopy as for test tube 1.

A wave-scan was performed from 250nm to 600nm on the sample from test tube 2 to establish the wavelength of maximal hemoglobin detection, which was determined to be 546nm. A standard curve was subsequently generated from the UV absorbance values of samples in test tubes 1 and 2. Analysis was undertaken in triplicate. Test samples in test tubes 3 to 6 were used to establish the hemolytic activity of optimized CHO-NLB and DSPE-NLB. Hemolysis was quantified employing Equation 6.1.

$$\text{Hemolysis (\%)} = (A_{\text{NLB}} - A_{\text{PBS}}) / A_{\text{NH}_4\text{Cl}} \times 100 \quad \text{Equation 6.1}$$

6.2.2.6 Assessing cellular uptake of nano-lipobubbles through fluorescence microscopy

Cells were seeded at a density of 1×10^5 cells/well in sterile, 6-well cell culture plates and incubated at 37°C in a humidified incubator with 95%O₂ and 5%CO₂. Fluorescently labeled CHO- and DSPE-NLB were prepared as previously described in Chapter 5, Section 5.3.2.7, with the addition of SRB during the emulsification process. Following attachment of the cells over a 24 hour period, cells were treated with SRB-labeled CHO- and DSPE-NLB as well as cell culture medium (1:1; 2mL), under sterile incubation conditions as described above. Following the incubation period, excess media and NLB suspension were removed and the cells were washed twice with PBS (pH 7.4; 37°C). PBS (pH 7.4; 37°C; 1mL) was added to each well to prevent dehydration of the cells during analysis. The fluorescent nature of SRB enabled qualitative determination of cellular uptake of the CHO- and DSPE-NLB through the application of fluorescence microscopy. Fluorescent images were super-imposed onto bright field contrast images to highlight the presence of fluorescently labeled CHO- and DSPE-NLB within the A2780 ovarian cancer cells.

6.2.2.7 Characterizing the cytotoxicity of formulated nano-lipobubbles

Cytotoxicity studies are employed to establish the degree of toxicity of the formulated NLB-DDS to the tumour cell line. In the present study toxicity of the formulation to the A2780 ovarian cancer cell was investigated, with the objective of maximizing toxicity and cell death. The cytotoxicity of formulations cannot be accurately defined without the use of experimental controls. Hence, in addition to the formulated coated and uncoated CHO- and DSPE-NLB, the cytotoxic activity of the controls outlined in Section 6.2.2.4 was investigated. The determination of cytotoxicity was assessed quantitatively employing flow cytometry, as well as analysis of real-time cell growth and cytotoxicity data employing the xCELLigence™ Real-Time Cell Analyzer (RTCA) (Roche Applied Science, Penzberg, Upper Bavaria, Germany and ACEA Biosciences Inc., San Diego, CA, USA). Moreover, counting of cells employing the automated cell counter as described in Section 6.2.2.3 before and after treatment, in order to determine and adjust the concentration for specific analytical procedures, provided a solid indication of cell viability.

6.2.2.7.1 Evaluating cytotoxicity employing flow cytometry

Following the determination of post-freezing cell viability, as outlined in Section 6.2.2.3, cells were seeded at a density of 5×10^5 cells per well in sterile 6-well cell culture plates and incubated at 37°C in a humidified incubator with 95%O₂ and 5%CO₂. When regular microscopic evaluation revealed cells had reached ~80% confluence, treatment of cells was undertaken in triplicate as illustrated in Table 6.1 and maintained in the humidified

incubator as previously described. The saturation solubility of CPT in DMSO is 10mg/mL, which was subsequently diluted 25-fold in PBS and then 2-fold in cell culture medium to negate the toxic effect of DMSO on cells. The final concentration of CPT with which the cells were treated was thus 0.20mg/mL. Suspensions of uncoated and optimized CHO- and DSPE-NLB formulations were prepared with a CPT concentration of 0.4mg/mL. A 2-fold dilution with cell culture medium thus produced preparations with CPT concentration of 0.20mg/mL. The concentration of SB in uncoated and optimized CHO-NLB was determined to be 1.02mg/mL and 0.99mg/mL, respectively. The concentration of SB in uncoated and optimized DSPE-NLB was determined to be 1.06mg/mL and 1.09mg/mL, respectively. Placebo suspensions were prepared at concentrations equal to the overall concentrations of optimized CHO- and DSPE-NLB. The maximum concentration of SB in DMSO that could be obtained was 15mg/mL, which was subsequently diluted 25-fold in PBS (pH 7.4; 37°C) and 2-fold in cell culture medium to create a final solution of 0.3mg/mL.

Table 6.1 Test and control preparations evaluated for their cytotoxic effect on A2780 ovarian cancer cells.

Test Samples	Control Samples
Optimized CHO-NLB	Untreated cells
Optimized DSPE-NLB	CPT
Uncoated CHO-NLB	SB
Uncoated DSPE-NLB	PBS
	DMSO+PBS
	Placebo CHO-NLB
	Placebo DSPE-NLB

The viability of cells following treatment with each preparation was assessed by flow cytometry 24, 48 and 72 hours post-treatment. The excess cell culture medium containing detached, no-viable cells was removed and added to sterile test tubes. Cells were rinsed with PBS (pH 7.4; 37°C) and trypsinized according to standard procedures outlined in Section 6.2.2.2. The cell suspensions were added to the respective sterile test tubes containing the previously removed non-viable cells. The total volumes were centrifuged at 800rpm for 3 minutes and the supernatant discarded. The cell sediments were resuspended in 100µL cell culture medium each and transferred to round-bottom polystyrene test tubes. The 7-AAD stain (5µL) was added to each test sample and incubated at room temperature in darkness for 10 minutes, in accordance with the manufacturer's guidelines. PBS (pH 7.4; 37°C; 500µL) was subsequently added to each test sample.

Prior to cell analysis, quality control assessment was undertaken on the flow cytometer (FACS Calibur, BD Biosciences, Tullastrasse, Heidelberg, Germany). Unstained cell

counting beads as well as 4 stains, namely FITC, PE, PerCP and APC, were employed to ensure the quality of fluorescence detection by each of the 4 fluorescence detectors. The FL3 detector was of particular relevance in this study as the 7-AAD dye employed during analysis is detected by the FL3 detector. Following the successful outcome of the quality control test, the test parameters were determined. Evaluation of the forward scatter and side scatter plots of completely viable and completely non-viable cells enabled accurate distinction of the voltage threshold and region of interest. Test samples were subsequently analyzed at low and medium flow rates with buffer rinses between each sample to avoid results reflecting the effects of residue from previous samples. No less than 10000 cells were analyzed in each sample. Cell viability was analyzed employing BD CellQuest™ Pro version 5.1 software (BD Biosciences, Tullastrasse, Heidelberg, Germany).

6.2.2.7.2 Real-time evaluation of formulation cytotoxicity

Cell growth and cytotoxicity of the NLB-DDS and relevant controls were determined in real-time as a measure of electrical impedance employing the xCELLigence™ RTCA (Roche Applied Science, Penzberg, Upper Bavaria, Germany and ACEA Biosciences Inc., San Diego, CA, USA). A background scan of the cell culture medium (100µL/well) was performed prior to each analysis. A cell titration was initially performed in triplicate with cell densities ranging from 1250 to 10000 cells/well. The growth pattern of cells was observed over a 100 hour period and a density of 10000 cells/well was deemed suitable for analysis. This further identified the most suitable time period (22-34 hours post-seeding) to initiate drug treatment. All subsequent drug treatment was undertaken 24 hours post-seeding.

A titration of CPT was subsequently undertaken to establish sensitivity of the cells to CPT and to determine an effective concentration of CPT for the achievement of adequate cytotoxic activity. A saturated solution of CPT in DMSO (10mg/mL) was prepared with subsequent serial dilutions resulting in a concentration range of 2-10mg/mL. The CPT solutions were diluted 25-fold PBS (pH 7.4; 37°C) and then 2-fold in cell culture medium due to the toxicity of concentrated DMSO to cells, resulting in final CPT solutions of 0.04-0.20mg/mL. Cells were seeded at 10000 cells/well and treated 24 hours later with serial dilutions of CPT and the response pattern of cells to the range of CPT concentrations was analyzed for 36 hours post-treatment. The final concentration of CPT determined to display the most appropriate response by the cells for the purposes of this study (0.20mg/mL following dilution in cell culture medium), coincided with the concentration employed for analysis by flow cytometry. Hence, all test and control samples were prepared in accordance with the description in Section 6.2.2.7.1.

6.3 Results and Discussion

6.3.1 Hemolytic impact of formulated nano-lipobubble drug delivery systems

For intravenous formulations, assessment of the hemolytic capacity of nanosystems is a pivotal determination and a foremost restriction to clinical application. Erythrocytes are negatively charged. The negative surface charge of optimized CHO- and DSPE-NLB was beneficial to intravenous application due to compatibility with the charge of erythrocytes. Formulations inducing <10% hemolysis are considered non-toxic, whilst those inducing >25% are considered to be of high risk (Elmowafy *et al.*, 2013; Sharma *et al.*, 2013). Optimized CHO- and DSPE-NLB demonstrated a concentration-dependent hemolysis. The hemolysis induced by CHO-NLB increased from 4.63% to 6.87% with an increase in concentration from 10mg/mL to 20mg/mL, as illustrated by the bar graph in Figure 6.1. A similar increase in concentration of DSPE-NLB resulted in a concomitant increase in hemolysis from 5.36% to 7.03%. However, NLB concentrations of 20mg/mL still demonstrated low hemolytic potential and were considerably below the hemolytic threshold delineating formulations that are considered safe for intravenous administration.

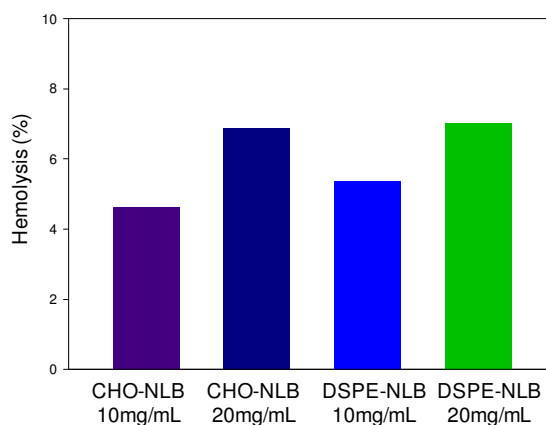


Figure 6.1 Quantitative analysis of the hemolysis induced by optimized CHO- and DSPE-NLS. Despite the concentration-dependent hemolysis displayed, all formulations assessed displayed hemolysis that was below the toxic threshold.

6.3.2 Cellular uptake of nano-lipobubbles

The application of fluorescence microscopy provided conclusive evidence of cellular uptake of the formulated NLB-DDS by the ovarian cancer cell line under investigation. Bright-field contrast images denote the cellular morphology, whilst super-imposed fluorescence images highlight the presence of the NLB-DDS within the cells. Successful cellular uptake of the formulated NLB-DDS and the subsequent release of CPT and SB within the tumour cells are critical to the achievement of augmented antineoplastic activity relative to that of native CPT and SB. Formulated CHO- and DSPE-NLB demonstrated a time-dependent cellular uptake, which was more pronounced in CHO-NLB. The distinct increase in fluorescence intensity evident in the fluorescence micrographs in the upper

panel of Figure 6.2 highlights the increase in CHO-NLB uptake by the A2780 cells 30 minutes post-treatment relative to that depicted 10 minutes post-treatment. Cellular uptake of DSPE-NLB was markedly higher and faster than observed for CHO-NLB, which was attributed to the smaller size of DSPE-NLB. Localization of both CHO- and DSPE-NLB highlight the potential for released CPT to be transported to the cell nucleus, which is the target for antineoplastic activity.

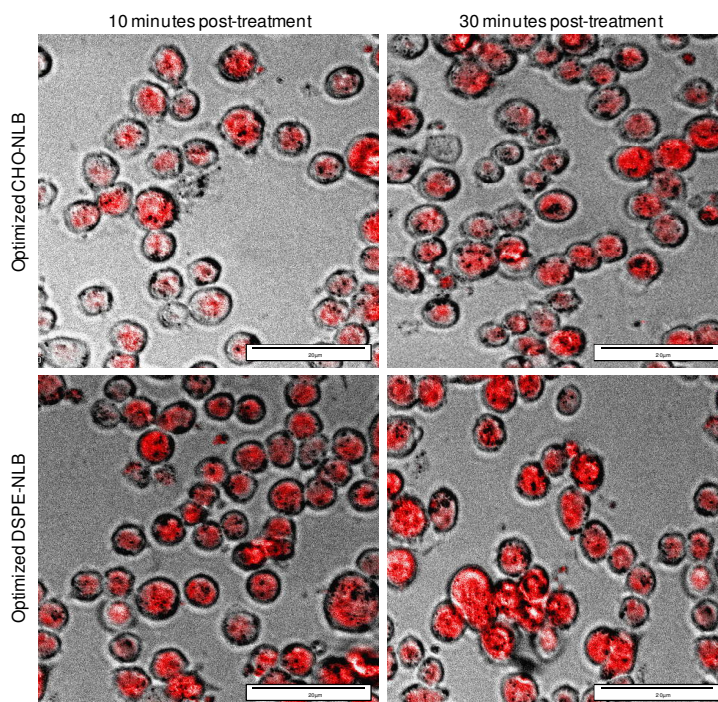


Figure 6.2 Qualitative evaluation of cellular uptake of SRB-labeled optimized CHO- and DSPE-NLB 10 and 30 minutes post-treatment.

6.3.3 Assessment of cytotoxicity by flow cytometry

Flow cytometry is a laser-based technology with a diverse range of applications from cell counting, differentiation between cells with various properties, detection of biomarkers, immunophenotyping and protein engineering. Fluorescence-activated cell sorting (FACS) flow cytometry was employed in this study to quantify cell viability following treatment with test and control formulations. The flow cell in the flow cytometer contains sheath fluid and the fluidics system therein ensures cells pass through the sensors in single file. Light scattering at different angles generates forward and side scatter data, which are indicative of cell size and complexity, respectively. The application of specific fluorescent dyes produces optical fluorescence signals that are converted to electronic signals for computation by the software (Brown and Wittwer, 2000). 7-AAD is a fluorescent dye that is widely employed in cell viability analyses. This fluorescent marker has a strong affinity for DNA and is able to effectively intercalate with double stranded DNA. 7-AAD is unable to permeate uncompromised cell membranes, hence it is excluded by viable cells.

Quantification of 7-AAD may, therefore, be employed to quantify non-viable cells in a sample.

Scatter plots and histograms depicted in Figures 6.3 and 6.4 provide graphical illustrations of the intensity of 7-AAD detected for each sample, which is directly related to the degree of cytotoxicity of the formulation under assessment. Evaluation of untreated cells provided an indication of natural cell death. As expected, the cell viability was >96% 24 hours post treatment and decreased over the next 2 days to 90.65% and 85.47%, respectively. Treatment of cells with PBS and DMSO+PBS did not demonstrate a significant increase in cell death. The high efficacy of CPT against A2780 tumour cells was readily highlighted, with 71.20% cytotoxicity recorded 24 hours post-treatment. However, there was a significant increase in cell viability 48-72 hours post-treatment. This increase in viability was attributed to the low stability of CPT and antineoplastic activity being restricted to cells in the S-phase of the cell cycle. CPT may have been readily internalized and had exerted high antineoplastic activity following initial treatment. However, rapid internalization may have also caused rapid saturation of cellular internalization mechanisms. CPT that was not initially internalized was converted to the inactive carboxylate form in the surrounding medium and was not able to exert any further antineoplastic effect. Surviving cells were able to recover and proliferate over the remaining analytical period leading to an increase in the ratio of viable cells:dead cells during analysis. On the contrary, SB displayed relatively low but increasing cytotoxic potential over the analysis period. SB is hypothesized to induce cell apoptosis, hence the effect is not restricted to a particular phase of the cell cycle. The cytotoxicity observed with cells treated with SB was 3.91%-8.41% higher than the natural cell death observed with untreated cells over the 72 hour analytical period.

Evaluation of the cytotoxic effect of the materials employed in the fabrication of optimized NLB as well as of the nano-construct itself was determined through treatment of cells with placebo CHO- and DSPE-NLB. Both formulations demonstrated similar cytotoxic activity against the A2780 cell line, as well as minimal variation to the cytotoxicity displayed by untreated cells. This confirms the cytotoxicity demonstrated by optimized NLB formulations are attributed only to the location and manner in which the antineoplastic agents are released and cannot be ascribed to the other materials in the formulation.

Treatment of A2780 cells with uncoated CHO- and DSPE-NLB was undertaken to provide insight on the effect of the release characteristics of these formulations on cells relative to those of the optimized polymer coated NLB formulations. The cytotoxicity observed 24 hours post-treatment was substantially (10.46%) higher for uncoated DSPE-NLB than

uncoated CHO-NLB. The more rapid release of CPT and SB from uncoated DSPE-NLB was associated with the greater cytotoxic activity. Over the following 2 days the cytotoxicity of cells treated with CHO-NLB was greater than that treated with DSPE-NLB. At the conclusion of the experiment, cytotoxicity induced by uncoated CHO-NLB was 12.58% greater than that induced by DSPE-NLB. The slower release of CPT and SB from uncoated CHO-NLB was attributed to the increased cytotoxic activity and provided an insight into the significant effect that drug release characteristics may have on the cytotoxic potential of formulated NLB. This was of particular significance given the consideration that CPT acts on a particular phase of the cell cycle, and displays instability in aqueous environments and at higher pH, which leads to loss of antineoplastic activity. The institution of polymeric coating considerably slowed the release of CPT and SB from CHO- and DSPE-NLB. The benefit of the slower release was distinctly evident in the consistent increase in cytotoxicity demonstrated by optimized CHO- and DSPE-NLB over the analytical period. The cytotoxicity of optimized CHO- and DSPE-NLB was 4.58% and 8.46% lower than their uncoated counterparts 24 hours post-treatment. The lower cytotoxic activity was associated with lower concentration of CPT and SB due to slower release. However, the advantage of polymeric coating and the consequent slower, more constant pattern of drug release was readily evident over the following 2 days of treatment. The slower drug release translated into sustained cytotoxic activity evidenced by the increasing uptake of 7-AAD by the non-viable cells. Cytotoxicity induced by optimized CHO-NLB 48 and 72 hours post-treatment were 69.93% and 85.9%, respectively. Optimized DSPE-NLB induced cytotoxicity 48 and 72 hours post-treatment were 72.93% and 94.93%, respectively. Slower release of CPT enabled more cells in the S-phase of the cell cycle to be exposed to CPT, resulting in higher cell death. This cytotoxic effect may have been further intensified by the synergistic activity of SB. The cytotoxicity resulting from treatment of cells with CHO- and DSPE-NLB 72 hours post-treatment was substantially higher than that observed with CPT and SB individually, or the sum thereof.

Flow cytometry is a highly favored technique in cell-based studies due to the ability to rapidly obtain a high volume of data with regards to various cellular characteristics. The use of different fluorochromes with similar excitation wavelengths but different emission wavelengths enables multi-variate qualitative and quantitative analysis (Brown and Wittwer, 2000). Moreover single cell characterization, small sample size and simple sample preparation are added benefits of this technique. However, this is an end-point analysis and as such does not provide data on continuous physiological and kinetic changes undergone by cells during the course of the study.

6.3.4 Assessing cellular status through continuous real-time evaluation

Continuous real-time evaluation of cellular cytotoxicity was undertaken through label-free quantitative assessment employing the xCELLigence™ RTCA system (Roche Applied Science, Penzberg, Upper Bavaria, Germany and ACEA Biosciences Inc., San Diego, CA, USA). The xCELLigence system comprises four main components, namely the RTCA analyzer, RTCA station, RTCA computer with integrated software, disposable E-plate 16. E-plates 16 are a single use, disposable device similar in structure to microtitre plates used in other cell-based studies. However the distinct feature of these plates is the presence of gold microelectrode cell sensors lining 80% of the bottom of each well, which enable the determination of electrical impedance (Urcan *et al.*, 2010). The E-plate 16 is fitted into the RTCA station, which is further housed within a sterile cell culture incubator and connected externally to a computer with integrated software.

The principle of this analytical technique is centered on the measurement of emerging electrical impedance of the cell population present in each well (Urcan *et al.*, 2010). The measurement of electrical impedance enables the detection and characterization of physiological cellular changes. Electrical impedance is influenced by electrode geometry, the degree of cellular attachment to the electrode, and ion concentration within the well. Ion concentration in the bulk solution as well as at the electrode/solution interface will be the primary contributor to electrical impedance in the absence of cells (Urcan *et al.*, 2010). The introduction of adherent cells and their subsequent attachment to the electrode sensors on the surface of the well has an insulating effect, thereby altering the local ion concentration at the electrode/solution interface. Changes in the ionic environment of the well are detected by the microelectrode sensors and can be related to the nature and intensity of cell attachment, the quantity of cells present and their morphology. The data is represented as cell index (CI), a unit-less parameter that relates the electrical impedance of the cell population in a well at a given time-point to the baseline electrical impedance determined at the initiation of the experiment (Urcan *et al.*, 2010). Fundamentally, the healthier cells are and the greater their proliferation the greater their attachment and the higher the CI (Moodley *et al.*, 2011). Morphological changes such as cytotoxicity reduce the attachment of cells and are thus indicated by a lower cell index.

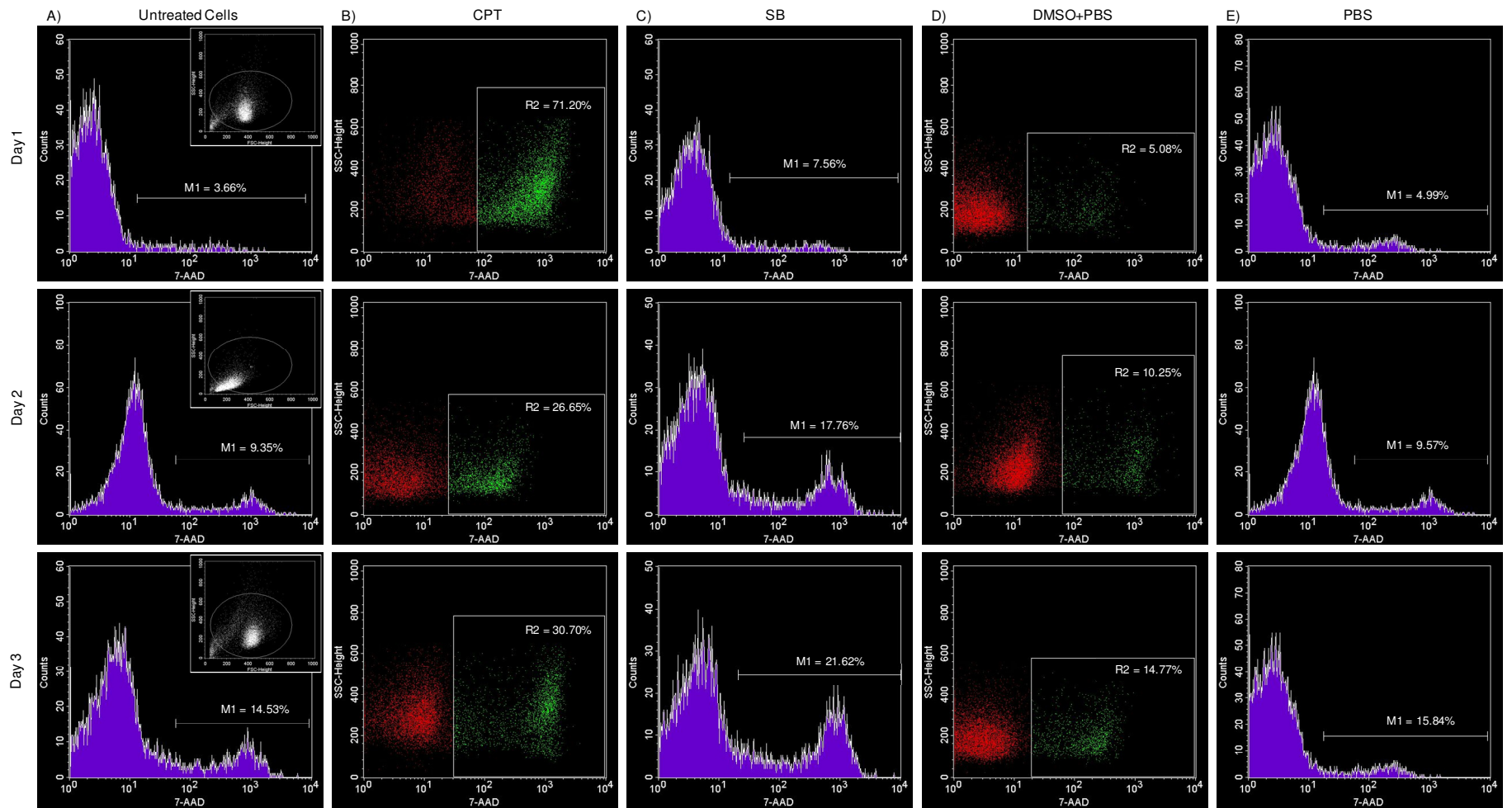


Figure 6.3 Histograms (A; C; E) and scatter plots (B; D) indicating the intensity of 7-AAD detected as a measure of the cytotoxicity of test controls, CPT and SB formulations. Histograms in the first column provide an indication of the natural cell death that occurred in untreated cells over the analytical period, with an inset of the forward versus side scatter plot for each day, depicting the cell characteristics on each day. (M1 = R2 = cell cytotoxicity).

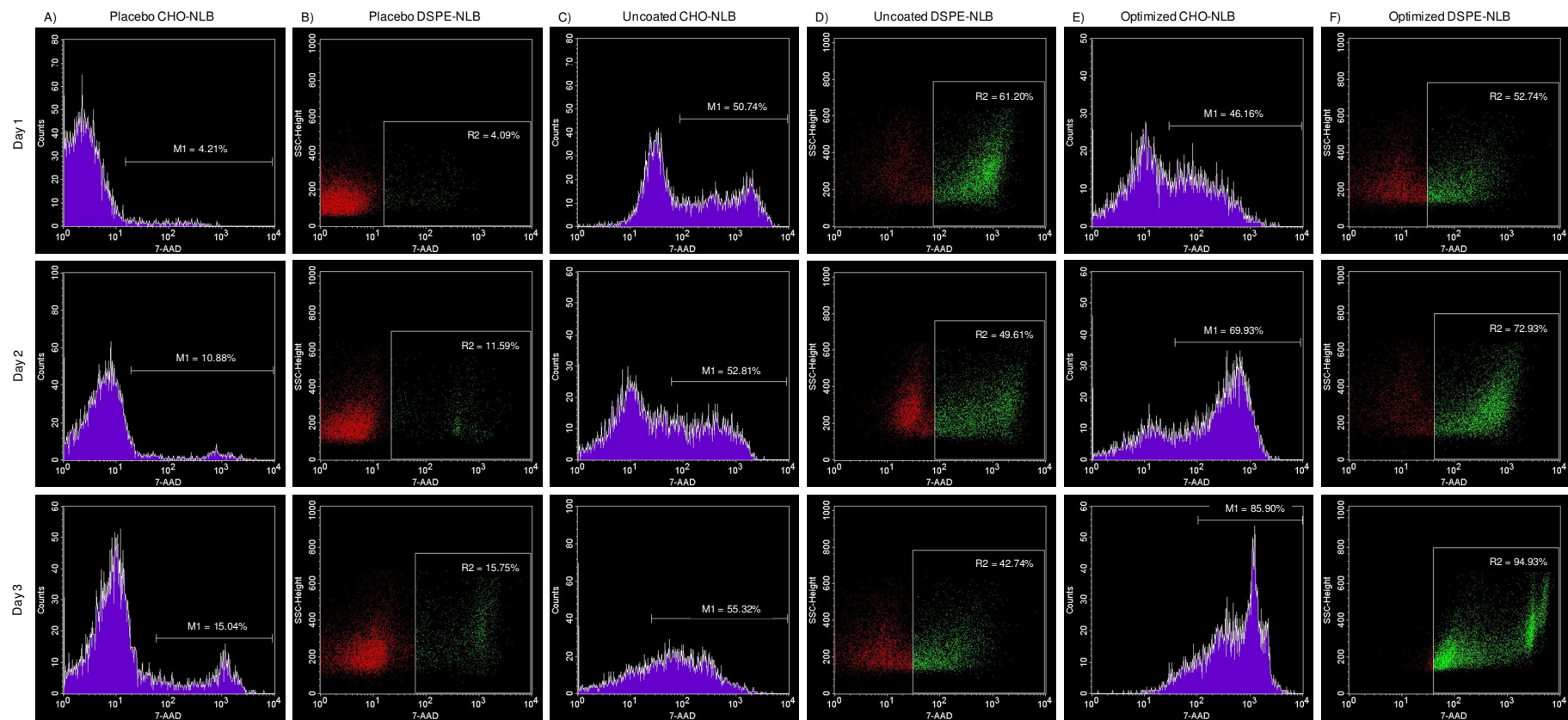


Figure 6.4 Histograms (A; C; E) and scatter plots (B; D; F) indicating the intensity of 7-AAD detected as a measure of cytotoxicity induced by placebo, uncoated and optimized CHO- and DSPE-NLB. (M1 = R2 = cell cytotoxicity).

A cell titration was initially performed in an attempt to firstly, determine the growth pattern of the A2780 ovarian cancer cell line and secondly, to identify an appropriate cell density that would demonstrate a rate of cell proliferation suitable to the purpose of the study. Measurements were taken at 15 minute intervals over a 100 hour period, however are represented graphically at 30 minute intervals. Each of the cell densities employed (1250-10000 cells/well) demonstrated reproducible cell growth patterns, the average of which is represented in Figure 6.5. The cell indices observed over the initial 6-8 hours were attributed to attachment of the cells introduced into the wells, based on previously observed cell behavior, and were congruent with the variation in cell concentrations in accordance with the cell titration. Following this period, the significant difference in the cell indices of each cell concentration was attributed to proliferation of the cells. The proliferation of cells at lower densities (1250 and 2500 cells/well) was notably slower than that observed at higher cell densities (5000 and 10000 cells/well). This was attributed to sub-optimal cell signaling required for adequate cellular replication, as a result of sparser cell populations. Cells at the highest density (10000 cells/well) exhibited a rapid rise in cell index which was related to a high proliferation rate. The maximum cell index at this density was achieved at approximately 47 hours, followed by natural cell death. At a density of 5000 cells/well cellular proliferation proceeded notably slower, reaching maximum cell density at approximately 72 hours post-seeding. The earlier onset of cell death at 10000 cells/well relative to that at 5000 cells/well was hypothesized to result from nutrients being exhausted faster at the higher cell density as well as a lack of space for attachment of more cells. Cells at density of 1250 cells/well and 2500 cells/well did not demonstrate maximum cell indices during the analytical period. A density of 10000 cells/well was delineated as the most appropriate for the purposes of this study, with a treatment period between 22-34 hours post-seeding.

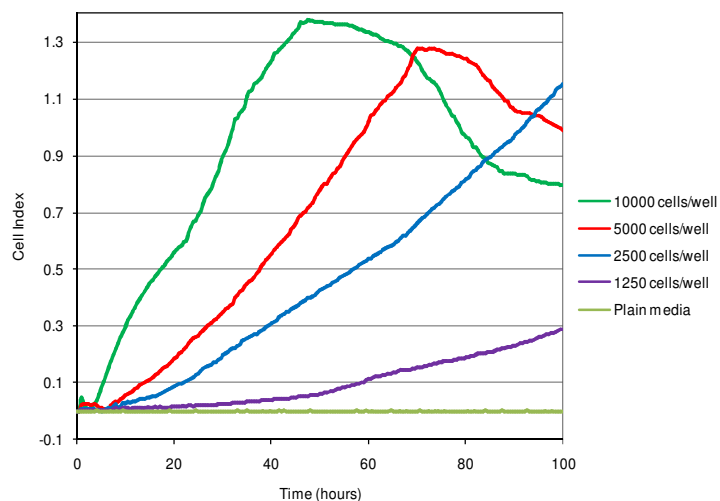


Figure 6.5 Growth profiles of A2780 cells at densities from 1250-10000 cells/well over a 100 hour period. (in all cases n=3 and SD<0.02)

A drug titration was subsequently performed with CPT to establish sensitivity of the cell line to the model drug, as depicted in Figure 6.6. Serial dilutions of CPT in DMSO were prepared, followed by dilution with PBS (pH 7.4; 37°C) to negate the toxic effects of DMSO on the cells. All samples were diluted with cell culture medium (1:1) prior to treatment of cells. Treatment of cells with DMSO+PBS was, therefore, assessed as a control. Cellular proliferation was noticeably reduced following treatment with the DMSO+PBS control relative to that of untreated cells. Whilst the DMSO+PBS solvent was not particularly toxic to the cells, their nutrient content is substantially lower than that of the cell culture medium environment in which the untreated cells grew. The rapid proliferation of this cell line is associated with high nutritional demands. Since the DMSO+PBS solvent is unable to cater adequately to these nutritional demands, the proliferation of cells will be compromised to a degree.

Sensitivity of the cell line to CPT was apparent, even at the lowest concentration tested. There was an observable direct relationship between CPT concentration and cytotoxic effect on the cells over the initial 10 hours post-treatment. At a CPT concentration of 0.20mg/mL there was a rapid and significant decline in cell index over the initial 10 hours post-treatment, succeeded by recovery of the cells as evidenced by the increase in cell index. Treatment with lower concentrations of CPT resulted in a similar response pattern, but with proportionally reduced intensity. Cellular internalization of CPT appears to have been highest during the first 10 hours resulting in cell death. However, conversion of CPT to the inactive carboxylate form over time led to reduced cytotoxicity. Moreover, the surviving cells were able to proliferate over time causing an increase in cell number. The rapidly diminished cell numbers following treatment with 0.20mg/mL CPT solution resulted in less nutrients being consumed and availability of sufficient nutrients for quicker recovery and proliferation of the surviving cells. Hence, the gradient of the portion of each curve associated with cell recovery and proliferation appears steeper with increasing concentration of CPT. Moreover, the swift recovery of cells treated with higher concentrations of CPT suggest some cells may have not been completely killed and detached. Rather, metabolic changes may have caused rounding of the cells, thereby covering a smaller surface and leading to lower cell index. Upon removal of the stress generated by the presence of active CPT, the cells were thus able to quickly recover. The considerable response of cells treated with 0.20mg/mL CPT was determined appropriate for analysis and comparison of the cytotoxic activity of optimized formulations.

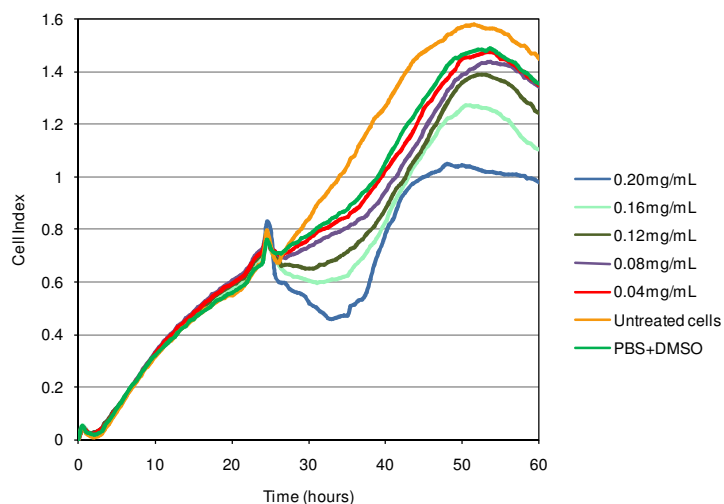


Figure 6.6 Cell index curves highlighting cellular response to serial dilutions of CPT relative to the growth pattern of untreated cells and treatment with the PBS:DMSO solvent system. (in all cases $n=3$ and $SD<0.02$)

Several controls were assessed in order to elucidate the potential of their effects on the overall cytotoxicity of the formulated nano-DDS's. The response of A2780 ovarian cancer cells to test and control formulations are presented in Figures 6.7A and 6.7B. The ionic environment of plain cell culture media remained constant throughout the analytical period and displayed no electrical impedance. Untreated cells were employed as an indication of unhindered cellular growth and proliferation within the confines of this study, limited only by the availability of nutrients and space for attachment. The growth pattern for cells following treatment with PBS, the solvent for the formulated NLB's, was analogous to that observed following treatment with the PBS:DMSO solvent combination. The slower growth pattern was attributed to the reduced availability of nutrients for cell replication, as previously discussed. Cells treated with placebo CHO-NLB demonstrated a growth pattern analogous to that following treatment with PBS, thus confirming the non-toxicity of the materials employed in nano-NLB, as well as the nano-construct itself. However, treatment with placebo DSPE-NLB resulted in a significantly lower cell index. Greater cellular internalization of the placebo DSPE-NLB relative to the larger placebo CHO-NLB is likely to have hindered cellular function to a slight degree, thereby reducing the proliferative capacity of the cells. However, this reduction in cell proliferation was not significant enough to have clinical relevance, particularly in such a rapidly proliferating cell line.

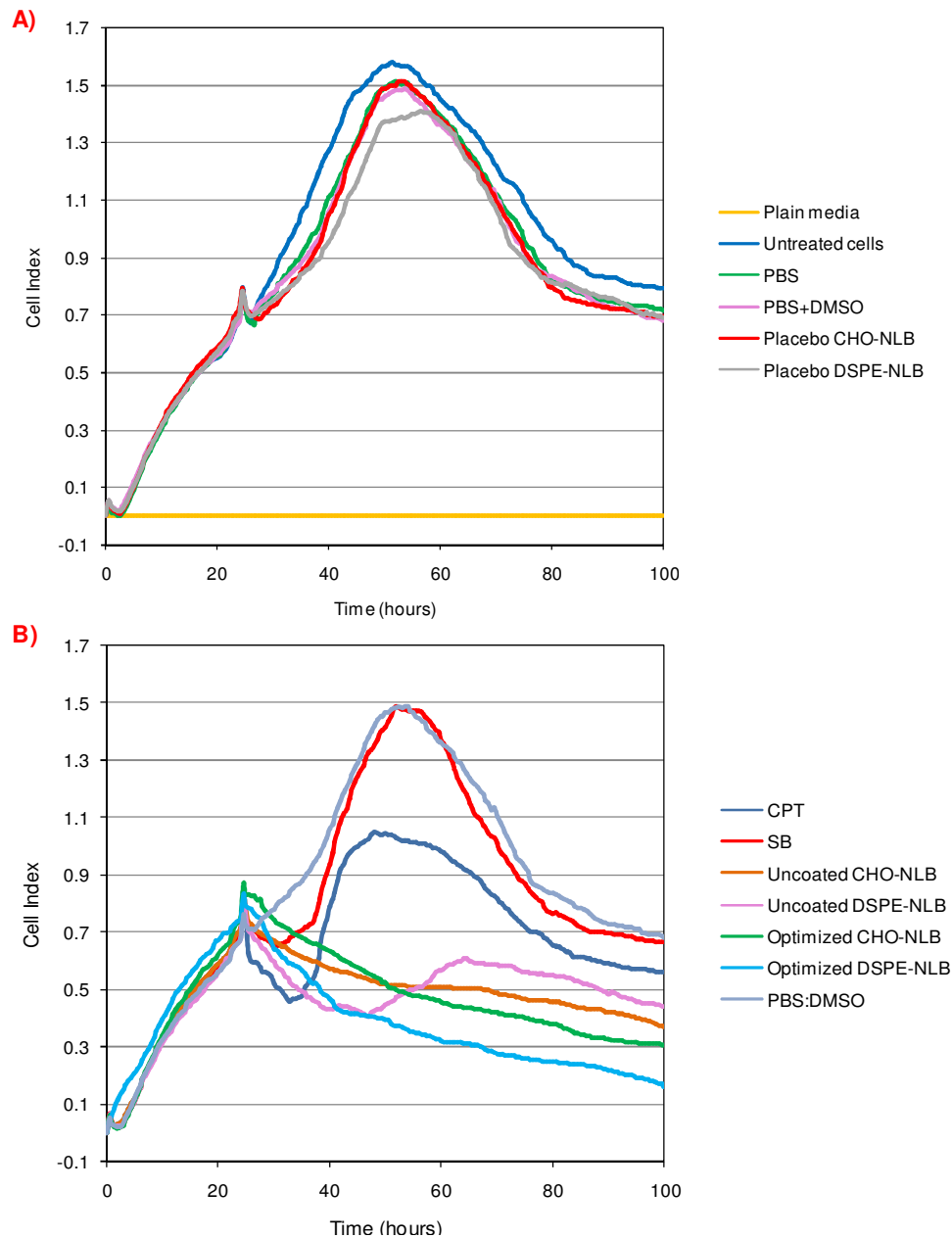


Figure 6.7 Graphical illustration of the growth and response of A2780 cells to various control preparations establishing the cytotoxic potential of each preparation. (in all cases $n=3$ and $SD < 0.02$).

The response of A2780 cells to treatment with native CPT has been previously expounded. The presence of native CPT may have led to saturation of cellular internalization of CPT, leading to rapid killing of cells in the S-phase of the cell cycle. However, the short duration of the cytotoxic stress presented by CPT had a marginal effect on cells in other phases of the cell cycle, resulting in expeditious recovery of the cells and subsequent proliferation. The cytotoxic activity of SB was notably less intense and of a shorter duration to that observed for CPT. The mechanisms of cell cytotoxicity outlined in Chapter 5, Section 5.2 that would be applicable in *ex vivo* studies include induction of apoptosis and cell cycle arrest. SB does not work on a particular phase of the

cell cycle and thus will have an indiscriminate cytotoxic effect on all cells. The initial decrease in cell index was attributed to this indirect effect. The solubility constraints of SB and the high dilution required due to the DMSO solvent resulted in a very low final concentration of SB for cell treatment and low cytotoxic activity. However, the analysis established a distinct sensitivity of A2780 cells to SB. Recovery and proliferation of cells was of a fairly swift nature with marginal differences in cell index relative to that of cells treated with PBS:DMSO from approximately 18 hours post-treatment.

Treatment of cells with uncoated CHO- and DSPE-NLS demonstrated an immediate and considerable reduction in cell index due to the release characteristics of CPT and SB from these formulations. The degree of cytotoxic activity deduced from the cell indices highlighted greater cytotoxicity by DSPE-NLB over a shorter duration, with subsequent recovery of cells from approximately 16 hours post-treatment. This correlates with the release characteristics of CPT from DSPE-NLB observed during *in vitro* analysis. Rapid release of CPT and SB from the uncoated DSPE-NLB resulted in a high degree of cell cytotoxicity, augmented further by the differing mechanisms of action of the 2 compounds. However, the achievement of cellular uptake saturation was a swifter process and CPT and SB that did not have an impact initially, failed to achieve significant cytotoxicity later in the experiment. Whilst recovery of cells was apparent, the peak of the curve was at a conspicuously lower cell index than that of cells treated with PBS:DMSO. The release of CPT from uncoated CHO-NLB displayed a bi-phasic pattern, with slower release from 6-24 hours relative to that of the initial 6 hours. Release of SB from this formulation was evidently more rapid. These characteristics proved beneficial in achieving a more sustained cytotoxic effect on A2780 cells than that observed with DSPE-NLB. The initial decrease in cell index may be attributed to synergistic activity of CPT and SB, whilst the prolonged activity may be a combination of continued CPT activity and the inability of cells to recover adequately.

Treatment of cells with optimized CHO- and DSPE-NLB proved substantially favorable and to a large extent corroborated the drug release data expounded in Chapter 5, Section 5.4.11. The slower release pattern of both CPT and SB following polymer coating translated into augmented and sustained cytotoxic activity of both optimized formulations. The achievement of superior cytotoxicity with DSPE-NLB was associated with enhanced cellular internalization due to the smaller size of this formulation. The enhanced cytotoxicity may also be attributed to a higher concentration of SB within the optimized formulations relative to that of native SB. The cell index curve of optimized DSPE-NLB treated cells displayed a steeper gradient over the initial 16 hours post-treatment, with a marginal decrease in cytotoxicity thereafter. The cell index profile of cells treated with

optimized CHO-NLB highlighted a fairly constant decrease in cell index, indicative of sustained cytotoxic activity. The slower release of CPT and SB from optimized CHO- and DSPE-NLB formulations prevented saturation of cell uptake of the compounds at an early stage resulting in constant exposure to the antineoplastic compounds. Moreover, prolonged release of CPT in particular allowed for more cells to be exposed to CPT whilst in the S-phase of the cell cycle, where CPT acts.

The advantages of this technique include the ability to immediately gauge changes in cellular behavior. Continuous monitoring provides a more complete and accurate representation of changes in cellular morphology, cell numbers and viability (Urcan *et al.*, 2010). The technique provides high sensitivity and reproducibility due to the extent of microelectrode coverage on the base of the wells. A small sample size is required and the entire cell population in a well can be monitored. This is a label-free analytical process which often saves labor and reagents whilst providing substantial information content. Furthermore, real-time evaluation provides an indication of the optimal period for treatment, which is decidedly more accurate than that deduced solely from microscopic observation (Moodley *et al.*, 2011). However, the specialized plates required for the experiment can prove costly.

6.4 Conclusions

The undertaking of *ex vivo* analyses was essential in the systematic characterization of formulated CHO- and DSPE-NLB, and the potential of these nano-DDS to enhance the cytotoxic activity of CPT and SB. The potential of formulated CHO-NLB to induce hemolysis was determined to be 4.36% and 6.87% for NLB concentrations of 10mg/mL and 20mg/mL, respectively. At equal concentrations, the hemolysis deduced for DSPE-NLB was 5.36% and 7.03%. This concentration-dependent hemolysis was not completely unexpected and the safety observed even at the higher concentration was highly favorable. The optimized CHO- and DSPE-NLB can be considered hemocompatible. The intracellular target of CPT, in particular, requires adequate uptake of the formulated NLB by tumour cells. Successful cellular internalization was demonstrated for both CHO- and DSPE-NLB over a short period post-treatment. The size difference between DSPE-NLB and CHO-NLB resulted in higher cellular internalization of DSPE-NLB. A time-dependent uptake was also evident, which would be beneficial for the achievement of sustained antineoplastic activity.

The evaluation of cell cytotoxicity was undertaken by flow cytometry, an end-point assay, and a continuous monitoring, real-time impedance-based study. The results of both studies demonstrated high correlation. The evaluation of control formulations highlighted

the inactivity of materials employed in the formulation of NLB, the structure of the nano-system in the absence of antineoplastic compounds and the solvents employed in the assays. Cells displayed a marginally slower growth rate when treated with control formulations due to reduced availability of nutrients to meet the high demand of rapidly proliferating cells. The slower release pattern of CPT and SB from optimized CHO- and DSPE-NLB proved significantly beneficial to the overall antineoplastic activity of CPT and SB, as evidenced by the sustained and highly favorable cytotoxicity results obtained over the 72 hour assessment. Moreover, the high degree of cellular internalization of the NLB may have further contributed to the favorable antineoplastic characteristics demonstrated by the NLB formulations. Treatment of A2780 ovarian cancer cells with optimized CHO- and DSPE-NLB resulted in a cytotoxicity of 85.90% and 94.93%, respectively over the 72 hour analysis, which was considerably higher than the cytotoxicity demonstrated by plain CPT and SB.

CHAPTER 7

CONCLUSIONS AND RECOMMENDATIONS

7.1 Conclusions

Ovarian cancer is an aggressive pathology affecting several thousand women across all demographic barriers. Late clinical diagnosis, extensive metastasis and a high rate of recurrence collectively add to a very poor prognosis and low 5-year survival rate. The multivariate challenges associated with successful ovarian cancer therapy severely compromise the outcome of therapy and patient quality of life. Chemotherapy is an essential adjuvant to surgical resection due to the high likelihood of metastasis. Intravenous chemotherapy is associated with deleterious side-effects due to indiscriminate activity on rapidly dividing cells. However, this route of administration remains convenient, relatively cost effective, minimally invasive and acceptable to patients. The aim of this study was to formulate a novel antineoplastic nano-lipobubble drug delivery system (NLB-DDS) that would demonstrate passive targeting to tumour tissue through the Enhanced Permeability and Retention phenomenon, following intravenous administration.

Camptothecin (CPT) was selected as the model drug due to the broad spectrum of antineoplastic activity as well as the formulation and physiologic stability challenges that hinder the clinical use of this compound. Nano-sizing was of paramount importance during this study with a maximum threshold size of 200 nm being delineated for the NLB in order to ensure passive targeting. Nano-liposomes (NLS) were formulated as a precursor to NLB and preliminary studies were undertaken on these NLS. The Reverse Phase Solvent Evaporation method was deemed the most appropriate method of formulation for the purposes of this study. Fixed formulation parameters defined during preliminary investigations included the lipid combinations employed, total lipid concentration, surfactant type, CPT concentration, ultrasonication and rotary evaporation parameters. The ratio of each lipid in the combination and surfactant concentration were identified as independent variables that needed to be optimized in order to achieve the desired zeta size, zeta potential, drug incorporation efficiency (DIE) and mean dissolution time.

A Face-centered Central Composite design was employed to statistically optimize the independent variables for the desired outcomes. The concentration of dioctyl sulfosuccinate [DOS] had a statistically significant impact on the MDT achieved with cholesterol-containing NLS (CHO-NLS), whilst lipid ratio and [DOS] proved statistically significant on the average size and zeta potential, respectively of

distearoylphosphatidylethanolamine-containing NLS (DSPE-NLS). The optimal formulation constitution of CHO-NLS was determined to be Distearoylphosphatidylcholine (DSPC): CHO = 3:1 and [DOS] of 0.3%^{w/v}. The optimal constitution of DSPE-NLS was DSPE:CHO = 1.33:2.67 and [DOS] = 0.3%^{w/v}. The composite desirability of both formulations exceeded 0.9.

Statistically optimized CHO- and DSPE-NLS were converted to NLB through the introduction of sulfur hexafluoride gas into the core of the NLS. Formulated NLB were well below the size limit of 200 nm delineated for passive targeting and displayed high drug incorporation. The zeta potential of CHO-NLB was substantially more favorable than that of DSPE-NLB. Moreover, the release profile of CPT from CHO-NLB was slower and more favorable than that observed from DSPE-NLB. Formulations were successfully lyophilized in the presence of a cryoprotectant to produce flaky powders which were easily re-dispersed and retained the NLB structure. Further modifications were undertaken to enhance the antineoplastic potential of the nano-DDS as well as minimize drug release in the systemic circulation. The incorporation of silibinin (SB) a phytochemical with well documented antineoplastic properties was intended to work synergistically with CPT. SB incorporation was satisfactory and had minimal effect of the properties of formulated NLB. Finally the application of sequential oppositely charged polymeric layers was instituted in order to enhance the stability profile of the formulation and delay release of CPT and SB from the NLB. Polymeric coating with CHT and PAA proved substantially beneficial on the surface charge of NLB, particularly DSPE-NLB whilst the average size of each formulation was successfully maintained below 200 nm. The release characteristics of CPT and SB were notably slower and the impact of this was highlighted in cytotoxicity evaluation.

Ex vivo studies were undertaken on fresh blood samples and the A2780 epithelial ovarian cancer cell line. Optimized CHO- and DSPE-NLS demonstrated excellent haemocompatibility as well as rapid and efficient uptake by tumour cells. Cytotoxicity studies highlighted markedly sustained cytotoxicity with low recovery of cells, relative to that observed with uncoated NLB and native CPT and SB. This was a direct result of the slower release of CPT, in particular, which exhibits cell cycle phase-specific activity.

In conclusion, formulated CHO- and DSPE-NLB were below the delineated size for passive targeting and demonstrated remarkable stability characteristics to substantiate feasibility of the formulation with regards to manufacturing, storage and clinical application. Materials employed were generally easily obtainable and cost-effective. The formulations demonstrated considerable safety and cytotoxicity against the ovarian cancer

cell line. The optimized CHO- and DSPE-NLB demonstrated significant potential for clinical application.

7.2 Recommendations

The passively targeted nature of this DDS lends applicability to other solid tumours since no targeting modalities that are specific to ovarian cancer have been employed. Hence, potential for use in other solid tumours should be investigated. To this end, the incorporation of other antineoplastic drugs that are currently employed in the treatment of other solid tumours such as colon, liver and lung cancer should be evaluated in this DDS. Moreover, *ex vivo* studies should extend to the respective cell lines that are applicable to other tumour subtypes.

Drug resistance presents an increasing challenge to antineoplastic therapy. The potential of the formulated NLB-DDS to overcome or bypass established mechanisms of drug resistance should be assessed. It is recommended that antineoplastic drugs to which resistance has been identified be incorporated into the NLB-DDS and tested against resistant cell lines. Furthermore, the potential of phytochemical incorporation in overcoming drug resistance should be considered. Tailored release of the phytochemical and antineoplastic drug may result in sensitization of the cells to the drug or the phytochemical may act as a preferential substrate, thereby preventing deactivation of the antineoplastic drug. In addition, the antineoplastic activity of various combinations of phytochemicals with different mechanisms of antineoplastic activity should be evaluated against resistant and non-resistant tumour cells to effectively assess their potential and clinical applicability in tumour therapy.

Uncoated CHO-NLB demonstrated immensely favourable characteristics during *in vitro* and *ex vivo* evaluation. The benefits of polymeric coating, although evident, were of lesser significance than that observed with DSPE-NLB. It is recommended that methods of delaying drug release from CHO-NLB, other than polymeric coating, be investigated. These methods should maintain the already favorable stability of the formulation and not significantly increase the size of the NLB.

An outstanding characteristic of nano-DDS is the increased surface area which facilitates the attachment of targeting moieties. Targeted therapy will be especially beneficial for antineoplastic drugs since site-specific delivery enhances cytotoxicity at the desired site while maintaining the condition of healthy tissue. It is thus recommended that future research delves into the feasibility of adding targeting moieties to coated and uncoated

NLB and the benefits of widely applicable, passively targeted nano-DDS relative to a tumour specific nano-DDS.

Nano-lipobubbles, as described in this dissertation, have theranostic potential and may be combined with ultrasound technology for tumour detection, imaging and monitoring the progress of therapy. *In vivo* studies are critical in assessing the clinical applicability of this DDS and will also shed valuable light on the imaging potential of this nano-structure. It is thus recommended that *in vivo* evaluation is undertaken in a suitable animal model, such as rats, to simultaneously assess the therapeutic and diagnostic potential of this nano-DDS.

The Reverse Phase Solvent Evaporation method employed in formulation of the optimized CHO- and DSPE-NLB was uncomplicated and did not require prolonged preparation times. This method can conveniently be adapted to industry-scale production, particularly through the employment of rotary evaporators similar to the one used in this study, that enable simultaneous solvent evaporation of numerous samples, without interference between samples. However, consistency in technique and timing was paramount to the achievement of consistently reproducible results and scientifically acceptable inter-formulation variance in this study. Hence, industry-scale production may require automation of the processes that were undertaken manually during this study, such as intermittent addition of phosphate buffered saline and subsequent ultra-sonication, in order to minimize personnel involvement and formulation variance. The production of a lyophilized powder end-product provides a dosage form that is easily and readily usable in clinical practice.

REFERENCES

1. Abu-Lila A, Suzuki T, Doi Y, Ishida T, Kiwada H. Oxaliplatin targeting to angiogenic vessels by PEGylated cationic liposomes suppresses the angiogenesis in the dorsal air sac mouse model, *Journal of controlled release*, (2009); 134: 18-25.
2. Akhlaghi S P, Saremi S, Ostad S N, Dinarvand R, Atyabi F. Discriminated effects of thiolated chitosan-coated pMMA paclitaxel-loaded nanoparticles on different normal and cancer cell lines, *Nanomedicine: Nanotechnology, Biology and Medicine*, (2010); 6(5): 689-697.
3. Aktas M, Wessel M, Hacker S, Klüsener S, Gleichenhagen J, Narberhaus F. Phosphatidylcholine biosynthesis and its significance in bacteria interacting with eukaryotic cells, *European Journal of Cell Biology*, (2010); 89(12): 888-894.
4. Alakhov V, Klinski E, Li S M, Pietrzynski G, Venne A, Batrakova E, Bronitch T, Kabanov A. Block copolymer-based formulation of doxorubicin. From cell screen to clinical trials, *Colloids and Surfaces B: Biointerfaces*, (1999); 16(1-4): 113-134.
5. Allen T M, Cullis P R. Liposomal drug delivery systems: From concept to clinical applications, *Advanced Drug Delivery Reviews*, (2013); 65(1): 36-48.
6. Allison R R, Mota H C, Bagnato V S, Sibata C H. Bio-nanotechnology and photodynamic therapy – State of the art review, *Photodiagnosis and Photodynamic Therapy*, (2008); 5(1): 19-28.
7. Alvarez-Núñez F A, Yalkowsky S H. Relationship between Polysorbate 80 solubilization descriptors and octanol-water partition coefficients of drugs, *International Journal of Pharmaceutics*, (2000); 200(2): 217-222.
8. American Cancer Society, 2012.
<http://www.cancer.org/cancer/ovariancancer/detailedguide/ovarian-cancer-detection> (Accessed: December 2012)
9. Amir-Aslani A. Toxicogenomic predictive modelling: Emerging opportunities for more efficient drug discovery and development, *Technological Forecasting and Social Change*, (2008); 75(7): 905-932.
10. Anand P, Nair H B, Sung B, Kunnumakkara A B, Yadav V R, Tekmal R R, Agarwal B B. Design of curcumin-loaded PLGA nanoparticles formulation with enhanced cellular uptake, and increased bioactivity in vitro and superior bioavailability in vivo, *Biochemical Pharmacology*, (2010); 79(3): 330-338.
11. Anitha A, Maya S, Deepa N, Cheenazhi K P, Nair S V, Tamura H, Jayakumar R. Efficient water soluble *O*-carboxymethyl chitosan nanocarrier for the delivery of curcumin to can cells, *Carbohydrate Polymers*, (2011); 83(2): 452-461.

12. Aqil F, Munagala R, Jeyabalan J, Vadhanam M V. Bioavailability of phytochemicals and its enhancement by drug delivery systems, *Cancer Letters*, (2013); 334(1): 133-141.
13. Balachandran M, Devanathan S, Muraleekrishnan R, Bhagawan S S. Optimizing properties of nanoclay-nitrile rubber (NBR) composites using Face Centered Central Composite Design, *Materials and Design*, (2012); 35: 854-862.
14. Bamias A, Karadimou A, Soupos N, Sotiropoulou M, Zagouri F, Haidopoulos D, Thomakos N, Rodolakis A, Antsaklis A, Dimopoulos M A. Prognostic factors for early-stage epithelial ovarian cancer, treated with adjuvant carboplatin/paclitaxel chemotherapy: A single institution experience, *Gynecologic Oncology*, (2011); 123(1): 37-42.
15. Barenholz Y. Liposome application: problems and prospects, *Current Opinion in Colloid & Interface Science*, (2001); 6(1): 66-77.
16. Bawarski W E, Chidlowsky E, Bharali D J, Mousa S A. Emerging nanopharmaceuticals, *Nanomedicine: Nanotechnology, Biology and Medicine*, (2008); 4(4): 273-282.
17. Bawa R, Fung S-Y, Shiozaki A, Yang H, Zheng G, Keshavjee S, Liu M. Self-assembling peptide-based nanoparticles enhance cellular delivery of the hydrophobic anticancer drug ellipticine through caveolae-dependent endocytosis, *Nanomedicine: Nanotechnology, Biology and Medicine*, (2012); 8(5): 647-654.
18. Bazell R. HER-2: The making of Herceptin, a revolutionary treatment for breast cancer, *Journal of the National Cancer Institute*, (1998); 91(15): 1329-1330.
19. Beig A, Miller J M, Dahan A. Accounting for the solubility-permeability interplay in oral formulation development for poor water solubility drugs: the effect of PEG-4000 on carbamazepine absorption, *European Journal of Pharmaceutics and Biopharmaceutics*, (2012); 81(2): 386-391.
20. Bellot R, Pouna P, Robert J. Separation and determination of liposomal and non-liposomal daunorubicin from the plasma of patients treated with Daunoxome, *Journal of Chromatography B: Biomedical Sciences and Applications*, (2001); 757(2): 257-267.
21. Bhatia N, Zhao J, Wolf D M, Agarwal R. Inhibition of human carcinoma cell growth and DNA synthesis by silibinin, an active constituent of milk thistle: comparison with silymarin, *Cancer Letters*, (1999); 147(1-2): 77-84.
22. Blagosklonny M V. Matching targets for selective cancer therapy, *Drug Discovery Today*, (2003); 8(24): 1104-1107.
23. Bogunia-Kubik K, Masanori S. From molecular biology to nanotechnology and nanomedicine, *Biosystems*, (2002); 65(2-3): 123-138.

24. Borba A, Lairion F, Disalvo A, Fausto R. Interaction of nicotinamide and picolinamide with phosphatidylcholine and phosphatidylethanolamine membranes: A combined approach using dipole potential measurements and quantum chemical calculations, *Biochimica et Biophysica Acta (BBA)-Biomembranes*, (2009); 1788(12): 2553-2562.
25. Brannon-Peppas L, Blanchette J O. Nanoparticle and targeted systems for cancer therapy, *Advanced Drug Delivery Reviews*, (2004); 56(11): 1649-1659.
26. Brown M, Wittwer C. Flow cytometry: Principles and clinical applications in hematology, *Clinical Chemistry*, (2000); 46(8): 1221-1229.
27. Buckley S T, Fischer S M, Fricker G, Brandl M. In vitro models to evaluate the permeability of poorly soluble drug entities: Challenges and perspectives, *European Journal of Pharmaceutical Sciences*, (2012); 45(3): 235-250.
28. Bray F, Jemal A, Grey N, Ferlay J, Forman D. Global cancer transitions according to the Human Development Index (2008-2030): a population-based study, *The Lancet Oncology*, (2012); 13(8): 790-801.
29. Cai L, Qui N, Li X, Luo K, Chen X, Yang L, He G, Wei Y, Chen L. A novel truncated basic fibroblast growth factor fragment-conjugated poly (ethylene glycol)-cholesterol amphiphilic polymeric drug delivery system for targeting to the FGFR-over expressing tumour cells, *International Journal of Pharmaceutics*, (2011); 408(1-2): 173-182.
30. Cancer Research UK: Cancer Stats Key Fact, 2013. http://publications.cancerresearchuk.org/downloads/Product/CS_KF_WORLDWIDE.pdf (Accessed: January 2013).
31. Cao X, Deng W, Fu M, Zhu Y, Liu H, Wang L, Zeng J, Wei Y, Xu X, Yu J. Seventy-two-hour release formulation of the poorly water soluble drug silybin based on porous silica nanoparticles: *In vitro* release kinetics and *in vitro/in vivo* correlations in beagle dogs, *European Journal of Pharmaceutics*, (2012); 7: 753-762.
32. Cerdeira A M, Mazzotti M, Gander B. Miconazole nanosuspensions: Influence of formulation variables on particle size reduction and physical stability, *International Journal of Pharmaceutics*, (2010); 396(1-2): 210-218.
33. Cesur H, Rubinstein I, Pai A, Önyüksel H. Self-associated indisulam in phospholipid-based nanomicelles: a potential nanomedicine for cancer, *Nanomedicine: Nanotechnology, Biology and Medicine*, (2009); 5(2): 178-183.
34. Chang S-J, Bristow R E, Ryu H-S. Prognostic significance of systematic lymphadenectomy as part of primary debulking surgery in patients with advanced ovarian cancer, *Gynecologic Oncology*, (2012); 126(3): 381-186.
35. Charrois G J R, Allen T, Drug release rate influences the pharmacokinetics, biodistribution, therapeutic activity, and toxicity of pegylated liposomal doxorubicin

- formulations in murine breast cancer, *Biochimica et Biophysica Acta (BBA)- Biomembranes*, (2004); 1663(1-2): 167-177.
36. Chatrabuthi S, Chirachanchai S. Chitosan core-corona nanospheres: A convenient material to tailor pH and solvent responsive magnetic nanoparticles, *Polymer*, (2013); 54(16): 4318-4324.
 37. Chaudhury A, Das S, Lee R F S, Tan K-B, Ng W-K, Tan R B H, Chiu G N C. Lyophilization of cholesterol-free PEGylated liposomes and its impact on drug loading by passive equilibration, *International Journal of Pharmaceutics*, (2012); 430(1-2): 167-175.
 38. (a) Chen H, Wang L, Yeh J, Wu X, Cao Z, Wang Y A, Zhang M, Yang L, Mao H. Reducing non-specific binding and uptake of nanoparticles and improving cell targeting with an antifouling PEO-*b*-PyMPS copolymer coating, *Biomaterials*, (2010); 31(20): 5397-5407.
 39. (b) Chen C, Han D, Cai C, Tang X. An overview of liposome lyophilization and its future potential, *Journal of Controlled Release*, (2010); 142(3): 299-311.
 40. Chen K-I, Li B-R, Chen Y-T. Silicon nanowire field-effect transistor-based biosensors for biomedical diagnosis and cellular recording investigation, *Nano today*, (2011); 6(2): 131-154.
 41. Chien J R, Aletti G, Bell D A, Keeney G L, Shridhar V, Hartmann L C. Molecular pathogenesis and therapeutic targets in epithelial ovarian cancer, *Journal of Cellular Biochemistry*, (2007), 102 (5): 1117-1129.
 42. Chin P T K, Buckle T, de Miguel A A, Meskers S C J, Janssen R A J, van Leeuwen F W B. Dual-emissive quantum dots for multispectral intraoperative fluorescence imaging, *Biomaterials*, (2010); 31(26): 6923-6832.
 43. Chirino Y I, Pedrazza-Chaverri J. Role of oxidative and nitrosative stress in cisplatin-induced nephrotoxicity, *Experimental and Toxicologic Pathology*, (2009); 61(3): 223-242.
 44. Cho Y W, Park S A, Han T H, Son D H, Park J S, Oh S J, Moon D H, Cho K-J, Ahn C-H, Byun Y, Kim I-S, Kwoni I C, Kim S Y. In vivo tumour targeting and radionuclide imaging with self-assembled nanoparticles: Mechanisms, key factors, and their implications, *Biomaterials*, (2007); 28(6): 1236-1247.
 45. Chou H-H, Wang K-L, Chen C-A, Wei L-H, Lai C-H, Hsieh C-Y, Yang Y-C, Twu N-F, Chang T-C, Yen M-S. Pegylated liposomal doxorubicin (Lipo-Dox®) for platinum-resistant or refractory epithelial ovarian carcinoma A Taiwanese gynecologic oncology group study with long-term follow-up, *Gynecologic Oncology*, (2006); 101(3): 423-428.

46. Chou T-H, Chu I-M. Thermodynamic characteristics of DSPC/DSPE-PEG₂₀₀₀ mixed monolayers on the water subphase at different temperatures, *Colloids and Surfaces B: Biointerfaces*, (2003); 27(4): 333-344.
47. Chu C S, Rubin S C. Screening for ovarian cancer in the general population, *Best Practice & Research Clinical Obstetrics and Gynecology*, (2006); 20(2): 307-320.
48. Chun J-Y, Choi M-J, Min S-G, Weiss J. Formation and stability of multiple-layered liposomes by layer-by-layer electrostatic deposition of biopolymers, *Food Hydrocolloids*, (2013); 30(1): 249-257.
49. Ciobanu M, Heyrtault B, Schultz P, Ruhlmann C, Muller C D, Frisch B. Layersome: Development and optimization of stable liposomes as drug delivery system. *International Journal of Pharmaceutics*, (2007); 344(1-2): 154-157.
50. Cirstoiu-Hapca A, Buchegger F, Lange N, Gurny R, Delie F. Benefit of anti-HER2-coated paclitaxel-loaded immune-nanoparticles in the treatment of disseminated ovarian cancer: Therapeutic efficacy and biodistribution in mice, *Journal of Controlled Release*, (2010); 144(3): 324-331.
51. Cloven N G, Kyshtoobayena A, Burger R A, Yu I-R, Fruehauf J P. In vitro chemoresistance and biomarker profiles are unique for histologic subtypes of epithelial ovarian cancer, *Gynecologic Oncology*, (2004), 92 (1): 160-166.
52. Cole L K, Vance J E, Vance D E. Phosphatidylcholine biosynthesis and lipoprotein metabolism, *Biochimica et Biophysica Acta (BBA)-Molecular and Cell Biology of Lipids*, (2012); 1821(5): 754-761.
53. Cortesi R, Esposito E, Luca G, Nastruzzi C. Production of lipospheres as carriers for bioactive compounds, *Biomaterials*, (2002); 23(11): 2283-2294.
54. Curry S H. Translational science: past, present and future, *BioTechniques*, (2008); 44(2): Pii-Pviii.
55. D'Incalci M, Steward W P, Gescher A J. Use of cancer chemopreventive phytochemicals as antineoplastic agents, *The Lancet Oncology*, (2005); 6(11): 899-904.
56. Dai R, Wu G, Weigang L, Zhou Q, Li X, Chen H. Gelatin/carboxymethylcellulose/dioctyl sulfosuccinate sodium microcapsule by complex coacervation and its application for electrophoretic display, *Colloids and Surfaces A: Physicochemical and Engineering Aspects*, (2010); 362(1-3): 84-89.
57. Danson S, Ferry D, Alakhov V, Margison J, Kerr D, Jowle D, Brampton M, Halbert G, Ranson M. Phase I dose escalation and pharmacokinetic study of pluronic polymer-bound doxorubicin (SP1049C) in patients with advanced cancer, *British Journal of Cancer*, (2004); 90(11): 2085-2091.

58. Das M, Sahoo S K. Epithelial cell adhesion molecule targeted nutlin-3a loaded immunonanoparticles for cancer therapy, *Acta Biomaterialia*, (2011); 7(1): 355-369.
59. Das R K, Kasoju N, Bora U. Encapsulation of curcumin in alginate-chitosan-pluronic composite nanoparticles for delivery to cancer cells, *Nanomedicine: Nanotechnology, Biology and Medicine*, (2010); 6(1): 153-160.
60. Dhule S S, Penfornis P, Frazier T, Walker R, Feldman J, Tan G, He J, Alb A, John V, Pochampally P. Curcumin-loaded γ -cyclodextrinliposomal nanoparticles as delivery vehicles for osteosarcoma, *Nanomedicine: Nanotechnology, Biology and Medicine*, (2012); 8(4): 440-451.
61. Dominguez A L, Lustgarten J. Targeting the tumour microenvironment with anti-neu/anti-CD40 conjugated nanoparticles for the induction of antitumor immune responses, *Vaccine*, (2010); 28(5): 1383-1390.
62. Dreis S, Rothweiler F, Michaelis M, Cinatl J Jr, Kreuter J, Langer K. Preparation, characterisation and maintenance of drug efficacy of doxorubicin-loaded human serum albumin (HSA) nanoparticles, *International Journal of Pharmaceutics*, (2007); 341 (1-2): 207-214.
63. du Toit L C, Govender T, Pillay V, Choonara Y E, Kodama T. Investigating the effect of polymeric approaches on circulation time and physical properties of nanobubbles, *Pharmaceutical Research*, (2011); 28(3): 494-504.
64. Elmowafy M, Viitala T, Ibrahim H M, Abu-Elyazid S K, Samy A, Kassem A, Yliperttula M. Silymarin loaded liposomes for hepatic targeting: In vitro evaluation and HepG2 drug uptake, *European Journal of Pharmaceutical Sciences*, (2013); 50(2): 161-171.
65. Ertl B, Platzer P, Wirth M, Gabor F. Poly(D,L-lactic-co-glycolic acid) microspheres for sustained delivery and stabilization of camptothecin, *Journal of Controlled Release*, (1999); 61(3): 305-317.
66. Etheridge M L, Campbell S A, Erdman A G, Haynes C L, Wolf S M, McCullough J. The big picture on nanomedicine: The state of investigational and approved nanomedicine products, *Nanomedicine: Nanotechnology, Biology and Medicine*, (2013); 9(1): 1-14.
67. Evjen T J, Nilssen E A, Rögnavaldsson S, Brandl M, Fosshem S L. Distearoylphosphatidylethanolamine-based liposomes for ultrasound-mediated drug delivery, *European Journal of Pharmaceutics and Biopharmaceutics*, (2010); 75(3): 327-333.
68. Fang J-Y, Hung C-F, Hua S-C, Hwang T-L. Acoustically active perfluorocarbon nanoemulsions as drug delivery carriers for camptothecin: Drug release and Cytotoxicity against cancer cells, *Ultrasonics*, (2009); 49(1): 39-46.

69. Fang J-Y, Hung C-F, Liao M-H, Chien C-C. A study of the formulation design of acoustically active lipospheres as carriers for drug delivery, *European Journal of Pharmaceutics and Biopharmaceutics*, (2007); 67: 67-75.
70. Farokhzad O C, Langer R. Nanomedicine: Developing smarter therapeutic and diagnostic modalities, *Advanced Drug Delivery Reviews*, (2006); 58(14): 1456-1459.
71. Fattal E, Bochot A. State of the art and perspectives for the delivery of antisense oligonucleotides and siRNA by polymeric nanocarriers, *International Journal of Pharmaceutics*, (2008); 364(2): 237-248.
72. Fernández-Murray J P, McMaster C R. Phosphatidylcholine synthesis and its catabolism by yeast neuropathy target esterase 1, *Biochimica et Biophysica Acta (BBA)-Molecular and Cell Biology of Lipids*, (2007); 1771(3): 331-336.
73. Ferrandina G, Legge F, Salutari V, Paglia A, Testa A, Scambia G. Impact of pattern of recurrence on clinical outcome of ovarian cancer patients: Clinical considerations, *European Journal of Cancer*, (2006); 24(14): 2296-2302.
74. Fishman D A, Cohen L, Blank S V, Shulman L, Singh D, Bozorgi K, Tamura R, Timor-Tritsch I, Schwartz P E. The role of ultrasound evaluation in the detection of early stage epithelial ovarian cancer, *American Journal of Obstetrics and Gynecology*, (2005); 192(4): 1214-1221.
75. Fonseca C, Simões S, Gaspar R. Paclitaxel-loaded PLGA nanoparticles: preparation, physicochemical characterization and in vitro anti-tumoral activity, *Journal of Controlled Release*, (2002); 83(2): 273-286.
76. Fujiwara K, Sakuragi N, Suzuki S. First-line intraperitoneal carboplatin-based chemotherapy for 165 patients with epithelial ovarian carcinoma: results of long-term follow-up, *Gynaecologic Oncology*, (2003), 90: 637-643.
77. Fukumura D, Jain R K. Tumour microvasculature and microenvironment: Targets for antiangiogenesis and normalization, *Microvascular Research*, (2007); 74 (2-3): 72-84.
78. Gallo D, Giacomelli S, Ferlini C, Raspaglio G, Apollonio P, Prislei S, Riva A, Morazzoni P, Bombardelli E, Scambia G. Antitumour activity of the silybin-phosphatidylcholine complex, IdB1016, against human ovarian cancer, *European Journal of Cancer*, (2003); 39(16): 2403-2410.
79. Ganesh S, Iyer A K, Morrissey D V, Amiji M M. Hyaluronic acid based self-assembling nanosystems for CD44 target mediated siRNA delivery to solid tumours, *Biomaterials*, (2013); 34(13): 3489-3502.
80. Ganta S, Paxton J W, Baguley B C, Garg S. Formulation and pharmacokinetic evaluation of an asulacrine nanocrystalline suspension for intravenous delivery, *International Journal of Pharmaceutics*, (2009); 367(1-2,9): 179-186.

81. Gao J, Zhong W, He J, Li H, Zhang H, Zhou G, Li B, Lu Y, Zou H, Kou G, Zhang D, Wang H, Guo Y, Zhong Y. Tumour targeted PE38KDEL delivery via PEGylated anti-HER2 immunoliposomes, *International Journal of Pharmaceutics*, (2009); 374(1-2): 145-152.
82. Gao Z, Kennedy A M, Christensen D A, Rapoport N Y. Drug-loaded nano/micro bubbles for combining ultrasonography and targeted chemotherapy, *Ultrasonics*, (2008); 48: 260-270.
83. García-Díaz M, Kawakubo M, Mroz P, Sagristà M L, Mora M, Nonell S, Hamblin M R. Cellular and vascular effects of the photodynamic agent temocene are modulated by the delivery vehicle, *Journal of Controlled Release*, (2012); 162(2): 355-363.
84. García-Jimeno S, Escribano E, Queralt J, Estelrich J. Magnetoliposomes prepared by reverse-phase followed by sequential extrusion: Characterization and possibilities in the treatment of inflammation, *International Journal of Pharmaceutics*, (2011); 405(1-2): 181-187.
85. Gelderblom H, Verweij J, Nooter K, Sparreboom A. Cremophor EL: the drawbacks and advantages of vehicle selection for drug formulation, *European Journal of Cancer*, (2001); 37(13): 1590-1598.
86. George M, Ghosh I. Identifying the correlation between drug/stabilizer properties and critical quality attributes (CQA's) of nanosuspension formulation prepared by wet media milling technology, *European Journal of Pharmaceutical Sciences*, (2013); 48(1-2): 142-152.
87. Geszkea M, Muriasc M, Baland L, Medjahdie G, Korczynskif J, Moritzb M, Lulekb J, Schneidera R. Folic-acid conjugated core/shell ZnS:Mn/ZnS quantum dots as targeted probes for two photon fluorescence imaging of cancer cells, *Acta Biomaterialia*, (2011); 7(3): 1327-1338.
88. Geusens B, Lambert J, Smedt S C, Buyens K, Sanders N N, van Gele M. Ultradeformable cationic liposomes for delivery of small interfering RNA (siRNA) into human primary melanocytes, *Journal of Controlled Release*, (2009); 133: 214-220.
89. Gill K K, Nazzal S, Kaddoumi A. Paclitaxel loaded PEG₅₀₀₀-DSPE micelles as pulmonary delivery platform: Formulation characterization, tissue distribution, plasma pharmacokinetics, and toxicological evaluation, *European Journal of Pharmaceutics and Biopharmaceutics*, (2011); 79(2): 276-284.
90. Global Facts and Figures 2nd Edition (GLOBOCAN), *American Cancer Society*, Georgia, USA, 2008.

91. Guinedi A S, Mortada N D, Mansour S, Hathout R M. Preparation and evaluation of reverse-phase evaporation and multilamellar niosomes as ophthalmic carriers of acetazolamide, *International Journal of Pharmaceutics*, (2005); 306(1-2): 71-82.
92. Guo M, Que C, Wang C, Liu X, Yan H, Liu K. Multifunctional superparamagnetic nanocarriers with folate-mediated and pH-responsive targeting properties for anticancer drug delivery, (2011), *Biomaterials*; 32 (1): 185-194.
93. Guyton A C. Textbook of Medical Physiology (8th edition), (1991), Philadelphia: W B Saunders, p. 274.
94. Hadinoto K, Phanapavudhikul P, Kewu Z, Tan R B H. Dry powder aerosol delivery of large hollow nanoparticulate aggregates as prospective carriers of nanoparticulate drugs: Effects of phospholipids, *International Journal of Pharmaceutics*, (2007); 333(1-2): 187-198.
95. Haeri A, Sadeghian S, Rabbani S, Anvari M S, Boroumand M A, Dadashzadeh S. Use of remote film loading methodology to entrap sirolimus into liposomes: Preparation, characterization and in vivo efficacy for treatment of restenosis, *International Journal of Pharmaceutics*, (2011); 414(1-2): 16-27.
96. Hao J, Wang F, Wang X, Zhang D, Bi Y, Gao Y, Zhao X, Zhang Q. Development and optimization of baicalin-loaded solid lipid nanoparticles prepared by coacervation method using central composite design, *European Journal of Pharmaceutical Sciences*, (2012); 47(2): 497-505.
97. Hatefi A, Amsden B. Camptothecin delivery methods, *Pharmaceutical Research*, (2002); 19 (10): 1389-1399.
98. Hatefi A, Knight D, Amsden B. A biological injectable thermoplastic for localized camptothecin delivery, *Journal of Pharmaceutical Sciences*, (2004); 93(5): 1195-1204.
99. Hawkins M J, Soon-Shiong P, Desai N. Protein nanoparticles as drug carriers in clinical medicine, *Advanced Drug Delivery Reviews*, (2008); 60(8): 876-885.
100. Hernot S, Klibanov A L. Microbubbles in ultrasound-triggered drug and gene delivery, *Advanced Drug Delivery Reviews*, 60 (2008), pp. 1153-1166.
101. Hess V, A'Hern R P, Gore M E. Relative platinum-resistance of mucinous carcinoma of the ovary, *The American Society of Clinical Oncology*, (2003), 22: 1797.
102. Hogan F S, Krishnegowda N K, Mikhailova M, Kahlenberg M S. Flavonoid, Silibinin, inhibits proliferation and promotes cell-cycle arrest of human colon cancer, *Journal of Surgical Research*, (2007); 143(1): 58-65.
103. Hossann M, Syunyaeva Z, Schmidt R, Zengerle A, Eibl H, Issels R D, Lindner L H. Proteins and cholesterol lipids vesicles are mediators of drug release from

- thermosensitive liposomes, *Journal of Controlled Release*, (2012); 162(2): 400-406.
104. Hossann M, Wang T, Wiggenghorn M, Schmidt R, Zengerle A, Winter G, Eibl H, Peller M, Reiser M, Issels R D, Lindner L H. Size of thermosensitive liposomes influences content release, *Journal of Controlled Release*, (2010); 147(3): 436-443.
105. Howlader N, Noone AM, Krapcho M, Neyman N, Aminou R, Altekruse SF, Kosary CL, Ruhl J, Tatalovich Z, Cho H, Mariotto A, Eisner MP, Lewis DR, Chen HS, Feuer EJ, Cronin KA (eds). SEER Cancer Statistics Review, 1975-2009 (Vintage 2009 Populations), National Cancer Institute, 2012.
106. Hsiao S-M, Chen C-A, Lin H-H, Hsieh C-Y, Wei L-H. Phase II trial of carboplatin and distearoylphosphatidylcholine pegylated liposomal doxorubicin (LipoDox®) in recurrent platinum-sensitive ovarian cancer following front-line therapy with paclitaxel and platinum, *Gynecologic Oncology*, (2009); 112(1): 35-39.
107. Hussein G A, Pitt W G. Micelles and nanoparticles for ultrasonic drug and gene delivery, *Advanced Drug Delivery Reviews*, 60 (2008): 1137-1152.
108. Ishida T, Harada M, Wang X Y, Ichihara M, Irimura K, Kiwada H. Accelerated blood clearance of PEGylated liposomes following preceding liposome injection: Effects of lipid dose and PEG surface-density and chain length of the first does liposomes, *Journal of Controlled Release*, (2005); 105(3): 305-317.
109. Ishida T, Kirchmeier M J, Moase E H, Zalipsky S, Allen T M. Targeted delivery and triggered release of liposomal doxorubicin enhances cytotoxicity against human B lymphoma cells, *Biochimica et Biophysica Acta (BBA)-Biomembranes*, (2001); 1515(2): 144-158.
110. Ishii T, Teramoto S, Matsuse T. GSTP 1 affects chemoresistance against camptothecin in human lung adenocarcinoma cells, *Cancer Letters*, (2004); 216 (1): 89-102.
111. Itamochi H, Kigawa J, Terakawa N. Mechanisms of chemoresistance and poor prognosis in ovarian clear cell carcinoma, *Cancer Science*, (2008), 99 (4): 653-658.
112. Jó T A, Petri D F S, Beltramini L M, Lucyszyn N, Sierakowski M R. Xyloglucan nano-aggregates: physic-chemical characterisation in buffer solution and potential application as a carrier for camptothecin, an anti-cancer drug, *Carbohydrate Polymers*, (2010); 82(2): 355-362.
113. Jacobs I J, Menon U. Progress and challenges in screening for early detection of ovarian cancer, *Molecular and Cellular Proteomics*, (2004); 3(4): 355-366.
114. Jemal A, Bray F, Center M M, Ferlay J, Ward E, Forman D. Global Cancer Statistics, *CA: A Cancer Journal for Clinicians*, (2011); 61(2): 69-90.

115. Ji X-T, Huang L, Huang H-Q. Construction of nanometer cisplatin core-ferritin (NCC-F) and proteomic analysis of gastric cancer cell apoptosis induced with cisplatin released from the NCC-F, *Journal of Proteomics*, (2012); 75 (11): 3145-3157.
116. Jia Y, Joly H, Omri A. Liposomes as a carrier for gentamicin delivery Development, and evaluation of the physicochemical properties, *International Journal of Pharmaceutics*, (2008); 359(1-2): 254-263.
117. John Hopkins Pathology, 2001. <http://www.ovariancancer.jhmi.edu/typesca.cfm> (Accessed: December 2012).
118. Junghanns J-U A H, Müller R H. Nanocrystal technology, drug delivery and clinical applications, *International Journal of Nanomedicine*, (2008); 3(3): 295-310.
119. Köbel M, Kalloger S E, Santos J L, Huntsman D G, Gilks C B, Swenerton K D. Tumour type and substage predict survival in stage I and II ovarian carcinoma: Insights and implications, *Gynecologic Oncology*, (2010); 116(1): 50-56.
120. Kang H, O'Donoghue M B, Liu H, Tan W. A Liposome-based nanostructure for aptamer directed delivery, *Chemical Communication*, (2010); 46(2): 249-251.
121. Kang J, Kumar V, Yang D, Chowdhury P R, Hohl R J. Cyclodextrin Complexation: influence on the solubility, stability and cytotoxicity of camptothecin, an antineoplastic agent, *European Journal of Pharmaceutical Sciences*, (2002); 15(2): 63-170.
122. Kapitza S B, Michel B R, van Hoogevest P, Leigh M L S, Imanidis G. Absorption of poorly water soluble drugs subject to apical efflux using phospholipids as solubilizers in the Caco-2 cell model, *European Journal of Pharmaceutics and Biopharmaceutics*, (2007); 66(1): 146-158.
123. Katragadda U, Teng Q, Rayaprolu B M, Chandran T, Tan C. Multi-drug delivery to tumour cells via micellar nanocarriers, *International Journal of Pharmaceutics*, (2011); 419(1-2): 281-286.
124. Kawaguchi E, Shimokawa K-i, Ishii F. Physicochemical properties of structured phosphatidylcholine in drug carrier lipid emulsions for drug delivery systems, *Colloids and Surfaces B: Biointerfaces*, (2008); 62(1): 130-135.
125. Kawakami S, Suzuzki S, Yamashita F, Hashida M. Induction of apoptosis in A549 human lung cancer cells by all-*trans* retinoic acid incorporated in DOTAP/cholesterol liposomes, *Journal of Controlled Release*, (2006); 110(3): 514-521.
126. Kent C. Regulatory enzymes of phosphatidylcholine biosynthesis: a personal perspective, *Biochimica et Biophysica Acta (BBA)-Molecular and Cell Biology of Lipids*, (2005); 1733(1): 53-66.

127. Khdair A, Handa H, Mao G, Panyam J. Nanoparticle-mediated combination chemotherapy and photodynamic therapy overcomes tumour drug resistance *in-vitro*, *European Journal of Pharmaceutics and Biopharmaceutics*, (2009); 71(2): 214-222.
128. Khosravi-Darani K, Pardakhty A, Honarpisheh H, Rao V S N M, Mozafari M R. The role of high-resolution imaging in the evaluation of nanosystems for bioactive encapsulation and targeted nanotherapy, *Micron*, (2007); 38(8): 804-818.
129. Kiesslich T, Berland J, Plaetzer K, Krammer B, Berr F. Comparative characterization of the efficiency and cellular pharmacokinetics of Foscan®-Foslip®-based photodynamic treatment in human biliary tract cancer cell lines, *Photochemical and Photobiological Sciences*, (2007); 6: 619-627.
130. Kim P S, Djazayeri S, , Zeineldin R. Novel nanotechnology approaches to diagnosis and therapy of ovarian cancer, *Gynecologic Oncology*, (2011), 120(3): 393-403.
131. Koo O M, Rubinstein I, Onyuksel H. Role of nanotechnology in targeted drug delivery and imaging: a concise review, *Nanomedicine: Nanotechnology, Biology and Medicine*, (2005); 1(3): 193-212.
132. Koroukian S M, Punjabi A, Schiltz N, Barnholz-Sloan J, Zanotti K. Ovarian cancer in older women: Clinical presentation and inpatient mortality, *Journal of Geriatric Oncology*, (2012); 3(1): S53.
133. Kratz F. Albumin as a drug carrier: Design of prodrugs, drug conjugates and nanoparticles, *Journal of Controlled Release*, (2008); 132(3): 171-183.
134. Kumar G P, Rajeshwarrao P. Nonionic surfactant vesicular systems for effective drug delivery – an overview, *Acta Pharmaceutica Sinica B*, (2011); 1(4): 208-219.
135. Kundu P, Mohanty C, Sahoo S K. Antiglioma activity of curcumin-loaded lipid nanoparticles and its enhanced bioavailability in brain tissue for effective glioblastoma therapy, *Acta Biomaterialia*, (2012); 8(7): 2670-2687.
136. Kunii R, Onishi H, Machida Y. Preparation and antitumor characteristics of PLA(PEG-PPG-PEG) nanoparticles loaded with camptothecin, *European Journal of Pharmaceutics and Biopharmaceutics*, (2007); 67(1): 9-17.
137. Kurian A W, Balise R R, Mcguire V, Whittemore A S. Histologic types of epithelial ovarian cancer: have they different risk factors, *Gynecologic Oncology*, (2005); 96(2): 520-530.
138. Kwon O S, Parka S J, Jang J. A high-performance VEGF aptamer functionalized polypyrrole nanotubes biosensor, *Biomaterials*, (2010); 31(17): 4740-4747.
139. Landriscina M, Amoroso M R, Piscazzi A, Esposito F. Heat shock proteins, cell survival and drug resistance: The mitochondrial chaperone TRAP1, a potential

- novel target for ovarian cancer therapy, *Gynecologic Oncology*, (2010); 117(2): 177-182.
140. Leamon C P, Low P S. Folate-mediated targeting: from diagnostics to drug and gene delivery. *Drug Discovery Today*, (2001); 6(1): 44-51.
141. Lee J H, Khor T O, Shu L, Su Z-Y, Fuentes F, Kong A-N T. Dietary phytochemicals and cancer prevention: Nrf2 signalling, epigenetics, and cell death mechanisms in blocking cancer initiation and progression, *Pharmacology and Therapeutics*, (2013); 137(2): 153-171.
142. Lee S-J, Kim Y J, Lee C S, Bae J. Combined application of camptothecin and the guanylate cyclase activator YC-1: Impact on cell death and apoptosis-related proteins in ovarian carcinoma cell lines, *Chemico-Biological Interactions*, (2009); 181(2): 185-192.
143. Lee S J, Hong G-Y, Jeong Y-I, Kang M-S, Oh J-S, Song C-E, Lee H C. Paclitaxel-incorporated nanoparticles of hydrophobized polysaccharide and their antitumor activity, *International Journal of Pharmaceutics*, (2012); 433(1-2): 121-128.
144. Lehner R, Wang X, Wolf M, Hunziker P. Designing switchable nanosystems for medical application, *Journal of Controlled Release*, (2012); 161(2): 307-316.
145. Lei T, Srinivasan S, Tang Y, Manchanda R, Nagesetti A, Fernandez-Fernandez A, McGoron A J. Comparing cellular uptake and cytotoxicity of targeted drug carriers in cancer cell lines with different drug resistance mechanisms, *Nanomedicine: Nanotechnology, Biology and Medicine*, (2011); 7(3): 324-332.
146. Lesoin L, Crampon C, Boutin O, Badens E. Preparation of liposomes using the supercritical anti-solvent (SAS) process and comparison with a conventional method, *The Journal of Supercritical Fluids*, (2011); 57(2): 162-174.
147. Li X, Zhao Q, Qiu L. Smart ligand: Aptamer-mediated targeted delivery of chemotherapeutic drugs and siRNA for cancer therapy. *Journal of Controlled Release*. 2013; 171(2): 152-162.
148. Ling D, Bae B-c, Park W, Na K. Photodynamic efficacy of photosensitizers under an attenuated light dose via lipid nano-carrier-mediated nuclear targeting, *Biomaterials*, (2012); 33(21): 5478-5486.
149. Liu J, Jiang Z, Zhang S, Saltzman W M. Poly(ω -pentadecalactone-co-butylene-co-succinate) nanoparticles as biodegradable carriers for camptothecin delivery, *Biomaterials*, (2009); 30(29): 5707-5719.
150. Liu J, Xu L, Liu C, Zhang D, Wang S, Deng Z, Lou W, Xu H, Bai Q, Ma J. Preparation and characterization of cationic curcumin nanoparticles for improvement of cellular uptake, *Carbohydrate Polymers*, (2012); 90(1): 16-22.

151. Lo Y-L. Phospholipids as multidrug resistance modulators of the transport of epirubicin in human intestinal epithelial Caco-2 cell layers and everted gut sacs of rats, *Biochemical Pharmacology*, (2000); 60(9): 1381-1390.
152. Lu Y, Park K. Polymeric micelles and alternative nanonized delivery vehicles for poorly soluble drugs, *International Journal of Pharmaceutics*, (2012); 453(1): 198-214.
153. Macklin P, Lowengrub J. Nonlinear simulation of the effect of microenvironment on tumour growth, *Journal of Theoretical Biology*, (2007); 245(4): 677-704.
154. Madrigal-Carballo S, Lim S, Rodriguez G, Vila A O, Krueger C G, Gunasekaran S, Reed J D. Biopolymer coating of soybean lecithin liposomes via layer-by-layer self-assembly as novel delivery system for ellagic acid, *Journal of Functional Foods*, (2010); 2(2): 99-106.
155. Mahmoudi M, Sant S, Wang B, Laurent S, Sen Tapas. Superparamagnetic iron oxide nanoparticles (SPIONs): development, surface modification and applications in chemotherapy, *Advanced Drug Delivery Reviews*, (2011); 63(1-2): 24-46.
156. Marconescu A, Thorpe P E. Coincident exposure of phosphatidylethanolamine and anionic phospholipids on the surface of irradiated cells, *Biochimica et Biophysica Acta (BBA)-Biomembranes*, (2008); 1778(10): 2217-2224.
157. Maringe C, Walters S, Butler J, Coleman M P, Hacker N, Hanna L, Mosgaard B J, Nordin A, Rosen B, Engholm G, Gjerstorff M L, Hatcher J, Johannesen T B, McGahan C E, Meechan D, Middleton R, Tracey E, Turner D, Richards M A, Rachet B. Stage at diagnosis and ovarian cancer survival: Evidence from the International Cancer Benchmarking Partnership, *Gynecologic Oncology*, (2012); 127(1): 75-82.
158. Martins S, Tho I, Reimold I, Fricker G, Souto E, Ferreira D, Brandl M. Brain delivery of camptothecin by means of solid lipid nanoparticles: Formulation design, *in vitro* and *in vivo* studies, *International Journal of Pharmaceutics*, (2012); 439(1-2): 49-62.
159. McCormack V A, Schüz J. Africa's growing cancer burden: Environmental and Occupational contributions, *Cancer Epidemiology*, (2012); 36(1): 1-7.
160. Meng F, Cheng R, Deng C, Zhong Z. Intracellular drug release nanosystems, *Materials Today*, (2012); 15(10): 436-442.
161. Merisko-Liversidge E, Liversidge G G, Cooper E R. Nanosizing: a formulation approach for poorly-water-soluble compounds, *European Journal of Pharmaceutical Sciences*, (2003); 18(2): 113-120.
162. Mertins O, Sebben M, Pohlmann A R, da Silveira N P. Production of soybean phosphatidylcholine-chitosan nanovesicles by reverse phase evaporation: a step by step study, *Chemistry and Physics of Lipids*, (2005); 138(1-2): 29-37.

163. Mi Y, Liu X, Zhao J, Ding J, Feng S-S. Multimodality treatment of cancer with Herceptin conjugated, thermomagnetic iron oxides and docetaxel loaded nanoparticles of biodegradable polymers, *Biomaterials*, (2012); 33(30): 7519-7529.
164. Miura H, Onishi H, Sasatsu M, Machida Y. Antitumour characteristics of methoxypolyethylene glycol-poly(DL-lactic acid) nanoparticles containing camptothecin, *Journal of Controlled Release*, (2004); 97(1): 101-113.
165. Modugno F, Ness R B, Wheeler J E. Reproductive risk factors for epithelial ovarian cancer according to histological type and invasiveness, *Annals of Epidemiology*, (2001), 11 (8): 568-574.
166. Mohanty C, Sahoo S K. The in-vitro stability and in-vivo pharmacokinetics of curcumin prepared as an aqueous nanoparticulate formulation, *Biomaterials*, (2010); 31(25): 6597-6611.
167. Moodley K, Angel C E, Glass M, Graham E S. Real-time profiling of NK cell killing of human astrocytes using xCELLigence technology. *Journal of Neuroscience Methods*, (2011); 200(2): 173-180.
168. Mu L, Elbayoumi T, Torchilin V P. Mixed micelles made of poly(ethylene glycol)-phosphatidylethanolamine conjugate and d-alpha-tocopheryl polyethylene glycol 1000 succinate as pharmaceutical nanocarriers for camptothecin, *International Journal of Pharmaceutics*, (2005); 306(1-2): 142-149.
169. Murday J S, Siegel R W, Stein J, Wright J F. Translational nanomedicine: status assessment and opportunities, *Nanomedicine: Nanotechnology, Biology and Medicine*, (2009); 5(3): 251-273.
170. Nabekura T, Yamaki T, Hiroi T, Ueno K, Kitagawa S. Inhibition of anticancer drug efflux transporter P-glycoprotein by rosemary phytochemicals. *Pharmacological Research*, (2010); 61(3): 259-263.
171. Nagle C M, Olsen C M, Webb P M, Jordan S J, Whiteman D C, Green A C. Endometrioid and clear cell ovarian cancers – A comparative analysis of risk factors, *European Journal of Cancer*, (2008); 44(16): 2477-2484.
172. Nair H B, Sung B, Yadav V R, Kannappan R, Chaturvedi M M, Aggarwal B B. Delivery of anti-inflammatory nutraceuticals by nanoparticles for the prevention and treatment of cancer, *Biochemical Pharmacology*, (2010); 80(12): 1833-1843.
173. Nakanishi T, Fukushima S, Okamoto K, Suzuki M, Matsumura Y, Yokoyama M, Okano T, Sakurai Y, Kataoka K. Development of the polymer micelle carrier system for doxorubicin, *Journal of Controlled Release*, (2001); 74(1-3): 295-302.
174. National Cancer Institute, 2012 - <http://www.cancer.gov/cancertopics/cancerlibrary/what-is-cancer> (Accessed: November 2012).

175. Nijhara R, Balakrishnan K. Bringing nanomedicines to market: regulatory challenges, opportunities, and uncertainties, *Nanomedicine: Nanotechnology, Biology and Medicine*, (2006); 2(2): 127-136.
176. Nishiyama N, Kataoka K. Current state, achievements, and future prospects of polymeric micelles as nanocarriers for drug and gene delivery, *Pharmacology and Therapeutics*, (2006); 112(3): 630-648.
177. Önyüksel H, Mohanty P S, Rubinstein I. VIP-grafted sterically stabilized phospholipid nanomicellar 17-allylamino-17-demethoxy geldanamycin: A novel targeted nanomedicine for breast cancer, *International Journal of Pharmaceutics*, (2009); 365(1-2,5): 157-161.
178. O'Cearbhaill R, Li D, Shi W, Thaler H, Sabbatini P J, Konner J, Hensley M L, Aghajanian C A, Lichtman S M, Tew W P. Intraperitoneal chemotherapy in older women with epithelial ovarian cancer, *Journal of Geriatric Oncology*, (2012); 3(3): 189-195.
179. Ohulchanskyy T Y, Roy I, Goswami L N, Chen Y, Bergey E J, Pandey R K, Oseroff A R, Prasad P N. Organically modified silica nanoparticles with covalently incorporated photosensitizer for photodynamic therapy of cancer, *Nano Letters*, (2007); 7(9): 2835-2842.
180. Pan J, Feng S-S. Targeting and imaging cancer cells by Folate-decorated, quantum dots (QDs)-loaded nanoparticles of biodegradable polymers, *Biomaterials*, (2009); 30(6): 1176-1183.
181. Paolino D, Licciardi M, Celia C, Giammona G, Fresta M, Cavallaro G. Folate-targeted supramolecular vesicular aggregates as a new frontier for effective anticancer treatment in *in vivo* model, *European Journal of Pharmaceutics and Biopharmaceutics*, (2012); 82(1): 94-102.
182. Papagiannaros A, Levchenko T, Hartner W, Mongayt D, Torchilin V. Quantum dots encapsulated in phospholipid micelles for imaging and quantification of tumours in the near-infrared region, *Nanomedicine: Nanotechnology, Biology and Medicine*, (2009); 5(2): 216-224.
183. Parveen R, Baboota S, Ali J, Ahuja A, Vasudev S S, Ahmad S. Oil based nanocarrier for improved oral delivery of silymarin: *In vitro* and *in vivo* studies, *International Journal of Pharmaceutics*, (2011); 413(1-2): 245-253.
184. Paszko E, Ehrhardt C, Senge O M, Kelleher D P, Reynolds J V. Nanodrug applications in photodynamic therapy, *Photodiagnosis and Photodynamic Therapy*, (2011); 8(1): 14-29.
185. Pathak P, Meziani M J, Desai T, Sun Y-P. Formation and stabilization of ibuprofen nanoparticles in supercritical fluid processing, *The Journal of Supercritical Fluids*, (2006); 37(3): 279-286.

186. Patil V V, Galge R V, Thorat B N. Extraction and purification of phosphatidylcholine from soybean lecithin, *Separation and Purification Technology*, (2010), 75(2): 138-144.
187. Petrak K. Essential properties of drug-targeting delivery systems, *Drug Discovery Today*, (2005); 10(23-24): 1667-1673.
188. Pien H H, Fischman A J, Thrall J H, Sorenson A G. Using imaging biomarkers to accelerate drug development and clinical trials, *Drug Discovery Today*, (2005); 10(4): 259-266.
189. Pilkington G A, Briscoe W H. Nanofluids mediating surface forces, *Advances in Colloid and Interface Science*, (2012); (179-182): 68-84.
190. Pradhan P, Giri J, Rieken F, Koch C, Mykhaylyk O, Döblinger M, Banerjee R, Bahadur D, Plank C. Targeted temperature sensitive magnetic liposomes for thermo-chemotherapy, *Journal of Controlled Release*, (2010), 142(1): 108-121.
191. Pujana M A, Pérez-Álvarez L, Iturbe L C C, Katime I. Water-dispersible pH-responsive chitosan nanogels modified with biocompatible cross-linking agents, *Polymer*, (2012); 53(15): 3107-3116.
192. Róg T, Pasenkiewicz-Gierula M. Cholesterol effects on a mixed-chain phosphatidylcholine bilayers: a molecular dynamics simulation study, *Biochimie*, (2006); 88(5): 449-460.
193. Rai P, Mallidi S, Zheng X, Rahmanzadeh R, Mir Y, Elrington S, Khurshid A, Hasan T. Development and applications of photo-triggered theranostics agents, *Advanced Drug Delivery Reviews*, (2010); 62(11): 1094-1124.
194. Ramasamy K, Agarwal R. Multitargeted therapy of cancer by silymarin, *Cancer Letters*, (2008); 269(2): 352-362.
195. Rapoport N. Physical stimuli-responsive polymeric micelles for anti-cancer drug delivery, *Progress in Polymer Science*, (2007); 32 (8-9): 962-990.
196. Rastogi R, Galati N, Konawa R K, Sharma U, Jayasundar R, Koul V. Evaluation of folate conjugated pegylated thermosensitive magnetic nanocomposites for tumour imaging and therapy, *Colloids and Surfaces B: Biointerfaces*, (2011); 82(1): 160-167.
197. Rauh-Hain J A, Krivak T C, del Carmen M G, Olawaiye A B. Ovarian cancer screening and early detection in the general population, *Reviews in Obstetrics and Gynecology*, (2011); 4(1): 15-21.
198. Rjiba-Touati K, Ayed-Boussema I, Belarbia A, Azzebi A. Protective effect of recombinant human erythropoietin against cisplatin cytotoxicity and genotoxicity in cultured Vero cells, *Experimental and Toxicologic Pathology*, (2013); 65(1-2): 181-187.

199. Roy I, Ohulchansky T Y, Pudavar H E, Bergey E J, Oseroff A R, Morgan J, Dougherty T J, Prasad P N. Ceramic-based nanoparticles entrapping water-insoluble photosensitizing anticancer drugs: A novel drug-carrier system for photodynamic therapy, *Journal of the American Chemical Society*, (2003); 125(26): 7860-7865.
200. Sadzuka Y, HIRAMA R, Sonobe T. Effects of intraperitoneal administration of liposomes and methods of preparing liposomes for local therapy, *Toxicology Letters*, (2002); 126(2): 83-90.
201. Sakai K, Tomizawa H, Tsuchiya K, Ishida N, Sakai H, Abe M. Characterizing the structural transition of cationic DPPC liposomes from the approach of TEM, SAXS and AFM measurements, *Colloids and Surfaces B: Biointerfaces*, (2008); 67(1): 73-78.
202. Santos N D, Mayer L D, Abraham S A, Gallagher R C, Cox K A K, Tardi P G, Bally M B. Improved retention of idarubicin after intravenous injection obtained for cholesterol-free liposomes, *Biochimica et Biophysica Acta (BBA)-Biomembranes*, (2002); 1562(2): 188-201.
203. Sato Y, Hatakeyama H, Sakurai Y, Hyodo M, Akita H, Harashima H. A pH-sensitive cationic lipid facilitates the delivery of liposomal siRNA and gene silencing activity *in vitro* and *in vivo*, *Journal of Controlled Release*, (2012); 163(3): 267-276.
204. Savić R, Luo L, Eisenberg A, Myasinger D. Micellar nanocontainers distribute to defined cytoplasmic organelles, *Science*, (2003); 300; 615-618.
205. Sawant R R, Sawant R M, Torchilin V P. Mixed PEG-PE/vitamin E tumour-targeted immunomicelles as carriers for poorly soluble anti-cancer drugs: Improved drug solubilisation and enhanced *in vitro* cytotoxicity, *European Journal of Pharmaceutics and Biopharmaceutics*, (2008); 70(1): 51-57.
206. Sezgin Z, Yüksel N, Baykara T. Preparation and characterization of polymeric micelles for solubilisation of poorly soluble anticancer drugs, *European Journal of Pharmaceutics and Biopharmaceutics*, (2006); 64(3): 261-268.
207. Schroedera J E, Shwekya I, Shmeedab H, Banina U, Gabizonb A. Folate-mediated tumour cell uptake of quantum dots entrapped in lipid nanoparticles, *Journal of Controlled Release*, (2007); 124 (1-2,4): 28-34.
208. Sellers T A, Schildkraut J M, Pankratz V S, Vierkant R A, Fredericksen Z S, Olson J E, Cunningham J, Taylor W, Liebow M, McPherson C, Hartmann L C, Pal T, Adjei A A. Estrogen bioactivation, genetic polymorphisms and ovarian cancer. *Cancer Epidemiology, biomarkers and prevention*, (2005), 14 (11): 2536-2543.

209. Setua S, Menon D, Asok A, Naira S, Koyakutty M. Folate receptor targeted, rare-earth oxide nanocrystals for bi-modal fluorescence and magnetic imaging of cancer cells, *Biomaterials*, (2010); 31(4): 714-729.
210. Shapira A, Livney Y D, Broxterman H J, Assaraf Y G. Nanomedicine for targeted cancer therapy: towards the overcoming of drug resistance, *Drug Resistance Updates*, (2011); 14(3): 150-163.
211. Sharma G, Modgil A, Layek B, Arora K, Sun C, Law B, Singh J. Cell penetrating peptide tethered bi-ligand liposomes for delivery to brain *in vivo*: Biodistribution and transfection, *Journal of Controlled Release*, (2013); 167(1): 1-10.
212. Shea J E, Nam K H, Rapoport N, Scaife C L. Genexol inhibits primary tumour growth and metastases in gemcitabine-resistant pancreatic ductal adenocarcinoma, *International Hepato-Biliary Association (Oxford)*, (2011); 13(3): 153-157.
213. Shehata T, Ogawara K-i, Higaki K, Kimura T. Prolongation of residence time of liposome by surface-modification with mixture of hydrophilic polymers, *International Journal of Pharmaceutics*, (2008); 359(1-2): 272-279.
214. Shen Y, Tang H, Zhan Y, Van Kirk E A, Murdoch W J. Degradable Poly(β -amino ester) nanoparticles for cancer cytoplasmic drug delivery, *Nanomedicine: Nanotechnology, Biology and Medicine*, (2009); 5(2): 192-201.
215. Shenderova A, Burke T G, Schwendeman S P. Stabilization of 10-hydroxycamptothecin in poly(lactide-co-glycolide) microsphere delivery vehicles, *Pharmaceutical Research*, (1997); 14(10): 1406-1414.
216. Shimizu K, Asai T, Fuse T, Sadzuka Y, Sonobe T, Ogino K, Taki T, Tanaka T, Oku N. Applicability of anti-neovascular therapy to drug resistant tumour: Suppression of drug-resistant P388 tumour growth with neovessel-targeted liposomal adriamycin, *International Journal of Pharmaceutics*, (2005); 296(1-2): 133-141.
217. Shiraishi K, Endoh R, Furuhashi H, Nishihara M, Suzuki R, Maruyama K, Oda Y, Jo J-I, Tabata Y, Yamamoto J, Yokoyama M. A facile preparation method of a PFC-containing nano-sized emulsion for theranostics of solid tumours, *International Journal of Pharmaceutics*, (2011); 421(2): 379-387.
218. Sibata M N, Tedesco A C, Marchetti J M. Photophysicals and photochemicals studies for zinc(II)phthalocyanine in long time circulation micelles for photodynamic therapy use, *European Journal of Pharmaceutical Sciences*, (2004); 23(2): 131-138.
219. Simões S I, Tapadas J M, Marques C M, Cruz M E M, Martins M B F, Cevc G. Permeabilisation and solubilisation of soybean phosphatidylcholine bilayers vesicles, as membrane models, by polysorbate, Tween 80, *European Journal of Pharmaceutical Sciences*, (2005); 26(3-4): 307-317.

220. Sobolev A S, Jans D A, Rosenkranz A A. Targeted intracellular delivery of photosensitizers, *Progress in Biophysics and Molecular Biology*, (2000); 73(1): 51-90.
221. Song L Y, Ahkong Q F, Rong Q, Wang Z, Ansell S, Hope M J, Mui B. Characterization of the inhibitory effect of PEG-lipid conjugates on the intracellular delivery of plasmid and antisense DNA mediated by cationic lipid liposomes, *Biochimica et Biophysica (BBA)-Biomembranes*, (2002); 1558(1): 1-13.
222. Sonnemann J, Palani C D, Wittig S, Becker S, Eichhorn F, Voigt A, Beck J F. Anticancer effects of the p53 activator nultin-3a in Ewing's sarcoma cells, *European Journal of Cancer*, (2011); 47(9): 1432-1441.
223. Soundararajan S, Wang L, Sridharan V, Chen W, Courtenay-Luck N, Jones D, Spicer E K, Fernandes D J. Plasma membrane nucleolin is a receptor for the anti-cancer aptamer AS1411 in MV4-11 leukemia cells, *Molecular Pharmacology*, (2009); 76(5): 984-991.
224. Spentzos D, Levine D A, Ramoni M F, Joseph M, Gu X, Boyd J, Libermann T A, Cannistra S A. Gene expression signature with independent prognostic significance in epithelial ovarian cancer, *Journal of Clinical Oncology*, (2004); 22(23): 4700-4710.
225. Spyratou E, Makropoulou M, Mourelatou M, Demetzos C. Biophotonic techniques for manipulation and characterization of drug delivery nanosystems in cancer therapy, *Cancer Letters*, (2012); 327(1-2): 111-122.
226. Stuart G C E. First-line treatment regimens and the role of consolidation therapy in advanced ovarian cancer, *Gynecologic Oncology*, (2003), 90(3): S8-S15.
227. Su Z, Graybill W S, Zhu Y. Detection and monitoring of ovarian cancer, *Clinica Chimica Acta*, (2013); 415: 341-345.
228. Sun J, Liu R H. Cranberry phytochemical extracts induce cell cycle arrest and apoptosis in human MCF-7 breast cancer cells, *Cancer Letters*, (2006); 241(1): 124-134.
229. Suzuki R, Takizawa T, Kuwata Y, Mutoh M, Ishiguro N, Utoguchi N, Shinohara A, Eriguchi M, Yanagie H, Maruyama K. Effective anti-tumor activity of oxaliplatin encapsulated in transferrin-PEG-liposome, *International Journal of Pharmaceutics*, (2008); 346(1-2): 143-150.
230. Tamilvanan S. Formulation of multifunctional oil-in-water nanosized emulsions for active and passive targeting of drugs to otherwise inaccessible internal organs of the human body, *International Journal of Pharmaceutics*, (2009); 381(): 62-76.
231. Tardi P G, Gallagher R C, Johnstone S, Harasym N, Webb M, Bally M B, Mayer L D. Coencapsulation of irinotecan and floxuridine into low cholesterol-containing

- liposomes that coordinate drug release in vivo, *Biochimica et Biophysica Acta Biomembranes*, (2007); 1768(3): 678-687.
232. Tew W P, Lichtman S M. Ovarian cancer in older women, *Seminars in Oncology*, (2008); 35(6): 582-589.
233. Tirelli N. Bio(Responsive) Nanoparticles, *Current Opinion in Colloid & Interface Science*, (2006); 11: 210-216.
234. Tiyaboonchai W, Tungpradit W, Plianbangchang P. Formulation and characterization of curcuminoids loaded solid lipid nanoparticles, *International Journal of Pharmaceutics*, (2007); 37(3-4): 395-404.
235. Tsay J M, Trzoss M, Shi L, Kong X, Selke M, Jung M E, Weiss S. Singlet oxygen production by peptide-coated quantum dot-photosensitizer conjugates, *Journal of the American Chemical Society*, (2007); 129(21): 6865-6871.
236. Tsukioka Y, Matsumura Y, Hamaguchi T, Koike H, Moriyasu F, Kakizoe T. Pharmaceutical and biomedical differences between micellar doxorubicin (NK911) and liposomal doxorubicin (Doxil), *Japanese Journal of Cancer Research*, (2002); 93: 1145-1153.
237. United States Food and Drug Administration, 2012. <http://www.fda.gov/Drugs/InformationOnDrugs/ApprovedDrugs/ucm323668.htm> (Accessed: December 2012)
238. Urcan E, Haertel U, Styllou M, Hickel R, Scherthan H, Reichl F X. Real-time xCELLigence impedance analysis of the cytotoxicity of dental composite components in human gingival fibroblasts, *Dental Materials*, (2010); 26(1): 51-58.
239. Van Hengel A J, Harkes M P, Wichers H J, Hesselink P G M, Buitelaar R M. Characterization of callus formation and camptothecin production by cell lines of *Camptotheca acuminata*, *Plant Cell, Tissue and Organ Culture*, (1992); 28: 11-18.
240. Vauthier C, Dubernet C, Chauvierre C, Brigger I, Couvreur P. Drug delivery to resistant tumours: the potential of poly(alkyl cyanoacrylate) nanoparticles, *Journal of Controlled Release*, (2003); 93(2): 151-160.
241. Veiseh O, Gunn J W, Zhang M. Design and fabrication of magnetic nanoparticles for targeted drug delivery and imaging, *Advanced Drug Delivery Reviews*, (2010); 62(3): 284-304.
242. Vergara D, Bellomo C, Zhang X, Vergaro V, Tinelli A, Lorusso V, Rinaldi R, Lvov Y M, Leporatti S, Maffia M. Lapatinib/paclitaxel polyelectrolyte nanocapsules for overcoming multidrug resistance in ovarian cancer, *Nanomedicine: Nanotechnology, Biology and Medicine*, (2012); 8 (6): 891-899.
243. Vizirianakis I S. Nanomedicine and personalized medicine toward the application of pharmacotyping in clinical practice to improve drug-delivery outcomes, *Nanomedicine: Nanotechnology, Biology and Medicine*, (2011); 7(1): 11-17.

244. Vo-Dinh T, Cullum B M, Stokes D L. Nanosensors and biochips: frontiers in biomolecular diagnostics, *Sensors and Actuators*, (2001); 74(1-3): 2-11.
245. Vogelstein B, Kinzler K W. Cancer genes and the pathways they control, *Nature Medicine*, (2004); 10 (8): 789-799.
246. Volodkin D, Ball V, Schaaf P, Voegel J-C, Mohwald H. Complexation of phosphocholine liposomes with polylysine. Stabilization by surface coverage versus aggregation, *Biochimica et Biophysica Acta (BBA)-Biomembranes*, (2007); 1768(2): 280-290.
247. Vonarbourg A, Passirani C, Saulnier P, Benoit J-P. Parameters influencing the stealthiness of colloidal drug delivery systems, *Biomaterials*, (2006); 27(24): 4356-4373.
248. Wang C-S, Wurtman R J, Lee R K K. Amyloid precursor protein and membrane phospholipids in primary cortical neurons increase with development, or after exposure to nerve growth factor or $A\beta_{1-40}$, *Brain Research*, (2000); 865(2): 157-167.
249. Wang J-J, Sung K C, Hu O Y-P, Yeh C-H, Fang J-Y. Submicron lipid emulsion as a drug delivery system for nalbuphine and its prodrugs, *Journal of Controlled Release*, (2006); 115(2): 140-149.
250. Wang R, Xiao R, Zeng Z, Xu L, Wang J. Application of poly(ethylene glycol)-distearoylphosphatidylethanolamine (PEG-DSPE) block copolymers and their derivatives as Nanomaterials in drug delivery, *International Journal of Nanomedicine*, (2012); 7: 4185-4198.
251. Wang W, Wang Y J, Wang D Q. Dual effects of Tween 80 on protein stability, *International Journal of Pharmaceutics*, (2008); 347(1-2): 31-38.
252. Wang X, Li J, Wang Y, Cho K J, Kim G, Gjyzezi A, Koenig L, Giannakakou P, Shin H J, Tighiouart M, Nie S, Chen Z G, Shin D M. HFT-T, a targeting nanoparticle enhances specific delivery of paclitaxel to folate-receptor positive tumours. *American Chemical Society Nano*, (2009); 3(10): 3165-3174.
253. Wang Y, Li X, Zhou Y, Huang P, Xu Y. Preparation of nanobubbles for ultrasound imaging and intracellular drug delivery, *International Journal of Pharmaceutics*, (2010); 384(1-2): 148-153.
254. Ward C, Langdon S P, Mullen P, Harris A L, Harrison D J, Supuran C T, Kunkler I H. New strategies for targeting the hypoxic tumour microenvironment in breast cancer, *Cancer Treatment Reviews*, (2013); 39(2): 171-179.
255. Wartlick H, Michaelis K, Balthasar S, Strebhardt K, Kreuter J, Langer K. Highly specific HER2-mediated cellular uptake of antibody-modified nanoparticles in tumour cells, *Journal of Drug Targeting*, (2004); 12(7): 461-471.

256. Wate P S, Banerjee S S, Jalota-Badwar A, et al. Cellular imaging using biocompatible dendrimer-functionalized grapheme oxide-based fluorescent probe anchored with magnetic nanoparticles. *Nanotechnology*. 2012; 23(41): 1-8.
257. Weber C E, Kuo P C. The tumour microenvironment, *Surgical Oncology*, (2012); 21(3): 172-177.
258. Weishár Z, Czúcz J, Révész C, Rosivall L, Szebeni J, Rozsnyay Z. Complement activation by polyethoxylated pharmaceutical surfactants: Cremophor-EL, Tween-80 and Tween-20, *European Journal of Pharmaceutical Sciences*, (2012); 45(4): 492-498.
259. Welti S, Fraterman S, D'Angelo I, Wilm M, Scheffzek K. The Sec14 homology module of neurofibromin binds cellular glycerophospholipids: Mass spectrometry and structure of a lipid complex, *Journal of Molecular Biology*, (2007); 366(2): 551-562.
260. Wilhelm C, Billotey C, Roger J, Pons J N, Bacri J-C, Gazeau F. Intracellular uptake of anionic Superparamagnetic nanoparticles as a function of their surface coating, *Biomaterials*, (2003); 24(6): 1001-1011.
261. Witz I P. The tumour microenvironment: The making of a paradigm, *Cancer Microenvironment*, (2009); 2(1): 9-17.
262. World Health Organization (WHO), 2013. <http://www.who.int/cancer/en/index.html> (Accessed: February 2013)
263. Wu J-W, Lin L-C, Tsai T-H. Drug-drug interactions of silymarin on the perspective of pharmacokinetics, *Journal of Ethnopharmacology*, (2009); 121(2): 185-193.
264. Wu X, Jiang H, Zheng J, Wang X, Gu Z, Chen C. Highly sensitive recognition of cancer cells by electrochemical biosensor based on the interface of gold nanoparticles/poly lactide nanocomposites, *Journal of Electroanalytical Chemistry*, (2010); 656(1-2): 174-178.
265. Xia S, Xu S. Ferrous sulphate liposomes: preparation, stability and application in fluid milk, *Food Research International*, (2005); 38(3): 289-296.
266. Xiao K, Li Y, Luo J, Lee J S, Xiao W, Gonik A M, Agarwal R G, Lam K S. The effect of surface charge on in vivo biodistribution of PEG-oligocholeic acid based micellar nanoparticles, *Biomaterials*, (2011); 32(13): 3435-3446.
267. Xu Z, Gu W, Huang J, Sui H, Zhou Z, Yang Y, Yan Z, Li Y. In vitro and In vivo evaluation of actively targetable nanoparticles for paclitaxel delivery, *International Journal of Pharmaceutics*, (2005); 288(2): 361-368.
268. Yang S C, Lu L F, Cai Y, Zhu J B, Liang B W, Yang C Z. Body distribution in mice of intravenously injected camptothecin solid lipid nanoparticles and targeting effect on brain, *Journal of Controlled Release*, (1999); 59(3): 299-307.

269. Yang S-H, Lin J-K I, Chen W-S, Chiu J-H. Anti-angiogenic effect of silymarin on colon cancer LoVo cell line. *Journal of Surgical Research*, (2003); 113(1): 133-138.
270. Yang X J, Liu X, Liu Z, Pu F, Ren J, Qu X. Near-infrared light-triggered, targeted drug delivery to target cells by aptamer gated nanovehicles, *Advanced Materials*, (2012); 24(21): 2890-2895.
271. Yurkovetskiy A V, Fram R J. XMT-1001, a novel polymeric camptothecin pro-drug in clinical development for patients with advanced cancer, *Advanced Drug Delivery Reviews*, (2009); 61(13): 1193-1202.
272. Zalba S, Navarro I, Trocóniz I F, de Ilarduya C T, Garrido M J. Application of different methods to formulate PEG-liposomes of oxaliplatin: Evaluation in vitro and in vivo, *European Journal of Pharmaceutics and Biopharmaceutics*, (2012); 81(2): 273-280.
273. Zhang L, Han L, Sun X, Gao D, Qin J, Wang J. The use of Pegylated liposomes to prolong the circulation lifetime of salvianolic acid B, *Fitoterapia*, (2012); 83(4): 678-689.
274. Zhang L, Yang M, Wang Q, Li Y, Guo R, Jiang X, Yang C, Lui B. 10-Hydroxycamptothecin loaded nanoparticles: preparation and antitumor activity in mice, *Journal of Controlled Release*, (2007); 119(2): 153-162.
275. Zheng X T, Li C M. Single living cell detection of telomerase over-expression for cancer detection by an optical fibre nanobiosensor, *Biosensors and Bioelectronics*, (2010); 25(6): 1548-1552.
276. Ziomkowska B, Kruszewski S, Siuda R, Cyrankiewicz M. Deactivation of camptothecin determined by factor analysis of steady-state fluorescence and absorption spectra, *Optica Applicata*, (2006); 36 (1): 137-146.

APPENDICES

APPENDIX A

Derusha Frank, Charu Tyagi, Lomas K. Tomar, Yahya E. Choonara, Lisa C. du Toit, Pradeep Kumar, Clement Penny, Viness Pillay. Overview of the role of nanotechnological innovations in the detection and treatment of solid tumours. *International Journal of Nanomedicine*, (2014); 9: 589-613.

International Journal of Nanomedicine

Dovepress

open access to scientific and medical research

Open Access Full Text Article

REVIEW

Overview of the role of nanotechnological innovations in the detection and treatment of solid tumors

This article was published in the following Dove Press journal:
International Journal of Nanomedicine
22 January 2014
Number of times this article has been viewed

Derusha Frank¹
Charu Tyagi¹
Lomas Tomar¹
Yahya E Choonara¹
Lisa C du Toit¹
Pradeep Kumar¹
Clement Penny²
Viness Pillay¹

¹Department of Pharmacy and Pharmacology, ²Department of Medical Oncology, Faculty of Health Sciences, University of the Witwatersrand, Johannesburg, South Africa

Abstract: Nanotechnology, although still in its infantile stages, has the potential to revolutionize the diagnosis, treatment, and monitoring of disease progression and success of therapy for numerous diseases and conditions, not least of which is cancer. As it is a leading cause of mortality worldwide, early cancer detection, as well as safe and efficacious therapeutic intervention, will be indispensable in improving the prognosis related to cancers and overall survival rate, as well as health-related quality of life of patients diagnosed with cancer. The development of a relatively new field of nanomedicine, which combines various domains and technologies including nanotechnology, medicine, biology, pharmacology, mathematics, physics, and chemistry, has yielded different approaches to addressing these challenges. Of particular relevance in cancer, nanosystems have shown appreciable success in the realm of diagnosis and treatment. Characteristics attributable to these systems on account of the nanoscale size range allow for individualization of therapy, passive targeting, the attachment of targeting moieties for more specific targeting, minimally invasive procedures, and real-time imaging and monitoring of in vivo processes. Furthermore, incorporation into nanosystems may have the potential to reintroduce into clinical practice drugs that are no longer used because of various shortfalls, as well as aid in the registration of new, potent drugs with suboptimal pharmacokinetic profiles. Research into the development of nanosystems for cancer diagnosis and therapy is thus a rapidly emerging and viable field of study.

Keywords: nanosystems, targeted drug delivery, nanotheranostics, antineoplastic drugs, poor aqueous solubility, solid tumors

Introduction

The global burden of cancer, compounded by an increase in incidence and regression in the age of onset, has created a strong resurgence into cancer research. Large amounts of financial aid have been dedicated to research in the field of cancer etiology, detection, and treatment. However, at present, we appear to be at the losing end of the battle against cancer, which is the second leading cause of death worldwide and accounted for 7.6 million deaths in 2008.¹ The burden of cancer in the African setting paints an increasingly dismal picture, with approximately 715,000 new cases of cancer diagnosed on the continent in 2008 and 542,000 deaths reported in the same period, against the backdrop of the financial burdens of this disease on the health systems of a developing continent.² Figure 1 presents the global distribution of cancer incidence, highlighting the magnitude of cancer burden across different regions.³ The World Health Organization has projected cancer-related mortalities to rise to over 11 million by 2030.¹

Correspondence: Viness Pillay
Department of Pharmacy and
Pharmacology, Faculty of Health
Sciences, University of the
Witwatersrand, 7 York Road, Parktown,
Johannesburg 2193, South Africa
Tel +27 11 717 2274
Fax +27 11 642 4355
Email viness.pillay@wits.ac.za

APPENDIX B

APPENDIX B1

Derusha Frank, Viness Pillay, Yahya E. Choonara, Lisa C. du Toit. Characterization of Chitosan-Poly(ϵ -caprolactone) Interpenetrating Polymeric Complexes. Poster presented at the 5th International Conference on Pharmaceutical and Pharmacological Sciences, 23-26 September 2009, Potchefstroom, South Africa.

Investigation of the effect of varying polymeric composition for chitosan and poly-caprolactone blends and characterisation of the resultant formulations

Derusha Frank, Viness Pillay*, Yahya E. Choonara and Lisa C. du Toit
University of the Witwatersrand, Department of Pharmacy and Pharmacology, 7 York Road,
Parktown, 2193, Johannesburg, South Africa

*Correspondence: viness.pillay@wits.ac.za

Purpose:

The sophistication of current drug delivery systems (DDS's) precludes the utilisation of advanced technology and innovative concepts to ensure progression in the field of drug delivery. Polymer blends offer the potential of exploiting the advantageous properties of individual polymers in the development of highly precise targeted DDS's. This study investigated the effect of varying the composition of chitosan (CHT), a biodegradable and biocompatible polymer, and poly-(caprolactone) (PCL), a pH-responsive polymer, on the resultant formulation and characterisation of these formulations.

Method:

Solutions of (CHT) (1% and 2% w/v) in 1M acetic acid and (PCL) (2% and 5% w/v) in chloroform was prepared. Phosphatidylcholine (10mg) was incorporated into the PCL solution. All solutions were stirred overnight by means of a magnetic stirrer. The CHT solution was subsequently added to the PCL solution under the influence of a homogeniser. A surfactant, Tween 80 (2mL), was added drop wise to the emulsion during homogenisation. The resultant milky-white emulsion was subjected to rotary evaporation under vacuum by means of a rotary evaporator (30rpm; 90°C) for 12 hours. The final semi-transparent solution was allowed to evaporate under a fume hood for 48 hours. The polymer composition of each formulation is as follows:

Formulation 1: Chitosan – 2% w/v; 100mL, Poly-(caprolactone) – 5% w/v; 25mL.

Formulation 2: Chitosan – 1% w/v; 50mL, Poly-(caprolactone) – 2%w/v; 100mL

Results:

Macroscopic analysis exhibited phase distinctions between the final products of each formulation. Formulation 1 produced porous macro-particles, whilst a semi-membranous structure with a microbead-like surface morphology resulted from Formulation 2. Microscopy studies revealed a more consistent size distribution in Formulation 2 (~100-200 μ m), as compared to Formulation 1. The formulations FT-IR spectra demonstrated minimal deviation from that of the spectra of individual polymers, signifying minor interaction between the polymers. This was further confirmed by DSC. Significant variation in the stability of these formulations was also highlighted by their zeta potential.

Conclusion:

Individual polymer concentrations and their relative proportions in polymeric blends have a substantial influence on the resultant formulation. This principal can be manipulated to develop materials with precise properties for specific drug delivery functions.

APPENDIX B2

Derusha Frank, Pradeep Kumar, Lisa C. du Toit, Yahya E. Choonara, Clement Penny, Viness Pillay. Fabrication and Evaluation of Camptothecin-loaded Nano-liposomes for Targeted Ovarian Cancer Therapy. Poster presented at the 12th NanoBio Conference, 18-20 June 2012, Varese, Italy.

FABRICATION AND EVALUATION OF CAMPTOTHECIN-LOADED NANO-LIPOSOMES FOR TARGETED OVARIAN CANCER THERAPY

Derusha Frank¹, Viness Pillay¹, Lisa C. du Toit¹, Yahya E. Choonara¹, Pradeep Kumar¹ and Clement Penny²

¹University of the Witwatersrand, Department of Pharmacy and Pharmacology, 7 York Road, Parktown, 2193, Johannesburg, South Africa.

²University of the Witwatersrand, Department of Medical Oncology, 7 York Road, Parktown, 2193, Johannesburg, South Africa.

*Corresponding author: viness.pillay@wits.ac.za

Introduction:

The gaping deficiency in current ovarian cancer therapy is substantiated by the elevated recurrence rate and appalling 5-year survival rate of ovarian cancer. Nano-enabled systems have been acutely successful in tumour imaging. The current research aims to extend this paradigm to targeted anti-tumour therapy with the formulation of a nano-liposomal (NL) drug delivery system that will be passively targeted to ovarian tumour tissue, via the EPR phenomenon, following intravenous administration. This system further aims to limit the solubility and toxicity to healthy tissue shortfalls that have hindered the clinical usefulness of the exceedingly potent anti-tumour drug Camptothecin (CPT).

Methods:

Preparation of CPT-loaded Nano-liposomes: Distearoylphosphatidyl choline (0.03% w/v) and cholesterol (0.01% w/v) were dissolved in chloroform:methanol (9:1). Dioctylsulfosuccinate (DOS) (0.01–0.03% w/v), CPT and PBS (pH 7.4) were added to the organic phase under ultra-sonication (Amplitude=60%, Time=2 minutes). The resultant monophasic emulsion was subjected to rotary evaporation under vacuum at 60°C for 2-3 hours, until complete evaporation of organic solvents was achieved. PBS (pH 7.4; 10mL) was added periodically during the evaporation process and ultra-sonication was undertaken at each addition as outlined above. This process culminated in the formation of CPT-loaded NL's suspended in PBS (pH 7.4).

Determination of Nano-liposomal Size and Size Distribution: NL suspensions were filtered through a 0.22µm filter and subjected to size and size distribution analysis employing a NanoZetasizer ZS. Analysis was conducted over a 3 hour period whilst maintaining the formulations at physiological temperature. Size and morphology were further confirmed by Transmission Electron Microscopy (TEM).

Evaluation of Drug Incorporation Efficiency (DIE): The solubility properties of CPT dictated that unincorporated drug would precipitate out in the suspending medium (PBS pH 7.4). Hence, the NL suspensions were double filtered through 0.22µm filters to remove free drug. The remaining suspensions were evaluated by UV spectroscopy at 366nm to quantify DIE.

Elucidation of Drug Release Profiles: Following the removal of unincorporated CPT, the NL suspensions were contained in dialysis tubing (12000kDa) and suspended in PBS (pH 7.4; 200mL) in sealed receptacles, maintained at 37°C in an orbital shaker bath (25rpm). At pre-determined intervals 5mL aliquots of the external phase were withdrawn and replaced with fresh PBS (pH 7.4). The samples were analyzed by UV spectroscopy.

Nano-liposomal Life-time studies: NL's were injected into a carrageenan hydrogel and observed employing a microultrasound imaging system.

Quantification of Nano-liposomal surface charge: The surface charge of NL suspensions was quantified as Zeta Potential employing a NanoZetasizer ZS. Samples were filled into specialized cuvettes and analyzed over a 3 hour period while being maintained at physiological temperature.

Results:

All formulations successfully produced stable, regular CPT-NL's, as evidenced by TEM images. Whilst all formulations fell into an acceptable size range (125nm-145nm) with narrow size distribution (PdI < 0.2) for successful extravasation through compromised tumour vasculature, DOS concentration appeared to have a significant effect on zeta potential. Increasing DOS concentration from 0.01% w/v to 0.03% w/v resulted in a ~14mV (-25.7 to -39.4mV) decrease in zeta potential. Zeta potential values for all formulations were significantly negative indicative of high stability and low propensity for aggregation. This could have significant impact on the stability (shelf-life and in-vivo) of the NL-DDS. In addition, increasing DOS concentrations resulted in an increase in DIE from ~61%-81%. The formulation with the highest DOS concentration was also more consistently reproducible. Drug release profiles revealed insignificant differences resulting from changes in DOS concentration. However, all 3 formulations exhibited favourable drug release characteristics, achieving ~50% drug release after 4 hours, thus allowing sufficient time for the accumulation of NL's within tumour tissue for targeted drug release. Microultrasound imaging displayed adequate diffusion of NL's through the gel medium and an absence of aggregation.

APPENDIX B3

Derusha Frank, Viness Pillay, Yahya E. Choonara, Lisa C. du Toit, Clement Penny. Design and Characterization of Intravenously Administered Nanolipobubbles for Targeted Ovarian Cancer Therapy. Podium presentation for the Young Scientist Competition at the 6th International Conference on Pharmaceutical and Pharmacological Sciences, 25-28 September 2011, Durban, South Africa.

Design and Characterization of Intravenously Administered Nanolipobubbles for Targeted Ovarian Cancer Therapy:

Derusha Frank¹, Viness Pillay^{*1}, Yahya E. Choonara¹, Lisa C. du Toit¹ and Clement Penny²

¹University of the Witwatersrand, Department of Pharmacy and Pharmacology, 7 York Road, Parktown, 2193, Johannesburg, South Africa.

²University of the Witwatersrand, Department of Medical Oncology, 7 York Road, Parktown, 2193, Johannesburg, South Africa.

**Corresponding author: viness.pillay@wits.ac.za*

Purpose:

This study aims to develop a camptothecin (CPT)-loaded nanolipobubble (NLB) intravenous formulation for the targeted treatment of ovarian cancer. This research is based on the pre-formulation studies undertaken to develop nanoliposomes (NL's), as the precursor to NLB preparation, ranging in size between 100-150nm, to facilitate adequate extravasation through the leaky vasculature present in tumour tissue. Furthermore, drug release kinetics of the formulation was elucidated at physiological and tumour pH (pH 7.4 and 6.0, respectively), to determine the targeting potential of the formulation.

Methods:

Preparation of CPT-loaded and placebo NL's: Varying concentrations and ratios of distearoylphosphatidyl choline (0.1-0.3% w/v) and either distearoylphosphatidylethanolamine-m-PEG (DSPE-m-PEG) or cholesterol (CHO) (0.1-0.3% w/v) was dissolved in chloroform:methanol (9:1; 10mL). PBS (pH 7.4; 10mL) was subsequently added to the organic phase under ultra-sonication (60% amplitude for 90 seconds). Tween® 80, Span® 80 and polyvinylpyrrolidone (PVP) (0.1-0.3mL) were employed as surfactants. The resultant emulsion was subjected to evaporation under vacuum (65°C) for 3 hours, forming a NL suspension. In CPT-loaded formulations, CPT was incorporated during ultrasonication.

Determination of NL size and size distribution: The NL suspension was analysed for size and size distribution profiles over a 3 hour period, whilst being maintained at 37°C. Effect of CPT loading on size of the NL's was investigated.

Elucidation of drug release profiles: NL's were centrifuged to remove unbound drug, and the sediment was re-suspended in PBS (pH 7.4 and 6.0; 100mL) and maintained in a shaker bath at 37°C at 25 rpm. Samples were withdrawn at pre-determined intervals and drug release was evaluated by UV spectroscopy.

Evaluating interactions of formulation components: Formulations were subjected to Fourier Transform Infra-Red (FTIR) analysis to determine the interactions of lipids and surfactants, and the effects of these interactions on the drug release kinetics and stability of the formulation.

Determination of NLB lifetime: Sulphurhexafluoride gas was incorporated into the NL, forming NLB's. The NLB's were injected into a hydrogel and observed using a microultrasound imaging system.

Results:

Variation in the lipid component and surfactant proved to be a factor in size and stability of the NL's. In general, the use of CHO instead of DSPE-m-PEG resulted in a 20-40nm increase in NL size and an unfavourable size distribution profile (PdI>0.2). Although more stable, PVP-containing formulations also displayed a dramatic increase in size (>200nm). Drug release was fairly rapid (100% in 15 minutes), thus polymer coating is being investigated as a means of retarding drug release. FTIR analysis highlighted only a physical interaction between lipids and surfactants, which had no significant influence on stability or drug release kinetics. NLB lifetime studies are currently underway.

APPENDIX B4

Derusha Frank, Yahya E. Choonara, Lisa C. du Toit, Clement Penny, Pradeep Kumar, Viness Pillay. Characterization and Optimization of Camptothecin Nano-liposomes for Targeted Ovarian Cancer Therapy. Podium presentation at the University of the Witwatersrand Faculty of Health Sciences Research Day, 19 September 2012, Johannesburg, South Africa.

Characterization and Optimisation of Camptothecin-loaded Nano-liposomes for Targeted Ovarian Cancer Therapy

Derusha Frank¹, Lisa C. du Toit¹, Yahya E. Choonara¹, Clement Penny², Viness Pillay^{*1}

¹University of the Witwatersrand, Department of Pharmacy and Pharmacology, 7 York Road, Parktown, 2193, Johannesburg, South Africa.


²University of the Witwatersrand, Department of Medical Oncology, 7 York Road, Parktown, 2193, Johannesburg, South Africa.

**Corresponding author: viness.pillay@wits.ac.za*

The gaping deficiency in current ovarian cancer therapy is substantiated by the elevated recurrence rate and appalling 5-year survival rate of ovarian cancer. Nano-enabled systems have been acutely successful in tumour imaging. The current research aims to extend this paradigm to targeted anti-tumour therapy with the formulation of a Camptothecin-Loaded Nano-Liposomal (NL) Drug Delivery System (DDS) that will be passively targeted to ovarian tumour tissue, via the EPR phenomenon, following intravenous administration. Extensive pre-formulation investigations culminated in the delineation of independent variables, namely phospholipid combination, phospholipid concentration and surfactant concentration. A Face-Centered Central Composite Design was employed to generate two sets of formulations based on the minima and maxima limits of the above-mentioned variables. Formulations were accurately prepared and analyzed in triplicate. Nano-sizing (<200nm) was highlighted as a vital measured outcome due to the intravenous nature of the formulation and the dependence of passive targeting on formulation size. Although all formulations were below 160nm, DSPC-containing formulations were ~20nm larger. Zeta potential was assessed as an indication of formulation stability. Increased surfactant concentration resulted in a more favourably negative zeta potential. Formulations from the DSPC-containing design proved significantly more stable (25-40mV). The nano-scale size range poses a challenge to the quantity of drug incorporated into nano-enabled DDS's. Hence, drug incorporation efficiency was determined by a novel method. The passively targeted nature of the DDS requires sufficient time for accumulation of the DDS within tumour tissue. Drug release profiles highlighted adequate time for extravasation before significant drug is released from the DDS, thereby favourably altering the biodistribution of camptothecin.

APPENDIX C

Targeted Ovarian Cancer Therapy. Lisa C. du Toit, Derusha Frank, Viness Pillay, Yayha E. Choonara. SA Patent Application No: 2012/07435, 4 October 2012.



CIPRO IP ONLINE SERVICES
close | print

Companies and Intellectual Property Commission
a member of the dti group

REPUBLIC OF SOUTH AFRICA REGISTER OF PATENTS PATENTS

Official Application No.		Lodging date: Provisional	Acceptance Date	
21	01	2012/07435	22	04-Oct-2012

International Classification No.		Lodging Date: Complete	Granted Date	
51		23		47

International Application No.	International Filing Date	Priority Date	

Full Name(s) of Patentee(s)	
71	1590939. UNIVERSITY OF THE WITWATERSRAND (THE) 1 JAN SMUTS AVENUE JOHANNESBURG 2050 Gauteng

Applicants Substituted	Date Registered
71	

Assignee(s)	Date Registered
71	

Full Name(s) of Inventor(s)	
72	2172760. LISA CLAIRE DU TOIT 2345426. DERUSHA FRANK 1709627. VINESS PILLAY 1800347. YAHYA ESSOP CHOONARA

Priority Claimed		
Country	Number	Date
33	31	32

Title of Invention	
54	TARGETED OVARIAN CANCER THERAPY

APPENDIX D

Waiver letter confirming this study did not require clearance from the Human Research Ethics Committee of the University of the Witwatersrand.

Human Research Ethics Committee (Medical)
(formerly Committee for Research on Human Subjects (Medical))

Secretariat: Research Office, Room SH-0005, 10th floor, Senate House • Telephone: 127 11 717 1334 • Fax: 127 11 389 6708
Private Bag 3, Wits 2050, South Africa

University
of the Witwatersrand,
Johannesburg



Ref: W-CJ-121026-1

26/10/2012

TO WHOM IT MAY CONCERN:

Waiver: This certifies that the following research does not require clearance from the Human Research Ethics Committee (Medical).

Investigator: Prof V Pillay, Miss D Frank (student no 0504046D).

Project title: The design and development of antineoplastic nano-lipobubbles for targeted chemotherapy.

Reason: This is laboratory study using a human epithelial tumour cell line (A2780). No humans are involved.

A handwritten signature in blue ink, appearing to read "Peter Cleaton-Jones".



Professor Peter Cleaton-Jones
Chair: Human Research Ethics Committee (Medical)

copy: Anisa Keshav, Research Office, Senate House, Wits